PORE SCALE STUDY OF CRUDE OIL DISTRIBUTION AND INTERFACIAL PROCESSES IN UNCONSOLIDATED POROUS MEDIA: AN APPLICATION OF SYNCHROTRON X-RAY MICROTOMOGRAPHY

by

JAYDEEP GHOSH

GEOFFREY R. TICK, COMMITTEE CHAIR
RONA J. DONAHOE
TIMOTHY MASTERLARK
JACK C. PASHIN
CHUNMIAO ZHENG

A DISSERTATION

Submitted in partial fulfillment of the requirements
for the degree of Doctor of Philosophy
in the Department of Geological Sciences
in the Graduate School of
The University of Alabama

TUSCALOOSA, ALABAMA

2011

ABSTRACT

A pore-scale study was conducted to determine model reservoir systems most amenable to oil recovery by investigating the behavior of three fractions of crude oil distribution and morphology in three types of porous media with increasing heterogeneity (in grain size distribution) during sequential surfactant flooding episodes. Multiple columns, packed with three types of sand, were established with residual saturations of light, heavy, and extra-heavy crude oil fractions, respectively. These columns were then flooded with anionic surfactant solution in various episodes. Synchrotron X-ray microtomography (SXM) was used to obtain high-resolution 3-D images before and after each surfactant flooding event. Results show homogeneous distributions of light and heavy oil fractions, as residual saturation conditions, within the homogeneous sand. Heterogeneous oil blob distributions were observed within the two higher heterogeneous porous media types. Oil blob distributions became more heterogeneous after surfactant flooding for all porous-media systems. Oil recovery was most effective from the homogenous sand (100% recovery) after 5 pore volumes (PVs) of flooding. Mildly-heterogeneous sand yielded a limited but consistent recovery after each flooding episode (23% and 43% recovery for light and heavy after 5-PV flood). The highly-heterogeneous sand showed greater recovery (42% and 16% for light and heavy) only after 5-PVs of flushing. SXM images effectively demonstrate trapping mechanism and mobilization of extra-heavy oil controlled by wettability of porous media. Homogeneous sand showed limited recovery (6%), whereas highly-heterogeneous sand showed consistent 20% recovery of extra-heavy oil after

each flooding episode. Although spontaneous in-situ-stable-emulsion was formed in the mildly-heterogeneous sand, no recovery was attained due to the "jamin" effect after the 2-PV flood and 7% recovery after the 5-PV flood. In general, oil blobs within the homogeneous and mildly-heterogeneous sands showed an increase in total surface area, but a gradual reduction of total surface area within the highly-heterogeneous sand after each surfactant flood. This innovative and cutting-edge research, for the first time, implemented SXM technology to understand the pore scale processes affecting enhanced oil recovery techniques. The results of this study can be extremely beneficial to establish 3-D model for pore-scale displacement efficiency for various reservoir media systems.

DEDICATION

I would like to dedicate this Doctoral Dissertation to my Advisor Dr. Geoffrey R. Tick for his constant support and tremendous help in completing this enormous research project.

I would also like to dedicate this work to my parents: Mr. Jaharlal Ghosh and Mrs. Sipra Ghosh, who have sacrificed many ways to help me complete this long journey of my academic career.

I would also dedicate this work to my wife, Antara Banerjee whom I have neglected many ways when she was recovering from a major car accident during last few years of my PhD research work.

LIST OF ABBREVIATIONS AND SYMBOLS

γ Interfacial tension between aqueous and non aqueous phases

θ Contact angle along the three phase liquid-liquid-solid interface

R Radius of curvature of the curved interface between crude oil-water

Δp Pressure difference/capillary pressure along the crude oil-water interface

hc Capillary rise of the wetting fluid (water)

η Viscosity of the flooding fluid (water)

v Velocity of the flooding fluid (water/surfactant solution)

ϕ Media porosity

k_i Intrinsic permeability,

ρ Density of flooding fluid (water)

g Acceleration due to gravity

ΔP Pressure gradient

N_C Capillary number

N_B Bond number

N_T Trapping number

C_U Uniformity coefficient

C_V Coefficient of variation

ACKNOWLEDGMENTS

Acknowledgement is made to the donors of the American Chemical Society Petroleum Research Fund for support of this research. Other grants/financial assistance was received from Geological Sciences Advisory Board, and Hook's Research Fund. I am pleased to express my gratitude to my advisor, Dr. Geoffrey R. Tick for all of his valuable ideas, and his tremendous help and support. I could not have accomplished this research project without Dr. Tick's encouragement. I would like to thank my Committee members, Dr. Rona J. Donahoe, Dr. Timothy Masterlark, Dr. Jack C. Pashin and Dr. Chunmiao Zheng, for their valuable comments and suggestions. I am indebted to Dr. Andrew M. Goodliffe for his generous support and help, and for allowing me to access Sun Server for most of image processing. I am also thankful to Dr. Timothy Masterlark for his valuable advices in many technical and academic issues. I would like to thank my friends David Slavic, Dorina Murgulet, Jason Harvel, Ghanashyam (Hari) Neupane and Joe Lambert for their helps in experimental/laboratory works. I would like to convey sincere thanks to Dr. Mark River at the Argonne National Laboratory for his help in capturing Synchrotron X-Ray images, Justin Marble (University of Arizona), and Mollie Costanza Robinson (Middlebury College, VT) for their help in many ways. Also I am indebted to Ron Fisher (BP), Anna Shafizadeh (Chevron), Tom Burghart, and R. Ravikiran (Stepan Chemical) for providing crude oil samples and surfactant sample for this research. My special thanks to my wife Antara Banerjee for her moral support, and my family members and friends, Swapna Banerjee, Siddhartha Bhattacharyya, Sikharini Majumder, Indrajit Kanjilal, Arunima Banerjee, Atanu Sengupta, and Shantanu Paul for taking some of my responsibilities, and helping me to concentrate on my goal.

CONTENTS

CONTENTS (CONTINUED)

LIST OF TABLES

LIST OF FIGURES

LIST OF FIGURES (CONTINUED)

LIST OF FIGURES (CONTINUED)

LIST OF FIGURES (CONTINUED)

LIST OF FIGURES (CONTINUED)

LIST OF FIGURES (CONTINUED)

INTRODUCTION

Research Problem

U.S. and global oil demand is projected to keep dramatically increasing into the future outpacing supply and posing severe challenges for more efficient extraction technologies in a currently oil-based economy. Due to increasing demand of crude oil and declining rate of production of conventional energy resources (Figure A1, Appendix) great interest in enhanced recovery methods for abandoned oil reservoirs has been initiated. For example, tertiary oil extraction technologies implementing the use of surfactant flooding, has become a promising technique to recover oil from existing reservoirs or from reservoirs that present challenges for primary and secondary extraction techniques. It has been estimated that existing economically feasible technologies (primary and secondary processes) may recover up to 50% of total original oil in place (OOIP) from an existing crude oil reservoir (Kerr 2005, Green and Willhite 1998). During water flooding, disconnected oil blobs or continuous ganglia type oil-phase are trapped into pore spaces by various controlling factors such as capillary action, crude oil viscosity, wettability of reservoir media, and crude oil-water interfacial tension. Other controlling factors include heterogeneity of reservoirs with respect to pore geometry, and sorting and packing of solid media grains. Chemical flooding using surfactants is an existing technology for tertiary extraction process from existing reservoirs. Unconventional resources such as extra-heavy oil or bitumen are receiving increased attention and importance as the crude oil prices increase. Surfactant induced cold recovery techniques are economically feasible, compare to conventional thermal recovery (Bryan and Kantzas 2009), for the heavy oil deposits of shallow (<200ft), thin

pay-zones in southeastern Missouri and Kansas (Hunky et al. 2010). Wettability changes (Hirasaki and Zhang 2004) and formation of heavy oil emulsification (McAuliffe 1973) are two important factors controlling the prospective success of this method. In both of the above mentioned oil extraction techniques, an understanding of crude oil trapping mechanisms and interfacial phenomena at the pore scale is required to optimize innovative techniques for microscopic displacement efficiency of crude oil from various porous media. Morphology of oil blobs and pattern of distributions too have an impact on available contact surfaces by controlling the interfacial processes. A thorough understanding of oil blob distribution patterns and changes in oil blob morphology, as function of media heterogeneity is critical for estimating the recovery potential from existing reservoirs.

Green and Willhite (1998) describe the overall displacement efficiency (E) of a reservoir as a measure of effective displacement of trapped oil blobs in response to displacing fluid flood, which is measured as a product of microscopic (E_D) and macroscopic (E_V) displacement efficiency.

$E = E_D E_V$

E_D can be estimated as the residual oil saturation (after chemical flood) as a fraction of initial trapped oil-saturation within a particular microscopic volume (laboratory scale) where the oil-phase is in contact with displacing fluid. The macroscopic displacement efficiency, E_V is a measure of the overall residual saturation (i.e. oil fraction remaining) for a macroscopic reservoir volume (field scale), which includes both swept and unswept zones with displacing fluid.

This innovative and cutting-edge research of this dissertation implemented synchrotron X-ray microtomography (SXM) technology to conduct the first detailed series of pore-scale experiments to understand the primary pore scale processes affecting oil recovery under tertiary

oil recovery techniques. This novel, noninvasive technique (SXM) was utilized to capture high-resolution images (10 μm) of various fractions of crude oil injected within columns packed with various types of porous media. Columns were flooded with an anionic surfactant over a series of episodes. Pore-scale images of the column systems were captured before and after the surfactant flooding events to study the temporal changes in oil-blob distribution pattern, oil-water surface area, oil morphology, and oil recovery. The outcome of this research will be beneficial in understanding interfacial processes at the pore-scale, improving knowledge about conditions appropriate for successful tertiary extraction of crude oil from existing reservoirs. Furthermore, this research will also be helpful in demonstrating the value of synchrotron X-ray microtomography as an effective tool for studying the primary pore-scale processes controlling crude oil mobilization, distribution, and recovery during surfactant flooding.

Previous Research

Following is a synopsis of previous research carried out to understand the transport mechanisms of non-aqueous-phase-liquid (NAPL) blob distribution patterns and changes in morphology within various types of porous media. Morrow and Heller (1985) presented a detailed description of the previous attempts carried out to understand and describe the pore geometry and oil-phase distribution in porous media using electron micrography techniques. Electron micrography is a high-resolution method for pore structure observation. Although electron micrography produces much detail of the pore structure, it is not appropriate for constructing a mathematical model of fluid flow (Morrow and Heller 1985). A more realistic model was costructed by Dullien (1979) and by Dullien and Dhawan (1974) by performing a computer analysis of two-dimensional slices of a real core. However, the application was limited

to only a few samples. Attempts have included using blob casting methods, two-dimensional micromodels, and imaging techniques to study trapping mechanisms and changes in distribution and blob morphology during residual saturation and during water and surfactant flooding in a laboratory setting. A styrene monomer was used to study nonwetting phase behavior in various types of media, including sandstone, limestone (Craze 1950, Morrow and Chatzis 1982 and Chatzis et al. 1983), glass beads (Mayer and Miller 1992), and unconsolidated media such as loose sands (Craze 1950, Powers et al. 1992). In this method, a styrene monomer liquid was injected to saturate a particular medium. Liquid styrene was then changed into a solid polymer by changing the temperature and pressure, and the solidified blobs were recovered from the media by acid dissolution or density fractionation. The morphology of the blobs was studied directly from the isolated beads. Sieve analysis has also been used for statistical analysis of the blob size distribution (Mayer and Miller 1992, Powers et al. 1992). However, the blob casting method was not always useful, as the styrene polymer would shrink in the solid phase and therefore quantitative results regarding shape and size would be erroneous. Moreover, there was a high potential of breaking the blobs into pieces during recovery and sieve analysis, and therefore, appropriate data for blob size distribution could not be obtained successfully. This technique also has other limitations such as difficulty in measuring the interfacial area, and the fact that the experiments only produce a single end-distribution result.

Oil flow and trapping mechanisms have been studied using two-dimensional micro-models, where two etched glass plates are fused with each other. Blob morphology and trapping mechanisms can be studied using this method, as well as temporal changes and dynamics in the fluid distribution through in situ imaging. Chatzis et al. (1983) described pore geometries favoring the two important trapping mechanisms known as “snap off” and “bypassing” (see

Figure A2 in Appendix for explanation). They have shown that heterogeneous blob distributions result from greater heterogeneity of the medium. A high aspect ratio (i.e. pore neck to pore body ratio) enhances the formation of spherical blob singlets through the snap off process, whereas interconnected ganglia distributions are more prevalent due to bypassing mechanisms caused by heterogeneities in the pore spaces. However, the two-dimensional micro-model techniques certainly have limitations characterizing three-dimensional distributions.

Three dimensional imaging techniques have received increasing attention over the last decade, and have been used extensively in understanding the pore-scale distribution of immiscible liquids. Recent researches using 3-D imaging techniques have been discussed in detail by Schnaar (2006). A brief synopsis of recent discoveries made by using various techniques such as photo imaging of refractive index, magnetic resonance imaging (MRI), and SXM is given herein. Although photo imaging of refractive index has high spatial resolution (1-10 μm), the porous media have to be transparent to light. Only a limited number of fluids, which possess a specific range of refractive indices, can be imaged by this method. MRI techniques can produce very high-resolution images ranging from 60 to 200 μm and have been used effectively to estimate the variation of fluid velocity along the pore spaces. SXM imaging can resolve image resolutions ranging from 1-10 μm and this technique is capable of imaging multiple phases simultaneously by changing the incident energy level. However, this technique can only be used to study relatively small systems, up to a few centimeters in thickness. Previous studies show that SXM imaging has been used successfully to observe and statistically analyze pore structure, immiscible phase blob morphology, distribution, transport (Wildenschild et al. 2002, Zhang et al. 2002, Al-Raoush et al. 2003), analyzing dissolution behavior, and measuring blob interfacial areas (Culligan 2004, Schnaar 2006a).

Objectives and Significance of the Research

The primary objective of this research was to understand the pore-scale processes controlling the mobilization and distribution of various fractions of crude oil within porous media of various heterogeneities using SXM as an innovative tool to understand these pore-scale processes. Following is the objectives of this research discussed in detail.

1. The nature of the oil blob distribution (3-D) was studied and characterized for light, heavy, and extra-heavy gravity crude oil in different types of porous media. As discussed previously, the interfacial tension, blob morphology and capillary action between oil and solid media are the primary factors controlling fluid migration through pore spaces. Attempts have been made in previous literature (Schnaar and Brusseau 2006a) to fit the particle size distribution of a non-aqueous phase liquid with a lognormal curve. For a multivariate system, log normal distribution is a good representation of size distribution. Attempt has been made to characterize the distribution (in terms of the particle size distribution coefficient of variation, or uniformity coefficient) as a function of crude oil fraction properties (such as API gravity, wettability).
2. Separate observations were carried out to characterize the distribution of each oil fraction in three types of porous media with increasing heterogeneity (pore scale). Multiple variables such as the porosity, sorting, and permeability of the solid media, as well as the diameter of the pore spaces, are the primary factors controlling the oil distribution pattern. The cumulative size distributions of oil blobs have been characterized by fitting the data to a log-normal distribution for various media. Attempts were made to develop correlative relationships between the porous media grain-size heterogeneity (i.e., the uniformity

coefficient) and blob-volume heterogeneity (i.e., the blob distribution uniformity coefficient or coefficient of variation) especially with respect to oil recovery.

3. Crude oil blob morphology is a function of both the crude oil fraction and the heterogeneity of the medium. During surfactant application, interfacial tension controls the morphology of the oil phase and its overall distribution. Oil blob shape and morphology can vary from single spheres (singlets) to complex interconnected ganglia (length and width much greater than thickness). Attempts have been made to characterize the shape distributions as deviations from a sphere of equal volume. The greater the shape deviation from a sphere, the greater the blob surface area and related morphological/geometrical complexity. Greater surface area of oil blobs favors surface activity in contact with surfactant solution, which in turn help in oil-phase mobilization or enhanced recovery process.
4. Transient changes in blob morphology have been studied, after a series of surfactant flooding events, as the oil-phase migrates through the pore spaces. Considering a water-wet media, it was assumed that the surface area available for crude oil is equivalent to the crude oil-surfactant surface area. The crude oil extraction capacity of the surfactant was estimated after each surfactant-flooding episode in terms of residual oil volume. The specific surface was calculated for each phase by normalizing the available surface area by the total imaged volume. Qualtitative observations were carried out to correlate residual volume with changing interfacial area.
5. Additional experiments were carried out to estimate critical micelle concentration (CMC), by means of interfacial tension measurement, for various crude oil with the particular anionic surfactant. Surfactant concentration below CMC ensures oil recovery by mobilization process with minimal or no dissolution of oil phase due to surfactant flood. Residual volume

is strongly influenced by the ratio of viscous to interfacial forces (estimated by capillary no.), and the density of oil fraction controlling the buoyancy forces (estimated by bond number). Capillary number and bond number were estimated using for each type of crude oil composition in each of three porous media types. These two parameters can have critical role in field scale application of this particular enhanced recovery experiment.

6. Finally, this research finds out the utility of Synchrotron X-ray Microtomography as an effective non-destructive tool for pore scale study of various crude oil fractions. With the high resolution (9-10μm) SXM provides, all phases (solid, aqueous and crude oil) can be resolved successfully. Quantitative data in terms of volume and surface area of the oil blobs were estimated. In addition the images were used to investigate wettability changes of the medium, resulting pore scale trapping or mobilization of oil phase.

Materials and Methods

Multiple columns were packed with three different sediments with increasing heterogeneity. The heterogeneity of medium is expressed in terms of uniformity coefficient, a ratio of the 60^{th} percentile to the 10^{th} percentile grain-size diameters of a grain-size distribution curve ($C_U = d_{60}/d_{10}$). Commercially available sediments, homogeneous 40/50 Accusand ($C_U = 1$, from Unimin Corporation, LeSueur, MN), heterogeneous mixed Accusand ($C_U = 5.8$), and heterogeneous, mixed Accusand and karst soil ($C_U = 10.6$) were used for column packing. In terms of sorting, the three types of porous media can be characterized as well sorted unimodal distribution (homogenous sand), and poorly sorted distribution for the two other heterogeneous sands. Sediment packed columns were saturated with water to simulate a water-wetting-reservoir and flooded with three different fractions (light, medium, and heavy) of crude oil (BP and

Chevron). The columns were then flooded with an anionic surfactant (Branched alcohol propoxy sulfate from Stepan Chemical Company, Northfield, IL) in two different episodes. Multiple SXM images of columns were captured before and after the flooding events. Oil samples were doped with 10% by volume iodobenzene (Acros Organics, NJ) to improve the image contrast for a particular X-ray absorption energy. The aqueous phase (double-deionized water) was doped with 60 g/L cesium chloride (Acros Organics, NJ) for the same purpose. A total of 27 images were taken for 9 columns. All images were taken using BM-13D at the GeoSoilEnviroCARS (GSECARS) located in the Advanced Photon Source (APS), Argonne National Laboratory, Illinois. Approximately 1500 to 1600 two-dimensional images were produced for 1.5 cm long column. Images were taken at three incident energy levels with a spatial resolution ranging from 9.9-10.3 μm. The images taken above (36.085KeV) and below (33.269 KeV) the cesium critical absorption edge can be subtracted to resolve the aqueous phase doped with cesium chloride. The images taken below the cesium edge (or above the iodine edge, 33.269 KeV), and below the iodine edge (33.0169) can be subtracted to resolve the oil phase (Figure A3, Appendix). The images were preprocessed and reconstructed using software called Tomo_Display at APS. Additional post-processing including quality control (noise reduction), grey-scale to binary transformation (Figure A4, Appendix), stacking of all two-dimensional images to generate a three-dimensional image of the entire column and quantitative measurements such as size, volume, and specific surface area distributions of blobs were performed using Blob3D software.

Findings and Relationships Between the Articles

The results of this research are compiled into four papers for publication as peer-reviewed journal articles. The Article 1 focuses on quantifying oil distribution and recovery as a function of oil fraction (light, heavy and extra-heavy). The oil recovery potential has been compared to the oil fraction distribution in homogeneous porous medium for each system in order to make quantitative assessments for systems most amenable to oil extraction under surfactant flooding. The Article 2 of this research takes a comprehensive approach quantifying two different fractions (light and heavy) of oil distribution (e.g., morphology, oil blob size distribution, specific surface area) as a function of pore scale heterogeneity (e.g. media uniformity coefficient, and permeability) of porous medium. Crude-oil recovery potential was compared to the oil distribution versus porous media heterogeneity relationships for each system in order to make quantitative assessments for systems most amenable to oil displacement under surfactant flooding. The Article 3 of this research synthesized the results of oil recovery under surfactant flushing in increasingly heterogeneous porous media configured with extra-heavy oil. Parts of the results from articles 1 has been integrated into third article investigating these relationships on extra-heavy oil recovery in the different systems studied. The fourth and last theme of this research comprises a short technical article (Article 4) quantifying the various surfactant-oil interfacial tension relationships under a range of surfactant concentrations. This is also the first known study investigating and quantifying the critical micelle concentration (CMC) for this particular surfactant and the various crude oil fractions utilized. Solubility of immiscible phase (oil in this case) increases drastically above CMC level. It was important to apply the surfactant solution below CMC level to ensure oil-phase removal, from this small laboratory scale system, entirely by mobilization process, limiting any dissolution activity.

HIGH RESOLUTION CHARACTERIZATION OF CRUDE OIL DISTRIBUTION IN HOMOGENEOUS POROUS MEDIUM: AN APPLICATION OF SYNCHROTRON X-RAY MICROTOMOGRAPHY

ABSTRACT

A pore-scale study was conducted to characterize three fractions of crude oil (light, heavy, and extra-heavy) distribution and morphology in homogeneous 40/50 Accusand (uniformity coefficient=1) after successive surfactant flooding events. Synchrotron X-ray microtomography was used to obtain high-resolution three-dimensional (3-D) images (10-μm image resolution) of the two-fluid-phase crude oil/water system, and quantify the distribution, the shape and size of the blobs in the pore spaces. Results show relatively homogeneous initial distribution of disconnected blobs of light and heavy gravity crude oil in residual saturation prior to surfactant flooding, whereas, extra-heavy oil shows trapping as continuous interconnected ganglia. Both light and heavy oil fractions show an increase in number of blobs and total blob surface area, and a reduction in the total blob-volume after 2 pore volumes (PV) of surfactant flooding. The light-oil distribution shows a 200% increase of total surface area after the 2 PVs surfactant flooding event. The heavy-oil distribution shows an 87% increase in total surface area after 2 PVs of surfactant flooding. This increase in surface area is attributed to the change in blob morphology from spherical to more complex non-spherical lenticular, laminar ganglia shape characteristics. Moreover, the observed increase in the number of oil blobs from larger to smaller particles after the 2-PV surfactant flood contributed to the greater cumulative oil surface area. In contrast, however,

the extra-heavy-oil distribution shows only 7% increase in surface area after 2 PVs of surfactant flooding and a 1.4% decrease in surface area after 5 PVs of surfactant flooding. Both the light and heavy oil experiments showed complete recovery after 5 PVs of surfactant flooding, whereas the extra-heavy oil experiment showed a minimal 7% recovery after the 5-PV surfactant flood, attributed to wettability change. The results of these experiments demonstrate the high extraction potential of light and heavy oil fractions within homogeneous medium-sized sand reservoirs when tertiary surfactant flooding is utilized. However, the results of the experiments reveal that the micro-scale displacement efficiency of extra-heavy oil fraction is expected to be severely limited even under significant surfactant flooding under these conditions.

Keywords: Interfacial tension, Synchrotron X-ray microtomography imaging, enhanced oil recovery

1.1 INTRODUCTION

A significant amount of crude oil is trapped in pore spaces as residual saturation during primary and secondary extraction processes. On average, only 35% of the original oil in place (OOIP) in a reservoir can be extracted by primary recovery process, which can be raised up to 50% by secondary recovery (such as water flooding) with current, economically feasible technologies (Kerr 2005). Therefore, the possibility exists that higher yields can be achieved from existing and abandoned reservoirs using innovative enhanced oil recovery techniques. Residual saturation is controlled by interaction between capillary and viscous forces, and buoyancy forces, which is determined by the differences in density between two phases (Wardlaw 1982, Mohanty et al. 1987). Numerous studies have been carried out to understand how residual saturation trapping varies as function of viscous versus capillary forces within various types of consolidated and unconsolidated porous media. Mobility of the displaced oil pool is partly restricted due to the capillary forces, which is controlled by wetting-nonwetting phase contact angle or the highly curved menisci of the oil front in tight porous medium pore networks. Oil mobility in these systems must rely on a change in the oil morphology and distribution, which eventually forms into smaller discontinuous blobs (Melores and Brandner 1974, Larson et al. 1981, Chatzis and Morrow 1984). Capillary force, on the other hand, is controlled by the interfacial tension between wetting and non-wetting phases. Residual saturation is a function of the heterogeneity of the reservoir media in terms of pore geometry, and pore size distribution, which is a function of sorting and packing of the solid media grains (Wardlaw 1982, Chatzis et al. 1983).

Morrow and Heller (1985) presented a detailed description of the previous attempts carried out to understand and describe the pore geometry and oil-phase distribution in porous media

using electron micrography. Electron micrography is a high-resolution method for characterizing pore structure. Although this method produces much detail of the pore structure, it is not appropriate for constructing a mathematical model of fluid flow (Morrow and Heller 1985). A realistic model was made by Dullien (1979) and by Dullien and Dhawan (1974) by performing a computer analysis of two-dimensional slices of a real core. However, the application was limited to only a few samples. Schnaar (2006) described various techniques that have been used to understand the parameters controlling the nonwetting phase (oil or any other immiscible phase) distribution in porous media. For example, attempts have included using blob casting methods, two-dimensional micromodels, and imaging techniques to understand trapping mechanisms, the distribution and changes in blob morphology during residual saturation and during water and surfactant flooding in a laboratory environment. Styrene monomer had been used to study nonwetting phase behavior in various types of media, including sandstone, limestone, glass beads (Craze 1950, Morrow and Chatzis 1982 and Chatzis et al. 1983) and unconsolidated media such as loose sands (Craze 1950, Powers et al. 1992). In this method, a styrene monomer liquid was injected to saturate a particular medium. Liquid styrene was then changed into a solid polymer by changing the temperature and pressure. The solid polymer blobs were then recovered from the media by acid dissolution or density fractionation. The morphology of the blobs was studied directly from the isolated beads. Also sieve analysis was used for statistical analysis of the blob size distribution. However, the blob casting method was not always useful, as the styrene polymer could shrink in the solid phase, and therefore quantitative results regarding shape and size would be erroneous. Moreover, there was always a possibility of breaking the blobs into pieces during recovery and sieve analysis, and therefore appropriate data for blob size distribution could not be attained great certainty. This technique also has other limitations such

as difficulty in measuring the interfacial area, and the fact that the experiments only produce a single end-distribution result (Schnaar 2006).

Oil flow and trapping mechanisms have been studied using two-dimensional micro-models (Chatzis and Dullien 1983, Chatzis et al. 1983), where two etched glass plates are fused with each other. Blob morphology and trapping mechanisms can be studied using this method, as well as temporal changes and dynamics in the fluid distribution through in-situ imaging. These authors described pore geometries favoring the two important trapping mechanisms known as "snap off" and "bypassing". They have shown that heterogeneous blob distributions result from greater heterogeneity of the medium. A high aspect ratio (i.e. pore neck to pore body ratio) enhances the formation of spherical blob singlets through the snap off process, whereas interconnected ganglia distributions are more inclined to be affected through bypassing mechanisms caused by heterogeneities in the pore spaces. These observations are consistent with the empirical formula discussed in detail later in the "Trapping Mechanisms" section. However, the two-dimensional micromodel certainly has limitations characterizing three-dimensional fluid phase distributions.

Three dimensional imaging techniques have received increasing attention over the last decade, and have been used extensively in understanding the pore-scale distribution of immiscible liquids/nonaqueous phase liquids (NAPLs). Recent research using a 3-D imaging technique has been discussed in detail by Schnaar (2006). A brief synopsis of recent discoveries made by using various techniques such as photo imaging of refractive index (Ng et al. 1978), magnetic resonance imaging (MRI) and SXM is given herein. Although photo imaging of refractive index has high spatial resolution (1-10 μm), the porous medium has to be transparent to light. Only a limited number of fluids which possess a specific range of refractive indices can

be imaged by this method. MRI techniques can produce high-resolution images ranging from 60 to 200 μm (Zhang et al. 2002) and have been used effectively to estimate NAPL dissolution process in sand. SXM imaging can resolve image resolutions ranging from 1-10 μm and this technique is capable of imaging multiple phases simultaneously by changing the incident energy level of the photon source (X-ray beam). However, this technique can only be used to study relatively small systems, up to a few centimeters in thickness. Previous studies show that SXM imaging has been used successfully to observe and statistically analyze porosity and residual saturation (Coles et al. 1998), pore structure, immiscible phase blob morphology, distribution, transport (Wildenschild et al. 2005, Al-Raoush et al. 2003), and measuring NAPL blob interfacial areas (Culligan 2004, Schnaar and Brusseau 2006a).

1.1.1 Trapping Mechanisms

Following secondary recovery with water flooding crude oil is trapped into the pore spaces as disconnected single blobs in single pores, or as continuous ganglia occupying multiple pores, mainly due to capillary pressure. This trapped volume is called the residual saturation. The other two factors contribute to the trapping mechanism are: interfacial tension and wettability. Interfacial tension between any two immiscible liquid surfaces is the difference between the cohesive force acting within the molecules of same liquid and the adhesive force acting within the molecules across the surface of two immiscible liquids (Mercer and Cohen 1990). If the adhesive force overcomes the cohesive force, the discontinuous liquid phase loses its mobility. In a wetting porous media, the aqueous phase is the continuous phase and the oil (nonwetting) phase is the discontinuous liquid phase. Wettability (measured with contact angle θ along the three phase liquid-liquid-solid interface) is another factor that estimates the extent of the

adhesive force acting along the immiscible interface. For a completely water wet system, $\theta = 0°$ or in other words no oil is adsorbed on solid surface, whereas, $\theta = 90°$ means oil is partially adsorbed along the solid surface (Mercer and Cohen 1990, Schramm 2000). Typically, residual saturation is established by injecting the nonwetting fluid (crude oil or NAPL) into a previously saturated system (water-wet porous reservoir) subsequently followed by a water flushing event at a particular flow velocity to mobilize any easily removed portion of oil/NAPL not trapped by capillary forces under normal operating hydraulic gradients. In the two-phase liquid system, a pressure difference is generated along the curved interface due to the interfacial tension, which is called the capillary pressure. A version of the Young-Laplace equation combines the three variables, which is the governing equation for entrapment of oil in pore spaces:

$$\Delta p = \frac{2\gamma \cos\theta}{R}$$

Where, γ = interfacial tension between aqueous and non aqueous phases,

θ = contact angle along the three phase liquid-liquid-solid interface,

R = radius of curvature of the curved interface, and

Δp= pressure difference/capillary pressure along the interface.

In a wetting porous media, it can be assumed that the pore spaces are initially filled with water. As oil tries to enter the pore spaces, the pore openings act as the interface boundary between the two phases. Therefore, in this case R would be the radius of the pore neck. For the oil phase to enter the pore spaces it has to overcome a threshold entry pressure exerted by the wetting fluid inside the pore. This threshold pressure for oil entrapment is equivalent to the head of the wetting fluid and can be expressed by the following equation (Mercer and Cohen 1990):

$$hc = \frac{2\gamma \cos\theta}{\rho g R}$$

where;

hc = capillary rise of the wetting fluid (water),

ρ = density of water, and

g = gravitational constant.

Two models have been proposed as the main trapping mechanisms in a residual saturated system: capillary snap off and bypass flow. The above equation shows that the capillary pressure is inversely proportional to the radius of the curved interface. In other words, the smaller the radius, the higher the capillary pressure of the water phase inside the pore. Therefore, it can be concluded that the oil blobs will preferentially be trapped into the pore spaces with larger openings (greater radius). As the oil phase enters a pore space, it becomes unstable due to a low pressure in the pore body and the oil blob snaps off from the pore neck (Roof 1970).

The other trapping mechanism can be explained in terms of a pore doublet model (Chatzis et al. 1983, Stegemeier 1976), which is a complex system containing alternate flow paths. This model considers capillaries of two different diameters, connected at both pore inlet and pore outlet. During residual saturation, the aqueous phase will preferentially penetrate the smaller diameter pores due to greater capillary pressure. Gradually, the smaller diameter pores will be filled completely with water, simultaneously squeezing the oil phase into the larger diameter pore channels. Eventually, the aqueous phase bypasses the oil phase and flows through the pore-doublet outlet, completely trapping the oil phase into the larger pore. As described by the bypassing mechanism, the oil phase will tend to be trapped into the larger pores. Therefore, under the premise of the local pore-doublet model, the trapped oil will preferentially be distributed in more than 50% of the available pore spaces.

From the above discussion, it can be hypothesized that the amount of oil entrapment, or the relative water and oil saturation, is a function of the heterogeneity of the media in terms of the pore diameter or grain size of the solid media. Snap off is more common in pore spaces with greater aspect ratios (the ratio of pore body to the pore neck radius) (Donaldson et al. 1985, Mercer and Cohen 1990), whereas, for low aspect ratio, the size of the pore neck and the pore body is almost equal which helps in displacing the oil blobs with no entrapment (Wilson and Conrad 1984). On the other hand, the bypassing mechanism is primarily responsible for trapping oil ganglia (network of oil blob) into the interconnected, larger pore spaces within the smaller pore matrix (Mercer and Cohen 1990).

1.1.2 Mobility/Driving Forces

The mobility or the displacement efficiency of crude oil is a function of its viscosity and the interfacial tension. Secondary recovery by water flooding can only recover 30% of oil-in-place, since the viscosity forces by water flood are not able to overcome the capillary forces, trapping oil blobs in the medium grain pores (Schramm 2000). Previous studies (e.g., Donaldson et al. 1985, Chatzis et al. 1983, Stegemeier 1976, Mercer and Cohen 1990) show a strong correlation between residual saturation and the ratio of viscous and capillary forces, expressed by a collective relationship called capillary number (N_C). The following equation is one of the various forms of capillary number used in previous literature (Morrow and Chatzis 1982):

$$N_C = \frac{\eta v}{\gamma \phi} = \frac{k_i \rho g \Delta P}{\gamma \phi}$$

Where, η = viscosity of the flooding fluid (water),
v = velocity of the flooding fluid (water),
γ = interfacial tension between oil and water,
ϕ = media porosity,

k_i = intrinsic permeability,
ρ = density of flooding fluid (water),
g = acceleration due to gravity, and
ΔP = pressure gradient.

A study conducted by Taylor and Hawkins (1990) showed that 45% of oil-in-place is trapped at $N_C = 10^{-6}$. Capillary numbers below this value represent the displacement of oil blobs mainly by capillary forces, rather than being dominated by viscous forces (Wardlaw and McKellar 1985, Schnaar and Brusseau 2006b). Mobilization of residual oil begins at a threshold value of $N_C = 2 \times 10^{-5}$, and 25% saturation is achieved at $N_C = 5 \times 10^{-3}$ (Schramm 2000). A similar experiment, conducted with isooctane in an unconsolidated bead (45-50 mesh) pack, showed that a greater pressure gradient is required to mobilize the trapped oil blobs resulting in higher N_C values for initial mobilization (Morrow and Chatzis 1982, Morrow et al. 1988). Residual saturation was reduced to 73% at $N_C = 2.29 \times 10^{-3}$, with a recovery up to 30% at $N_C = 4.22 \times 10^{-3}$. This additional entrapment force can be attributed to the high aspect ratio due to relatively greater radius of the bead pack pores and can be compared with capillary numbers estimated in this research. There is a constant endeavor to increase the value of N_C at the field scale for increasing the recovery potential of immiscible fluids. Increasing the hydraulic gradient is one way to increase N_C, which is limited by the fracture pressure. The other realistic approach would be to reduce the interfacial tension by the injection of a surfactant solution (Donaldson et al. 1985). Larson et al. (1981) tried to correlate residual saturation as function of blob length distribution. According to this study the capillary number is inversely proportional with blob length along the direction of Darcy flow. Therefore, higher capillary numbers are required to mobilize smaller blob length. They also showed from the results from previous literature that for a constant pressure gradient higher

recovery can be attained from a system with connected oil ganglia than from a system with disseminated oil blobs.

The bond number (N_B) is a comprehensive term which describes the ratio between buoyancy and interfacial forces. This ratio controls the mobility of the trapped oil phase (Morrow and Chatzis 1982, Boving and Brusseau 2000):

$$N_B = \frac{k_i \Delta\rho g}{\gamma}$$

where, $\Delta\rho$ is the density difference between aqueous and oil phases. Mobilization of the trapped oil phase occurs when the above discussed forces (i.e. buoyancy and interfacial) overcome a critical capillary force responsible for trapping. The coupling effect of N_C and N_B can be expressed by the total trapping number (N_T), where $N_T = \left(N_C^2 + N_B^2\right)^{1/2}$ for horizontal flow and N_C and N_B are additive for vertical flow conditions (Pennell et al. 1996). The trapping number is controlled by the heterogeneity, packing, and particle size distribution of the porous medium (Boving and Brusseau 2000).

Using surfactants to lower interfacial tension is an existing technology by which the mobility of the oil blobs is facilitated, thereby, increasing the recovery potential from the reservoirs. Capillary force and residual saturation are related to the available contact surface between the wetting phase (i.e. water-wet reservoir) and the non-wetting phase (i.e. oil) (Hassanizadeh and Gray 1990, Reeves and Celia 1996). An understanding of the interfacial phenomena is required to optimize innovative techniques for tertiary extraction of oil. Oil blob morphology and pattern of distribution have an impact on available contact surface, and therefore control interfacial processes. A thorough understanding of oil blob morphology and

distribution at the pore-scale level will be critical for estimating the enhanced oil recovery (EOH) potential from existing reservoirs. Knowledge acquired from this research can later be applied to better understanding the primary mobilization mechanisms in intermediate and field-scale processes and applications.

The purpose of this research is to characterize oil blob distribution in homogeneous porous medium and study the morphology of oil blobs as a function of various crude oil fractions. Attempts have been made to study the changes in blob morphology for varying crude oil fractions after successive surfactant flooding events, thereby changing the available interfacial area between the aqueous, nonaqueous, and solid phases. Oil recovery is estimated for each system as a function of crude oil fraction. Column experiments have been carried out to examine the transient nature of oil blob distribution before and after multiple surfactant flooding events. These surfactant-flooding experiments will help elucidate some of the flushing dependent factors related to the oil recovery potential for various types of crude oil composition.

This research uses a novel, noninvasive technique to study the crude oil distribution in various porous media. Synchrotron X-Ray Microtomography (SXM) was used to capture high-resolution images of the columns before and after the surfactant flooding events. Initially developed CAT-scan technology for the medical field (Flannery et al. 1987, Jasty et al. 1993) was also used in the petroleum-engineering field to understand the geometry of pores in the reservoir. Later on, advancements in SXM began to be used for understanding porosity, relative permeability and oil saturation in porous media (Coles et al. 1998). The outcome of this research will be beneficial in understanding interfacial processes at the pore-scale level, improving knowledge about conditions appropriate for successful tertiary extraction of crude oil from existing reservoirs.

1.2 MATERIALS AND METHODS

A comprehensive pore-scale study was conducted in a controlled environment to study the distribution and the morphology of various fractions of crude oil in different types of porous media. Multiple columns were packed with three different types of sands with increasing heterogeneity. The columns were saturated with water to simulate water-wetting- reservoir conditions, and flooded (imbibed) with three different fractions (light, medium, and heavy) of crude oil. The columns were flushed with an anionic surfactant in two different episodes. Multiple SXM images were taken, including one initial image (pre-surfactant flush) and two images after each subsequent surfactant-flooding event.

1.2.1 Materials

Three fractions of crude oil were chosen as model liquids with high (14.0°), medium (29.6°), and light (41.4°) API gravity, which are known as West Texas Intermediate crude (BP), Poseidon crude (BP) and San Joaquin Valley crude (Chevron), respectively. The oil samples were doped with 10% by volume iodobenzene (Acros Organics, NJ) to improve the image contrast for a particular X-ray absorption energy. The aqueous phase (double-deionized water) was doped with 60 g/L cesium chloride (CsCl, 99.99%, Optical grade from Acros Organics, NJ) for the same purpose. All experiments showed negligible or insignificant change in interfacial tension due to the addition of CsCl dopant in aqueous phase (Schnaar and Brusseau 2006b). However, oil phase doping with iodobenzene (IB) showed changes in interfacial tension for the bulk oil. These dopants showed least partitioning to the non-target fluids (Schnaar and Brusseau 2006b). Doping with IB, which has a density (1.82 g/cm^3) higher than water, has some control on the API gravity of crude oil. After recalculation, the crude oil samples were characterized as light

(23.4˚API), heavy (14.8˚API) and extra-heavy (4.2˚API), respectively (according to USGS standard). According to USGS standard, conventional crude oil which has API gravity of 22º or more and a viscosity less than 100 centipoise (cP) is considered as light crude oil. Heavy crude oil is characterized by API gravity ranging from 22 º to 10º, and viscosity ranges from 100 cP to 10,000 cP, whereas, crude oil containing higher than these values is considered as natural bitumen. In the absence of viscosity data any crude oil sample less than 10 ºAPI (heavier than water) is considered as extra-heavy crude oil.

A 0.1% (by volume) solution of an anionic surfactant branched alcohol propoxy sulfate, or commercially called Petrostep S-1 (Stepan Chemical Company, Northfield, IL) was used for the surfactant flooding experiments. This surfactant was chosen for its ability to develop low interfacial tension at very low concentrations. This surfactant was developed for oil extraction purposes and has also been effectively used to mobilize and remove crude oil and non-wetting fluids (i.e. remediation) from shallow aquifers. It also exhibits a high salinity and temperature tolerance, and is therefore assumed to be applicable for reservoirs with high salinity. In addition, this surfactant also showed minimal adsorption to the solid phase (Goddard et al. 2004).

A series of experiments were carried out in simple systems, where three different fractions of crude oils were injected into different columns, respectively, each packed with a physically homogeneous 40/50 accusand porous medium (Unimin Corporation, Ottawa, MN). Sorting of the medium grain size is expressed in terms of the uniformity coefficient ($C_U = d60/d10$), the ratio of the 60^{th} percentile to the 10^{th} percentile grain-size diameters in a grain-size distribution curve. The C_U for this homogeneous sand is approximately 1. This sand is characterized by high porosity (33%) and permeability ($k_i = 9.0 \times 10^{-11}$ m^2), and the median grain size is 0.35mm.

1.2.2 Residual Saturation and Surfactant Flooding

Thin-walled anodized aluminum columns were dry-packed with porous media. The columns were approximately 4.4 cm long, with Swagelok end-fittings on the top and bottom. The inner diameter of the columns was approximately 0.5 cm. However, a considerable part of the column image was cropped from top and bottom due to resolution problem attributed to the Swagelok end-fittings, and the available imaging length was approximately 1.2-1.7 cm after image cropping along the vertical direction. Polypropylene frits were used between the porous medium and the aluminum caps to hold the loose particles intact along the column boundaries, and to avoid any preferential flow of the fluids through the porous medium.

The columns were packed using the dry 40/50-mesh accusand in incremental steps to attain a consistent and homogeneous packing. Once the packing was completed, the columns were purged with carbon-dioxide to displace all of the air present in the pore spaces. The columns were then saturated with de-aired double-deionized (nanopure) water for several pore volumes (PV) vertically upward, using a single piston, HPLC pump (Acuflow series II). The saturation process continued for 48 hours with a linear pore velocity ranging from 6-7 cm/hour. After the initial aqueous phase saturation was completed, columns were injected with 4 PVs of various fractions of crude oil at a linear velocity of 4 cm/hour with a syringe pump (Model: 780100, KD Scientific, Holliston, MA). The columns were then flushed with a 60 g/L cesium chloride solution to attain a residual saturation, by displacing the oil blobs, in a discontinuous distribution. The residual saturation process was carried out in two steps: 2 PV with a flushing rate of 6-10 cm/hour (linear pore velocity) and 10 PV with a flushing rate of 20-32 cm/hour. Capillary numbers calculated for this displacement process range from 4.5×10^{-4} (for extra-heavy oil) to 1.2×10^{-3} (the two lighter fractions, in table 1.1). Previous research (Wardlaw and Mckellar 1985,

Morrow et al. 1988) shows that for unconsolidated media (such as bead packs or sand) the residual saturation in the range of 50% to more than 75% can be attained in this range. After residual saturation was completed, the columns were sealed and imaged by SXM to attain the initial crude oil distribution prior to surfactant flooding events.

For the subsequent surfactant flooding events, the columns were flooded with 0.1% anionic surfactant solution (in 60g/L cesium chloride). In separate experiments it was confirmed that this surfactant concentration is below the critical micelle concentration level corresponding to all three crude oil fractions (Detail in chapter 4). The motivation for these experiments was to ensure maximum recovery by mobilization process and no crude-oil removal by dissolution processes. As mentioned previously, surfactant flooding was performed in two successive steps. First, the initial residual saturation distributed crude oil columns were flushed with surfactant solution for 2 PVs at a linear velocity of 20 cm/hour and then imaged using the SXM. The columns were then flooded for the second successive surfactant-flushing step under the same flushing conditions for an additional 3 PVs and then imaged again using SXM. A total of three SXM scans were made for each column, including one initial scan and two scans after each surfactant flooding event.

1.2.3 Synchrotron X-Ray Microtomography

A total of 27 images were taken for 9 columns. All images were taken at the GeoSoilEnviroCARS (GSECARS) BM-13D, at the Advanced Photon Source (APS) Argonne National Laboratory, Illinois. The advantages of using SXM (bending magnet source) include the high penetrating energy source which is monochromatic, extremely uniform across the entire beam, and highly collimated, resulting in exceptionally high-resolution imaging capabilities

(Flannery et al. 1987). Images of different phases can be taken simultaneously by changing the X-ray incident energies using a monochromator. When the X-ray beam passes through a particular object, it is absorbed and scattered, therefore, attenuated at particular threshold energy, called the critical absorption energy (Ketcham 2001). The final image shows a linear depth-integrated grayscale image (darker gray indicates greater absorption). This gray scale level is a function of the atomic number and the X-ray energy, and can strongly be correlated with the density of the imaged object (Ketcham 2005). Approximately 1500 to 1600 two-dimensional (2-D) slices were produced for the 1.5 cm imaging length of a column. Images were taken at three incident energy levels with a spatial resolution ranging from 9.9-10.3 μm. The images taken above (36.085 KeV) and below (33.269 KeV) the cesium critical absorption edge were subtracted to resolve the aqueous phase doped with cesium chloride. The images taken below the cesium edge (or above the iodine edge, 33.269 KeV), and below the iodine edge (33.0169) were subtracted to resolve the oil phase.

The images were preprocessed and reconstructed using software called Tomo Display (written by Mark Rivers, ANL) at the APS. Preprocessing removes artifacts and dark currents, and corrects for flat field variations. The reconstruction process adjusts for the central axis of rotation, removes ring artifacts, and reverses the grayscale and absorption relationship. The fluid phases with high absorption look brighter after the reconstruction process. Following the reconstruction process, the software generates a series of 2-D slices in the X-Y plane from the raw data. This process is followed by stacking several column sections, and by cropping off the unwanted part of the images, along with the column boundary.

Additional post-processing software called Blob3D was used to stack all of the two-dimensional images to generate three-dimensional images of the entire column. Ketcham (2005)

describes the computational methodologies for this software. Several tools available in Blob3D were used to improve image quality prior to stacking. Median smoothing (grayscale-to-grayscale algorithm) was used to reduce inherent noise and to enhance the edge of the oil blobs from the surrounding non-target phases. Median smoothing applies a particular grayscale value, which is the median value of all other gray-scale values for a particular chosen radius. This filter has a minimum effect on altering the geometry of the targeted phase. A gray-scale to binary filter was applied to separate the targeted oil phase from non-target phase. A particular gray-scale value was assigned as the threshold value for each oil fraction to convert the images from gray-scale to binary (two-component). In general, a gray-scale value intermediate to the target phase and non-target phase is considered as the threshold value (ASTM 1992). Binary images separate the target fluid as white (grey-scale value 255) from any other phases as black. Quantitative measurements were also computed using Blob3D, in terms of blob size distribution, blob volume distribution, and specific blob/ganglia surface area.

1.3 RESULTS AND DISCUSSIONS

1.3.1 Capillary number

Results obtained for the change in interfacial tension due to 0.1% surfactant flooding, and as a result the increases in the capillary number are reported in table 1.1. Extra-heavy oil shows maximum reduction in the interfacial tension from 42.3 mN/m to 24.7 mN/m. Light and heavy oil show change from approximately 16 mN/m to 10.6 and 11.8 mN/m, respectively. Although both the capillary and the bond numbers increase for all three fractions, capillary number is 8 to 9 orders of magnitude greater than the bond numbers, and therefore is the main controlling factor in estimating the trapping number. This observation implies that the capillary force is the dominant parameter controlling the trapping mechanism and mobilization of oil blobs, whereas the buoyancy force has less or no control into these systems.

1.3.2 Crude oil distribution in 2-D and 3-D

Figure 1.1 shows the reconstructed thin sections showing the residual distribution of all three fractions of crude oil in homogeneous media. The images of all three columns clearly reveal the distribution pattern *in situ* for all three fractions with unprecedented resolution. The water (wetting) and crude-oil (non-wetting) phases have been separated as binary images, and then overlain with false color application. It can be observed that the fluid phases such as water and oil have been imaged properly, and can be distinguished by the image subtraction process using Tomo_Display software. All three images show a homogeneous packing of the 40/50 accusand with interconnected pore spaces. All three fractions of crude oil show random distribution as expected under residual saturation conditions. However, the distribution of chains of blobs along the column walls can be attributed to the development of preferential flow paths.

In order to avoid the boundary effects, the images have been cropped (approximately 4mm × 4mm section after cropping) and analyzed along the core of each column. The extra-heavy oil distribution, in the initial residual saturation, has a higher degree of connected blobs, called "ganglia". In contrast, the distribution of the other two oil fractions (light and heavy) are dominantly characterized by disconnected individual oil blobs called "singlets" and "doublets". The extra-heavy-oil also shows greater contact surface with the solid media grains, unlike the light and the heavy oil fractions, which have more interfacial contact with the aqueous phase. From this observation it can be concluded that surfactant flooding would be more effective for the light and the heavy gravity crude oil recovery, as the lighter gravity oil blobs are in greater contact with the aqueous surfactant solution compared to the extra-heavy crude oil blobs. It is interesting to note that the length of an oil blob can have control over mobilization, since the pressure gradient acts over the length of the oil blob (Taber 1969). For larger ganglia, occupying series of connected pores requires higher-pressure gradient to achieve greater recovery. In this research the velocity-of-flooding applied for the surfactant-enhanced-recovery was constant for all three systems; therefore it can be hypothesized that relatively less recovery can be achieved for the extra-heavy oil in comparison to the other two lighter fractions.

Figure 1.2 shows the time series of reconstructed thin sections in X-Z direction showing the distribution of the light-gravity-oil in the homogeneous medium for the residual saturation, and after 2PV, and 5 PV surfactant-flooding events. Figures 1.3 and 1.4 represent the same as above for the heavy and the extra-heavy gravity oils. Various fluid phases such as: the aqueous, the crude-oil and the trapped air bubbles can be distinguished in figures 1.2 and 1.3. These images were taken above the critical iodine energy level. Figure 1.4, on the other hand shows the subtracted binary image of the extra-heavy oil only. All other phases have been subtracted in this

image. Visual inspection reveals significant changes in oil saturation for both the light and the heavy gravity crude oil after 2 PV surfactant flooding event; and a complete recovery was attained after 5 PVs of surfactant flooding. The extra-heavy oil shows relatively less recovery compared to the other two lighter fractions. Mobilization of the extra-heavy oil mainly occurred along particular preferential flow paths (Figure 1.4). Mobilization of the light oil fraction can be clearly observed in figure 1.2 after 2 PVs of surfactant flushing. This observation supports the previous assumption on enhanced recovery by mobilization process. This also minimizes the possibility of dissolution of oil blobs and confirms recovery of crude oil in raw phase. The light and the heavy oil blobs show an overall change in the morphology after 2 PVs of surfactant flooding becoming more flattened, coating the media grain boundaries. The extra-heavy oil shows interconnected blobs for all three stages with visually negligible change in the distribution pattern. All the above discussed results are in agreement with the blob-morphology-distribution-pattern as observed in 3-D images, and with the graphical representation of the quantitative data, which will be discussed in later sections.

Figures 1.5, 1.6 and 1.7 show 3-D distribution pattern of three crude-oil-fractions within the cropped sections (approximately 3.9-mm×3.9-mm×1.6-mm). These figures show temporal changes in the distribution of a particular fraction before and after the surfactant flooding events. Observations in 2-D sections are in agreement with that in 3-D sections. These figures clearly show that the light and the heavy oil fractions are segregated into discrete smaller blobs in the residual saturation, and the number of blobs increases after the 2-PV surfactant flooding events (Tables 1.2 and 1.3). Visual observation of blob morphology pattern reveals a change from spherical or elliptical to a more flattened shape, covering the solid grain boundaries. This change in the morphology results in yielding greater surface area to be in contact with the surfactant

solution. As discussed earlier, greater surface area in contact with the surfactant solution can help in enhanced recovery. The extra-heavy oil distribution in 3-D section shows a complex interconnected network, which supports the observation carried out in the 2-D sections shown in figure 1.4.

Analyses were conducted to compare oil blob morphology for three different oil fractions (i.e. light, heavy and extra-heavy) as residual saturation and describe the temporal changes in blob morphology after successive surfactant flooding events. Chatzis et al. (1983) used scanning electron microscope to study and compare blob morphologies distributed in bead packs and in the homogeneous Berea sandstone. Blob shape was characterized into three main categories: singlets, doublets, and complex networks called ganglia. According to this study the trapping mechanism is a function of the aspect ratio of the connected pore spaces. For high aspect ratio, where the pore body diameter is much larger than pore neck, oil blobs are trapped by "snap off " processes, resulting in isolated disconnected singlets. In contrast, low pore-body/pore-neck aspect ratios result in continuous interconnected ganglia type networks. Figure 1.8 shows three types of light-oil blob morphologies, similar to that have been characterized by Chatzis et al. (1983). Figure 1.8 shows the trapped oil blobs in the homogeneous medium in both 3-D view and in the section view (X-Y slices) perpendicular to the Z-direction of the column. The heavy-oil fraction is also distributed as disconnected blobs in the residual saturation, and also shows morphologies similar to above described categories (figure not shown). After the 2-PV surfactant flooding event most of the blobs become flattened and are transported as thin lamina along the grain boundaries (Figure 1.9). Relative positions of the sand grains can be clearly identified in both the section view and 3-D image showing blob morphologies after 2PV surfactant flooding.

1.3.3 Quantitative estimation of crude oil volume and surface area

Quantitative results for potential recovery from each crude-oil/porous-medium column system have been extracted using the software Blob3D (Tables 1.2, 1.3 and 1.4). When compared for overall saturation, the extra-heavy oil shows a relatively greater volume trapped as residual saturation compared to the other two lighter oil fractions. The light and the heavy-oil experiments show approximately 44% and 10% recovery, respectively, after 2 PVs of surfactant flooding. Complete recoveries (100%) were obtained for both the light and the heavy-oil fractions after each 5 PV surfactant flooding event. However, the extra-heavy oil, within the physically homogeneous medium, exhibited a -4.5% recovery, which indicates a gain in total saturation. This discrepancy in mass balance can be explained by the addition of extra-heavy-oil, which may have been trapped into the Swagelok end-fittings associated with the column and subsequently added into the system during the 2-PV surfactant flood. Moreover, the wettability change of silica sand due to pH condition can have control over trapping mechanism of this additional oil-phase. The wettability factor in trapping and recovery of extra-heavy-oil phase has been described in detail in the chapter 3. The extra-heavy oil shows a recovery of 6% after the 5-PV surfactant flooding event. It is to be noted that compared to the recovery of the other two lighter fractions, 6% recovery is not that important; however, this can be significant volume in the field scale. Additionally, it should be noted that 100% recovery of the other two fractions, which has been attained in the laboratory condition, has never been achieved in field scale situation with the existing production technology. Quantitative data also shows increase in the number of blobs after 2 PVs of surfactant flood with a corresponding order-of-magnitude decrease in the mean blob volume for both the light, and the heavy-oil fraction column experiments.

Estimations were conducted for total surface area of the oil blob volumes. Total surface area includes the contact surface along the solid-media-grain/oil phase, and the oil/water phase boundaries. The light-oil shows an increase of 200% in terms of total oil surface area, after the 2-PV surfactant flooding event. The heavy-oil shows 87% increase in the total oil surface area after 2 PVs of surfactant flooding. This increase in surface area is attributed to the change in blob morphology from spherical to more non-spherical, laminar shape as was observed in the 3-D SXM-generated images. In addition, this observed surface area increase may be explained by the increase in number of blobs from larger to smaller fragments, thereby generating greater cumulative surface area. The extra-heavy oil, however, shows 7% increase in surface area after the 2-PV surfactant flood, and a marginal decrease in surface area after the 5-PV surfactant flood attributed to 6% recovery.

1.3.5 Blob volume and morphology distribution pattern

Chatzis et al. (1983) studied the nature of distribution of styrene monomer in unconsolidated bead packs and within homogeneous Berea sandstone. More than 50% of the styrene blobs were distributed as 'singlets', occupying single pore bodies, resulting in a relatively homogeneous distribution. In this research analyses were conducted to characterize the blob size distribution for three fractions of oil existing as residual saturation, as well as after each prescribed surfactant-flooding event (i.e. 2 PV, 3 PV; total of 5 PVs). It was observed that the oil blob volume distributions for all three oil fractions were highly skewed, characterized by a large number of smaller blobs and a decreasing number of large blobs. This type of distribution can be characterized as a log normal distribution (Davis 2002). The results show relatively homogeneous distribution of the light-oil blobs in residual saturation (Figure 1.10). It should be

noted that the lateral spreading (over great range of particle sizes) of the distribution curve represents higher heterogeneity. Under this concept it can be concluded that heavy-oil shows a relatively greater heterogeneous distribution and the extra-heavy oil blob volume shows the greatest and most significant heterogeneous distribution. However, as mentioned previously, the extra-heavy oil blob volume distribution is characterized by a large fraction of interconnected ganglia (Figures 1.4 and 1.7), which incorporates most of the oil-phase volume present within the system, and is represented by a single large blob as a residual saturation distribution. Therefore, quantitative representation of the extra-heavy oil blob distribution is subject to and also requires qualitative evaluation.

Figures 1.12 and 1.14 present the cumulative distribution of light and heavy oil blob volumes before and after the 2-PV surfactant-flooding event. Both light and heavy oil fractions show greater heterogeneous distribution after 2 PVs of surfactant flooding. Heterogeneity in oil blob volume distribution was also quantified by the uniformity coefficient (C_U) and the coefficient of variation (C_V) (Tables 1.2 and 1.3). C_V for light oil changes from 1.86 to 12.94 and heavy oil blob volume shows a change from 2.56 to 8.47 after 2 PVs o surfactant flooding. C_U for light and heavy oil blob volumes change from 1.74 to 5.2 and from 1.97 to 2.59, respectively, after 2 PVs of surfactant flood. Both light and heavy oil fractions have been segregated into smaller blobs after 2PV surfactant flood. Light oil was segregated into relatively smaller fragments and generated higher number of blobs (Table 1.2) compared to the heavy oil. The resulting heavy oil distribution shows a similar trend but produced fewer numbers of smaller particles or fragments (Table 1.3) than the light oil. Although both the oil fractions show a reduction in mean-blob- volume (approximately an order of magnitude), a portion of the light oil fraction (Figure 1.12) produced larger oil blobs after 2 PVs of surfactant flood. This phenomenon

can be attributed to coalesce of smaller blobs into larger blobs during the flood. Attempt has been made to plot cumulative distribution (Figure 1.16) for extra-heavy oil, where the majority of the blobs are insignificant in size. There is no change in distribution pattern after 2 PVs of surfactant flooding and only a small amount of spreading, re-distribution, or pattern change can be observed after 5 PVs of surfactant flooding. The large interconnected ganglion, which incorporates the bulk of the trapped extra-heavy oil, is represented by one single blob volume in this diagram for the residual saturation and after two flooding.

Analyses were conducted to compare the change in blob morphology pattern for three different oil fractions at residual saturation (Figure 1.11). In addition, changes in blob morphology, after each surfactant-flooding event, have been graphically plotted for all three oil fractions (Figures 1.13, 1.15, and 1.17). Oil blob specific-surface area has been plotted as function of blob volume to estimate the deviation of blob surface area from a spherical shape for a particular blob volume. A particular blob volume possesses a minimum surface area as a spherical shape (i.e. sphere) and any deviation from a sphere will result in oil blobs with a greater surface area, contributing more exposed surface to the surfactant solution. For both light and heavy oil, blob volumes ranging from 10^{-2} mm^3 to 10^{-4} mm^3 show varying morphologies from spherical to non-spherical. However, for all oil fractions the larger blobs, which are typically branching ganglia, exhibit maximum deviation from the spherical shape. These ganglia are trapped into multiple connected pores. The threshold of ganglia formation can be estimated as 10^{-2} mm^3 as observed in figure 1.11 (shown by dashed arrow) below which, the blobs primarily exist as ‘singlets’ or ‘doublets’. The light-oil blobs show relatively greater deviation from spherical shapes in comparison to the heavy oil in the residual saturation. It should be noted that the graphical representation of blob deviations from a sphere are more robust for

distributions of disconnected blobs. Therefore, these analyses and associated graphical plots cannot be successfully applied when the majority of the oil phase is connected as ganglia as observed by the extra-heavy oil distribution. For example, the largest blob of extra-heavy oil, which is more than 10 mm in volume (Figure 1.11), incorporates most of the trapped oil phases. Smaller blobs, although large in number are insignificant in cumulative volume.

Significant changes in blob morphology can be observed for both the light and the heavy-oil blobs after 2 PVs of surfactant flood (Figures 1.13 and 1.15). Smaller blobs less than 10^{-5} mm^3 show a mixture of spherical and non-spherical shape. On the other hand, the entire blob population larger than 10^{-5} mm^3 shows non spherical shape resulting in an increase in total surface area. For both cases the larger blobs comprise a significant portion of the total volume and the smaller blob-volumes although greater in numbers, comprise a smaller fraction of the total volume. The smallest fragments (particles) of extra-heavy oil blobs (Figure 1.16) show spherical deviation in surface area after 5 PVs of total surfactant flushing. However, the connected ganglia phase, which comprises most of the trapped volume, has shown no significant change in volume morphology. All of the above results clearly demonstrate the utility of synchrotron imaging to study the heterogeneity in oil blob distribution pattern, and the distinctive behavior of the morphology pattern, in the residual saturation and after surfactant flooding episodes for the three oil fractions in the homogeneous porous medium. These results will be beneficial to take important decisions in production design in terms of well location, flooding technique and the surfactant chemistry etc. in favor of greater recovery for a particular oil fraction.

Results from this research also show higher recovery potential for the light and heavy oil, which can be attributed to the significant increase in oil blob surface area after surfactant

flooding. This observation supports the lattice simulation model performed by Reeves and Celia (1996), which shows a correlation of the interfacial area of the trapped oil phase (non-wetting fluid) as function of both the capillary pressure and the residual saturation within the porous media system. Additionally, it is to be noted the larger fraction blobs/ganglia of the extra-heavy oil show no significant change in surface area, resulting in a relatively insignificant recovery from the homogeneous porous medium. Although the SXM image efficiently distinguished the blob distribution along the pore spaces, it has limited application for the oil phase adsorbed onto the media surface. While negligible in volume, this adsorbed oil phase is assumed to have a larger surface area, and therefore can play an important role in interfacial processes (Schnaar and Brussau 2006a). The smallest fragments of extra-heavy oil blobs may or may not be the part of the oil phase. This small fraction of oil phase may be adsorbed onto the grain surface or may be an artifact generated due to the threshold value allocated for separating the oil phase during binary image separation.

1.3.6 Sensitivity Analysis

In this research, the volume and surface area calculations depend solely on the threshold value assigned to the targeted fluid phase. Even after taking the utmost care, significant error can be associated with the fluid volumes measured by gravimetric methods. The source of this error can be the additional liquid trapped in the pore spaces between the caps and the porous frits. Therefore, a gravimetric mass balance is not reliable and beyond the scope of this research. Uncertainty associated with the surface area and volume calculations have been estimated by performing a sensitivity analysis with respect to various values of threshold applied on the same section of a column containing the same type of media and fluid phases. Sensitivity analysis has

been carried out to estimate the effect of degrees of median smoothing on calculated surface areas and volume ratios. Table 1.5 and figure 1.18 show the results for sensitivity analysis on integrated specific surface area calculated for all the light oil blobs distribution in homogeneous porous medium. Specific surface area is defined as the ratio between the individual blob volume and the surface area. Figure 1.18 shows that these results are sensitive with the threshold grey scale value applied in Blob3D software. Sensitivity coefficient shows changes of 2.65%, -2.58% and 6.33% in specific surface area for a corresponding change of +5%, -5% and +10% in threshold grayscale values applied for light-oil phase. The second most sensitive parameter on blob specific surface area is the intensity range applied to visualize 2-D slices in the Tomo_Display software, which uses the IDL (Interactive Data Language) routine TV and TVSCL for 2-D visualization. Results show changes of -5.9% and 9.08% in total specific surface area for two different intensity ranges. It is to be noted that the intensity range is one quality control parameter applied in Tomo_Display software to get the best contrasting image for the oil phase in 2-D slices (sections) extracted from the preprocessed images that become input parameters in Blob3D software. Median smoothing processes, is another quality control parameter in Blob3D however, have less control on the total blob specific surface area. Specific surface area was reduced by 1.9%, 2.6% and 3.1% for 2, 3 and 4 times repetition of median smoothing.

1.4 CONCLUSIONS

Synchrotron X-ray microtomography has been used successfully to image various phases including wetting and non-wetting phases in high resolution. Temporal change in oil blob distribution has been characterized by log-normal distribution, and compared for three fractions of crude oil in homogeneous 40/50 accusand. Quantitative analyses were conducted for changing morphology demonstrating an overall increased surface area of oil blobs after subsequent surfactant flooding events. Enhanced recovery potential for each oil-fraction/porous-medium system was determined based on quantitative and qualitative assessments from the results of this study. Following is a list of key results derived from this research.

1. Both light and heavy gravity crude oil show significant displacement (recovery 44% and 10% respectively) in residual saturation after the 2-PV surfactant flooding event; and complete recovery (100%) resulted after 5 PVs of surfactant flooding. Extra-heavy oil shows relatively less recovery of 6% after 5PVs flood. It is to be noted that 6% is not a significant recovery in laboratory scale, when compared with the recovery volume for other two fractions. However, in the field scale this volume can be a significant value. However, it is to be noted that the displacement efficiency estimated at laboratory scale is much higher than that can be found in field scale as the later is controlled by complex heterogeneties in larger scale.
2. The residual saturation of light and heavy oil fractions is characterized by disconnected individual oil blobs called “singlets” and “doublets”; whereas, extra-heavy oil distribution includes more connected blobs, called ganglia. It should be noted that interconnected ganglia need higher linear velocities to mobilize as the pressure gradient acts along the entire length of the blobs/ganglia compared to disconnected blobs such as “singlets” or “doublets”.

3. Both light and heavy oil fractions show relatively homogeneous distribution in the residual saturation. For both oil fractions, the distribution pattern shows greater heterogeneity after the 2-PV surfactant flooding event. Extra-heavy oil shows no significant change in the distribution pattern after all surfactant flooding events.
4. Quantitative data show an increase in the number of oil blobs attributed to reduction in interfacial tension due to surfactant application, with a corresponding order-of-magnitude decrease in mean blob volume for both the light and heavy oil fractions after the 2-PV surfactant flooding event.
5. The light oil shows a 200% increase in the total surface area after the 2-PV surfactant flooding event. The heavy oil shows an 87% increase in the total surface area for 2 PV flooding. This substantial increase in the surface area is attributed to the change in blob morphology from spherical to a more non-spherical, laminar shape. Other reason for the increase in the surface area after surfactant flooding is due to the increase in the number of blobs from larger to smaller fragments, thereby generating more cumulative surface area within the column system. The extra-heavy oil, however, shows a slight increase in the surface area after 2 PVs of surfactant flooding, and only 1.4% decrease in the surface area after the 5-PV surfactant flood.
6. The light and the heavy oil blobs show significant change in morphology after the 2-PV surfactant flooding event, and became more laminar and flattened, coating the media grain boundaries to a greater extent. The extra-heavy oil exhibits an interconnected distribution of blobs, primarily as large ganglia mass after all three stages of flushing (i.e. residual establishing aqueous flush, and the two successive surfactant flushes) with negligible visual or quantifiable change in distribution pattern.

REFERENCES

Al-Raoush, R.I., Abu-Salem Z., and Willson, C.S. (2003). Characterization of non-wetting phase fluids in porous media systems using high-resolution, three-dimensional, synchrotron x-ray microtomography. *American Chemical Society Conference Proceeding, Division of Environmental Chemistry, 43*, 1031-1035.

Boving, T.B., and Brusseau, M.L. (2000). Solubilization and removal of residual trichloroethene from porous media: comparison of several solubilization agents. *Journal of Contaminant Hydrology, 42*, 51–67.

Chatzis I., and Morrow N.R. (1984). Correlation of Capillary Number Relationships for Sandstone. *SPE Journal, 24(5),* 552-562.

Chatzis I., Morrow N.R., and Lim H.T. (1983). Magnitude and detailed structure of residual oil saturation. *Soc. Pet. Eng*., 23, 311-326.

Chatzis I., and Dullien, F.A.L. (1983). Dynamic immiscible displacement mechanisms in pore doublets: Theory versus experiment. *Journal of Colloid Interface Science, 91(1),* 199-222.

Coles, M.E., Hazlett, R.D., Spanne, P., Soll, W.E., Muegge, E.L., and Jones, K.W. (1998). Pore level imaging of fluid transport using synchrotron x-ray microtomography. *Journal of Petroleum Science and Engineering 19 (1-2)*, 55–63

Culligan, K.A., Wildenschild, D., Christensen, B.S.B., Gray, W.G., and Rivers, M.L. (2004). Pore-scale characteristics of multiphase flow in porous media: a comparison of air-water and oil water experiments. *Advances in Water Resources., 29*, 227-238.

Craze, R.C. (1950). Performance of limestone reservoirs. *Trans. Amer. Inst. Min. Eng., 189*, 287-294.

Davis, J. C. (2002). Statistics and Data Analysis in Geology, Third Ed., Wiley, New York, 646 pp.

Donaldson, E.C., Chillingarian, G.V., and Yen, T.F. (1985). *Enhanced Oil Recovery, I: Fundamentals and Analysis.* Elsevier, New York

Dullien, F.A.L. (1979). *Porous Media: Fluid Transport and Pore Structure.* Academic Press, New York

Dullien, F.A.L., and Dhawan, G.K. (1974). Characterization of pore structure by a combination of quantitative photomicrography and mercury porosimetry. *Colloid Interface Science*, *47*, 337-349.

Flannery, B.P., Deckman, H.D., Roberge, W.G., and D'Amico, K.L. (1987). Three-dimensional X-ray microtomography, *Science, New Series*, *237* (4821), 1439-1444

Goddard, W.A., Tang, Y., Shuler, P., Blanco, M., Jang, S.S., Lin, S.T., Maiti, P., Wu, Y., Iglauer, S., and Zhang, X. (2004). Lower cost methods for improved oil recovery via surfactant flooding: final report. Department of Energy DE-FC26-01BC15362

Hassanizadeh, S.M., and Gray, W.G. (1990). Mechanics and thermodynamics of multiphase flow in porous media including interphase boundaries. *Advances in Water Resources, 13 (4),* 169 -186.

Jasti, J.K., Jesion, G., and Feldkamp, L. (1993). Microscopic imaging of porous media with X-ray computer tomography, *SPE Formation Evaluation, 8 (3)*, 189-193

Kerr, R. A. (2005). Bumpy road ahead for world's oil, *Science, 310 (5751),* 1106-1108

Ketcham, R.A. (2005). Computational methods for quantitative analysis of three-dimensional features in geological specimens. *Geosphere, 1*, 32-41.

Ketcham, R.A., and Carlson, W.D. (2001). Acquisition, optimization and interpretation of x-ray computed tomographic imagery: application to the geosciences. *Comput. Geosci*., *27*, 381-400.

Larson, R. G., Davis H. T., Scriven, L.E. (1981). Displacement of residual nonwetting fluid from porous media. *Chemical Engineering Science, 36(1),* 75-85.

Melrose, J. C., and Brander, C. F. (1974). Role of capillary Forces in determining microscopic displacement efficiency for oil recovery by waterflooding. *Journal of Canadian. Petroleum. Technology. 13(4)*, 54-62

Mercer, J.W., and Cohen, R.M. (1990). *Journal of Contaminant Hydrology, 6*,107-163.

Mohanty, K.K., Davis, H.T., and Scriven, L.E. (1987). Physics of oil entrapment in water wet rocks. *Soc. Pet. Eng. Reservoir Eng*. 2, 113–127.

Morrow, N.R., Chatzis, I., and Taber, J.J. (1988). Entrapment and mobilization of residual oil in bead packs. *Soc. Pet. Eng. Reserv. Eng., 3(3)* 927-934.

Morrow, N.R., and Heller, J.P. (1985). Fundamentals of enhanced recovery. In Donaldson, E.C.; Chillingarian, G.V.; and Yen, T.F. (1985). *Enhanced Oil Recovery, I: Fundamentals and Analysis.* Elsevier, New York

Morrow, N.R., and Chatzis, I. (1982). Measurement and correlation of conditions for entrapment and mobilization of residual oil. *Dept. Energy Report, 10310* (20), 59.

Ng K.M., Davis H.T., Scriven L.E. (1978). Visualization of blob mechanics in flow through porous media. *Chem Eng Sci , 33(8),*1009-1017.

Pennell, K.D., Pope, G.A., and Abriola, L.M. (1996). Influence of viscous and buoyancy forces on the mobilization of residual tetrachloroethylene during surfactant flushing. *Environ. Sci. Technol., 30*(4), 1328–1335.

Powers S.E., Abriola L.M., and Weber W.J. (1992). An experimental investigation of nonaqueous phase liquid dissolution in saturated subsurface systems: steady state mass transfer rates. *Water Resour. Res., 28*, 2691-2705.

Reeves, P. C., and Celia, M. A. (1996). A functional relationship between capillary pressure, saturation, and interfacial area as revealed by a pore-scale network model, *Water Resour. Res., 32(8),* 2345–2358.

Roof, J.G. (1970). Snap off of droplets in water-wet cores. *Society of Petroleum Engineering Journal*, *10*(1), 85-90.

Schnaar, G. (2006). Pore-scale characterization of organic immiscible liquid in natural porous media using synchrotron X-ray microtomography. dissertation, University of Arizona.

Schnaar, G. and Brusseau, M.L. (2006a). Characterizing pore scale configuration of organic liquid in multiphase systems with synchrotron X-ray microtomography. *Vadose Zone Journal*, *5*, 641-648.

Schnaar, G., and Brusseau, M.L. (2006b). Characterizing pore-scale dissolution of organic immiscible liquid in natural porous media using synchrotron X-ray Microtomography. *Environ. Sci. Technol*., *40*, 6622-6629.

Schramm, L.L. (2000). *Surfactants: fundamentals and applications in the petroleum industry.* Cambridge, N.Y., Madrid. Cambridge University Press.

Stegemeier, G.L. (1976). Mechanism of entrapment and mobilization of oil in porous media. In Shah, D. O., Schechter, R. S. (Eds.), *Improved Oil Recovery by Surfactant Flushing and Polymer Flooding*. Academic Press, New York.

Taber, J. J. (1969). Dynamic and static forces required to remove a discontinuous oil phase from porous media containing both oil and water. *Soc. Pet. Eng. Journal. Vol. 9*, 3-12.

Taylor, K. T., and Hawkins, B. (1990). In petroleum emulsions and applied emulsion Technology, Schramm, L. L. (Ed.). Petroleum Recovery Institute, Calgary, AB.

Wardlaw, N. C., and McKellar, M. (1985). Oil blob populations and mobilization of trapped oil in unconsolidated packs. *Canadian Journal of Chemical Engineering*, *63*, 525-531.

Wardlaw, N. C. (1982). The effects of geometry, wettability, viscosity, and interfacial tension On trapping in single pore-throat pairs. *Journal of Canadian Petroleum Technology*, *21*, 21-27.

Wildenschild, D., Hopmans, J.W., Rivers, M.L., and Kent, J. R. (2005). Quantitative analysis of flow processes in a sand using synchrotron based X-ray microtomography, *Vadose Zone Journal, 4,* 112-126

Wilson, J.L., and Conrad, S.H. (1984). Is physical displacement of residual hydrocarbons a realistic possibility in aquifer restoration? In: Proceedings of the National Water Well Association /API Conference on Petroleum Hydrocarbons and Organic Chemicals in Ground Water. Natl. Water Well Assoc., Worthington, Ohio, pp. 274-298.

Zhang, C.Y., Werth, C.J., Webb, and A.G. (2002). A magnetic resonance imaging study of dense nonaqueous phase liquid dissolution from angular porous media. *Environmental Science and Technology, 36*, 3310-3317.

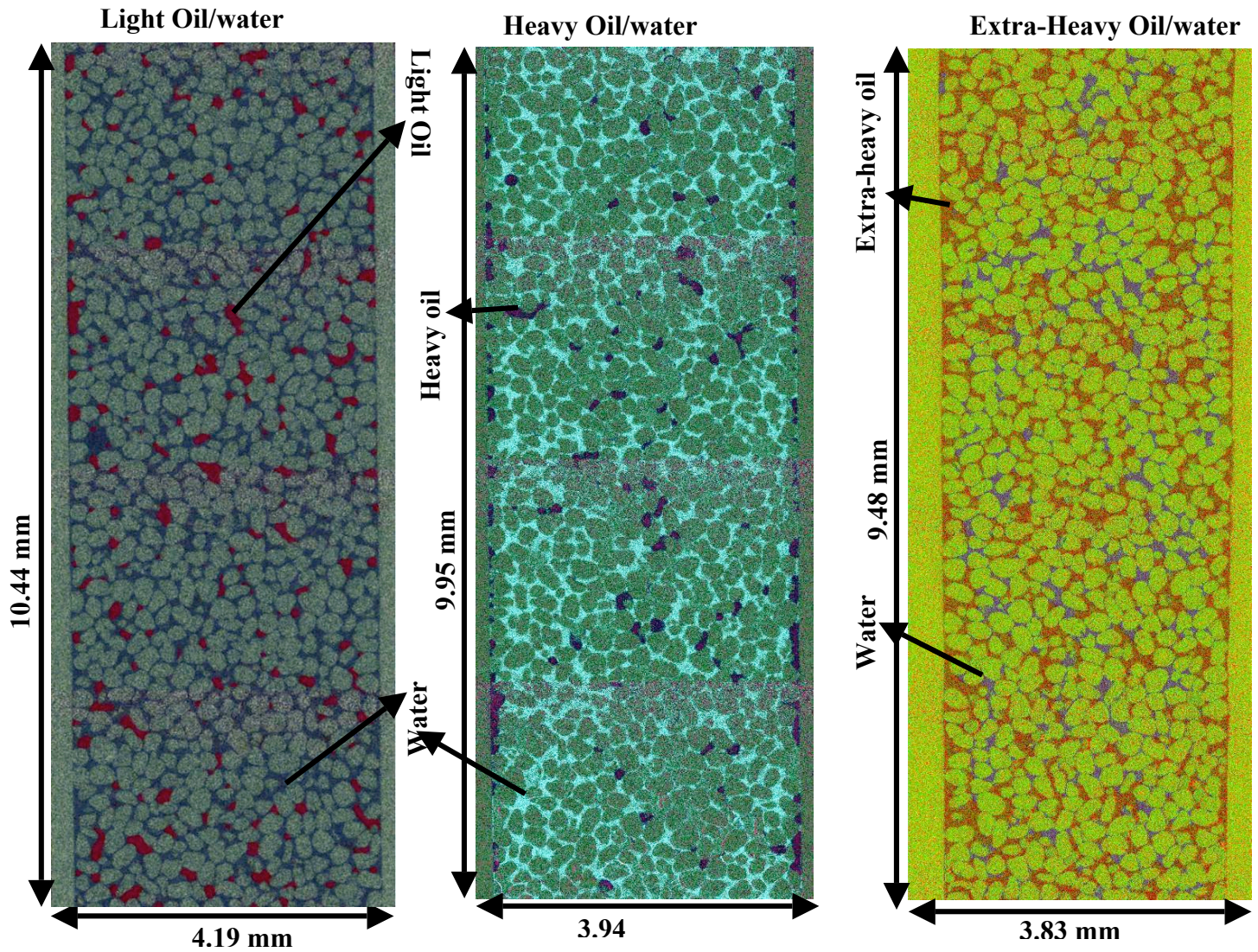

Figure 1.1. Vertical sections of columns along the X-Z direction showing the residual saturation of three fractions of crude oil and the aqueous phase in the homogeneous porous medium (40/50 Accusand). The aqueous and oil phases were separated as binary images and then overlain with false color application.

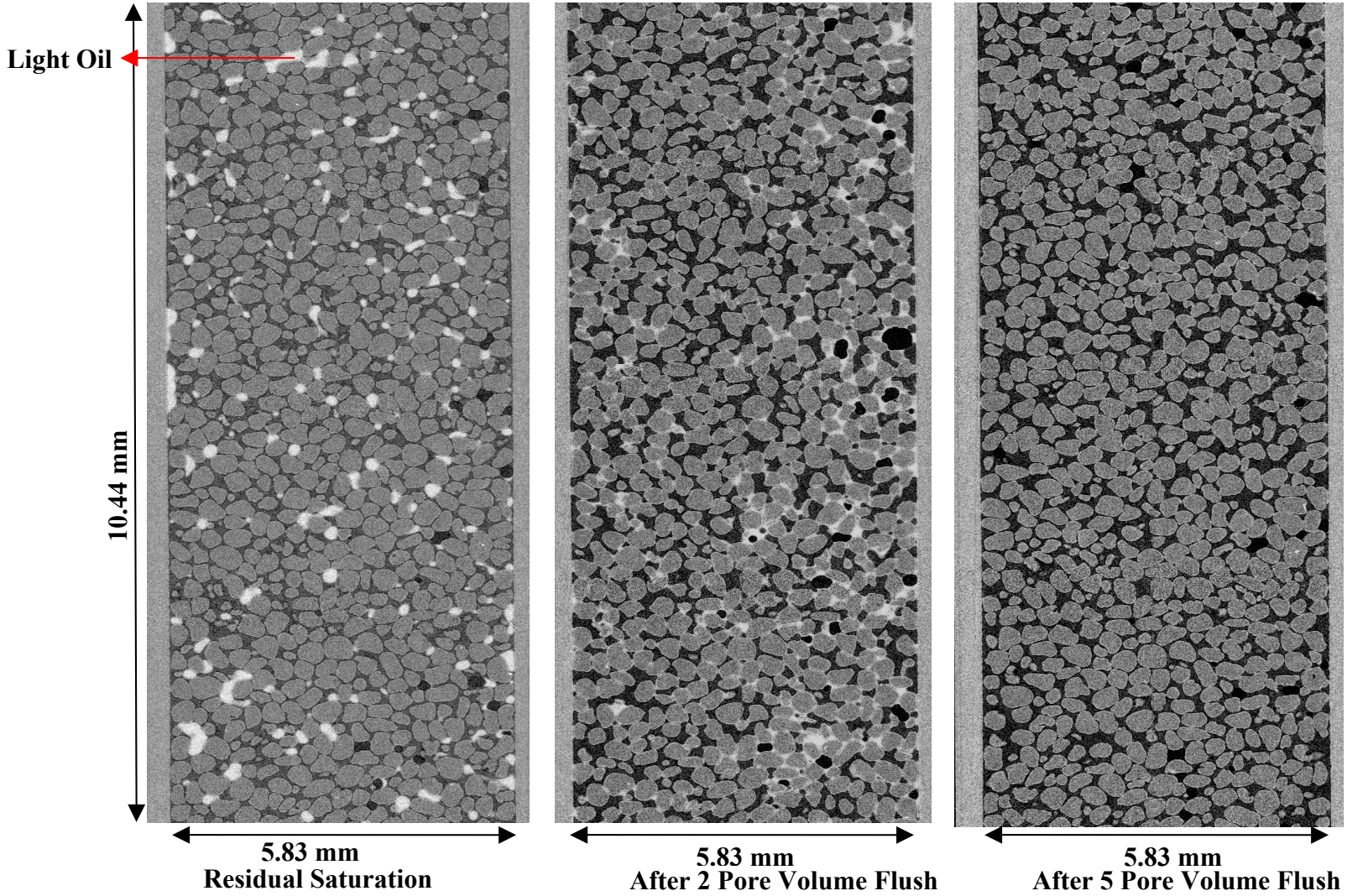

Figure 1.2. Vertical sections of a column along the X-Z direction showing the distribution of light crude oil (23.4˚ API) and aqueous phase in the homogeneous porous medium (40/50 Accusand). From left to right: residual saturation and after the 2-PV and 5-PV surfactant (0.1% v/v) flooding events.

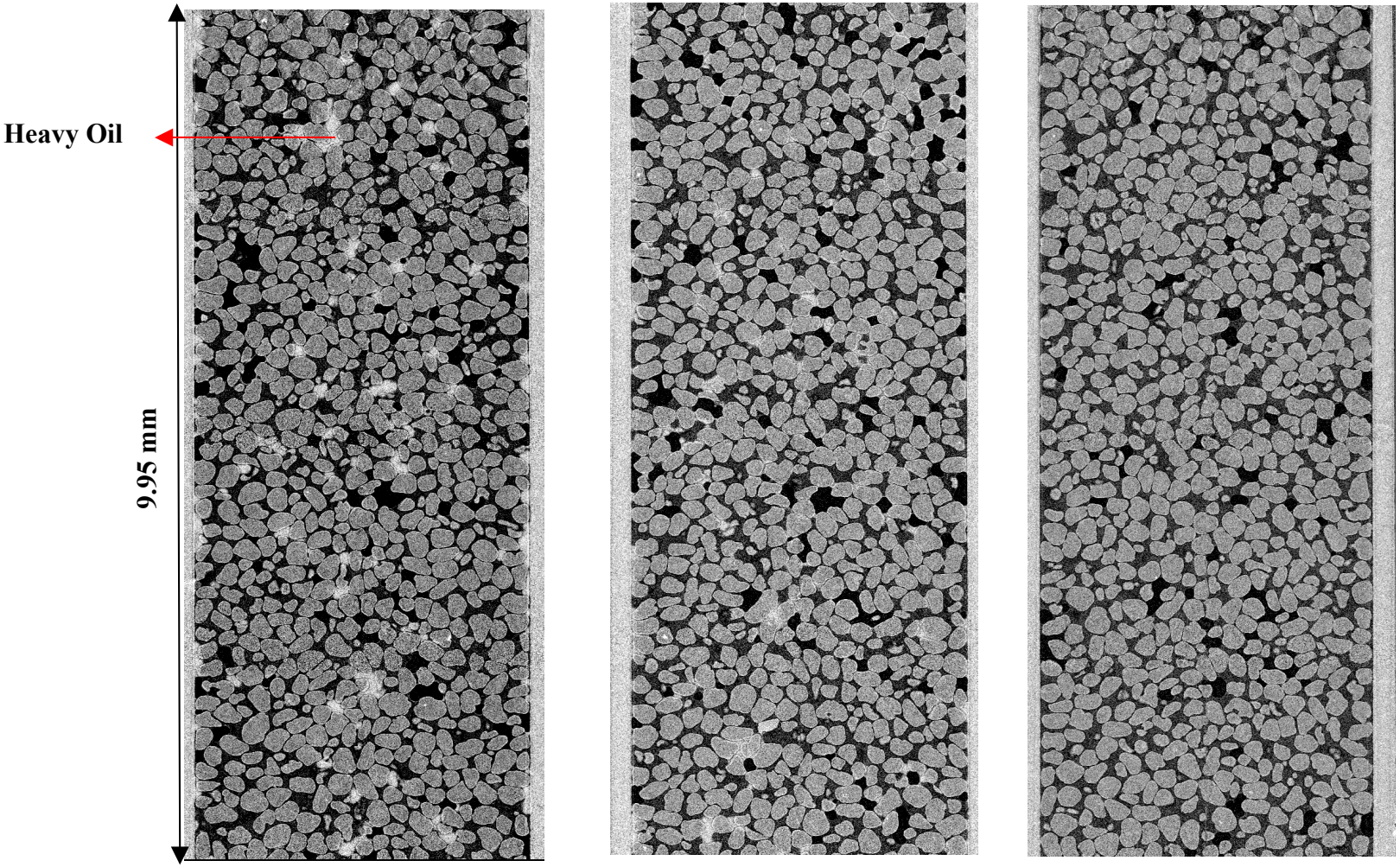

Figure 1.3. Vertical sections of a column along the X-Z direction showing the distribution of heavy crude oil (14.8˚ API) and aqueous phase in the homogeneous porous medium (40/50 Accusand). From left to right: residual saturation and after the 2-PV and 5-PV surfactant (0.1% v/v) flooding events.

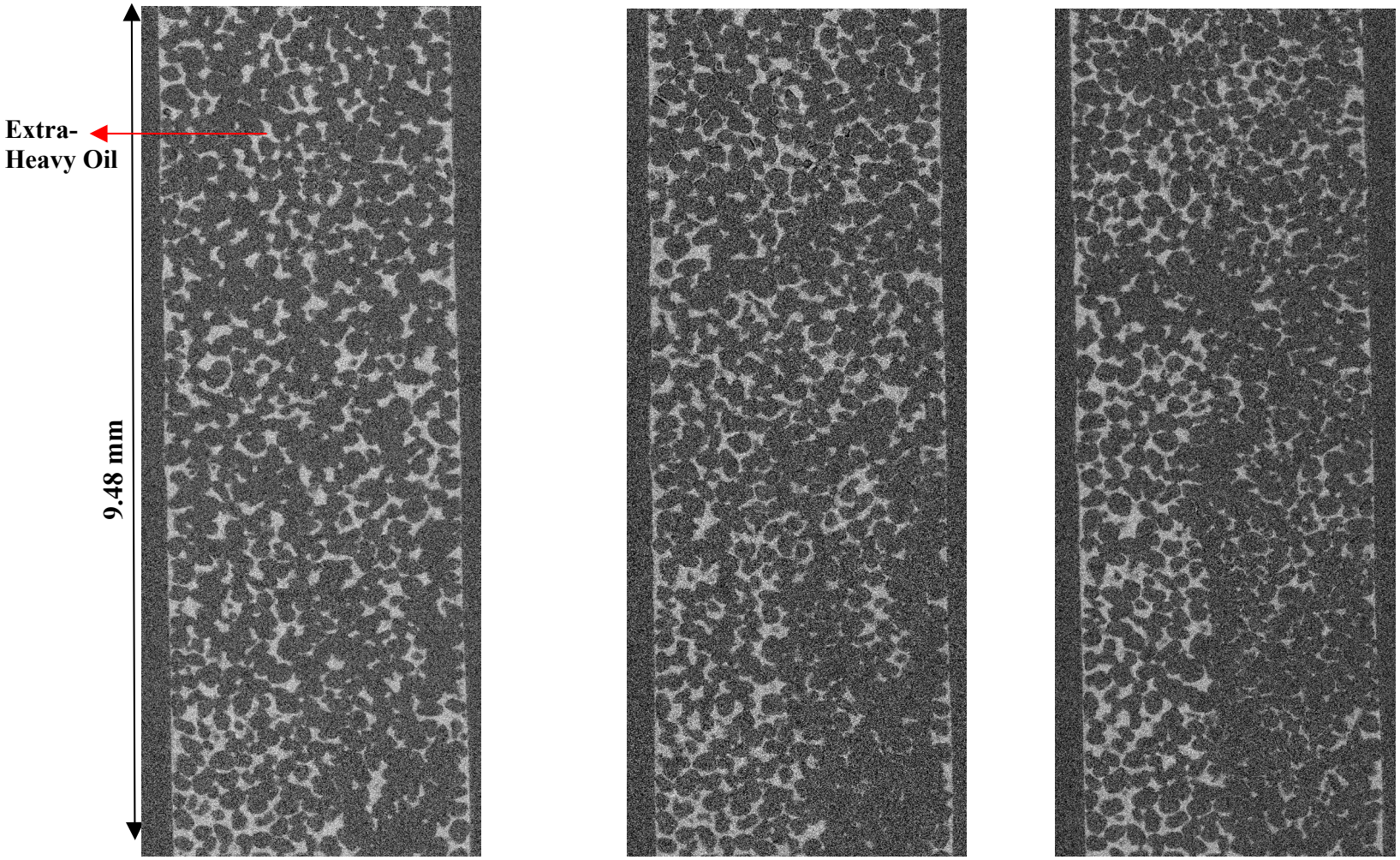

Figure 1.4. Vertical section of a column along the X-Z direction show the distribution of extra-heavy crude oil (4.2˚ API) and aqueous phase in the homogeneous porous medium (40/50 Accusand). From left to right: as residual saturation and after the 2-PV and 5-PV surfactant (0.1% v/v) flooding events.

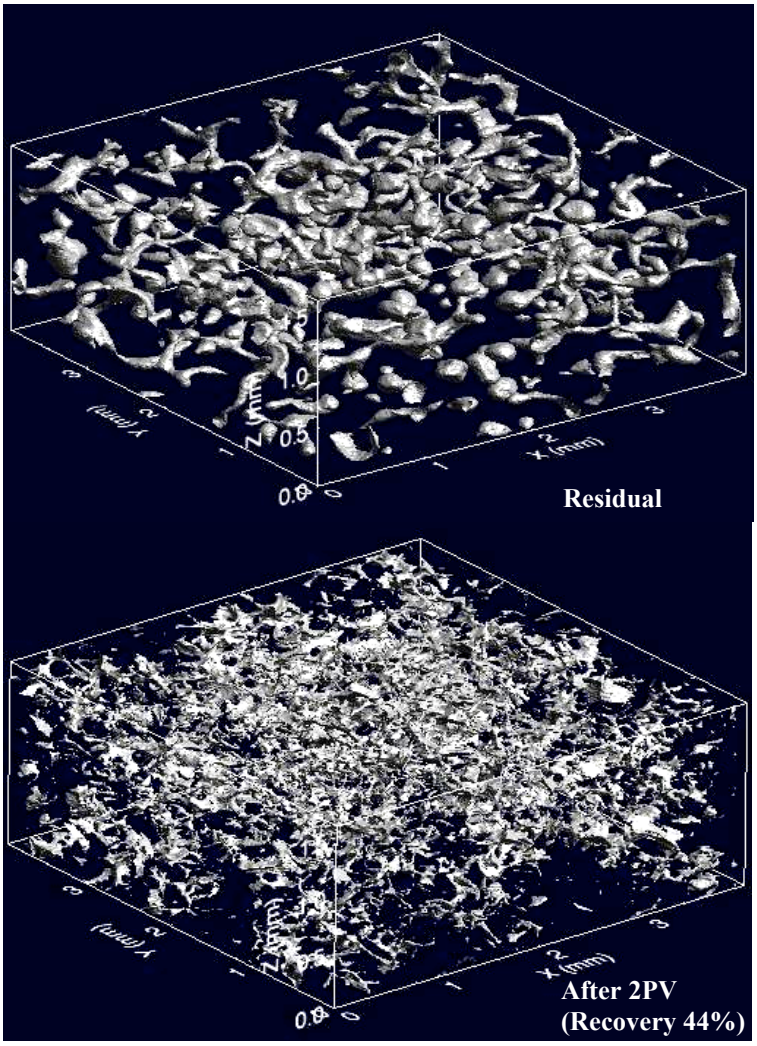

Figure 1.5. 3-D images of cropped sections (4mm×4mm×1.5mm) of the column showing the distribution of light crude oil in the homogeneous porous medium (40/50 Accusand). Light oil is segregated into discrete smaller blobs and become flattened after 2 PVs of surfactant (0.1% v/v) flooding, exposing greater surface area in contact with the surfactant solution. Complete recovery for the light oil was obtained after the 5-PV surfactant flooding event (see figure 1.2).

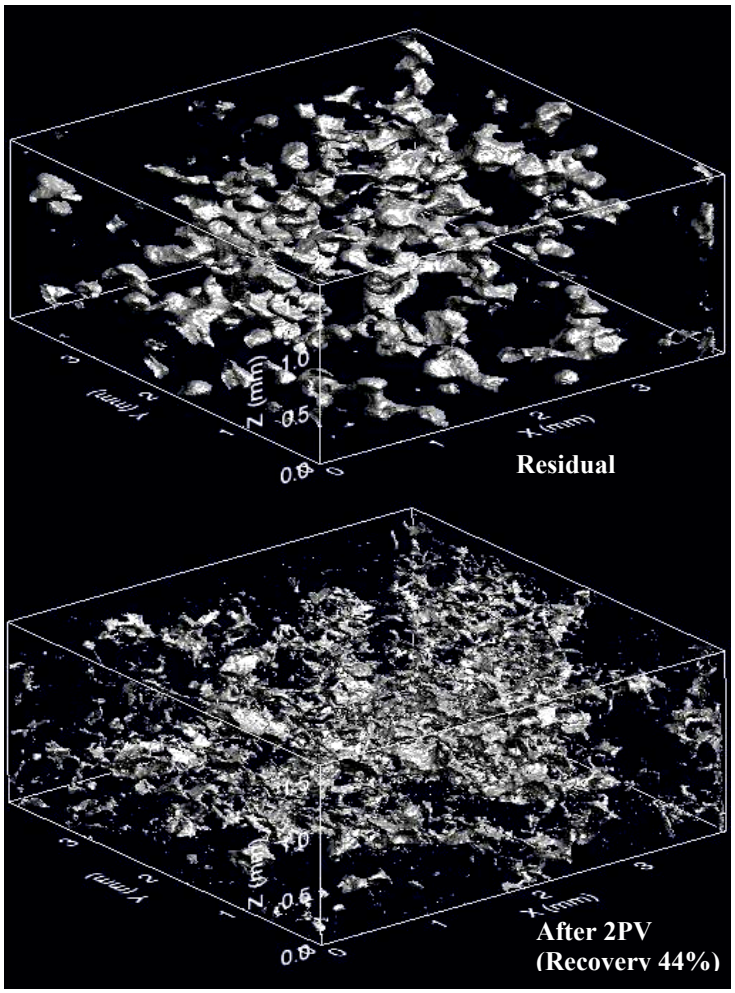

Figure 1.6. 3-D images of cropped sections (3.94mm×3.94mm×1.5mm along the Z-direction) of the column showing the distribution of heavy gravity (14.8˚ API) crude oil in the homogeneous porous medium (40/50 Accusand). After 2PV surfactant flood the heavy oil phase segregates into discrete smaller blobs and total surface area increases exposing greater surface area in contact with surfactant solution (see figure 1.3).

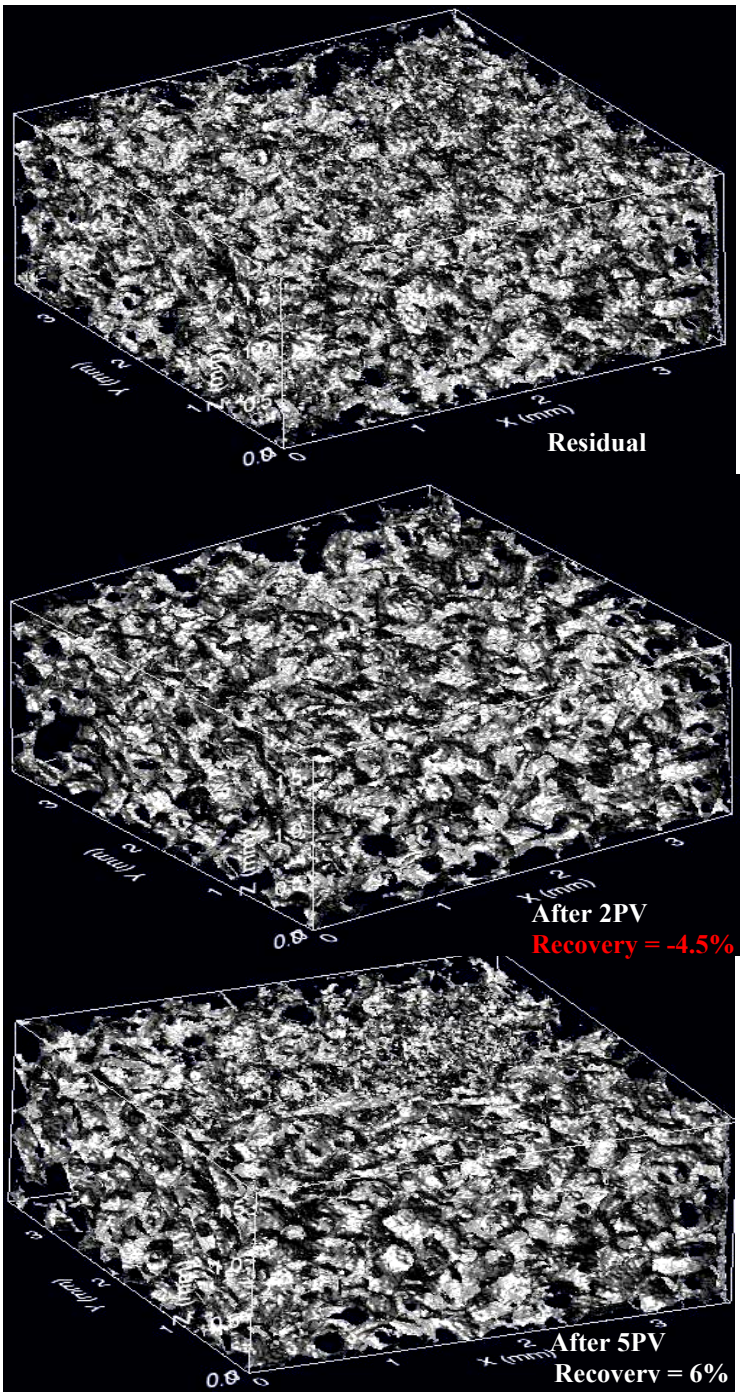

Figure 1.7. Cropped sections (3.83mm×3.83mm×1.5mm) of the column showing the distribution of extra-heavy crude oil (4.2˚ API) in the homogeneous porous medium (40/50 Accusand). The oil distribution is characterized by interconnected ganglia attributed to the oil-wet conditions of the porous medium at pH < 7. Negative recovery was obtained after the 2-PV surfactant flood, attributed to addition of oil into the system. 6% recovery was achieved after the 5-PV surfactant-flooding event. (also see figure 1.4)

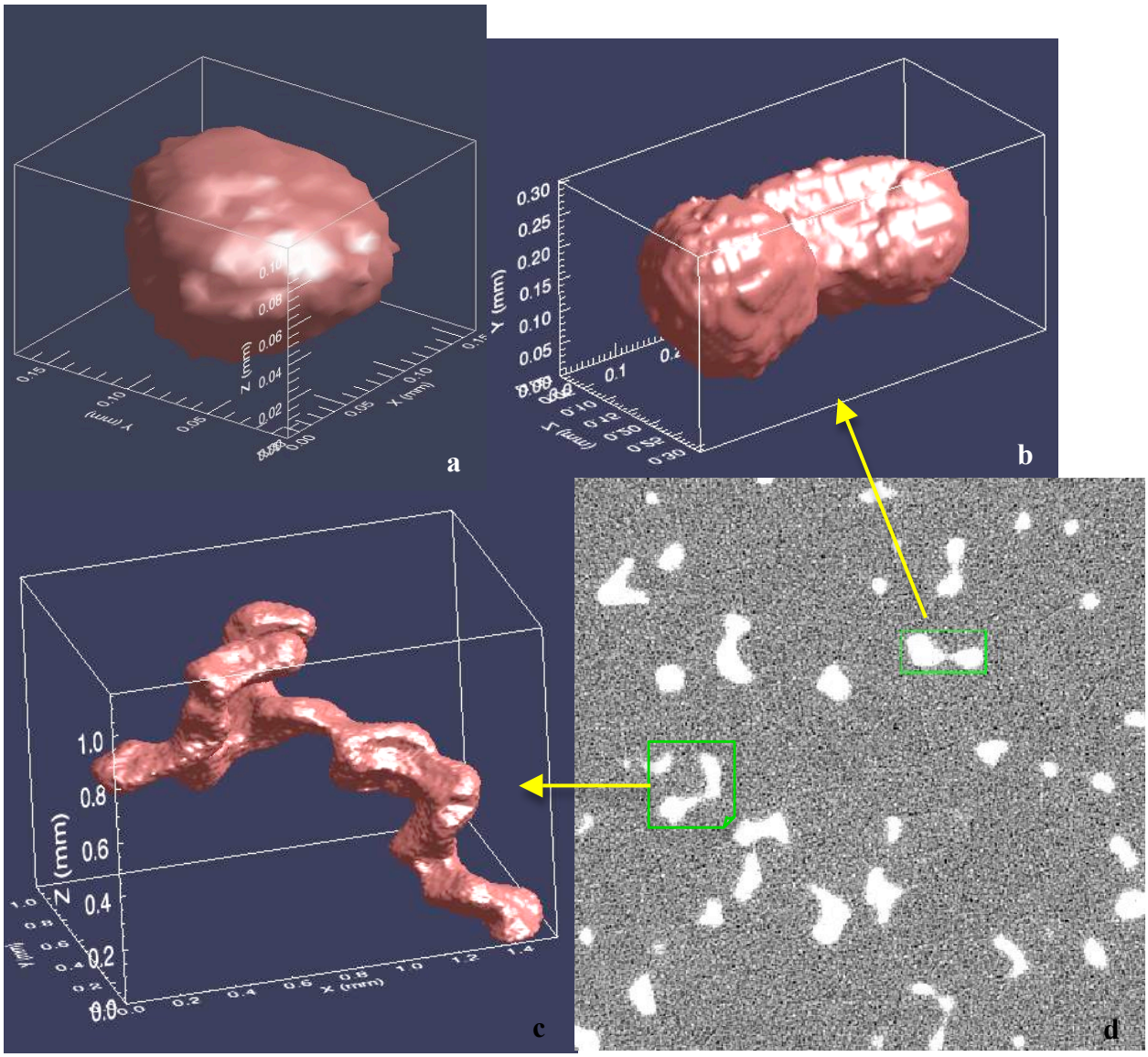

Figure 1.8. Morphology of trapped light oil blobs as residual saturation. Three main types were characterized by Chatzis et al. (1993). Various types are "singlet" (a), "doublet" (b) and "interconnected ganglia" (c). Figure d shows the 82nd slice (perpendicular to the Z-direction) of the column containing light oil blobs in the homogeneous porous medium. Note that the "singlet" blob (exaggerated in all three directions) is one third the size of the "doublet", and one tenth the size of the "ganglia" along the Z-direction.

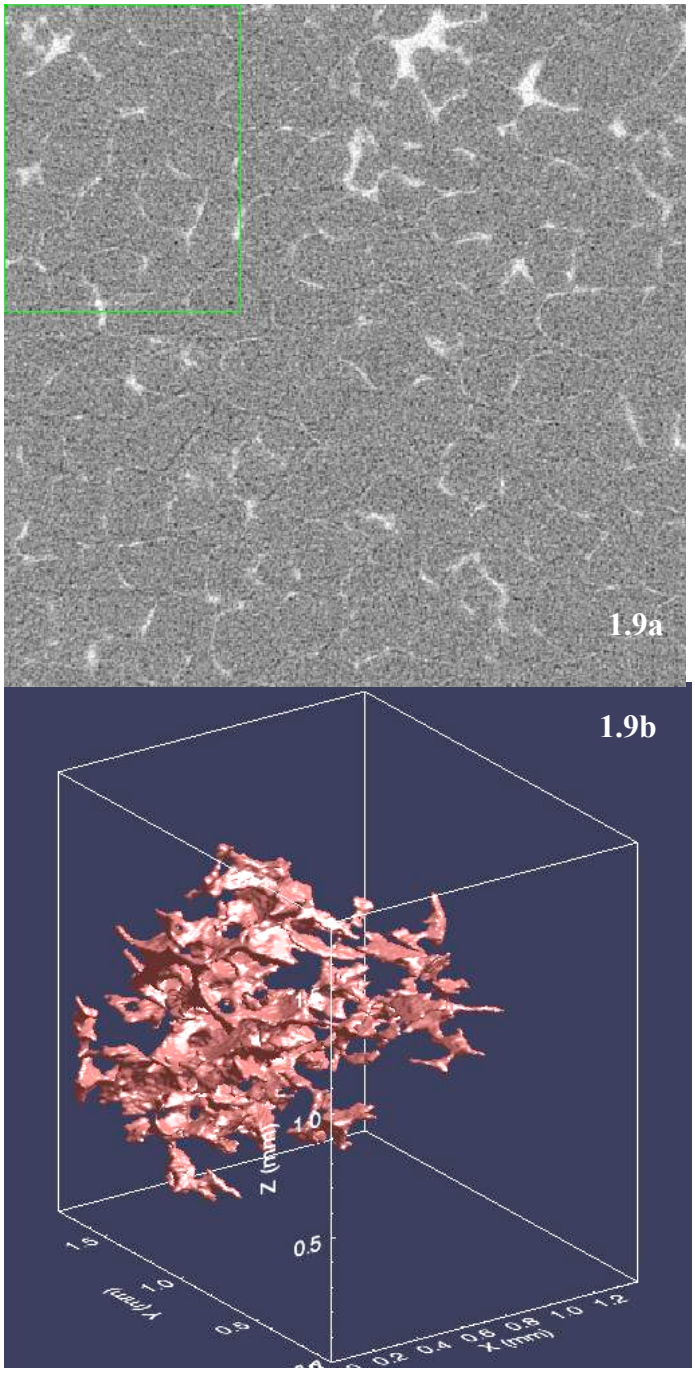

Figure 1.9. Light oil blob morphology changes observed after the 2-PV surfactant flood (homogeneous porous medium). Figure 1.9a shows the section view of one ganglia type oil-phase perpendicular to Z-direction. Figure 1.9b shows the same ganglia in 3-D. The length of the ganglia is approximately 2mm along the Z-direction. Oil phase morphology changed to a more tabular shape, exposing greater oil-phase surface area. Relative positions of the sand grains can be identified in both figures (1.9a and 1.9b).

Table 1.1 List of physical parameters controlling the mobilization process for three oil fractions.

	Light oil	Heavy oil	Extra-Heavy oil
Residual Saturation			
IFT (γ) dyne/cm	16.32	16.42	42.25
Capillary number (N_c)	1.16E-03	1.15E-03	4.48E-04
Bond Number (N_B)	6.65E-12	3.72E-12	1.24E-13
Trapping number (N_T)	1.16E-03	1.15E-03	4.48E-04
Flooding with 0.1% Surfactant			
IFT (γ) dyne/cm	10.66	11.80	24.68
Capillary number (N_c)	1.78E-03	1.61E-03	7.68E-04
Bond Number (N_c)	1.02E-11	5.18E-12	2.12E-13
Trapping number	1.78E-03	1.61E-03	7.68E-04

Table 1.2 Quantitative data for the light oil (23.4˚ API) in the homogeneous porous medium.

Parameters	Residual	After 2PV flood	After 5PV flood
No. of blobs (single particles)	1628	12541	N/A
Mean Volume (cu mm)	4.496E-3	3.282E-4	N/A
Blob Uniformity Coefficient (C_U)	1.737	5.209	N/A
Coefficient of variation (C_V)	1.864	12.937	N/A
Total Surface Area (mm^2)	284.924	840.989 (Change 200%)	N/A
Total volume (mm^3)	7.318	4.116 (Recovery 44%)	0 (Recovery 100%)

Table 1.3 Quantitative data for the heavy oil (14.8˚ API) in the homogeneous porous medium

Parameters	Residual	After 2PV flood	After 5PV flood
No. of blobs (single particles)	740	5381	N/A
Mean Volume (cu mm)	5.738E-3	7.101E-4	N/A
Blob Uniformity Coefficient (C_U)	1.967	2.592	N/A
Coefficient of variation (C_V)	2.585	8.474	N/A
Total Surface Area (mm^2)	151.571	282.708 (Change 87%)	N/A
Total volume (mm^3)	4.246	3.821(Recovery 10%)	0(Recovery 100%)

Table 1.4 Quantitative data for the extra-heavy oil (4.2˚ API) in the homogeneous porous medium

Parameters	Residual	After 2PV flood	After 5PV flood
No. of blobs	Interconnected ganglia	Interconnected ganglia	Interconnected ganglia
Mean Volume (cu mm)	N/A	N/A	N/A
Coefficient of variation (C_V)	N/A	N/A	N/A
Total Surface Area (mm^2)	1034.456	1108.619 (change 7%)	1092.859 (Change -1.4 %)
Total volume (mm^3)	34.036	35.553(Recovery -4.5%)	32.045(Recovery 6%)

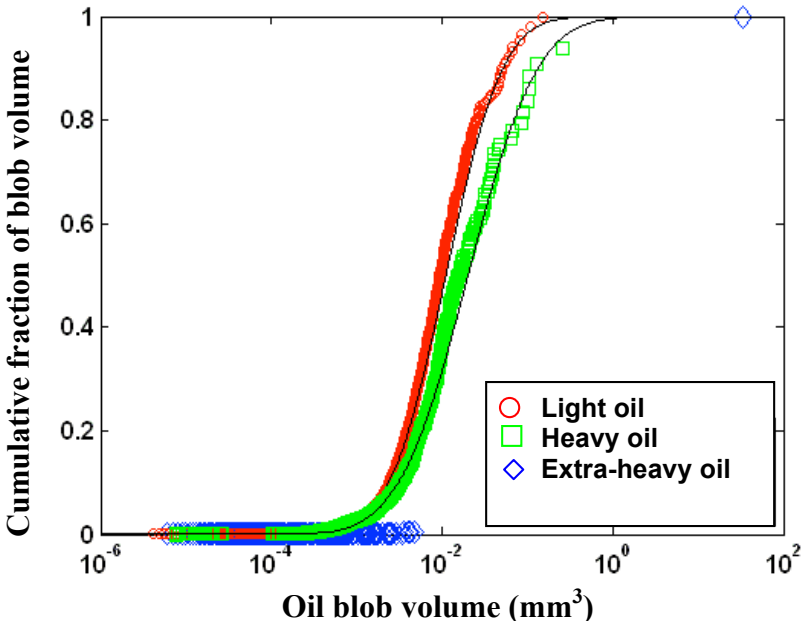

Figure 1.10. Cumulative distributions of light, heavy and extra-heavy-oil blobs as residual saturation (in the homogeneous medium) show a relatively homogenous distribution of the light oil blobs. The single large extra-heavy oil blob represents large interconnected ganglia which includes most of the oil-phase volume present within the system.

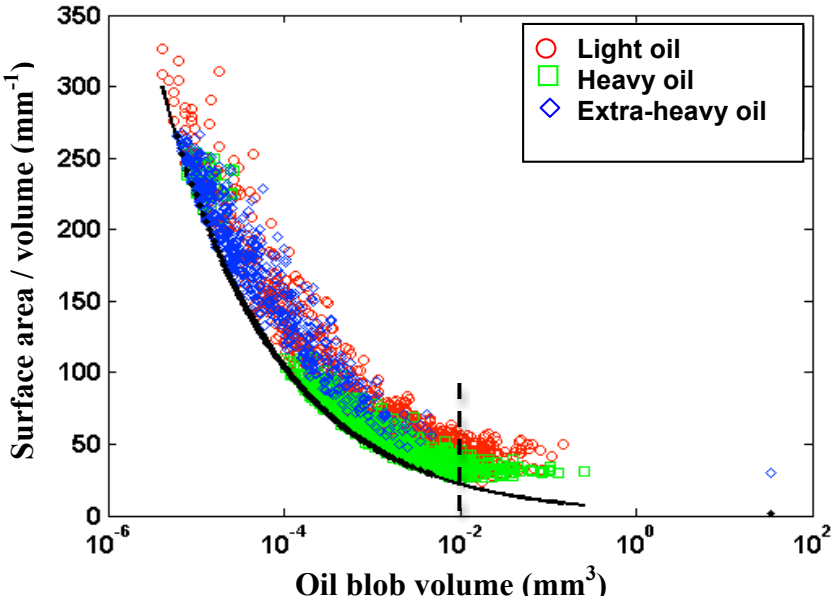

Figure 1.11. Graph shows deviation of oil blobs from spherical shape (bold black line: model curve for spherical shape for a particular volume) for the above system (figure 1.10). Greater deviation represents greater (increased) oil surface area. Light oil blobs show greater deviation from spherical shape in comparison to the heavy and extra-heavy oil as residual saturation. Maximum deviation from spherical shape is represented by larger volume blobs (dashed line), which are typically represented by interconnected ganglia, trapped within interconnected pore spaces.

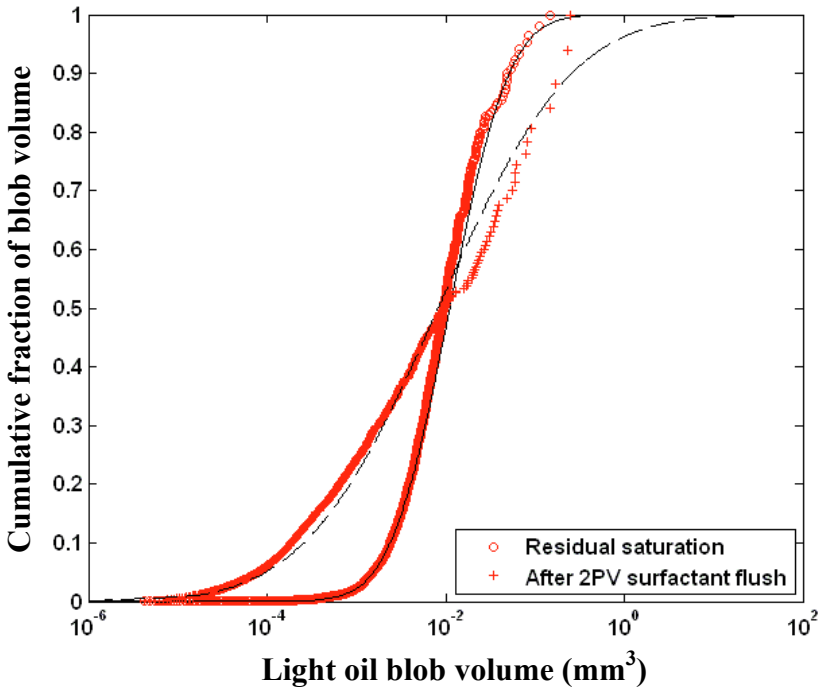

Figure 1.12. Graph shows the cumulative distribution of light oil blob volume within the homogeneous medium, before (homogeneous distribution) and after the 2-PV surfactant flood (heterogeneous distribution). Mean oil blob volume was reduced by one order of magnitude after surfactant flooding (also see figures 1.2 and 1.5).

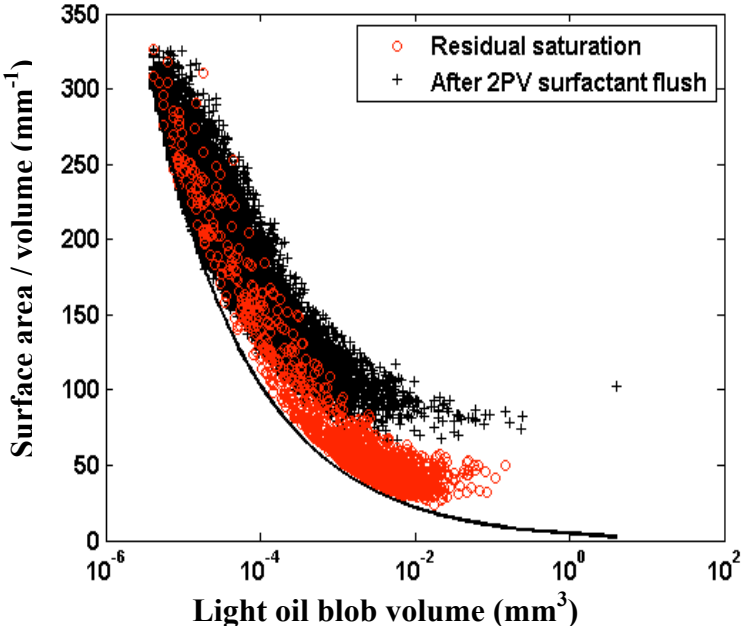

Figure 1.13. Graph shows the distribution of light oil blob morphology of the above system (figure 1.12). Light oil blobs show greater deviation from spherical shape (bold black model curve) after the 2-PV surfactant flood exposing more surface area, attributed to increased contact with the surfactant solution (also see figures 1.2 and 1.5).

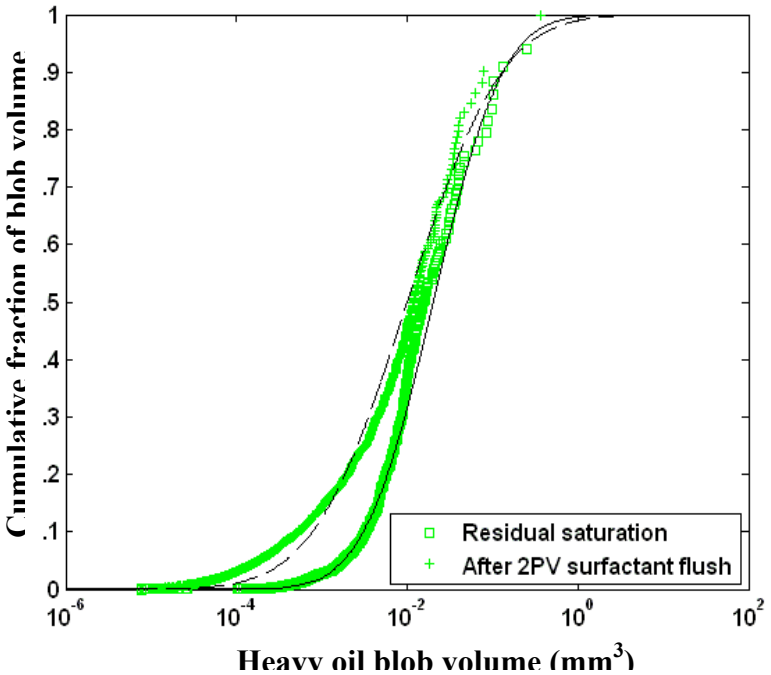

Figure 1.14. Cumulative distribution of heavy oil blob volume, within the homogenous medium, before and after the 2-PV surfactant flood. The distribution becomes more heterogeneous, and the mean blob volume was reduced by one order of magnitude after the surfactant flooding event (see figures 1.3 and 1.6).

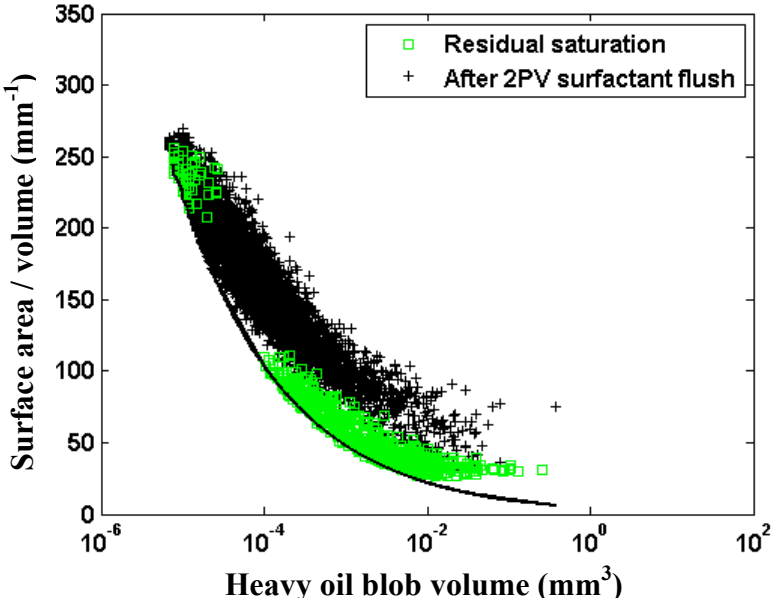

Figure 1.15. Graph shows the distribution of heavy oil blob morphology of the above system (figure 1.14). The deviation from spherical shape (black model curve) represents greater surface area. The heavy oil blobs show greater deviation from spherical shape after the 2-PV surfactant flooding event exposing more surface area, attributed to increased contact with the surfactant solution (see figures 1.3 and 1.6).

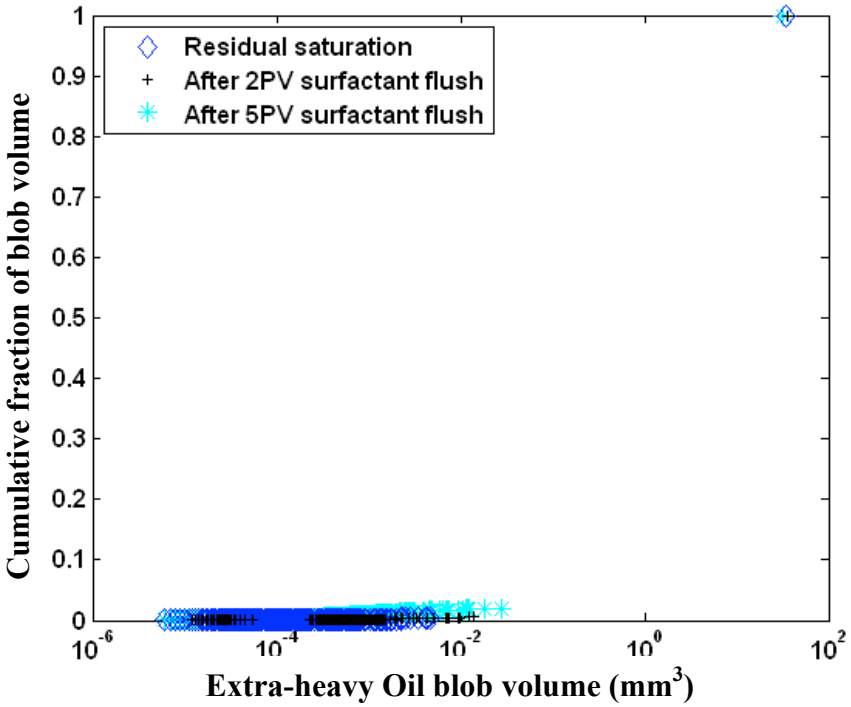

Figure 1.16. Cumulative distribution of extra-heavy oil blob volume, within the homogeneous medium, as residual saturation, and after the 2-PV and 5-PV surfactant flooding events. The results show no significant change in distribution pattern. The single large heavy oil blob represents large interconnected ganglia, which included most of the oil-phase volume present within in the system.

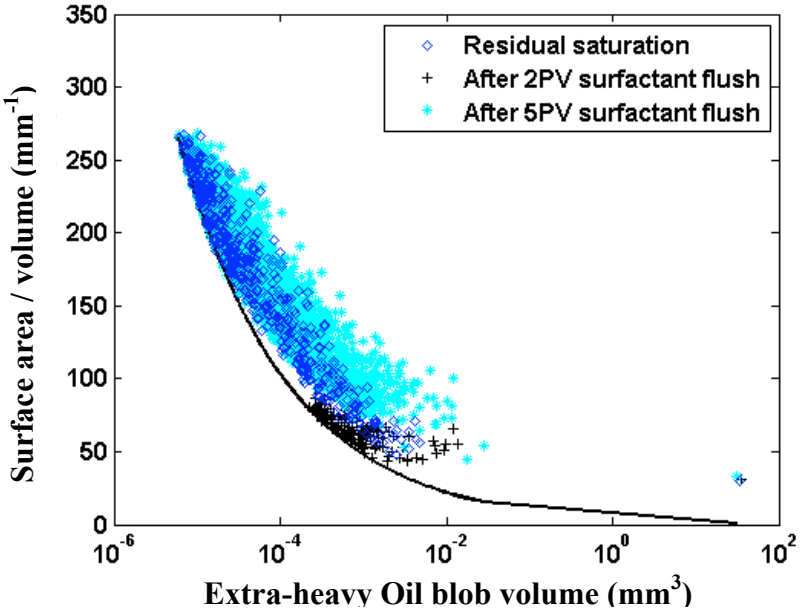

Figure 1.17. Although insignificant in total trapped volume, the smaller extra-heavy oil blobs show maximum deviation from spherical shape after the 5-PV surfactant flood. Only 6% recovery was achieved, primarily due to the nature of the interconnected ganglia represented as a single large blob volume (extreme right).

Table 1.5. Sensitivity analyses on total oil blob (light oil in the homogeneous 40/50 Accusand) specific surface area as function of several controlling factors.

Median smoothing	Contrast (tomo_display)	Initial Threshold	Final Threshold	Initial Specific Surface	Final Specific Surface	Sensitivity (%)
1	range =-2500 to +2500	190	199 (4.7%)	44.29231993	45.47	2.65
1	range =-2500 to +2500	190	180 (-5.2%)	44.29231993	43.15	-2.58
1	range =-2500 to +2500	190	209 (10 %)	44.29231993	47.10	6.33
1	range =-2500 to +2500	190	228 (20%)	44.29231993	52.87	19.37
2	range =-2500 to +2500	190	190	44.29231993	43.45	-1.91
3	range =-2500 to +2500	190	190	44.29231993	43.13	-2.63
4	range =-2500 to +2500	190	190	44.29231993	42.91	-3.13
1	range =-1500 to +1500	190	190	44.29231993	41.65	-5.96
1	range =-3500 to +3500	190	190	44.29231993	48.31	9.08

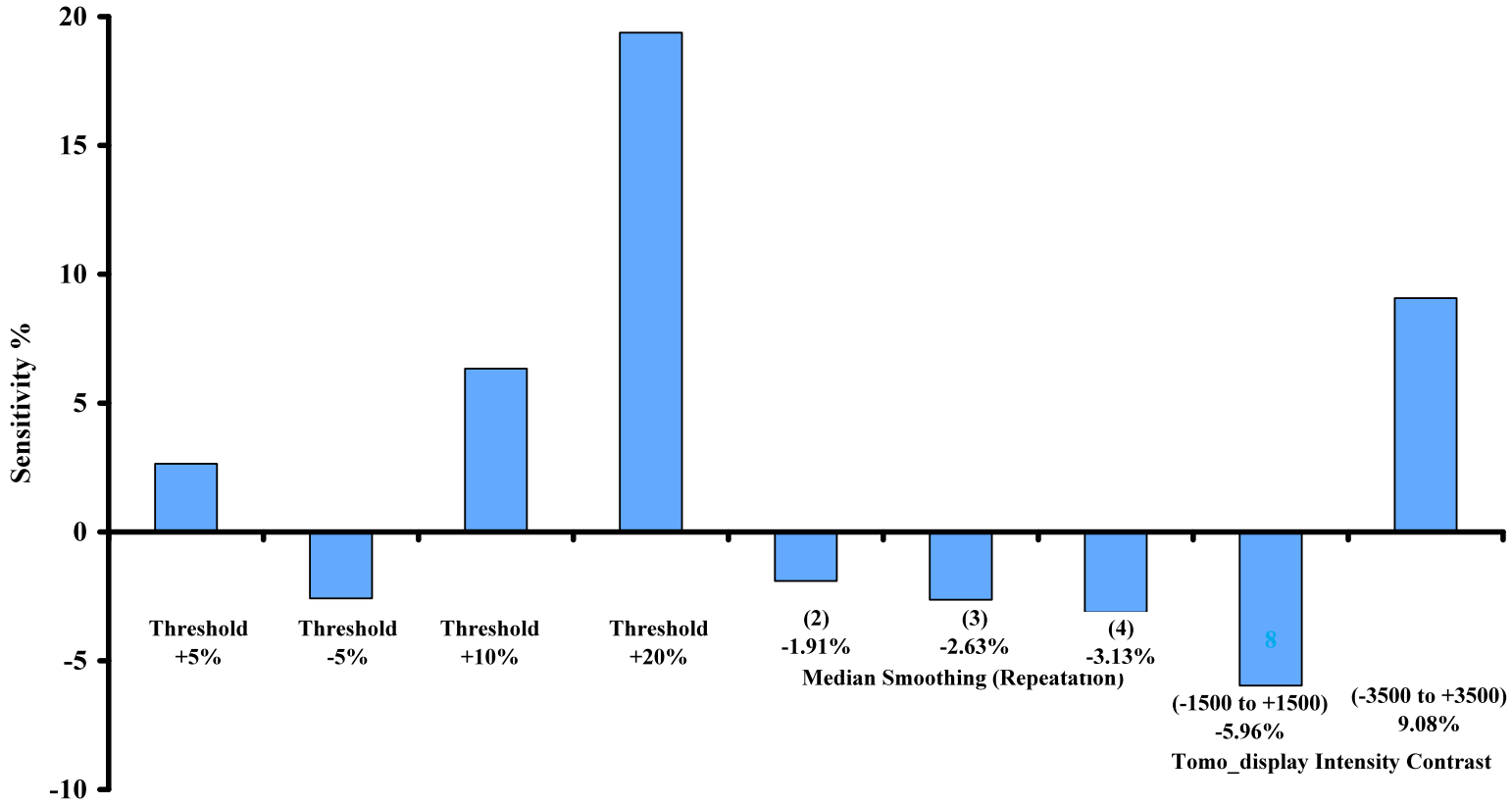

Figure 1.18. Bar diagram showing the sensitivity analysis on quantitative results (specific surface area) calculated for the light oil blobs distributed in the homogeneous porous medium (Table 1.5). Figure shows maximum sensitivity for binary transformation (threshold/grey-scale value assigned for the oil phase) process applied in Blob 3D software, followed by the intensity range applied in Tomo_Display software. Median smoothing (image quality control) has less control on the quantitative results.

PORE SCALE DISTRIBUTION OF CRUDE OIL BLOBS AS FUNCTION OF POROUS MEDIA HETEROGENEITY: AN APPLICATION OF SYNCHROTRON X-RAY MICROTOMOGRAPHY

ABSTRACT

Synchrotron X-ray Microtomography (SXM) imaging technology was used to study three-dimensional (3-D) distributions of crude oil blobs as function of pore-scale heterogeneity. A significant amount of crude oil can be trapped into pore spaces during primary and secondary recovery processes. Surfactant flooding into the reservoir system reduces interfacial tension between oil and water, resulting in enhanced mobility of the trapped oil blobs. Reducing interfacial tension also has control over oil blob morphology and the distribution pattern. The aim of this research is to understand the interfacial phenomena at the pore scale, the resulting residual saturation of oil blob distribution pattern as function of media heterogeneity (i.e. before and after surfactant flooding events), and oil recovery processes from different porous media systems. Multiple columns were packed with three types of sand of increasing heterogeneity in grain size distribution (sorting) and were injected with residual saturations of light and heavy crude oil fractions, respectively. These oil-distributed columns were then imbibed with 0.1% anionic surfactant solution in various episodes. SXM images of the crude oil distribution were captured before and after each surfactant flooding event. Results show a homogeneous distribution of oil blobs (both oil fractions) as residual saturation, within the homogeneous sand. Heterogeneous oil blob distributions were observed within the two higher heterogeneous porous media types. Oil blob distributions became more heterogeneous after each subsequent surfactant

flooding episode for all porous-media systems. The heterogeneity of the porous media (i.e. sorting) was a dominant control on the oil-blob-size-distribution trapped as residual saturation. The mobility of the oil blobs, as a result of surfactant flooding, was primarily controlled by the relative permeability of the medium and the reduction of interfacial tension between the wetting phase (water) and non-wetting phase (oil). Maximum oil recovery resulted from the homogeneous porous medium, whereas, the mildly heterogeneous porous medium produced a limited but consistent recovery after each surfactant flooding episode. The highly heterogeneous porous medium produced greater oil recovery only after multiple pore volumes of surfactant flooding, at which point the oil blobs become disseminated into the smaller fragments in response to the reduced interfacial tension.

2.1 INTRODUCTION

Crude oil mobility in a reservoir is controlled by several physical parameters such as viscosity, capillary action, and the interfacial tension existing between the oil-water, and the oil and solid-media-grain boundary. Other controlling factors include heterogeneity of the reservoir in terms of porosity, permeability, and pore-size-distribution (Wardlaw et al. 1988). These parameters, on the other hand are controlled by sorting and packing of the solid media grains (Wardlaw 1982, Chatzis et al. 1983, Morrow 1971). A significant amount of crude oil is trapped into the pore spaces as residual saturation during primary and secondary extraction processes. Surfactants have been used since the 1970s to lower oil-water interfacial tension, which increases the mobility of the oil blobs during water flooding, thereby, increasing the recovery potential. Interfacial tension has a control on available contact surface area between the wetting and non-wetting phases (water and oil in this case). Additionally, heterogeneity of the reservoir pore-size-distribution has an impact on oil blob morphology and pattern of distribution which controls the mobilization process (Wardlaw and Mckellar 1985, Chatzis et al. 1983, Larson et al. 1981). Therefore, a thorough understanding of interfacial phenomena, in terms of oil blob morphology and distribution at the pore-scale level, will be critical for estimating the enhanced oil recovery (EOR) potential from existing reservoirs. The goal of this research is to understand and quantify: 1) the three-dimensional (3-D) oil blob distribution patterns within various porous media, 2) the trapping mechanisms that exist within these different systems, and 3) the mobilization processes involved in EOR from the pore scale to laboratory scale. Knowledge acquired from this research can later be applied for better understanding the primary mobilization mechanisms in intermediate and field-scale systems.

2.1.1 Heterogeneity in Porous Media

Previous studies show the importance of capillary entrapment in homogeneous and heterogeneous porous media during secondary recovery by water flooding and EOR. Experimental studies were performed to understand the trapping mechanism in homogeneous porous medium such as glass bead packs and Berea sandstone (Powers et al. 1992, Morrow et al. 1988, Wardlaw and Mckellar 1985, Morrow and Chatzis 1982, Ng et al. 1978, Stegemeier 1976, Taber 1969), and heterogeneous glass capillary tubes (Chatzis and Dullien 1983, Chatzis et al. 1983). Lattice simulations (Larson et al. 1981) and numerical modeling were carried out to understand the trapping mechanisms in homogeneous pore network models (Reeves and Celia 1996), and heterogeneous cross-bedded reservoir environments (van Lingen et al. 1996, Ringrose et al. 1992, Kortekaas 1985). In small scale (pore-laboratory systems), the pore-scale heterogeneity of a porous medium can be identified by the variation in sorting, porosity and permeability. Patterns of pore spaces in a clastic reservoir are controlled by grain - size, shape, sorting and chemical composition, and the distribution pattern and chemical composition of the matrix and cement material (Levorsen 2001). In general, bulk reservoir porosity varies from 5-30%, which can change with depth and time. Porosity generally decreases with depth. Compaction and cementation are the two main processes for porosity reduction in a reservoir. Compaction is the main process of porosity reduction during shallow burial of unconsolidated sand, whereas the rate of cementation increases as the age and depth increases. Local scale variation in porosity at higher depth is a common occurrence. For example, un-cemented sandstone with a porosity of 30-33% is found within the Gulf of Mexico at a depth of about 2000-4000 meters (Gluyas and Cade 1997). Porosity of un-cemented sandstone varies from 20% (Norwegian Continental shelf) to 38% (Warwink, Texas).

Evans et al. (1997) describes permeability variations for clastic reservoirs. The absolute permeability for a clastic reservoir varies from < 0.1 milli-Darcy's (mD) to >10 Darcy's. Small-scale variation in heterogeneity within the same reservoir is a common characteristic. Most clastic reservoir rocks are associated with sand grains transported and deposited by air and water. Alternating small-scale distribution of coarse and fine grain sizes are common in graded bedding. Thin lamina may vary in thickness from one-grain diameter to a thickness which depends upon the time and the nature of depositional processes occurring (Ringrose et al. 1993). Pore throat diameter, and the connectivity of the pore spaces are the two main factors controlling the permeability of a reservoir. Compaction and cementation can affect the reduction in pore throat size thereby reducing overall reservoir permeability. Grain size and sorting are also important factors for variation in permeability in unconsolidated sands. Larger grain sizes which possess larger pore throats are responsible for the associated higher permeability of a reservoir or porous unit. In contrast, poorly sorted unconsolidated sands possess lower pore throat diameters compared to relatively well-sorted sands of same mean grain diameter (Evans et al. 1997).

2.1.2 Factors Controlling Trapping Mechanisms

The three primary fluid trapping mechanisms in porous media, dependent upon the porosity and permeability (pore throat diameter), are interfacial tension, capillary force, and the wetability of the liquid media (oil and water) on solid porous grain boundary. Levorsen (2001) described the fundamental role of these three parameters on the trapping mechanism process. The molecules of a particular liquid are bonded together by cohesive forces in all directions maintaining equilibrium of that fluid phase. The molecules along the surface, however, are attracted only inward, resulting in a dynamic contracting surface area. Surface tension, existing

between a particular liquid and air or vacuum, can be defined as the force required expanding a boundary surface (e.g., air-water) over a particular distance (mN/m). Interfacial tension is the term used when two immiscible phases are in contact, acting to reduce the area of existing interface to achieve thermodynamic equilibrium (lowest energy state). This force is equivalent to the surface free energy of the boundary per unit area. Greater interfacial tension causes higher immiscibility between two phases in contact with each other. Another force acts at the interface, by which two different substances when in contact are attracted by Van Der Walls forces. This energy of adhesion is the cause of wettability of a liquid on another liquid or solid surface. Wettability is also controlled by the interfacial tension between two substances. A wetting phase (i.e. water) has a tendency to be trapped into the smaller pore spaces of the porous media, whereas the relatively more non-wetting phase (oil in this case) should preferentially occupy the larger pore spaces (Mercer and Cohen 1990). Lowering interfacial tension allows expansion of oil-water interfacial surface. One way to achieve this expansion in interface is by breaking down the oil blobs, and dispersing them into water as smaller fragments. When the interfacial tension tends to zero, the two immiscible phases will prefer to exist as a single phase. However, since the interfacial tension between oil-water can never be zero, the mixture can produce an emulsion. Therefore, the purpose of flooding with a surfactant solution during EOR is to increase the mixing of oil and water in order to recover/mobilize more oil blobs, otherwise trapped as residual saturation during primary and secondary recovery processes.

Capillary pressure existing along the oil-water interface is one important controlling factor. As described above, the high interfacial tension along an immiscible-liquid interface acts to reduce the amount of interfacial area, resulting in a pressure difference between the two liquid phases. The liquid phase present at the concaved side of a curved interface has a higher pressure

condition. This pressure difference which exists along the curved interface is called capillary pressure, and is expressed by Young-Laplace equation (Bear 1979):

$$\Delta p = \frac{2\gamma \cos\theta}{R}$$

Where, Δp = pressure difference/capillary pressure along the interface.

γ = interfacial tension between aqueous and non-aqueous phases,

θ = contact angle along the three phase liquid-liquid-solid interface,

R = radius of curvature of the curved (assuming spherical) interface.

In a water saturated porous medium, the oil phase must overcome a threshold entry pressure applied by the wetting fluid inside the pore to invade the pore spaces (Mercer and Cohen 1990), known as 'capillary displacement pressure' (Levorsen 2001, Hubbert 1953). It can be assumed that the radius of curvature of the interface is equal to the radius of the pore (capillary) diameter. With this assumption, from the above expression, it can be inferred that smaller the pore throat diameters require greater capillary pressure to initiate displacement and fluid invasion. Hubbert (1953) showed that the amount of the capillary displacement pressure required in clay sized particle is 1 to 2 orders of magnitude higher than that for sand sized particles. From the above discussion, it can be hypothesized that relatively greater number of oil blobs can be trapped in a poorly sorted medium, due to the existence of large and small pore diameters. The difference in densities between the oil and water phases result in a buoyancy force which acts as an additional vertical component to the capillary pressure. The combined effect of capillary pressure, interfacial tension, and the buoyancy force can be quantified by two parameters called 'capillary' and 'bond' numbers. Types of trapping mechanisms (e.g. snap off, bypass flow, pore doublet model, etc.), and the effect of capillary and bond number on oil blob mobility and residual saturation have been discussed in detail in Chapter 1.

Previous research has been carried out to understand the blob distribution pattern in particular reservoir media, and various controls on oil residual saturation. A strong correlation has been established between the residual saturation and the capillary number. For a compacted tightly packed medium, such as sandstone, the capillary number required for trapped oil mobilization process is on the order of 10^{-6} (Schramm 2000). In contrast, trapped oil phase in unconsolidated porous media is harder to mobilize requiring higher capillary number. For example crude oil trapped in bead packs and unconsolidated sand requires capillary numbers 2-3 orders higher (10^{-3}) for mobilization to occur (Morrow et al. 1988). Ng et al. (1978) proposed an inverse relationship existing between the blob length and the capillary number required to mobilize a particular blob. Based on this result, Larson et al. (1981) estimated the blob length distribution using a statistical concept of percolation theory, and compared the statistical results obtained for the residual saturation as function of varying capillary number. Wardlaw and Mckellar (1985) proposed a term called "critical capillary number" required for blob mobilization. Any increase in capillary number before achieving the critical number is associated with blob separation and rearrangement of blob distribution.

Recent research has been carried out to understand the nature of pore distribution in different types of reservoir media, and groundwater aquifer systems. Different imaging methods have been used to study, and model the 2-D and 3-D distribution of pore spaces, and transport mechanisms of crude oil and other nonaqueous phase liquids (NAPLs) in many types of porous media. A detailed discussion is given in Chapter 1 on types of imaging techniques used for understanding pore distribution, fluid distribution, fluid transport, and trapping mechanisms within porous-media systems. However, few attempts have been made to understand the nature and factors controlling oil blob morphology distribution and oil extraction and recovery

processes. Of these limited studies, most were ‘destructive’ in nature, whereby the porous medium was destroyed to recover the oil or the NAPL blobs for quantitative measurement. In addition, the ex-situ extraction and separation process of the oil/NAPL blobs themselves, subject to breaking, proves to be difficult to preserve in-situ blob structure, morphology, and distribution. In contrast, this research uses a novel, noninvasive technique to study the crude oil distribution in unconsolidated homogeneous to heterogeneous sands. Synchrotron X-Ray Microtomography (SXM) has been used to capture high-resolution images of the oil-saturated water-wet sand-packed columns before and after prescribed surfactant flooding events. SXM technology works in the same way as the conventional computed tomography (CT) technology; however, it has many advantages over conventional CT applications. High resolution SXM images have been successfully used previously to study porosity, relative permeability, and oil saturation in porous media (Coles et al. 1998). Temporal variations in three dimensional (3-D) distributions of nonaqueous phase liquid (NAPL) in multiphase system has also been successfully studied using this imaging technique (Schnaar and Brusseau 2006a, 2006b).

The objectives of this research focuses on a better understanding of the processes controlling oil recovery by tertiary surfactant flushing applications, through detailed characterization and quantification of oil-blob-distribution and morphology as a function of porous media heterogeneity. Both qualitative and quantitative approaches have been utilized to understand the trapping and transport mechanisms of crude-oil-blobs in increasingly heterogeneous porous media. SXM was used to capture high-resolution three-dimensional images of the saturated-sand-packed-columns injected with two different oil fractions (i.e. light and heavy oil). Quantitative data (such as oil-blob-volume and surface area) for various phases have been determined from the depth integrated grayscale values proportional to the density of

those particular phases. Blob distribution of both oil fractions have been characterized and modeled as function of blob-volume-distribution heterogeneity. The nature of the oil blob morphology, as residual saturation, has been quantified and modeled with respect to available total blob surface area. For a wetting reservoir (previously water saturated), the aqueous phase is the primary phase adsorbed next to the grain boundaries, and the non-wetting phase (oil in this case) is trapped into the inner side of the larger pore spaces. With this idea, it can be assumed that the total blob surface area for a particular blob is equivalent to the oil-water interfacial area. These relationships will be important and highly useful for predicting the trapping mechanisms and saturation potential of a particular type of oil reservoir formation.

Additionally, this research attempts to describe the oil recovery efficiency of a particular medium, in terms of residual saturation and during the surfactant flooding process. Column experiments have been carried out to examine the transient nature of oil blob distribution before and after multiple surfactant flooding events. These experiments will help elucidate some of the issues related to the oil displacement efficiency of the surfactant, distributed in homogeneous sand and mixed sand-carbonate media with varying heterogeneity (in terms of sorting or grain size distribution). Attempts have been made to quantify and model the changes in blob morphology after each flooding event, thereby changing the available interfacial area between the aqueous and solid phases. Also, studies have been carried out to see how the heterogeneities of the media control the shape and distribution of the blobs after each flooding event. Lastly, a comprehensive approach has been taken to establish an empirical relationship between crude oil distribution and morphology, and heterogeneity of the medium.

2.2 MATERIALS AND METHODS

A total of six columns were packed with three types of sands in two sets. The columns were saturated with double deionized water. Each set of three columns was then injected with light and medium gravity crude oil. The columns were flushed with an anionic surfactant in two to three sequential episodes. Multiple SXM images were taken, including one initial image prior to surfactant flooding and images collected after each subsequent surfactant-flooding event (2 to 3 sequential surfactant flooding events).

2.2.1 Materials

Two different fractions of crude oil were chosen as model liquids, West Texas Intermediate crude (BP), with light (41.4°) API gravity and Poseidon crude (BP) with medium (29.6°) API gravity. The oil samples were doped with 10% by volume iodobenzene (Acros Organics, NJ) to improve the image contrast for a particular X-ray absorption energy. The aqueous phase (double-deionized water) was doped with 60 g/L cesium chloride (CsCl, 99.99%, Optical grade from Acros Organics, NJ) for the same purpose. Previous experiments showed no or insignificant change in interfacial tension due to the addition of CsCl dopant in aqueous phase (Schnaar and Brusseau 2006b). However, oil phase doping with iodobenzene (IB) showed slight changes in interfacial tension. These dopants showed the least partitioning to the non-target fluids (Schnaar and Brusseau 2006b). Doping with IB, which has a density (1.82 g/cm^3) higher than water has a slight effect on API gravity of crude oil. After recalculation, the crude oil samples were characterized as light (23.4˚API), and heavy (14.8˚API), respectively (USGS standard). However, the viscosity change, due to this doping effect, was not measured. According to USGS standard, conventional crude oil which has API gravity of 22º or more and a viscosity less than

100 centipoise (cP) is considered as light crude oil. Heavy crude oil is characterized by API gravity ranging from 22 º to 10º, and viscosity ranges between 100cP to 10,000 cP.

A 0.1% (by volume) solution of an anionic surfactant branched alcohol propoxy sulfate, or commercially called Petrostep S-1 (Stepan Chemical Company, Northfield, IL) was used for the surfactant flooding experiments. The relatively low concentration of surfactant was prepared to maximize interfacial tension reduction while still being below the critical micelle concentration (CMC) to initiate oil removal through mobilization processes rather than by micellar solubilization. Experiment regarding CMC estimation for various crude oil fractions with the surfactant solution has been described in detail in chapter 4. This surfactant was chosen for its ability to reduce interfacial tension at very low concentrations. This surfactant has been effectively used to mobilize crude oil remediation from shallow aquifers. It has also showed high salinity tolerance and is therefore assumed to be applicable for reservoirs with high salinity. In addition, this surfactant also showed minimal adsorption to the solid phase (Goddard et al. 2004).

Three types of sediments, with increasing heterogeneity, have been used to represent the porous media. The heterogeneity of the medium can be expressed in terms of uniformity coefficient ($C_U = d_{60}/d_{10}$), estimated by the ratio of the 60th percentile to the 10th percentile grain-size diameters in a grain-size distribution curve. The Accusand® sediments are commercially available (Unimin Corporation, Ottawa, MN), and were classified as homogeneous 40/50 Accusand ($C_U = 1$), mildly heterogeneous mixed Accusand ($C_U = 5.8$), and highly heterogeneous, accusand mixed with fine grained carbonate clay ($C_U = 10.6$). The latter two heterogeneous mixed accusands were prepared in the laboratory, in order to achieve specific uniformity coefficients of interest. Porosity and permeability for the homogeneous 40/50 accusand are 0.33 and 9×10^{-11} m^2, respectively. Porosity and absolute permeability have been

measured for the two heterogeneous media in the laboratory. Mildly heterogeneous medium (MHM) has a porosity of 0.27, and a permeability 3.6×10^{-11} m^2, and the highly heterogeneous medium (HHM) has a porosity of 0.25 and a permeability of 5.4×10^{-11} m^2. Table 2.1 shows the properties of these three porous media in detail.

2.2.2 Residual Saturation and Surfactant Flooding

Thin-walled aluminum columns were dry-packed with porous media. The columns were approximately 4.4 cm long, with Swagelok end-fittings on the top and bottom. The inner diameter of the columns was approximately 0.5 cm. However, the available imaging length varied from approximately 1.0-1.7 cm because the top and the bottom of the columns were fitted with Swagelock end-fittings which inhibited the penetration of the X-ray beam through these portions. Therefore, two aluminum caps were used at the column top and bottom, to occupy these obscured shaded regions. Polypropylene frits were used between the porous medium and the aluminum caps to hold the loose particles intact along the column boundaries, and to avoid any preferential flow of the fluids through the porous medium.

The sand pack columns were purged with carbon-dioxide (CO_2) to displace all of the air captured within the pore spaces. The columns were then saturated with de-aired double-deionized water for several pore volumes (PV) vertically upward, using a single piston, HPLC pump (Acuflow series II). The saturation process continued for 48 hours with a linear velocity of 6 cm/hour. After the initial saturation was completed, columns were injected with 4 PVs of crude oil, vertically downward, at a linear velocity of 4 cm/hour with a syringe pump (Model: 780100, KD Scientific, Holliston, MA). The columns were then flushed with a CsCl solution to establish residual saturation, by displacing the oil blobs, as a discontinuous distribution. The residual

saturation process was carried out in two steps: 2 PV with a flushing rate of 6-10 cm/hour (linear velocity) and 10 PV with a flushing rate of 20 cm/hour. Capillary number (Table 2.2), calculated for this displacement process was estimated to be approximately 1.2×10^{-3} for both light and heavy gravity oil flow in the 40/50 homogeneous accusand porous medium. Capillary number for the other two heterogeneous media experiments varied in the range of 1.41×10^{-3}. Previous research related to trapping and mobilization oil phase in unconsolidated bead packs (Wardlaw and McKellar 1985, Morrow et al. 1988) showed that the residual saturation in the range of 50% to more than 75% can be attained in this range. This additional entrapment force can be attributed to the high aspect ratio due to relatively greater radius of the bead pack pores and can be compared with the capillary number estimated in this research. After residual saturation was completed, the columns were sealed and imaged by SXM.

The columns were flooded with 0.1% anionic surfactant solutions doped with 60 g/L aqueous concentration of cesium chloride. It was assumed that no or insignificant dissolution of crude oil would have taken place below CMC level and during the time-scale of the experiments. Therefore, as mentioned previously, it is expected that the oil blobs would be mobilized and extracted from the system only due to reduce interfacial tension. Subsequent to the establishment of residual oil saturation and initial SXM scan, surfactant flooding was implemented in two to three steps. First, 2-PVs of surfactant solution were pumped through initial oil saturated column at a linear pore velocity of 20 cm/hr, and then scanned using SXM to resolve the oil distribution. The column was then pumped with 3-PVs (5-PVs total) of surfactant solution at the same velocity (20 cm/hr) and then scanned using SXM to resolve the resulting oil distribution within the column. An additional 4-PVs of surfactant flushing (9-PVs total) at 20 cm/hr was conducted for the medium gravity oil (recalculated as heavy oil) saturated in the mildly heterogeneous

porous medium (C_U = 5.8). A total of three SXM scans were made for each column, including one initial scan and two scans after each surfactant flooding event. One additional image was taken, for the heavy gravity oil saturated in the mildly heterogeneous medium, after the third 4-PV surfactant flooding event.

2.2.3 Synchrotron X-Ray Microtomography

All images were taken at the GeoSoilEnviroCARS (GSECARS) BM-13D, at the Advanced Photon Source (APS) Argonne National Laboratory, Illinois. Synchrotron X-ray Microtomography has many advantages such as the high intensity (high photon flux density), highly collimated and monochromatic or single energy rays, which are uniform across the entire beam, resulting in exceptionally high-resolution imaging capabilities (Wildenschild 2002, Flannery et al. 1987). Images of different phases (oil and water) can be taken simultaneously by changing the X-ray incident energies using a monochromator. When the X-ray beam passes through a particular object, it is absorbed and attenuated at particular threshold energy, called the critical absorption energy. After passing through the object the X-rays pass through a synthetic scintillator to be converted into the visible light. These visible rays are then reflected at an angle of 45˚ and magnified, before being captured by CCD camera (Al-Raoush and Willson 2005). A series of images can be captured from multiple directions by rotating the object at particular angular interval. The final image shows a linear depth-integrated grayscale image, where the darker gray indicates greater absorption. This gray scale level is a function of the atomic number and the X-ray energy, and can closely be correlated with the density of the imaged object (Ketcham 2001, Wildenschild 2002). Approximately 1400 to 1600 two-dimensional slices were produced for the 1.0-1.5 cm imaging length of one column. The images were preprocessed

(correction for dark current and white field) and reconstructed using software called Tomo_Display (written by Dr. Mark Rivers, ANL) at the APS. The reconstruction process was performed in multiple steps associated with the building of sinograms in terms of logarithmization, and correction of rotation axis with respect to the center of the image. The reconstruction process also involves removing any artifacts, and it applies a reconstruction algorithm to estimate the spatial variation of the attenuated values in inverse method, producing 2-D reconstructed slices. After the reconstruction process is completed, the fluid phases with high absorption appear brighter.

The images of the three phases have been captured at three incident energy levels with a spatial resolution ranging from 9.9-10.3 μm. The columns were scanned at energies above (36.085 KeV) and below (33.269 KeV) the cesium critical absorption edge, and were subtracted to resolve the aqueous phase doped with cesium chloride. The images scanned at energies below the cesium edge (or above the iodine edge, 33.269 KeV), and below the iodine edge (33.0169) have been subtracted to resolve the oil phase (i.e. non-aqueous fluid). Additional post-processing was carried out to stack all two-dimensional images of a single column, to generate a three-dimensional image for the entire column and portions along the column boundary were "cropped" to avoid unwanted artifacts due to wall effects such as preferential flow or unrealistic pools. Ketcham (2005) describes all these post processing methodologies, in detail, carried out by software called Blob3D. Several tools available in Blob3D have been used to improve image quality prior to stacking. Median smoothing (grayscale-to-grayscale algorithm) was used to reduce inherent noise in order to enhance the edge of the oil blobs from the surrounding non-target phases. This process involves the application of a particular grayscale value, which is the median value of all other gray-scale values for a chosen radius. A determined gray-scale value

was assigned as the threshold value for each oil fraction to convert the images from gray-scale to binary (two-component). In general, a gray-scale value intermediate to the target phase and non-target phase is considered as the threshold value (ASTM 1992). Binary images separate the target fluid as white (gray-scale value 255) from any other phases as black. Finally the images were cropped along X and Y directions (approximately 4mm×4mm) to ignore any saturation attributed to the preferential flow along the column wall. Quantitative data such as volume and surface area for each individual blob have been extracted after binary image separation.

2.3 RESULTS AND DISCUSSION

2.3.1 Capillary Number and Bond Number

The changes in the capillary number and the bond number in response to the application of surfactant solution are reported in table 2.2. The main goal of extraction process was to increase the capillary number by reducing the interfacial tension along oil-water interface. Experimental results show that the true interfacial tension was reduced from16.32 mN/m to 10.66 mN/m for light oil; and from 16.4 mN/m to 11.8 mN/m for the heavy oil fraction. Capillary number for each oil-media system increases for 0.1% (v/v) surfactant flood attributed to reduced interfacial tension. Capillary numbers for the light and heavy oil fractions, in the homogeneous medium, increase from 1.2×10^{-3} to more than 1.6×10^{-3}. The other two heterogeneous media experiments show a capillary number increase ranging from approximately 1.4×10^{-3} to 2×10^{-3} during the extraction of both oil fractions (i.e. light and heavy). However, no separate experiment has been carried out to determine the critical capillary number for each oil-porous medium system. SXM images captured the processes related to trapping and temporal changes of oil blob distribution after surfactant flooding events. A significant amount of raw phase oil was also recovered after surfactant flooding events. These observations reveal that the computed capillary numbers herein would have initiated the mobilization processes and are above the critical capillary numbers. The bond number is a function of the density difference between oil-water, permeability of the porous medium, and the interfacial tension between oil and water. Although, the bond number, for all three systems increase due to the lowering of the interfacial tension, it is only on the order of 10^{-12}, and therefore, has insignificant or no effect on trapping mechanism for these systems.

2.3.2 Light Oil Distribution in Porous Media

The applied Synchrotron X-ray Microtomography imaging technique successfully captured all three phases, oil-water-solid medium, with high resolution. Disconnected oil distribution patterns for both the oil fractions (i.e. light and heavy) can be observed in the images taken above the iodine critical energy incident interval (e.g., figures 2.1, 2.2, 2.3 etc.). The binary transformation process, in Blob-3D software, has successfully separated out the oil phase, which is shown as small 3-D sections (Figures 2.4, 2.5, 2.6 etc.). The light oil fraction experiments show disconnected distribution of blob-volumes, indicating that residual saturation was attained in all three types of porous media. After a total of 5-PVs of surfactant flooding, the light oil fraction shows complete recovery from the homogeneous media, and partial recovery from the other two heterogeneous media (i.e. "mildy heterogeneous" and "highly heterogeneous"). The change in blob morphology, and the interfacial processes are in agreement with the conceptual model described in the introduction section. Surface area of the oil blobs has been increased after each surfactant flooding episode, and the blobs become fragmented into smaller particles, and segregated before being extracted from the system. The blob-volume-distribution patterns for all systems have been modeled as log-normal distribution, and quantitative comparisons were made in terms of distribution-heterogeneity, as residual saturation and before and after the surfactant flooding events. Statistical analyses of crude-oil-blob distribution pattern show possible correlation of the distribution heterogeneity with sorting (porous media grain distribution) and permeability of porous media. Both qualitative and quantitative approaches were carried out to describe the oil-blob-volume distribution pattern, and the changes in oil blob morphology as residual saturation and after each surfactant flooding event. Following is a detailed discussion on the above observations.

Figures 2.4, 2.5 and 2.6 show the cropped sections of the columns packed with three types of porous media, containing light gravity crude oil. 3-D distribution of light oil, as residual saturation, shows a homogeneous distribution of comparatively larger blobs present in the homogeneous 40/50 accusand (Figure 2.4). Residual saturation of light oil, in the two other heterogeneous media (mildly heterogeneous and highly heterogeneous) was dominated by smaller blob volumes. In these two systems the oil phase saturation occurred only along one side of the columns (Figures 2.5 and 2.6), indicating the presence of preferential flow path due to the sorting (poorly sorted) of the grain size, and small scale variation in permeability. The light oil fraction experiments show a maximum change in blob morphology within the homogeneous sand after successive surfactant flooding episodes. The initial light oil residual saturation distribution, prior to surfactant flooding, exist dominantly as rounded blobs but become flattened and fragmented after 2-PVs of surfactant flooding increasing the oil distribution's total surface area dramatically. The initially spherical rounded blobs of light oil present within the mildly heterogeneous porous media do not show any significant change in morphology after surfactant flooding; however, the oil blobs become fragmented into increasingly smaller blobs. Increasing number of smaller blobs also indicates an increase in surface area in response to reduced interfacial tension along water-oil interface. Blobs in the highly heterogeneous porous medium exhibited a significant reduction in blob volume after 5-PVs of surfactant flooding, whereas the mildly heterogeneous sand resulted in relatively smaller reduction in volume for individual oil blobs. Additionally, it can be observed that light oil blobs in the two heterogeneous media are trapped along the relatively high permeability zone of the section. After 5-PV surfactant flood the smaller oil blobs in the highly-heterogeneous porous medium invaded the less permeable section of the medium. With subsequent flooding the solution was able to invade the less

accessible (i.e. reduced-permeability) zones thereby increasing the sweep efficiency allowing enhanced mobilization and re-distribution of oil-blobs within the column. This phenomenon is called “jamin” effect (McAuliffe 1973), which has been described in detail in chapter 3.

Quantitative data (Tables 2.3, 2.4 and 2.5) show a 44% recovery of the light oil from the homogeneous porous medium after the 2-PV surfactant flood. However, there is only 1.3% recovery (i.e. light oil) from the mildly heterogeneous medium and a -3.5% recovery (addition into the system) from the highly heterogeneous medium after 2-PVs of surfactant flooding. The net gain of oil after the first 2-PV surfactant flush can be attributed to an addition of oil fraction that was trapped at an external source beyond the imaged zone. Any gravimetric mass balance for this system is limited due to the potential of significant error associated with this small scale system. Therefore, the saturation estimation has been made based on the image data only. A significant oil recovery (light fraction) was achieved after 5-PVs of surfactant flooding. Complete recovery was attained from the homogeneous sand, whereas 23% and 42% of the total trapped light oil were recovered from the mildly heterogeneous and the highly heterogeneous media respectively. The data show that the total number of light oil blobs, trapped in all three systems, gradually increase after each surfactant flooding event. This trend is consistent with visual observation from the tomographic 3-D distribution images. Total surface area for all the oil blobs have also been increased, for all three systems, after the 2-PV surfactant flood. However, the magnitude of increase is more significant in the homogeneous porous medium (+195%) and highly heterogeneous porous medium (+48%), and far less for the blobs trapped in the mildly heterogeneous medium (+7%). A relatively small reduction in the total blob surface area can be observed for both heterogeneous (i.e. mildly and highly) media after a total of 5-PVs of surfactant flooding (Tables 2.4 and 2.5), which is attributed to the reduction of oil volume due

to the extraction process. The mean-blob-volume of the light oil blobs trapped in the homogeneous and the highly heterogeneous medium are one order higher in volume relative to that are trapped in the mildly heterogeneous medium. Quantitative data show a significant reduction in mean blob volume, approximately one order of magnitude less, for the homogeneous and highly heterogeneous porous media after each surfactant flooding event. Whereas, the blobs trapped into the mildly heterogeneous medium, show less reduction in mean blob volume after each successive surfactant flooding event. These results indicate that both grain size distribution and the permeability have a significant control over the recovery process. As a result, it should be noted that the homogeneous porous medium is characterized by the maximum permeability structure and the mildly heterogeneous medium possesses the minimum permeability among all three media types for the experiments conducted as part of this study.

Statistical analyses were conducted to understand the nature of oil blob distribution pattern and the change in blob morphology for each system. For each system, the cumulative blob distribution pattern was modeled and characterized by log normal distribution (Figures 2.7, 2.9 and 2.11). The lower slope (more spread across a larger grain or oil blob diameter range) of the cumulative distribution curve indicates greater heterogeneity in the distribution pattern. The heterogeneity of the oil blob distribution has been measured by two parameters called the uniformity coefficient (C_U) and coefficient of variation (C_V). C_U is defined as the ratio of the blob-diameters at the 60^{th} and 10^{th} percentile positions in volume distribution curve. C_V is defined as the standard deviation for a particular grain or oil blob size distribution divided by the mean volume for the same distribution. Change in blob morphology and associated amount of available surface area is an important interfacial process that contributes to enhanced recovery processes. Smaller blobs of an immiscible liquid have a tendency to be spherical in shape due to

high interfacial tension. Hence, reduced interfacial tension due to the application of surfactant solution may act to redistribute or fragment oil blobs into different morphologies thereby increasing interfacial area. Figures 2.8, 2.10 and 2.12 show the distribution of light oil blob volume morphology in three types of porous media (homogeneous, mildly heterogeneous, and highly heterogeneous), respectively. The bold black line, in all three figures, represents a model curve for a spherical shape, which depicts the minimum specific surface area for any particular blob volume. Any deviation from the model curve (spherical shape) represents greater surface area. Smaller blobs are usually trapped in a single pore space and can be identified as "singlets", whereas the larger blobs are mainly interconnected "ganglion" type spanning multiple interconnected pore spaces. As a result the larger blobs show the maximum deviation from the spherical shape.

The light oil blob volume distribution, in the homogeneous medium, changes from a homogeneous pattern in residual saturation to a more heterogeneous pattern after the 2-PV surfactant flooding event (Figure 2.7). The oil distribution, as residual saturation, reveals two distinct blob populations. The smaller blob volumes range from 10^{-6} to 10^{-3} mm^3. The larger oil blob population shows more homogeneous distribution and the volume-size varies between 10^{-3} and $\pm 10^{-2}$ mm^3. It is interesting to note that a mixture of large and smaller blob volumes were produced after the 2-PV surfactant flood resulting in a highly heterogeneous blob population. Blob size ranged from 10^{-6} to 10^{-1} mm^3. The smaller oil blob fragments were produced by the segregation of the larger blobs; whereas, the larger blobs can be effectively be produced by the coalescing of smaller blobs. The process of coagulation/coalescence of more than one blob is possible in the high permeability homogeneous unconsolidated medium. Images of the oil phase distribution through the entire column (Figure 2.1) shows the distribution of the larger

coagulated blobs spanning through multiple well-connected pores. The C_U and the C_V measured for residual saturation are 1.7 and 1.9, respectively (Table 2.3). After 2 PVs of surfactant flooding, these values increase to 5.2 and 12.9, respectively, describing a highly heterogeneous blob distribution and indicating a change in distribution as a result of the introduction and flushing with surfactant. Water flushing alone over these short experimental flushing time-scales did not result in any significant change in residual saturation oil blob distribution or morphology. As described above, the smaller blobs as residual saturation are close to a spherical shape (Figure 2.8), whereas the larger blobs ($>10^{-2}$ mm^3), which are mainly ganglia type, showed the greatest deviation from a spherical shape. After the 2-PV surfactant flood all of the blobs trapped in the homogeneous sand showed a maximum deviation from spherical shape, indicating greater expansion or reconfiguration of oil blob surface area. Complete recovery was attained after an additional 3-PV (a total of 5 PV) surfactant flood.

The light oil blobs trapped within the mildly heterogeneous porous medium show a relatively more heterogonous distribution as residual saturation (Figure 2.9). The C_U and the C_V were estimated as 2.6 and 5.1, respectively (Table 2.4), for the initial residual saturation oil distribution. The range of the blob volume varies from 10^{-5} to greater than 10^{-2} mm^3 as residual saturation. The entire blob population becomes smaller after each surfactant flooding event, however, only a small change in the distribution pattern can be observed. The distribution becomes relatively more homogeneous after each flooding event. The C_U and the C_V were calculated as 2.5 and 3.9, respectively, after 2 PVs of surfactant flooding. The oil blob volumes only slightly change after each of the surfactant floods, and the largest blob sizes were reduced to less than 10^{-2} mm^{-3} after the 2-PV surfactant flood. Most of the blobs in the mildly heterogeneous medium do not show a discernable or significant change in the blob morphology (Figure 2.10) or

surface area after the 2-PV surfactant flood, which can be observed in the 3-D distribution SXM images (Figure 2.5). The distribution shows that there was increase (Figure 2.10) in surface area for few blobs (ranging from 10^{-4} to10^{-2} mm^{-3}), however the total blob surface area was decreased by 11%. This result is attributed to the greater recovery (23%) after 5-PV surfactant flood, which resulted in a decrease in the total surface area of all blobs (Table 2.4).

Crude oil (i.e. light fraction) blob distribution in the highly heterogeneous medium (Figure 2.11) shows a homogeneous pattern as initial residual oil saturation and more heterogeneous pattern after the 2-PV surfactant flood. The C_U and the C_V have been calculated as 2.1 and 2.6, respectively, as residual saturation. The pattern of blob distribution as residual saturation is similar to that observed in the homogeneous porous medium. The oil blob population primarily existed as two groups. The smaller blob population ranged in size from 10^{-5} to 10^{-3} mm^3. The larger blobs exhibited a relatively homogeneous distribution with a narrow range in size of approximately $\pm 10^{-3}$ mm^3. The sequential change in oil distribution pattern in the highly heterogeneous medium was similar to the trends observed for the experiments (i.e. light oil) within the homogeneous medium. However, the distribution is slightly more heterogeneous prior to and after all surfactant episodes. After 2 PVs of surfactant flushing, the C_U and the C_V increased to 3.2 and 6.5, respectively, resulting in a relatively higher heterogeneous blob distribution (Table 2.5). This phenomenon indicates that the surfactant flushing event is in fact redistributing the oil trapped within the column. The mean blob volume changed from 1.1×10^{-3} mm^3 as residual saturation to 2.6×10^{-4} mm^3 after the 2-PV surfactant flood. A mixture of both the larger and smaller blobs resulted after the 2-PV surfactant flood. The overall oil distribution pattern also showed a highly heterogeneous trend after this flooding event. The C_U and the C_V were calculated as 3.2 and 6.5 respectively. Blob volume became

significantly smaller after the 5-PV surfactant flooding event, which is represented by the displacement of the distribution curve towards the left hand side (smaller blob particles). The mean oil blob volume was significantly reduced by one order of magnitude (8.2×10^{-5} mm^3) after the 5-PV flood. The segregation of the larger oil blobs into the smaller ones due to reduced interfacial tension (Figure 2.6) may be the primary physical mechanism acting to re-distribute the particles through the highly heterogeneous porous medium system.

The initial residual light oil saturation in the highly heterogeneous porous medium can be characterized by smaller blobs ($<10^{-2}$ mm^3) close to spherical shape, and the largest blobs, greater than $10^{-2}mm^3$, distinctly deviated from a spherical shape. The changes in oil distribution pattern and blob volume morphology were similar to that observed in the homogeneous porous medium. After the 2-PV surfactant flood, a maximum deviation from a spherical shape was observed for the smaller blobs ranging in volume from 10^{-5} to 10^{-3} mm^3. All the larger blobs appear to have been fragmented and disintegrated into smaller particles after 5 PVs of surfactant flushing. Nearly all of the oil blobs showed deviation from the spherical shape after this flooding episode. The maximum deviation in oil blob morphology can be observed in the newly formed larger blobs (ranging from 10^{-4} to10^{-2} mm^3) after the 5-PV surfactant flood. Maximum oil recovery was attained in this system after this 5 PV of surfactant flooding event (42%).

Figure 2.13 shows a comparison of the light oil blob volume distribution as residual saturation for all three porous media types. As described above, the homogeneous and the highly heterogeneous porous media show similar trends in changing blob distribution pattern after each surfactant flooding episode. The difference was only in the size of the blobs. The mean blob volume for the homogeneous medium was larger (4.5×10^{-3} mm^3) in comparison to the highly heterogeneous media (1.1×10^{-3} mm^3). Additionally, both of the media showed a bimodal

distribution of the blobs as residual saturation. In contrast, the blob distribution for the residual oil saturation within the mildly heterogeneous medium was highly heterogeneous and the distribution of blob population was uniformly distributed from small to large, unlike the two distinct blob populations observed in the other two media. With these observations it can be concluded that heterogeneity in the grain size (or sorting) has control over the oil blob volume (size) trapped as residual saturation. A well-sorted homogeneous porous medium with larger overall grain sizes should trap larger blobs, unlike a poorly sorted medium which can trap smaller blob volumes and a greater variance blob volumes due to the smaller and greater range of pore diameters. The permeability of the porous medium also has a significant control over the oil blob distribution pattern. Higher permeability porous media can trap larger blobs with generally more homogeneous distribution patterns, whereas heterogeneous blob distributions are more likely to be established within low permeability media whereby the oil phase can only mobilize through relatively higher permeability networks or zones.

A comparison of the light oil blob volume morphologies, as residual saturation (Figure 2.14) for all three types of porous media, shows that almost all oil blobs in the homogeneous sand, irrespective of size, demonstrate greater deviation from spherical shape. Whereas, the larger blobs in the mildly heterogeneous sand are relatively more non-spherical than the large blobs distributed in the other two media. Moreover, It is to be noted that some of the larger blobs trapped into this medium are bigger in volume than that are trapped in the homogeneous sand (Figure 2.13). Most of the blobs trapped in the highly heterogeneous medium are smaller in size; therefore they tend to be relatively spherical in comparison to the blob sizes trapped in other two media (i.e. homogeneous and mildly heterogeneous). All light oil blobs trapped in the homogeneous sand exhibits maximum deviations from spherical shape, produced maximum

recovery after 2PV flood in comparison to the other two heterogeneous media. The mildly heterogeneous medium, oil blobs became significantly more homogeneous with each subsequent surfactant flood whereby the oil blobs initially existed as a highly heterogeneous distribution as residual saturation. In addition, a continuous but low oil recovery was achieved after each flooding episode. In contrast, the poorly sorted (highly heterogeneous) medium initially can be unproductive in terms of oil recovery, but can result in maximum recovery after many pore volumes of surfactant flushing. In this particular system the initial surfactant flood helps by disintegrating ("breaking up") the larger blobs into smaller blobs, which can then be easily mobilized later, through the smaller pores as the surfactant flooding continues.

2.3.2 Heavy oil distribution in porous media

Experiments were carried out to study the distribution of medium gravity oil in the same three types of media. As mentioned in the material section, the API gravity of the medium gravity oil was increased (recalculated API is 14.8˚) due to the doping process, and henceforth will be called as heavy oil. Figures 2.15, 2.16 and 2.17 show the X-Z sections of the entire columns distributed with heavy oil in the three porous media types. These images show the oil blob distribution as residual saturation, and after each surfactant flooding event. The above images were taken above iodine critical incident energy level, primarily to capture the crude oil phase doped with iodobenzene. It also shows the other phases such as water and solid grain with unaided eye. Low permeability fine grained carbonate particles (< 270 mesh size) (Figure 2.17), however, show a grayscale value close to that of the oil phase, which was removed by image subtraction and grayscale-binary image transformation process (Figures 2.18, 2.19, 2.20). The X-

Z sections of the entire columns show disconnected distribution of the heavy oil blobs in all three media, which indicate that the residual saturation was established.

The three-dimensional (3-D) distribution of the heavy oil in the homogeneous porous medium shows that the oil blobs primarily exist as a distribution of rounded blobs with complex morphologies (Figure 2.18), similar to that observed for the light oil distribution in the same porous medium. Oil blobs were fragmented and flattened after the 2-PV surfactant flush, resulting in a maximum change in the blob morphology and available interfacial area. The heavy oil distribution patterns in the other two heterogeneous media are also similar to those observed for the light oil in those two media. The heavy-oil blobs in the mildly heterogeneous medium also show a homogeneous distribution in the residual saturation and after subsequent flooding events as well (Figure 2.19). Generally, the oil blobs are rounded and close to spherical shape as residual saturation. No significant change was observed in the blob morphology after each surfactant flooding event, however, the number of blobs decreased gradually after each flushing event. Significant oil recovery resulted after the 5-PV and 9-PV surfactant flooding events. Figure 2.19 shows that nearly all of the larger blobs fragment into smaller blobs in the latter phases of surfactant flooding.

The residual saturation of heavy oil in the highly heterogeneous medium (Figure 2.20) showed relatively larger blobs with a high variance in morphology from very rounded and spherical to very complex (i.e. lenses and ganglia) in shape. The number of blobs increased after each surfactant flooding event. Some of the blobs became flattened, resulting in a maximum increase in blob surface area after each subsequent surfactant flood. Most of the large blobs were fragmented into smaller blobs after 5 PVs of surfactant flooding. One important characteristic to note in this medium (highly heterogeneous) is related to the observed temporal changes in the oil

distribution pattern after each surfactant flooding episodes. Initially the blob distribution is characterized by local high oil saturation, which is limited within specific zones along preferential flow paths. These zones of high oil saturation may be attributed to trapping within high permeability zones and restricted (hydraulically inaccessible) by the low permeability carbonate clay (Figure 2.17). Larger oil blobs became fragmented due to reduced interfacial tension and gradually occupied the less impermeable section into the porous medium. After 5 PVs of surfactant flooding smaller blob fragments mobilized and captured the entire 3-D section. This phenomenon is very similar to the light oil distribution in this particular medium (Figure 2.6). This process explains the role of surfactant application to enhance sweep efficiency in the highly heterogeneous medium. In this connection, it is important to note that the heterogeneity for all three media was defined by the grain size distribution or sorting of the media grains. Laboratory measurements showed that that the permeability, which is another important factor of heterogeneity, was the maximum for the homogeneous medium (9 Darcy), and the minimum (3.6 Darcy) for the medium heterogeneous porous medium. Permeability of the highly heterogeneous medium was 5.4 Darcy, although the C_U for this medium was the highest (poorly sorted) and the porosity was the least in comparison to the other two media.

Quantitative data for the heavy oil blob volume and morphology pattern (Table 2.6) in the homogeneous medium show a trend similar to the light oil distribution in the same medium (Table 2.3). The number of blobs and the total surface area of all blobs increased after the 2-PV surfactant flooding episode. The mean blob volume was reduced by one order of magnitude, and the total surface area increased by 87% after the 2-PV flood. A relatively less, 10% oil recovery resulted after the 2-PV flood, and complete recovery resulted after 5 PVs of flooding. In contrast to all other systems, the heavy oil distribution in the mildly heterogeneous medium (Table 2.7)

showed a gradual reduction in the number of blobs after each surfactant flooding event. No significant change occurred in the amount of total blob surface area and the mean blob volume after 2 PVs of flooding. However, after 5 PVs of surfactant flooding, the mean-blob-volume was reduced by one order in magnitude and the total surface area reduced by 30%. The total surface area continued to decrease gradually upon further surfactant flooding resulting in a 41% reduction after 9 PVs of flooding. Increasing oil recovery resulted with continuous surfactant flooding exhibiting a 10%, 41% and 66% recovery after 2, 5 and 9 PVs of flooding, respectively. It is to be noted that the initial distribution of the blobs in this medium were dominated by relatively smaller blobs, approximately one order in magnitude smaller in mean volume than the blobs distributed in the other two media. Additional reduction in blob mean volume occurred after both the 5-PV and 9-PV surfactant flooding events and was attributed to the fragmentation and disintegration process of the small blobs into the smaller singlets. However, the number of the extracted blobs exceeds the number of blobs produced by disintegration process As a result all of the quantitative parameters, such as the number of blobs, mean blob volume, and the total surface area were reduced gradually with each sequential surfactant flood. The blob distribution in the highly heterogeneous medium (Table 2.8) shows a similar mobilization process as has been observed in the homogeneous medium. For example, the number of blobs and the total surface area increased after each surfactant flooding event, and the mean blob volume decreased after the 2-PV flood. One exception observed in this system was the noted gain in oil saturation by 28% (oil added into the system) after the 2-PV flood. However, after the 5-PV surfactant flooding event, the number of blobs increased, the blob mean volume was reduced by one order of magnitude, and oil recovery of 16% occurred from this medium. The gross oil recovery (after the 5-PV flood) was 34%, which includes the 28% gain after 2PV flush. The surface area was

reduced by 5% after 5 PVs of surfactant flooding. All of these results from the highly heterogeneous medium are similar in trend as that observed for the light oil distribution in highly heterogeneous medium.

Following is a statistical and quantitative analysis of blob distribution heterogeneity and the morphological changes of heavy-oil blobs in all three porous media systems for initial residual conditions and subsequent surfactant flooding events. The cumulative blob volume distribution of heavy oil blobs in all three media types are also modeled by log-normal curves. The cumulative distribution of the oil blobs reveal the same trend as that observed for the light oil distribution within the three media types. Changes in the pattern of oil blob morphology also show similarity with the light oil distribution in all three media. The residual distribution of heavy oil in the homogeneous medium (Figure 2.21) is more heterogeneous when compared to the light oil fraction distribution. It can be characterized by a bimodal distribution of larger and smaller blobs. Smaller blobs ranged in size from 10^{-5} to 10^{-3} mm^3, and the larger blobs varied in size from 10^{-3} to 10^{-1} mm^3. Mean blob volume was estimated as 5.7×10^{-3} mm^3 (Table 2.6) as residual saturation. C_U and C_V for the heavy-oil blob distribution (in homogeneous porous media) were approximately 2.0 and 2.6, respectively. After 2 PVs of surfactant flooding the blob distribution became highly heterogeneous, characterized by a blob volume distribution ranging from 10^{-5} to 10^{-1} mm^3 (mean volume 7.1×10^{-4} mm^3). Both C_U and C_V for this resulting blob distribution had higher associated values of 2.6 and 8.5 representing a higher heterogeneous oil blob distribution after 2 PVs of surfactant flooding. The larger blobs present as the initial residual saturation, greater than 10^{-2} mm^3 by volume, exhibit morphologies that deviate greatest from spherical shape (Figure 2.22). These blobs represent the ganglion type oil phase trapped within multiple pore networks. Mean grain diameter of the homogeneous sand is 0.35 mm. If it is

considered that the median diameter for the pores are in the same range, then the estimated pore volume, assuming a spherical pore would be approximately 2.2×10^{-2} mm^3. Blob volumes above this range occupy multiple pores, and the smaller blobs below this volume exist primarily as spherical singlets. For example, smaller blobs, less than10^{-2} mm^3, show less deviation from spherical shape (Figure 2.22). Most of the larger blobs were fragmented into smaller blobs after the 2-PV flooding event. After this flooding event, both large and smaller blobs, ranging in size from 10^{-5} mm^3 to greater than 10^{-2} mm^3, show notable deviation from spherical shape. Recovery was approximately 44% after this surfactant flooding episode (2-PV), and as mentioned before, a complete recovery resulted after 5 PVs of surfactant flooding.

Heavy oil blob distribution in mildly heterogeneous medium (Figure 2.23) is relatively more heterogeneous as residual saturation, and no significant change occurs after subsequent flooding events. Blob volume distribution ranges from 10^{-5} to 10^{-2} mm^3 (Mean volume 1.1×10^{-4} mm^3), which does not change significantly after 2-PV flood. Mean blob volume reduces one order of magnitude after 5-PV flood (8.8×10^{-5} mm^3), and only reduces insignificantly after 9PV flood. C_U varies within $\pm$ 2.3 for all episodes (Table 2.7), and C_V values are 3.3, 4.1 and 3.4 in residual saturation, after 2-PV and 5-PV flood respectively. C_V value for the distribution after 9PV flood is 2.6, which is slightly more homogeneous than before. There is also similarity in trapping and recovery pattern of heavy oil in this medium with that of light oil distribution in the same medium. Heavy oil shows maximum deviation from the spherical shape in residual saturation (Figure 2.24).With subsequent flooding events, as the blobs become smaller, show a tendency to be more close to the spherical shape. This system also produces a consistent and increasing recovery after each flooding event. Quantitative data reveals a gradual reduction in

total surface area of all the blobs after each flood. This diagram shows that this reduction in surface area is primarily due to the extraction of the blobs, from the system.

Heavy oil blob distribution in highly heterogeneous medium (Figure 2.25) shows similarity in the temporal change of distribution in various episodes, as was observed in the homogeneous medium. The trend is also similar with the light oil distribution in the same highly heterogeneous medium. A relatively homogeneous blob distribution as residual saturation changes to more heterogeneous distribution after 2-PV flood, and again became homogeneous after 5-PV flood. C_U varies from 2.3 in residual saturation to 4.5 after 2-PV and to 3.1 after 5-PV flood. C_V values are 3.2, 8.9 and 6 respectively for all three episodes. The residual saturation shows bimodal distribution of small and large blob populations. Smaller blobs range in volume from 10^{-5} to greater than 10^{-4} mm^3, whereas the larger blobs vary within $\pm\ 10^{-3}$ mm^3. Mean blob volume for this distribution is 8.8×10^{-4} mm^3, which decreases to 2.5×10^{-4} mm^3 after 2-PV flood. The heterogeneous distribution after 2-PV flood contained smaller blobs and few larger blobs as well, which were greater in volume than the larger blob present in residual saturation. The quantitative data indicates a gain of oil pool in this period that can be related to the formation of these larger blobs. This added fraction either had an external source, or they were formed from coagulation of the smaller blobs. Coalesce phenomenon is rare for less permeable medium, therefore, the source of these larger blobs were most likely the oil pool trapped into the Swage-lock fitting or into the impermeable carbonate clay of un-imaged section during residual saturation, and was transported and added into the system in later time. The blobs are reduced in mean volume by one order of magnitude (9.2×10^{-5} mm^3) after 5PV flush, and the distribution pattern can be characterized as heterogeneous, though relatively more homogeneous than after 2PV flood. Blob volume ranges in size from 10^{-5} to greater than 10^{-4} mm^3. As has been seen

before, both light and heavy oil show similar behavior in distribution pattern in homogeneous and the highly heterogeneous media. Heavy oil blobs trapped in highly heterogeneous medium (Figure 2.26) also show greater deviation of the blob morphology from the spherical shape after each surfactant flood. The larger blobs, greater than 10^{-3} mm^3, trapped as residual saturation and after subsequent flood showed maximum deviation. However, increasing surface area after 2PV flood does not help in recovery process. Recovery has been achieved only after 5PV flood, when mean blob volume decreased in size and most of the larger blobs were broken into smaller blobs.

With these observations in the background, additional comparison has been carried out to analyze the initial blob distribution pattern (Figure 2.27) and blob morphology (Figure 2.28) of heavy oil in residual saturation trapped in all three media. As described before the distribution pattern in homogeneous and highly heterogeneous media has similar trend, except the blob volumes in the highly heterogeneous medium is one order smaller by volume. Both distributions are characterized by bimodal distribution. The distribution pattern in the mildly heterogeneous sand on the other hand shows continuous distribution of smaller to larger volume blobs and the distribution is slightly more heterogeneous. The initial distribution in the heterogeneous media has approximately same heterogeneity, which is slightly higher than that in the homogeneous medium. The blobs in the mildly heterogeneous medium are one order smaller by mean volume than that in the highly heterogeneous medium and two orders of magnitude smaller by mean volume from that in the homogeneous medium. Since the permeability of the medium is comparatively smaller, most of the blobs trapped in this medium were singlets in compare to the other two media. Although smallest in mean volume the blobs in the mildly heterogeneous medium shows significant deviation from the spherical shape, in residual saturation. The blobs trapped in the highly heterogeneous medium are also relatively smaller in volume than that are

trapped in the homogeneous medium, however, showed a tendency of deviating from spherical shape irrespective of their size. In comparison the larger blobs trapped in the homogeneous medium only showed maximum deviation from spherical shape and the smallest blobs were close to the spherical shape. Blob volume distribution C_U and C_V were plotted in residual saturation as function of the uniformity coefficient of the three media. A value of 1 for these two parameters represents homogeneous distribution. A highly heterogeneous distribution of oil blobs, for both light and medium gravity crude oil can be found for the mildly heterogeneous porous medium. The distribution is relatively more homogeneous, for both oil fractions, in the homogeneous 40/50 accused, and relatively more heterogeneous in highly heterogeneous sand. It is to be noted that the heavy oil fraction shows a relatively higher heterogeneous distribution in residual saturation than that of light oil in the homogeneous medium.

2.4 SUMMARY AND CONCLUSIONS

Experiment has been done to understand the interfacial processes of oil blobs in various types of porous media with increasing heterogeneity in grain size distribution. Trapping mechanism and the mobility of oil blobs through porous media have been studied in terms of blob distribution pattern and change in blob morphology in residual saturation. Blob morphology and therefore available interfacial area changes as a function of interfacial tension. 0.1% anionic surfactant solution has been injected to reduce oil-water interfacial tension. An attempt has been made to correlate the enhanced recovery process, and the change in distribution pattern with respect to the porous medium heterogeneity. Light and heavy gravity (after doping with iodobenzene for imaging purpose) gravity crude oil have been injected in previously saturated sand packed columns. Three types of media have been used with varying uniformity coefficient: homogeneous ($C_U = 1$), mildly heterogeneous ($C_U = 5.8$), and highly heterogeneous ($C_U = 10.6$). Intrinsic permeability for the homogeneous medium is 9 Darcy, and the absolute permeability of the other two heterogeneous media has been measured as 3.6 and 5.4 Darcy respectively. Median grain diameters of these three media are 0.35 mm, 0.27mm. and 0.37 mm respectively. Synchrotron X-ray micro-tomography was used to capture 3-D images of crude oil distribution in residual saturation and after subsequent flooding events with surfactant solution.

Results show homogeneous distribution of both the oil fractions, in residual saturation, within the homogeneous medium. The heavy oil fraction shows relatively higher C_U and C_V for the blob distribution in this particular medium. This homogeneous distribution in residual saturation changes to highly heterogeneous distribution after 2PV flood. Application of surfactant solution reduces interfacial tension, resulting increment in oil-water interfacial area. This increment is also complemented by breaking down of the oil blobs into smaller particles

after surfactant flood. 3D images and the quantitative data (volume, surface area etc.) show maximum change in blob morphology have been attained after 2PV flood for both the fractions, resulting in increasing surface area. Number of blobs also increases after 2PV flood. 44% and 10% recovery has been attained for light and heavy oil fractions respectively after 2PV flood, and complete recovery has been achieved after 5PV flood.

Both oil fractions show relatively more heterogeneous distribution of oil blobs in residual saturation, within the two heterogeneous media. Residual distribution in mildly heterogeneous medium shows the highest heterogeneity for both the light and the heavy oil fractions. It is important to note that the distribution in this medium contains the smallest mean blob volume, for both fractions compared to any other systems. Additionally, it should be noted that although mildly heterogeneous in grain size distribution, this sand has the minimum permeability among all three types. Permeability of a medium is function of the connectivity and the diameter of the pore spaces. Formation of the smallest blobs may be associated with the smaller pore diameter. Additionally, poor permeability does not allow forming complicated ganglia structure spanning multiple pores. The distribution heterogeneity does not change significantly after surfactant flooding events. After 2PV flood light oil fraction shows increment in blob numbers, and a small increase in blob surface area, whereas the heavy oil shows a continuous decrease in blob number and the total surface area. Both the oil fractions show continuous steady recovery after each flooding vent from mildly heterogeneous medium.

The oil blob distribution in the highly heterogeneous medium shows similar distribution pattern with that in the homogeneous medium. However, the mean blob volume trapped in the highly heterogeneous medium are one to two order magnitude smaller in all the episodes. The residual saturation blob distribution curve for both light and heavy oil fractions follow the same

trend in changing distribution pattern as has been found in homogeneous medium. The residual saturation for both the fractions in highly heterogeneous medium is heterogeneous: C_U and C_V are 2.1 and 2.6 respectively for light oil, and 2.3 and 3.2 for heavy oil. The distribution changes to more heterogeneous after 2PV flood for both oil fractions. The mean blob volume for both oil fractions also reduces by one order of magnitude after this flooding event. The distribution for both the fractions remains heterogeneous after 5PV flood; however, the mean blob volume reduces to approximately 2 orders of magnitude. Blob morphology for both fractions also show significant deviation from the spherical shape after each flooding episode. No significant recovery has been achieved for both oil fractions after 2PV flood. However, significant recovery has been attained after 5PV flood: 44% for light oil and 34% gross recovery for heavy oil. Permeability can be one controlling factor for morphological change, which allows the oil blobs to expand in surface area in response to surfactant flooding event. This highly heterogeneous medium has permeability higher than the mildly heterogeneous medium. Therefore, more surface expansion can be observed in this system. However, it can be inferred that a certain blob mean volume should be attained for a particular system, before the blobs can be mobilized and extracted from the medium.

With all these observation, it can be concluded that the heterogeneity of porous media in terms of sorting or grain size distribution can control the heterogeneity of blob distribution in residual saturation. However, the permeability of the medium also has the control over blob mobilization and distribution pattern. The size of the blobs in residual saturation is an important factor controlling recovery process after subsequent surfactant flooding process. The smaller the blobs in residual saturation should produce consistently higher recovery. The sorting (heterogeneity) of a porous medium has bigger impact on blob volume determination for a

particular system. For highly porous and permeable homogeneous medium easy recovery can be attained by surfactant solution flood, however, the process can be complicated for the highly heterogeneous medium. In order to achieve significant recovery the increase in surface area should be complimented by the segregation of larger blobs into smaller blob forming an emulsion, and requires more pore volume surfactant flood for significant recovery process.

RFERENCES

Al-Raoush, R. I., and Willson, C. S. (2005). Extraction of physically realistic pore network properties from three-dimensional synchrotron X-ray microtomography images of unconsolidated porous media systems, *Journal of Hydrology 300 (1-4)*, 44-64. doi: 10.1016/j.jhydrol.2004.05.005.

Bear, J. (1972). *Dynamics of fluids in porous media*. American Elsevier Pub. Co., New York

Chatzis, I. and. Dullien, A. L. (1983). Dynamic Immiscible Displacement Mechanisms in Pore Doublets: Theory versus Experiment, *Journal of Colloid and Interface Science,* 91(1), 199-222, doi: 10.1016/0021-9797(83)90326-0.

Chatzis I., Morrow N.R., and Lim H.T. (1983). Magnitude and detailed structure of residual oil saturation. *Soc. Pet. Eng*., 23, 311-326.

Coles, M.E., Hazlett, R.D., Spanne, P., Soll, W.E., Muegge, E.L., Jones, K.W. (1998). Pore level imaging of fluid transport using synchrotron x-ray microtomography. *Journal of Petroleum Science and Engineering 19 (1-2)*, 55–63

Flannery, B.P., Deckman, H.D., Roberge, W.G. and D'Amico, K.L. (1987). Three-dimensional x-ray microtomography, *Science, New Series*, *237* (4821), 1439-1444

Evans, J., Cade, C., and Bryant, S. (1997). A geological approach to permeability prediction in clastic reservoirs, In Kupecz, J. A., Gluyas, J. and Bloch, S., AAPG Memoir 69, Reservoir quality prediction in sandstones and carbonates, 19 – 27. The American Associatiation of Petroleum Geologist, Tulsa, Oklahoma.

Gluyas, J., Cade, C. A, (1997). Prediction of porosity in compacted sands, In Kupecz, J. A., Gluyas, J. and Bloch, S., AAPG Memoir 69, Reservoir quality prediction in sandstones and carbonates, 19 – 27. The American Associatiation of Petroleum Geologist, Tulsa, Oklahoma.

Goddard, W.A., Tang, Y., Shuler, P., Blanco, M., Jang, S.S., Lin, S.T., Maiti, P., Wu, Y., Iglauer, S., and Zhang, X. (2004). Lower cost methods for improved oil recovery via surfactant flooding: final report. Department of Energy DE-FC26-01BC15362

Hubbert , M. K. (1953). Entrapment of petroleum under hydrodynamic conditions *American Association of Petroleum Geologist Bulletin, 37,* 1954-2026doi: 10.1306/5CEADD61-16BB-11D7-8645000102C1865D

Ketcham, R.A. (2005). Computational methods for quantitative analysis of three-dimensional features in geological specimens. *Geosphere, 1*, 32-41.

Ketcham, R.A., Carlson, W.D. (2001). Acquisition, optimization and interpretation of x-ray computed tomographic imagery: application to the geosciences. *Comput. Geosci*., *27*, 381-400.

Kortekaas, T. (1985). Water/oil displacement in crossbedded reservoir zones, *SPE Journal, 25 (6)*, 917-926, doi: 10.2118/12112-PA

Larson, R. G., Davis, H. T., and Scriven, L. E. (1981). Displacement of residual nonwetting fluid from porous media, *Chemical Engineering Science, 36*, 75-85, doi:10.1016/0009-2509(81)80049-8.

Levorsen, A. I. (2001). *Geology of petroleum (2nd Ed.).* The AAPG Foundation. Tulsa, Oklahoma.

McAuliffe, C. D., (1973). Oil-In-Water Emulsions And Their Flow Properties In Porous Media, *Journal of Petroleum Technology, 25, (6),* 727-733, doi: 10.2118/4369-PA

Mercer, J.W., and Cohen, R.M. (1990). A review of immiscible fluids in the subsurface: properties, models, characterization and remediation, *journal of Contaminant Hydrology, 6 (2)*,107-163. doi:10.1016/0169-7722(90)90043-G

Morrow, N.R., Chatzis, I., and Taber, J.J. (1988). Entrapment and mobilization of residual oil in bead packs, *SPE Reservoir Engineering, 3 (3)*, 927-934, doi: 10.2118/14423-PA

Morrow, N.R., and Chatzis, I. (1982). Measurement and correlation of conditions for entrapment and mobilization of residual oil. *Dept. Energy Report, 10310* (20), 59.

Morrow, N. R. (March 1971). Small-scale packing heterogeneities in porous sedimentary rocks, *The American Association of Petroleum Geologists Bulletin 55 (3)*, 514-522, doi: 10.1306/5D25CF6F-16C1-11D7-8645000102C1865D

Ng, K. M., Davis, H.T. and Scriven, L.E.(1978). Visualization of blob mechanics in flow through porous media, *Chemical Engineering Science, 33 (8)*, 1009-1017, doi: 10.1016/0009-2509(78)85004-0.

Powers S.E., Abriola L.M., and Weber W.J. (1992). An experimental investigation of nonaqueous phase liquid dissolution in saturated subsurface systems: steady state mass transfer rates. *Water Resour. Res., 28*, 2691-2705.

Reeves, P., and M. Celia (1996). A Functional Relationship Between Capillary Pressure, Saturation, and Interfacial Area as Revealed by a Pore Scale Network Model, Water Resource Research, 32(8), 2345-2358.

Ringrose, P.S., Sorbie, K.S., Corbett, P.W.M., Jensen, J.L. (1993). Immiscible flow behaviour in laminated and cross-bedded sandstones, *Journal of Petroleum Science and Engineering,* 9 (2),103-124, doi: 10.1016/0920-4105(93)90071-L.

Schnaar, G., and Brusseau, M.L. (2006a). Characterizing pore scale configuration of organic liquid in multiphase systems with synchrotron X-ray microtomography. *Vadose Zone Journal*, *5*, 641-648.

Schnaar, G., and Brusseau, M.L. (2006b). Characterizing pore-scale dissolution of organic immiscible liquid in natural porous media using synchrotron X-ray Microtomography. *Environ. Sci. Technol*., *40*, 6622-6629.

Schramm, L.L. (2000). *Surfactants: fundamentals and applications in the petroleum industry.* Cambridge, N.Y., Madrid. Cambridge University Press.

Stegemeier, G.L. (1976). Mechanism of entrapment and mobilization of oil in porous media. In Shah, D. O., Schechter, R. S. (Eds.), *Improved Oil Recovery by Surfactant Flushing and Polymer Flooding*. Academic Press, New York.

Taber, J.J. (1969). Dynamic and static forces required to remove a discontinuous oil phase from porous media containing both oil and water, *SPE Journal, 9(1)*, 3 – 12, doi: 10.2118/2098-PA.

Van Lingen, P.P., Bruining, J., and van Kruijsdijk, C.P.J.W (1996). Capillary Entrapment Caused by Small-Scale Wettability Heterogeneities, *SPE Reservoir Engineering 11, (2)*, 93-100, doi: 10.2118/30782-PA.

Wardlaw, N. C., McKellar, M. and Yu, L. (1988). Pore and throat size distributions determined by mercury porosimetry and by direct observation. *Carbonates and Evaporites. 3(1),* 1-16. doi: 10.1007/BF03174408

Wardlaw, N. C., and McKellar, M. (1985). Oil blob populations and mobilization of trapped oil in unconsolidated packs. *Canadian Journal of Chemical Engineering*, *63*, 525-531, doi: 10.1002/cjce.5450630401

Wardlaw, N. C. (1982). The effects of geometry, wettability, viscosity and interfacial tension on trapping in single pore-throat pairs, *Journal of Canadian Petroleum Technology, 21(3)*, 21-27, doi:10.2118/82-03-01

Wildenschild, D., Hopmans, J.W., Vaz, C.M.P., Rivers, M.L., Rikard, D., and Christensen, B.S.B. (2002). Using X-ray computed tomography in hydrology: systems, resolutions and limitations. *Journal of Hydrology, 267*, 285-297.

Table 2.1 Properties of three types of porous media

Properties	Homogenous sand (Accusand 40/50)	Mildly Heterogeneous sand	Highly Heterogeneous sand
Median Grain Diameter, d_{50} (mm)	0.35	0.27	0.37
Uniformity Coefficient, C_U	1.00	5.8	10.6
Bulk Density (disturbed) [g/cm^3]	1.75	1.97	1.95
Wet Porosity	0.33	0.27	0.25
Permeability (m^2)	9E-11	3.6E-11	5.4E-11

Table 2.2 List of physical parameters controlling the mobilization process in three types of porous media.

Media type	Homogeneous sand 40/50 accusand (C_U = 1)		Mildly Heterogeneous sand Mixed accusand (C_U = 5.8)		Highly Heterogeneous sand Mixed accusand carbonate (C_U = 10.6)	
Oil fraction	Light	Heavy	Light	Heavy	Light	Heavy
Residual Saturation						
True IT (γ) dyne/cm	16.32	16.42	16.32	16.42	16.32	16.42
Capillary number	1.16E-03	1.15E-03	1.42E-03	1.41E-03	1.53E-03	1.52E-03
Bond Number	6.65E-12	3.72E-12	2.22E-12	1.24E-12	3.69E-12	2.07E-12
Trapping number	1.16E-03	1.15E-03	1.42E-03	1.41E-03	1.53E-03	1.52E-03
After Surfactant Flooding						
True IT (γ) dyne/cm	10.66	11.80	10.66	11.80	10.66	11.80
Capillary number	1.78E-03	1.61E-03	2.17E-03	1.96E-03	2.35E-03	2.12E-03
Bond Number	1.02E-11	5.18E-12	3.39E-12	1.73E-12	5.65E-12	2.88E-12
Trapping number	1.78E-03	1.61E-03	2.17E-03	1.96E-03	2.35E-03	2.12E-03

Table 2.3 Quantitative data for light oil (23.4˚ API) in homogeneous (C_U =1) sand

Parameters	Residual	After 2PV flood	After 5 PV flood
No. of blobs (single particles)	1628	12541	N/A
Mean Volume (cu mm)	4.496E-3	3.282E-4	N/A
Blob Uniformity Coefficient (C_U)	1.737	5.209	N/A
Coefficient of variation (C_V)	1.864	12.937	N/A
Total Surface Area (mm^2)	284.924	840.989 (+195%)	N/A
Total volume (mm^3)	7.318	4.116 (Recovery 44%)	0 (Recovery 100%)

Table 2.4 Quantitative data for light oil (23.4˚ API) in mildly- heterogeneous (C_U =5.8) sand

Parameters	Residual	After 2PV flood	After 5 PV flood
No. of blobs (single particles)	4357	5367	7504
Mean Volume (cu mm)	7.715E-4	6.181E-4	3.473E-4
Blob Uniformity Coefficient (C_U)	2.616	2.471	2.403
Coefficient of variation (C_V)	5.067	3.88	3.787
Total Surface Area (mm^2)	231.914	248.826 (+7%)	220.368 (-11%)
Total volume (mm^3)	3.361	3.317 (Recovery 1.3%)	2.605 (Recovery 23%)

Table 2.5 Quantitative data for light oil (23.4˚ API) in highly-heterogeneous (C_U =10.6) sand

Parameters	Residual	After 2PV flood	After 5 PV flood
No. of blobs (single particles)	2107	8957	15673
Mean Volume (cu mm)	1.053E-3	2.561E-4	8.209E-5
Blob Uniformity Coefficient (C_U)	2.137	3.159	3.133
Coefficient of variation (C_V)	2.567	6.527	30.758
Total Surface Area (mm^2)	119.019	175.684 (+48%)	174.133 (-1%)
Total volume (mm^3)	2.217	2.294 (Recovery -3.5%)	1.287 (Recovery 42%)

** 42% is the net recovery compared to residual saturation. Gross recovery after 5PV was 44%*

Table 2.6 Quantitative data for heavy oil (14.8˚ API) in homogeneous sand

Parameters	Residual	After 2PV flood	After 5 PV flood
No. of blobs (single particles)	740	5381	N/A
Mean Volume (cu mm)	5.738E-3	7.101E-4	N/A
Blob Uniformity Coefficient (C_U)	1.967	2.592	N/A
Coefficient of variation (C_V)	2.585	8.474	N/A
Total Surface Area (mm^2)	151.571	282.708 (Change 87%)	N/A
Total volume (mm^3)	4.246	3.821(Recovery 10%)	0(Recovery 100%)

Table 2.7 Quantitative data for heavy oil (14.8˚ API) in mildly-heterogeneous (Cu =5.8) sand

Parameters	Residual	After 2PV flood	After 5 PV flood	After 9 PV flood
No. of blobs (single particles)	18278	17295	14146	8886
Mean Volume (cu mm)	1.074E-4	1.02E-4	8.241E-5	7.473E-5
Blob Uniformity Coeff. (C_U)	2.303	2.349	2.265	2.245
Coefficient of variation (C_V)	3.322	4.057	3.380	2.615
Total Surface Area (mm^2)	203.839	198.943 (-2%)	140.326 (-30%)	82.467 (-41%)
Total volume (mm^3)	1.962	1.764 Recovery 10%)	1.166 (Recovery 41%)	0.664 (Recovery 66%)

Table 2.8 Quantitative data for heavy oil (14.8˚ API) in highly- heterogeneous (Cu =10.6) sand

Parameters	Residual	After 2PV flood	After 5 PV flood
No. of blobs (single particles)	3252	14809	24345
Mean Volume (cu mm)	8.799E-4	2.475E-4	9.926E-5
Blob Uniformity Coefficient (C_U)	2.329	4.451	3.104
Coefficient of variation (C_V)	3.188	8.932	6.088
Total Surface Area (mm^2)	167.036	341.465 (+104%)	325.070 (-5%)
Total volume (mm^3)	2.860	3.665 (Recovery -28%)	2.416 (Recovery 16%)*

** 16% is the net recovery compared to residual saturation. Gross recovery after 5PV was 34%*

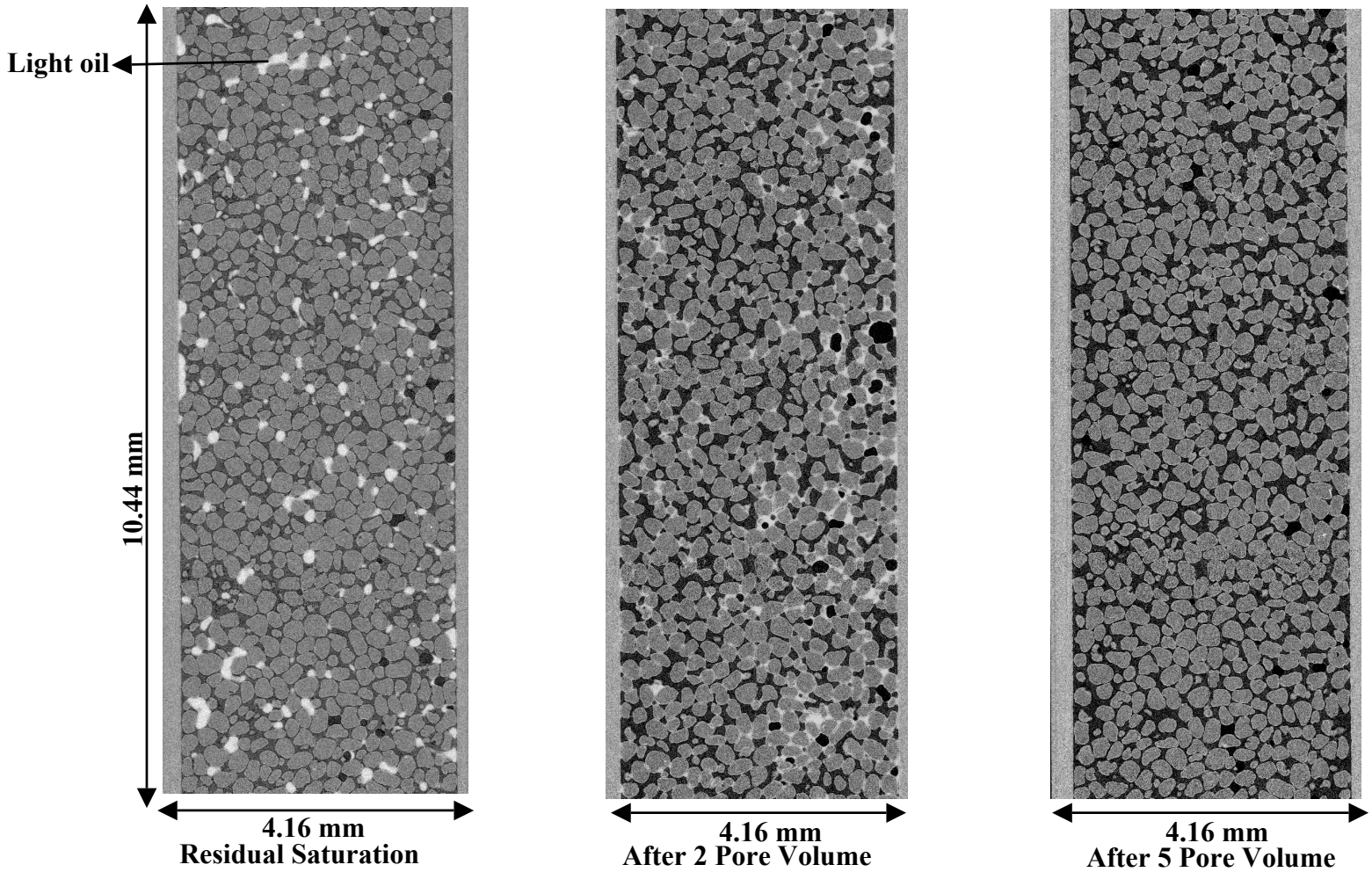

Figure 2.1. Vertical sections of a column along the X-Z direction showing the distribution of light crude oil (23.4˚ API) and aqueous phase within the homogeneous porous medium (40/50 Accusand, $C_U = 1$). From left: residual saturation, and after the 2, and 5-pore-volume (PV) surfactant (0.1% v/v) flooding events. Complete recovery was achieved after the 5-PV flood.

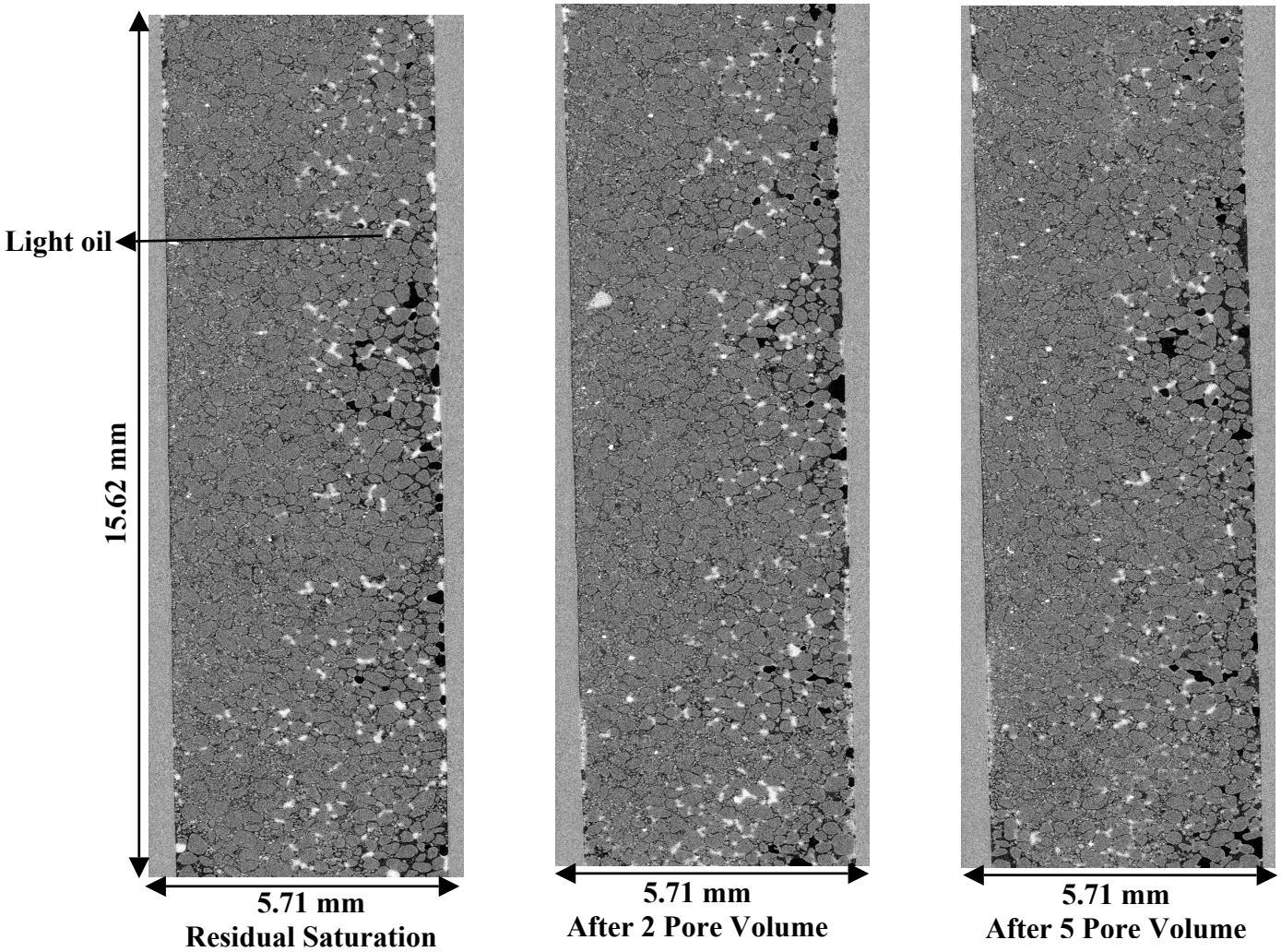

Figure 2.2. Vertical sections of a column along the X-Z direction showing the distribution of light crude oil (23.4˚ API) and aqueous phase within the mildly-heterogeneous porous medium (mixed Accusand, $C_U = 5.8$).

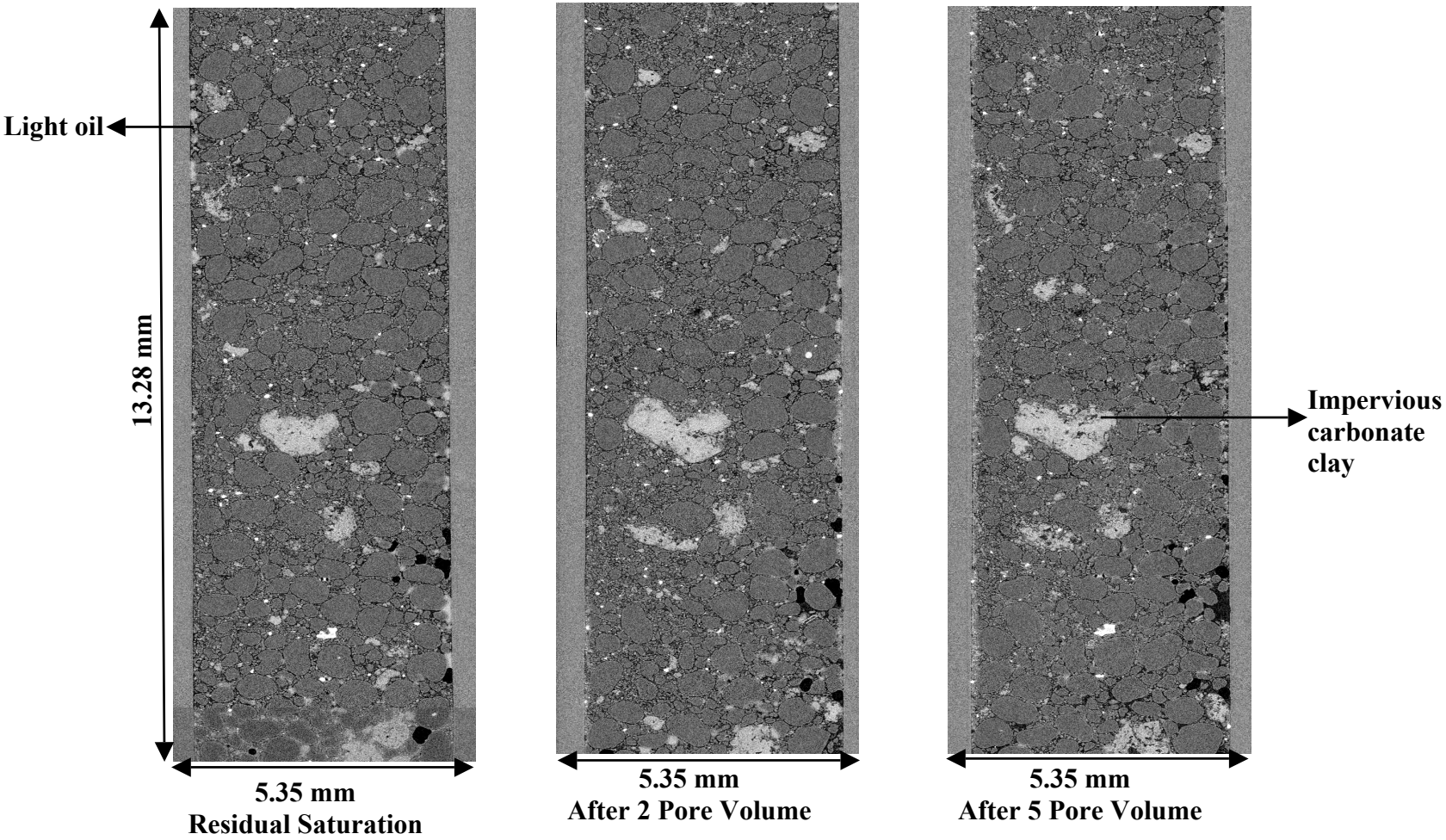

Figure 2.3. Vertical sections of a column along the X-Z direction showing the distribution of light crude oil (23.4˚ API) and aqueous phase in the highly-heterogeneous porous medium (mixed Accusand C_U = 10.6).

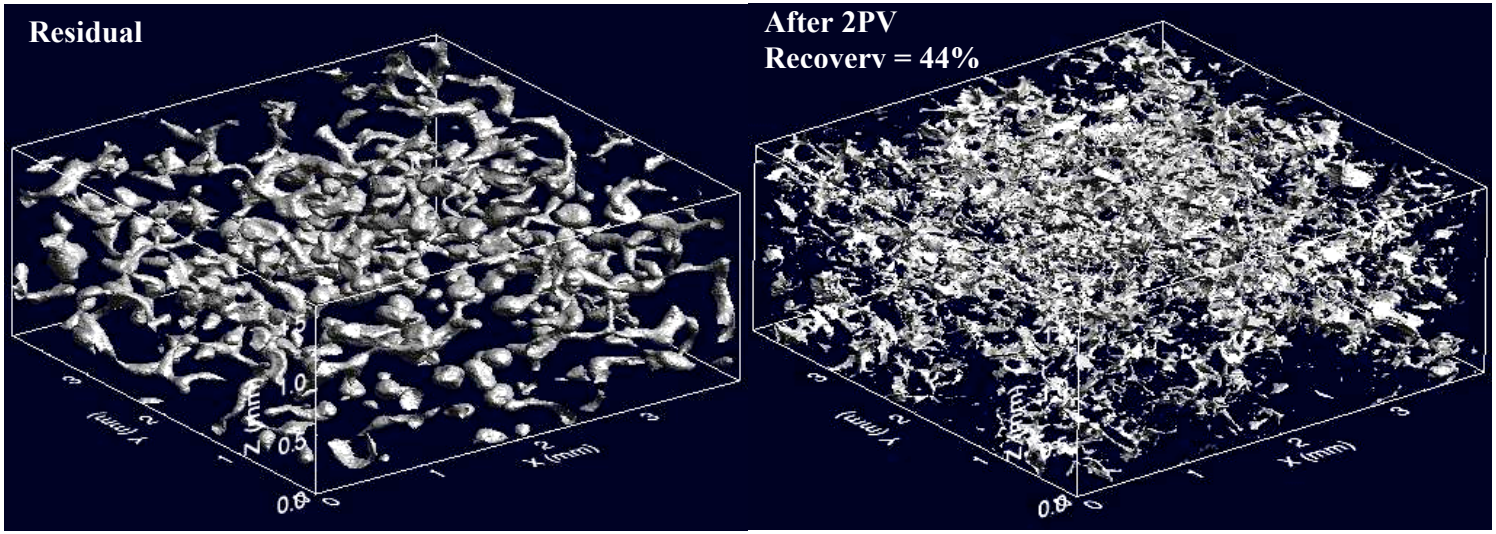

Figure 2.4. 3-D images showing time series of a cropped section (4mm×4mm×1.5mm) of the column (see figure 2.1) containing the light (23.4˚ API) crude oil in the homogeneous porous medium (40/50 Accusand). Light oil segregates into discrete smaller blobs resulting in significant changes in blob morphology after the 2-PV surfactant (0.1% v/v) flood. Complete recovery was obtained after the 5-PV surfactant flood.

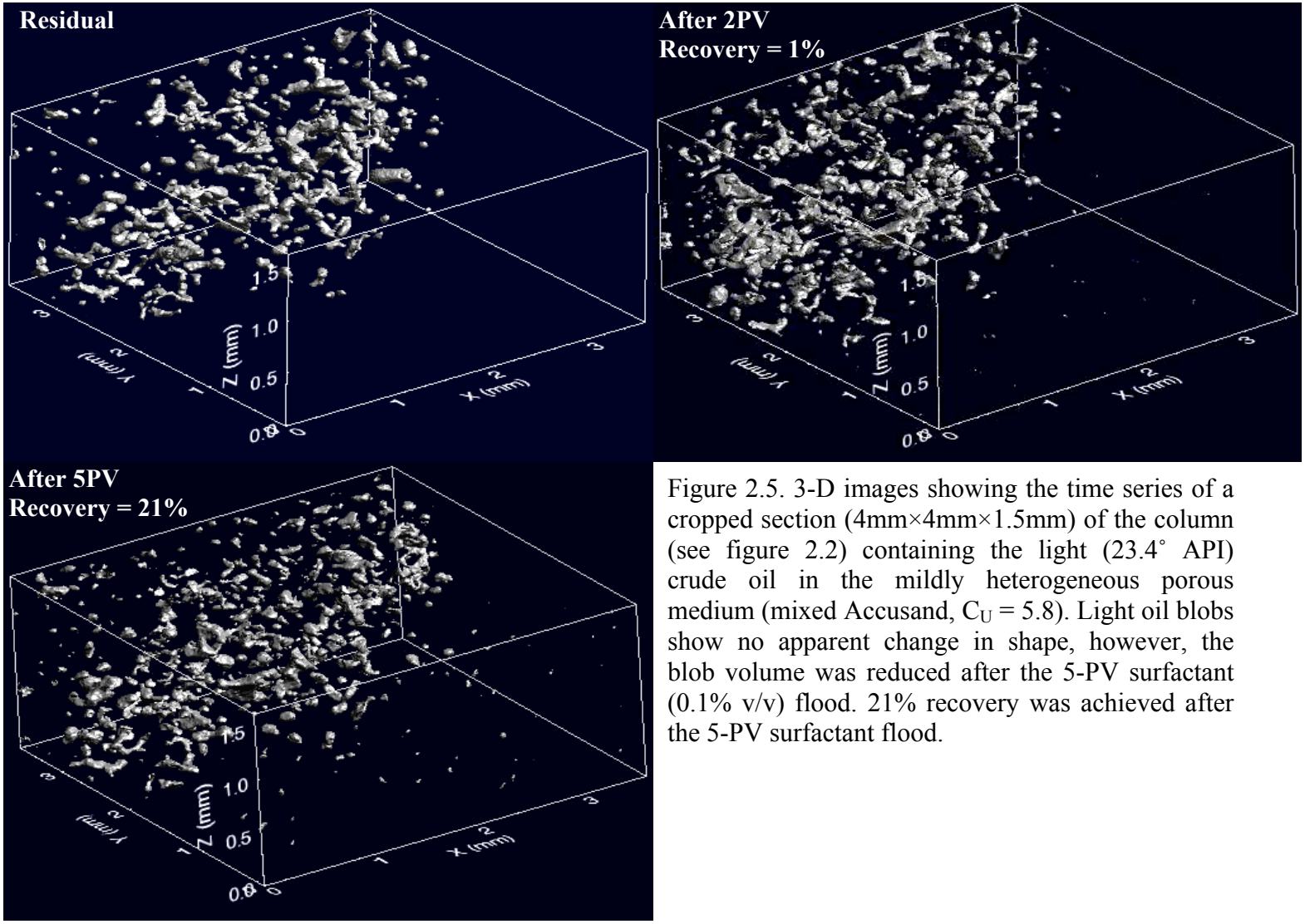

Figure 2.5. 3-D images showing the time series of a cropped section (4mm×4mm×1.5mm) of the column (see figure 2.2) containing the light (23.4˚ API) crude oil in the mildly heterogeneous porous medium (mixed Accusand, C_U = 5.8). Light oil blobs show no apparent change in shape, however, the blob volume was reduced after the 5-PV surfactant (0.1% v/v) flood. 21% recovery was achieved after the 5-PV surfactant flood.

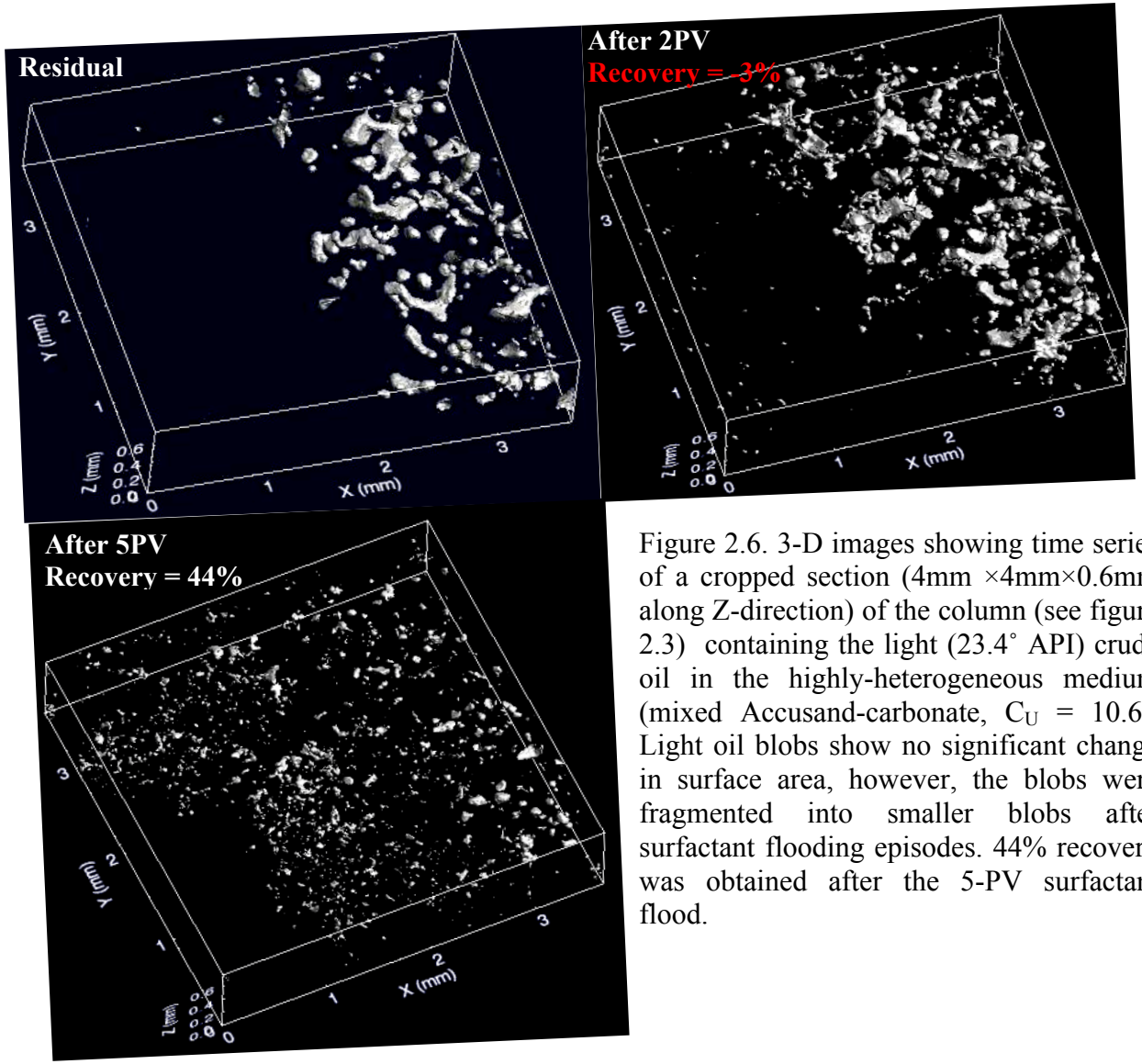

Figure 2.6. 3-D images showing time series of a cropped section (4mm ×4mm×0.6mm along Z-direction) of the column (see figure 2.3) containing the light (23.4˚ API) crude oil in the highly-heterogeneous medium (mixed Accusand-carbonate, C_U = 10.6). Light oil blobs show no significant change in surface area, however, the blobs were fragmented into smaller blobs after surfactant flooding episodes. 44% recovery was obtained after the 5-PV surfactant flood.

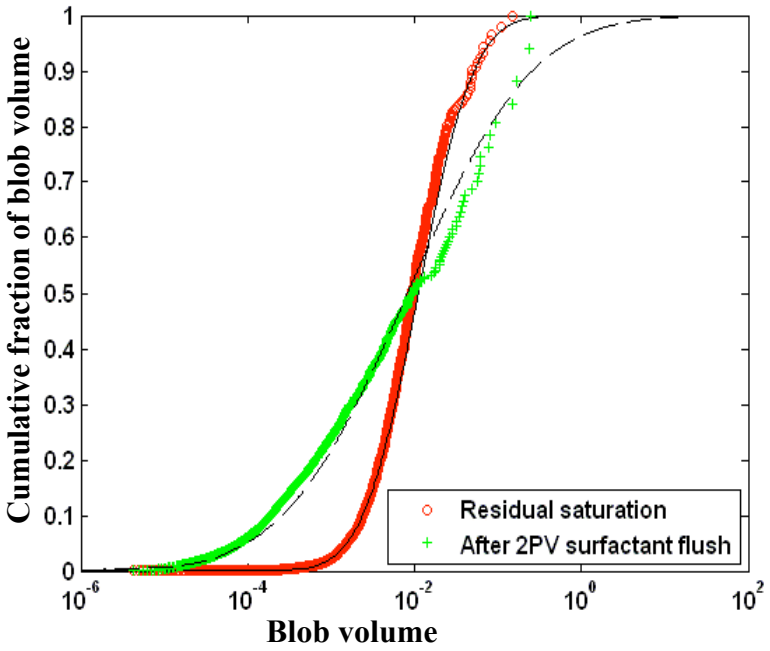

Figure 2.7. Cumulative distributions of the light oil blob volume in the homogeneous 40/50 Accusand (see figures 2.1 and 2.4). Blob-volume-distribution trends changed from homogeneous (initial residual saturation) to more heterogeneous after the 2-PV surfactant flood.

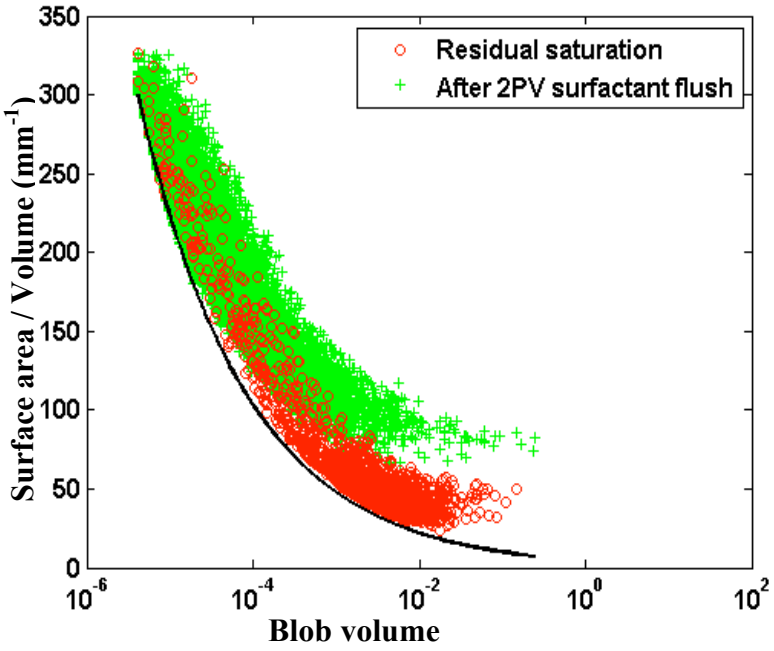

Figure 2.8. Plot showing the distributions of light-oil blob surface area in the homogeneous 40/50 Accusand (also refer figures 2.1 and 2.4). The bold black line represents model curve for a spherical shape for any particular volume. Deviation from spherical shape represents greater surface area. Light oil blobs show greater deviation from spherical shape after the 2-PV flood, resulting in increased blob surface area in response to the reduced interfacial tension by surfactant flooding.

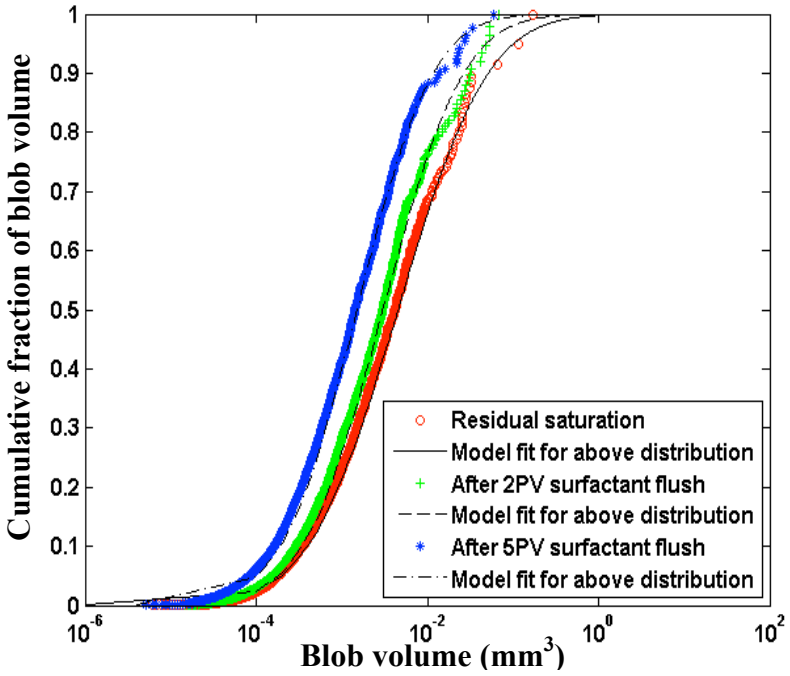

Figure 2.9. Cumulative distributions of light oil blob volume within the mildly-heterogeneous porous medium (C_U = 5.8, see figures 2.2 and 2.5). Oil blobs become smaller after each surfactant-flooding event, and the distribution pattern becomes slightly more homogeneous after each flood.

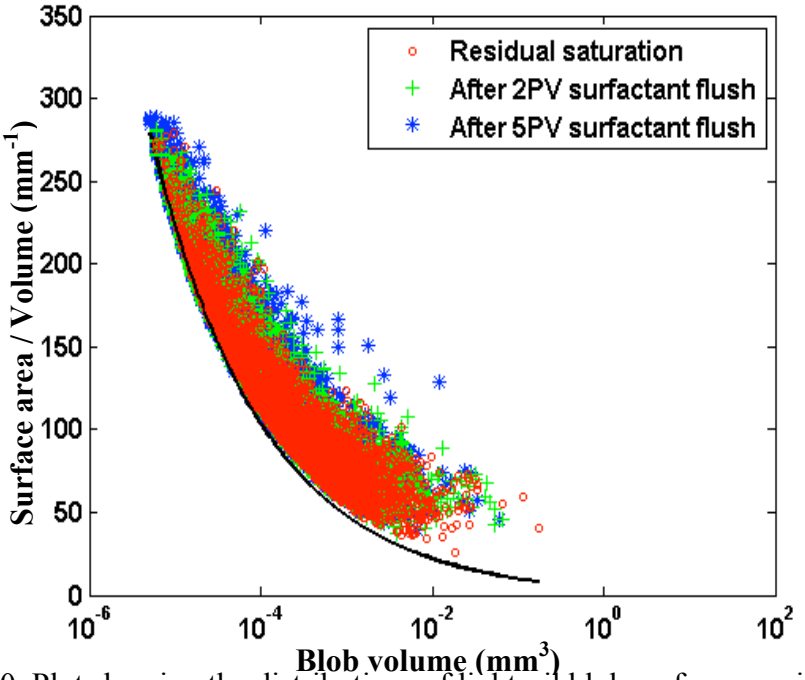

Figure 2.10. Plot showing the distributions of light-oil blob surface area in the mildly-heterogeneous porous medium (C_U = 5.8, see figures 2.2 and 2.5). The bold black line represents a model curve for a spherical shape for a particular blob volume. Any deviation from spherical shape represents greater surface area. Light oil blobs in this system show significant deviation from spherical shape primarily for only the relatively of the larger blobs, after the 5-PV surfactant flood.

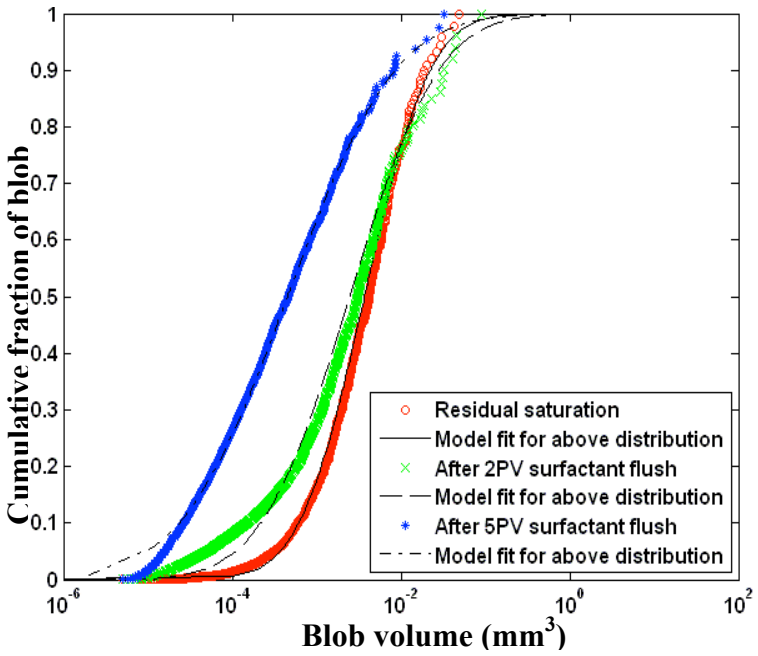

Figure 2.11. Cumulative distributions of light-oil blob volumes in the highly-heterogeneous porous medium (C_U = 10.6, see figures 2.3 and 2.6). Blob-volume-distribution trends changed from homogeneous (initial residual saturation) to increasingly heterogeneous after the 2-PV and 5-PV surfactant floods. Mean blob volume gradually became smaller after subsequent surfactant flooding events.

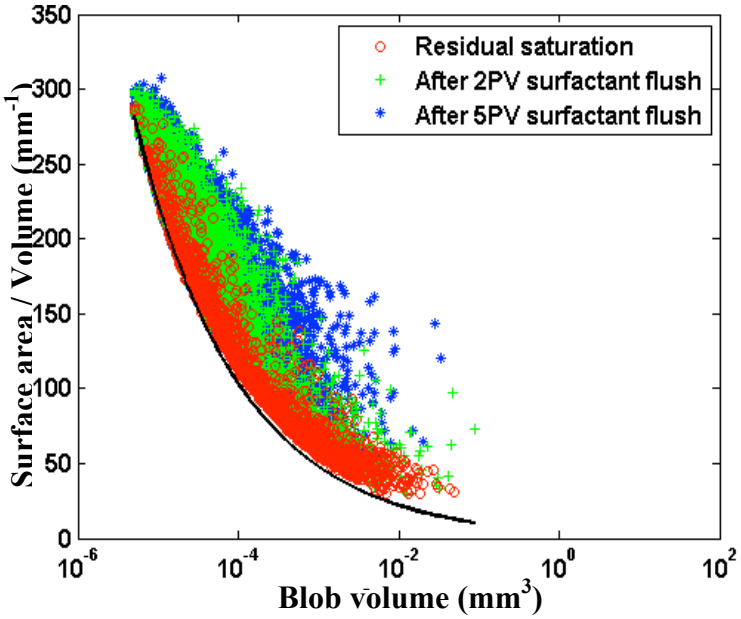

Figure 2.12. Plot showing the distributions of light-oil blob surface area volumes in the highly-heterogeneous porous medium (C_U = 10.6, see figures 2.3 and 2.6). The bold black line represents a model curve for spherical shape for a particular blob volume. Any deviation from the spherical shape represents greater surface area. Smaller blobs show greater deviation from spherical shape after the 2-PV flood, whereas the larger blobs primarily show greater deviation after the 5-PV surfactant flood.

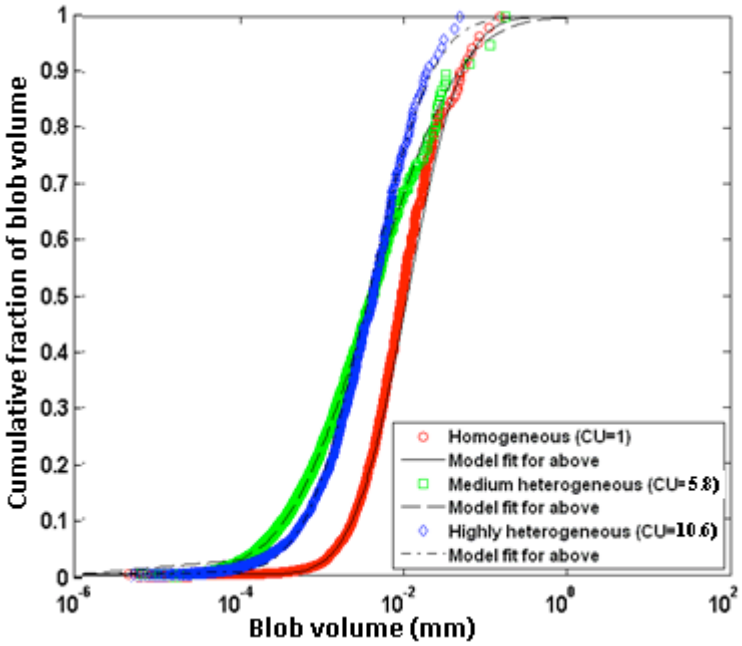

Figure 2.13. Cumulative distributions of light-oil blob volumes as initial residual saturation within all three media types. The oil distribution pattern is relatively more homogenous within both the homogenous (C_U = 1) and highly-heterogeneous media (C_U = 10.6); and more heterogeneous within the mildly-heterogeneous sand (C_U = 5.8). Smaller oil blob volumes were trapped within the two heterogeneous media type compared to blobs trapped within the homogenous medium (distribution of larger blobs).

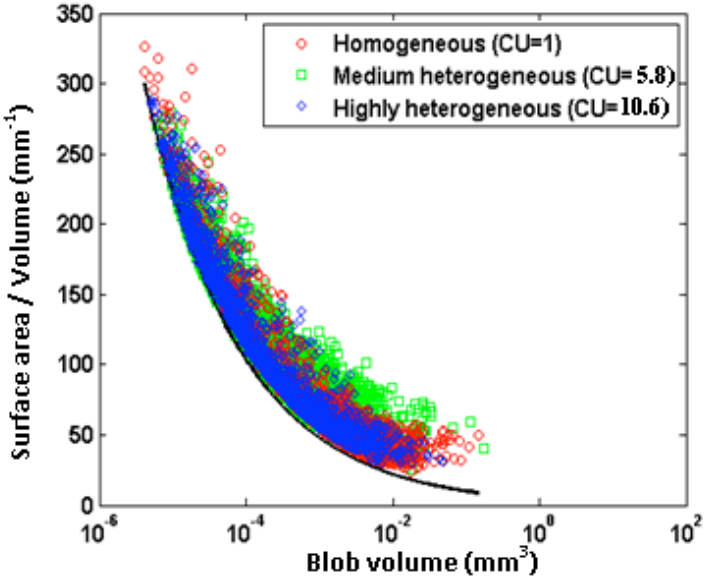

Figure 2.14. Plot showing the change in light-oil blob morphology for the three media systems (see figure 2.13). Deviation from spherical shape (Bold black line: model curve for spherical shape) represents greater surface area. Larger ganglia, trapped into multiple pores, show maximum deviation from spherical shape for all three systems. Finer blobs in the homogeneous medium, and the larger blobs trapped in the mildly heterogeneous medium show maximum deviation from spherical shape.

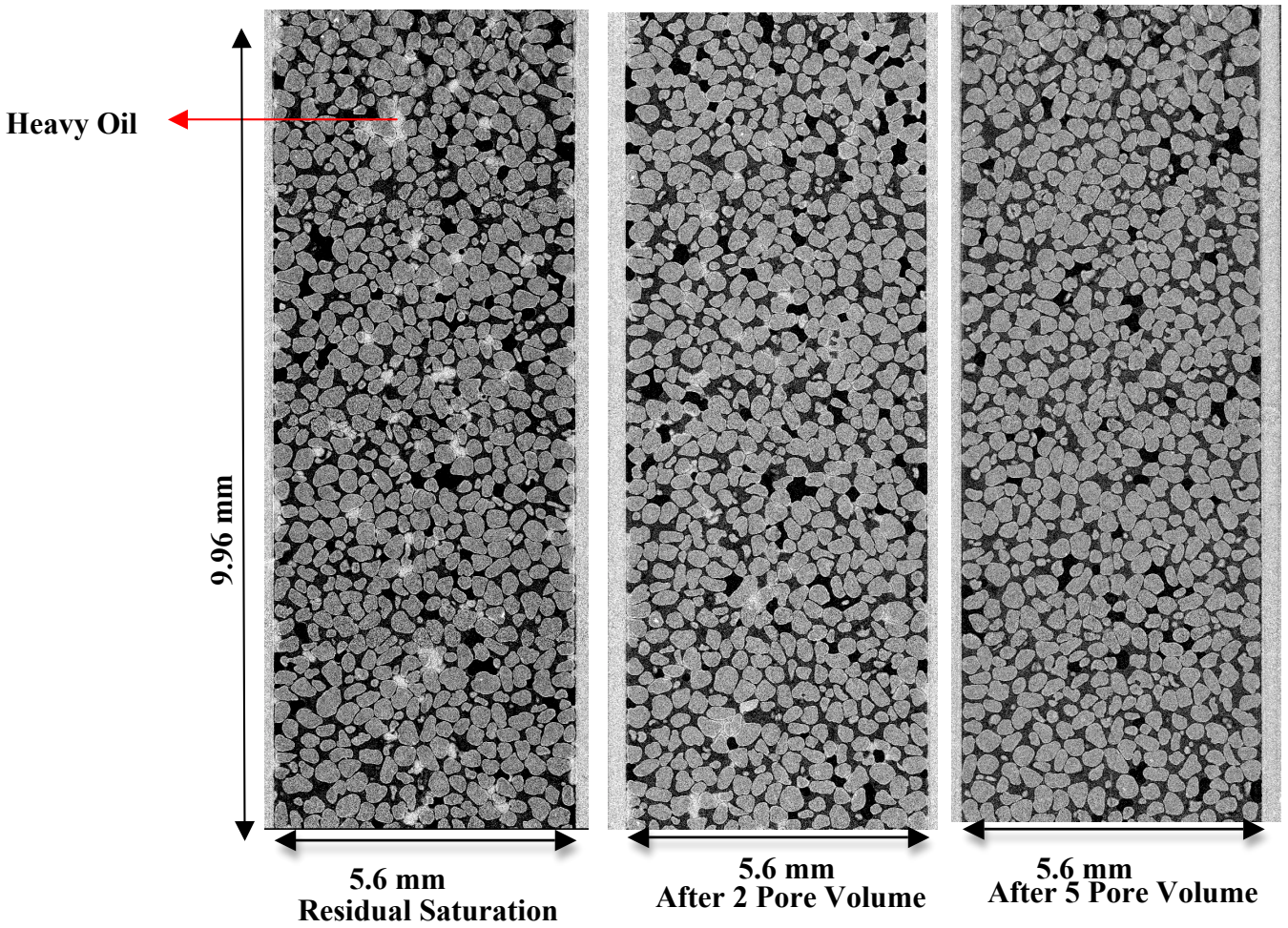

Figure 2.15. Vertical sections of a column, along the X-Z direction, showing the distribution of heavy crude oil (14.8˚ API) and aqueous phase within the homogeneous porous medium (40/50 Accusand, $C_U = 1$). Images show the sections of the same column as residual saturation and after the 2-PV and 5-PV surfactant (0.1% v/v) flooding events.

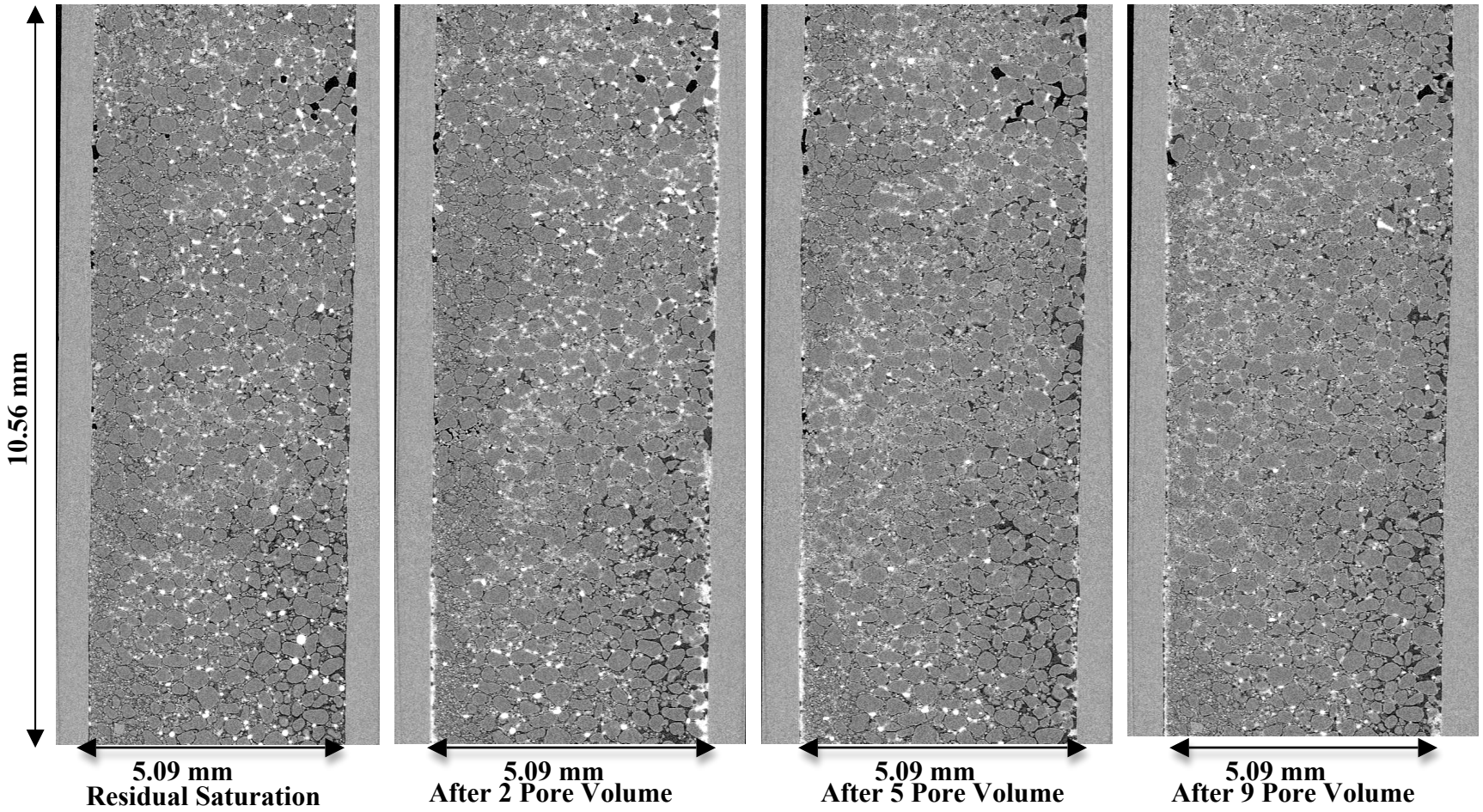

Figure 2.16. Vertical sections of a column, along the X-Z direction, showing the distribution of heavy crude oil (14.8˚ API, bright white color) and aqueous phase (dark grey-black) within the mildly-heterogeneous porous medium (mixed Accusand, $C_U = 5.8$). These are the sections of the same column displaying oil distribution as residual saturation and after 2, 5 and 9-PV surfactant (0.1% v/v) flooding events.

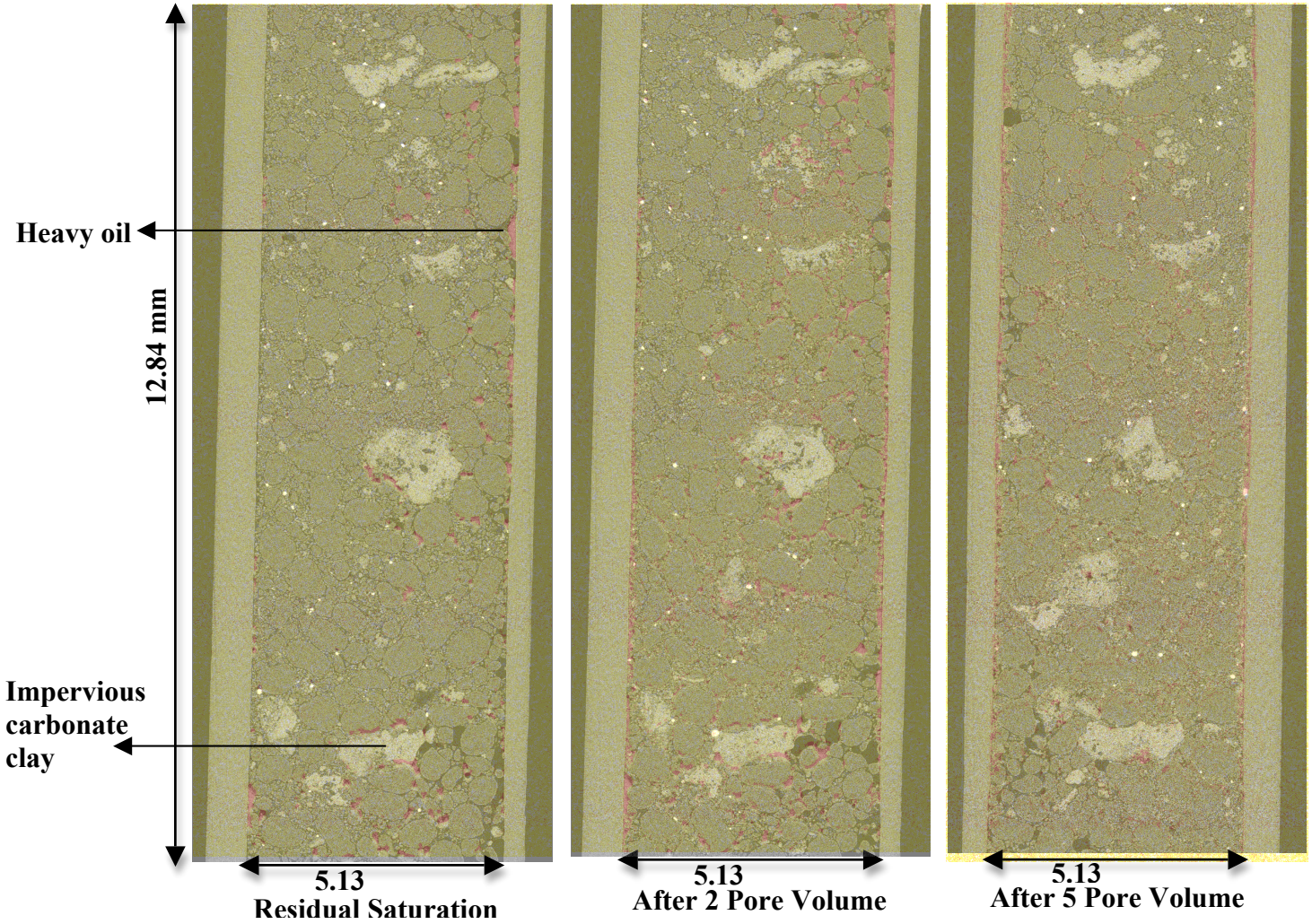

Figure 2.17. Vertical sections of a column along the X-Z direction showing the distribution of heavy crude oil (14.8˚ API) and the aqueous phase within the highly-heterogeneous sand (C_U =10.6). Sections of the same column show blob distribution and displacement after the 2-PV and 5-PV surfactant (0.1% v/v) flooding events.

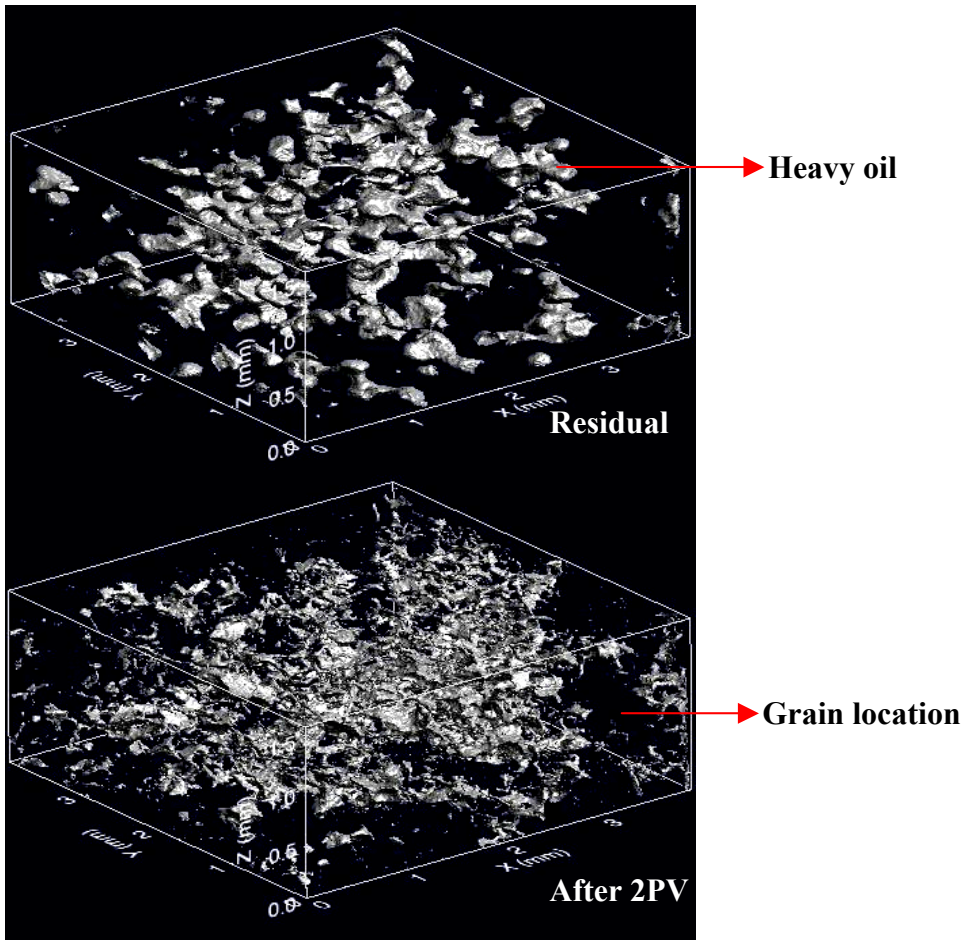

Figure 2.18. 3-D images of the cropped sections (approximately 4mm×4mm×1.5mm) of the column (see figure 2.15) containing heavy (14.8˚ API) crude oil within the homogeneous porous medium (40/50 Accusand, C_U =1) as residual saturation and after the 2-PV surfactant (0.1% v/v) flood. The oil phase segregated into smaller blobs as a result of progressive surfactant flooding. Changes in blob morphology were observed, resulting in greater surface area and greater contact with the surfactant solution. Complete oil recovery was obtained after the 5-PV surfactant flood. Relative locations of rounded sand grains can be observed in these images.

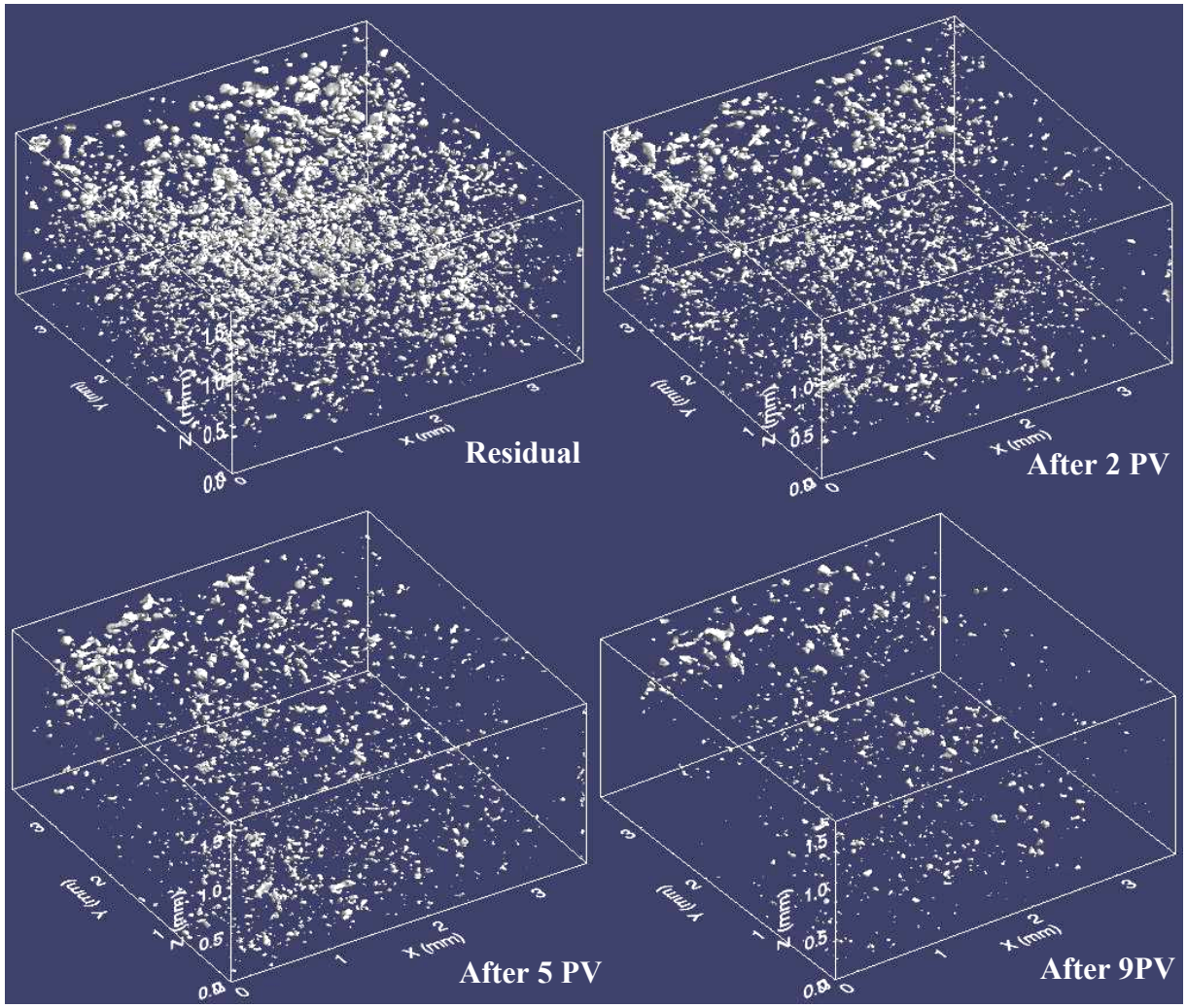

Figure 2.19. 3-D distributions of heavy crude oil (14.8˚ API) in cropped sections (3.6015 x 3.6015 x 1.64352 mm^3) of the column shown in figure 2.16. Binary transformed images show the distribution of the heavy crude oil in the mildly-heterogeneous sand (C_U = 5.8) as residual saturation, and after each surfactant flood. The number of the blobs decreased gradually, after each flooding episode.

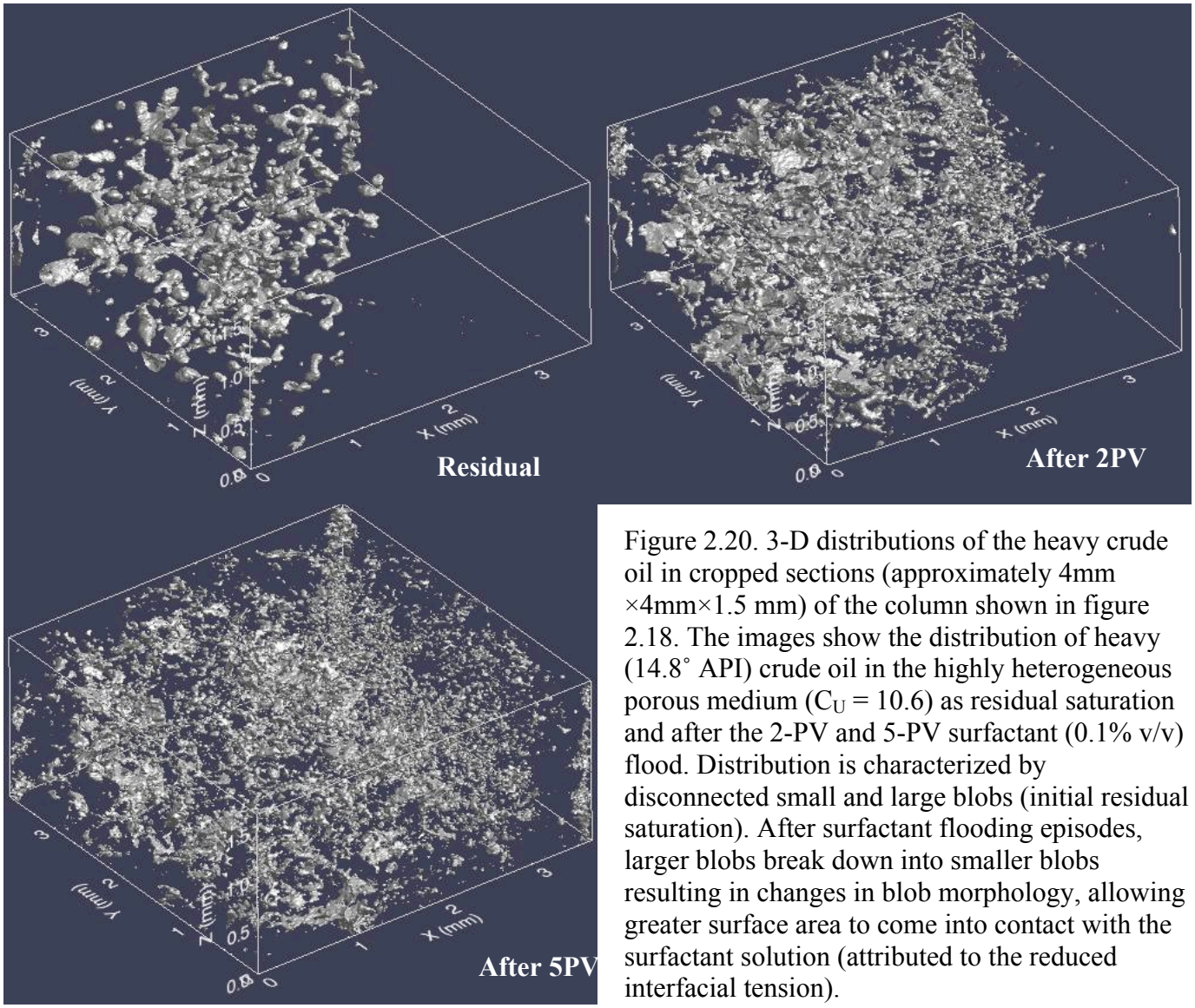

Figure 2.20. 3-D distributions of the heavy crude oil in cropped sections (approximately 4mm ×4mm×1.5 mm) of the column shown in figure 2.18. The images show the distribution of heavy (14.8˚ API) crude oil in the highly heterogeneous porous medium (C_U = 10.6) as residual saturation and after the 2-PV and 5-PV surfactant (0.1% v/v) flood. Distribution is characterized by disconnected small and large blobs (initial residual saturation). After surfactant flooding episodes, larger blobs break down into smaller blobs resulting in changes in blob morphology, allowing greater surface area to come into contact with the surfactant solution (attributed to the reduced interfacial tension).

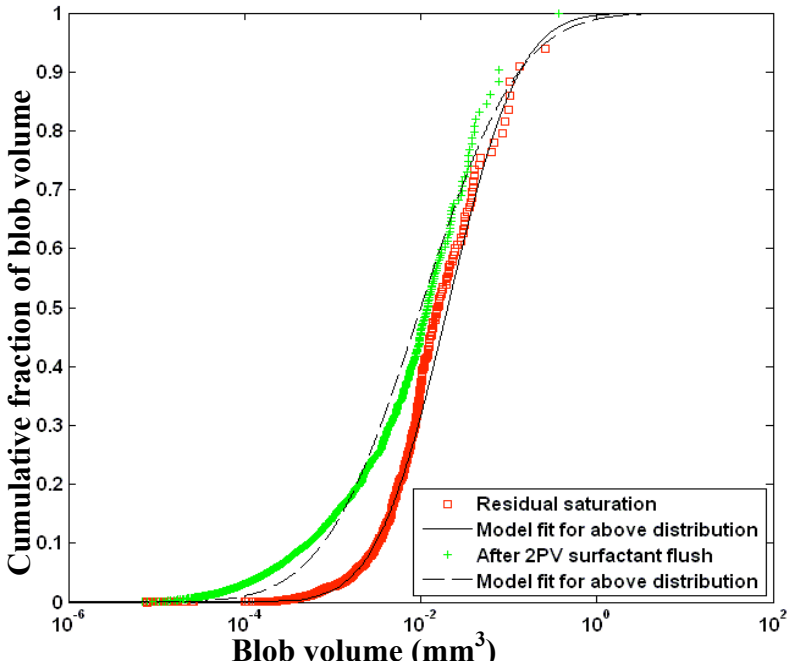

Figure 2.21. Cumulative distributions of the heavy crude oil blob volume in the homogeneous 40/50 Accusand (C_U = 1, see figures 2.15 and 2.18). Oil-blob volume distribution trends changed from homogeneous (initial residual saturation) to more heterogeneous after the 2-PV surfactant flood. Mean blob volume was also reduced after the 2-PV surfactant flooding event.

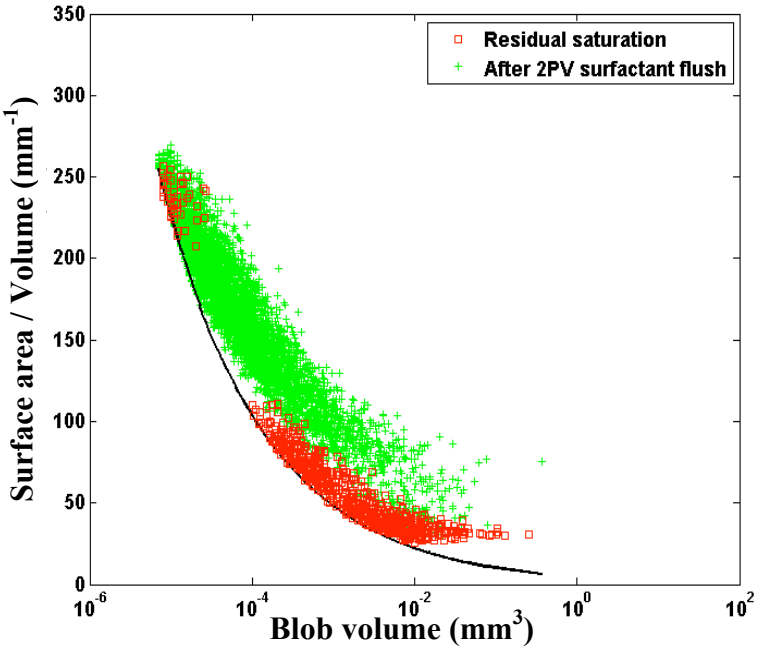

Figure 2.22. Plot showing the distributions of the blob surface area shown in the homogeneous 40/50 Accusand (C_U = 1,see figures 2.15 and 2.18). Deviation from a spherical shape (bold black line represents model curve for spherical shape) represents greater surface area. Heavy oil blobs show greater deviation from spherical shape after 2-PV flood, attributed to increase in total surface area in response to reduced interfacial tension induced by the surfactant solution.

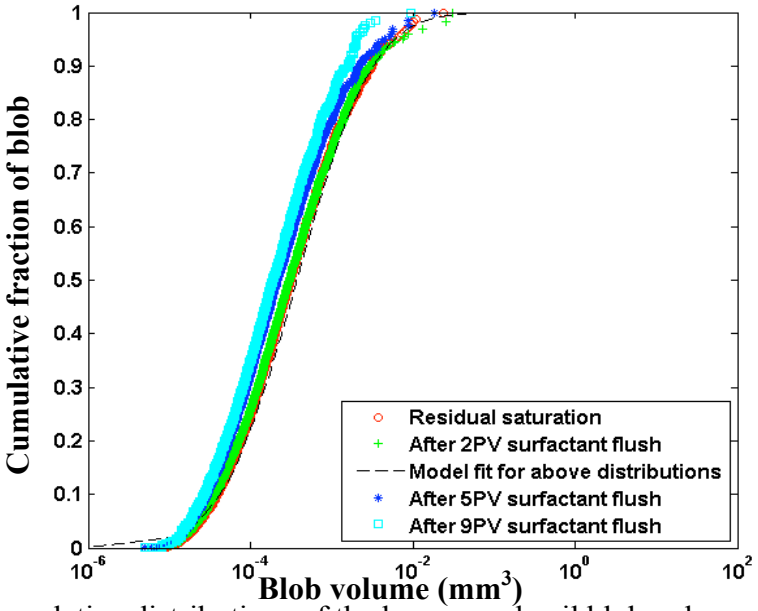

Figure 2.23. Cumulative distributions of the heavy crude oil blob volume in the mildly heterogeneous mixed Accusand (C_U = 5.8, see figures 2.16 and 2.19). The oil blob volume distribution trend was relatively more heterogeneous (initial residual saturation), and no significant change occurred after subsequent surfactant flooding events.

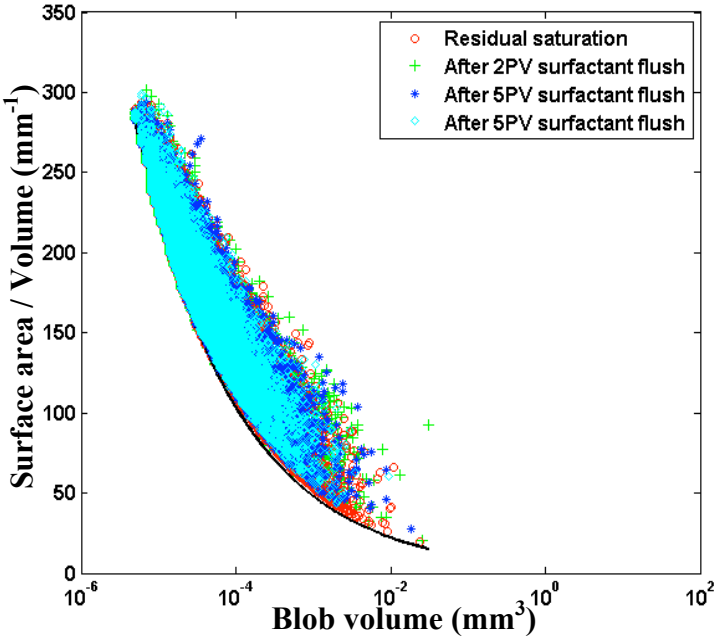

Figure 2.24. Plot showing the distributions of the heavy-oil blob surface area for the system shown in Figure 2.23 (also see figures 2.16 and 2.19). The bold black line represents a model curve for a spherical shape for any particular volume. Deviation from a spherical shape represents greater surface area. Heavy oil blobs show maximum deviation from spherical shape, as initial residual saturation, and after the 2-PV (red and green data points) surfactant flooding event.

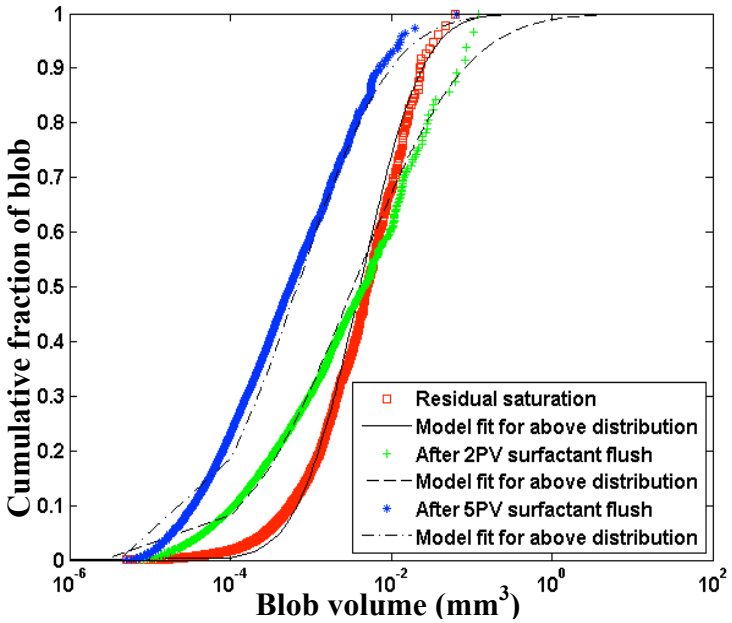

Figure 2.25. Cumulative distribution of the heavy crude oil blob volume in the highly heterogeneous mixed Accusand (C_U = 10.6, see figures 2.17 and 2.20). The oil blob volume distribution trend changed from homogeneous (initial residual saturation) to relatively more heterogeneous after the 2-PV surfactant flood, and then becoming slightly more homogeneous after the 5-PV of flooding event.

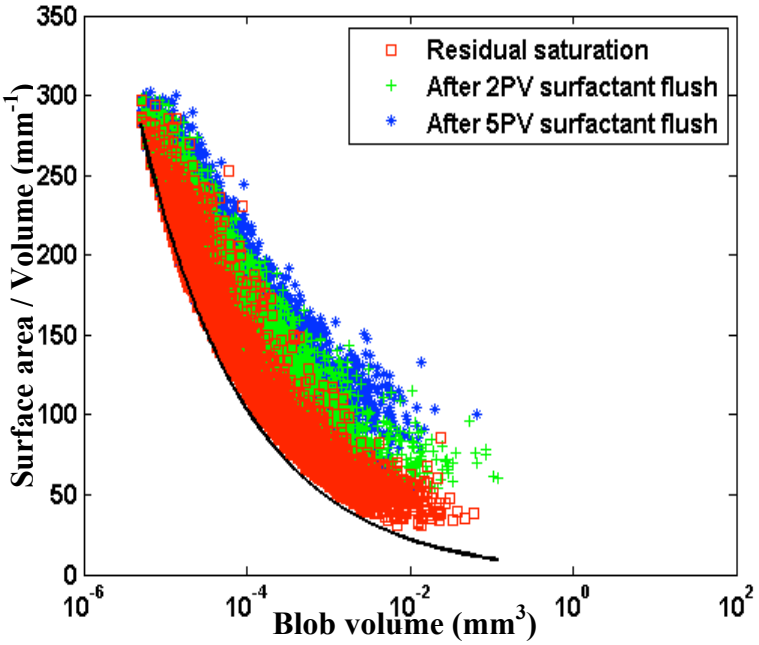

Figure 2.26. Distributions of the heavy-oil blob surface area in the highly heterogeneous mixed Accusand (C_U = 10.6, see figures 2.17 and 2.20). The bold black line represents the model curve for a spherical shape for a particular blob volume. Deviation from spherical shape represents greater surface area. The heavy-oil blobs show greater deviation from spherical shape after the 2-PV and 5-PV surfactant floods in response to reduced interfacial tension induced by the surfactant solution.

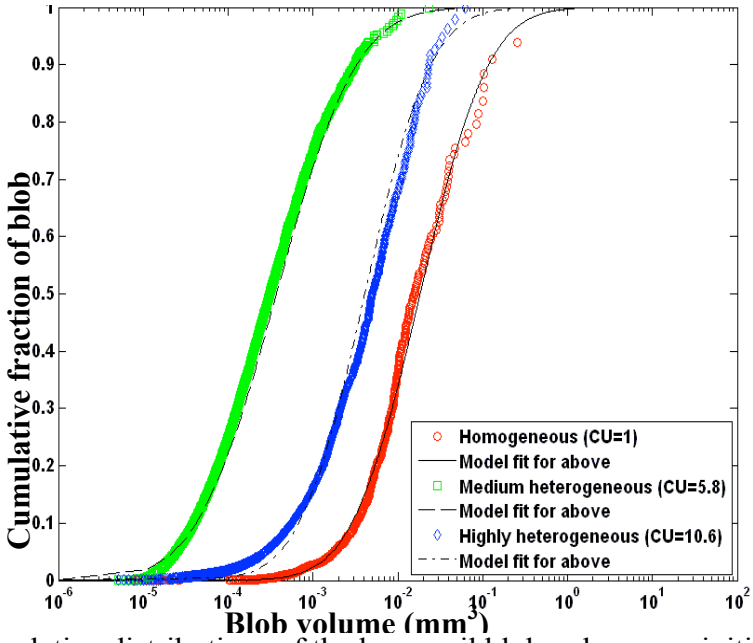

Figure 2.27. Cumulative distributions of the heavy oil blob volumes as initial residual saturation in three different porous media. The curves (heavy-oil blobs) exhibit a relatively more heterogeneous distribution compared to that of the light oil (figure 2.13) in each medium type. Mean blob volume was greatest in the homogeneous sand, followed by that in the highly-heterogeneous medium. Smallest mean blob volumes were observed in the mildly-heterogeneous medium system.

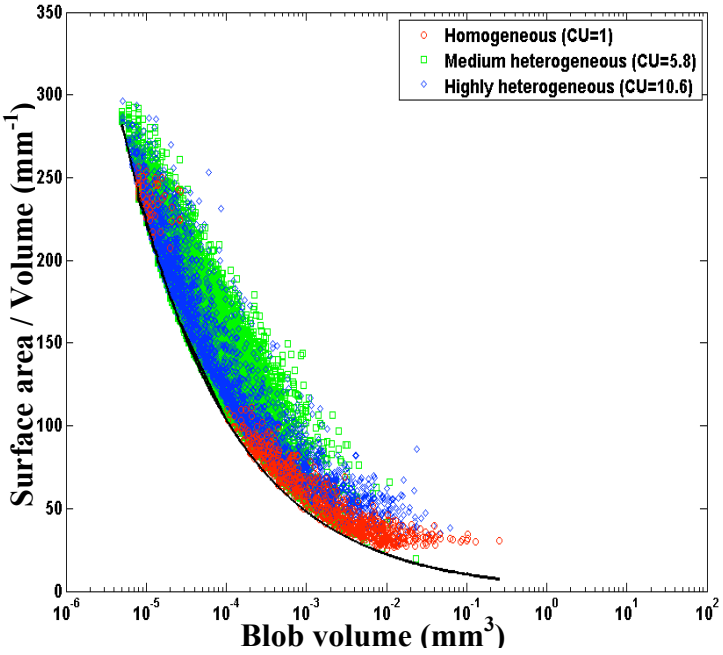

Figure 2.28. Distributions of the heavy oil blob surface area as residual saturation in three different porous media. Any deviation from spherical shape (bold black line) represents greater surface area. Larger blobs exhibit a maximum deviation from spherical shape or greater interfacial area for all three systems. Smaller blobs, trapped within the mildly-heterogeneous medium, show a maximum deviation from spherical shape.

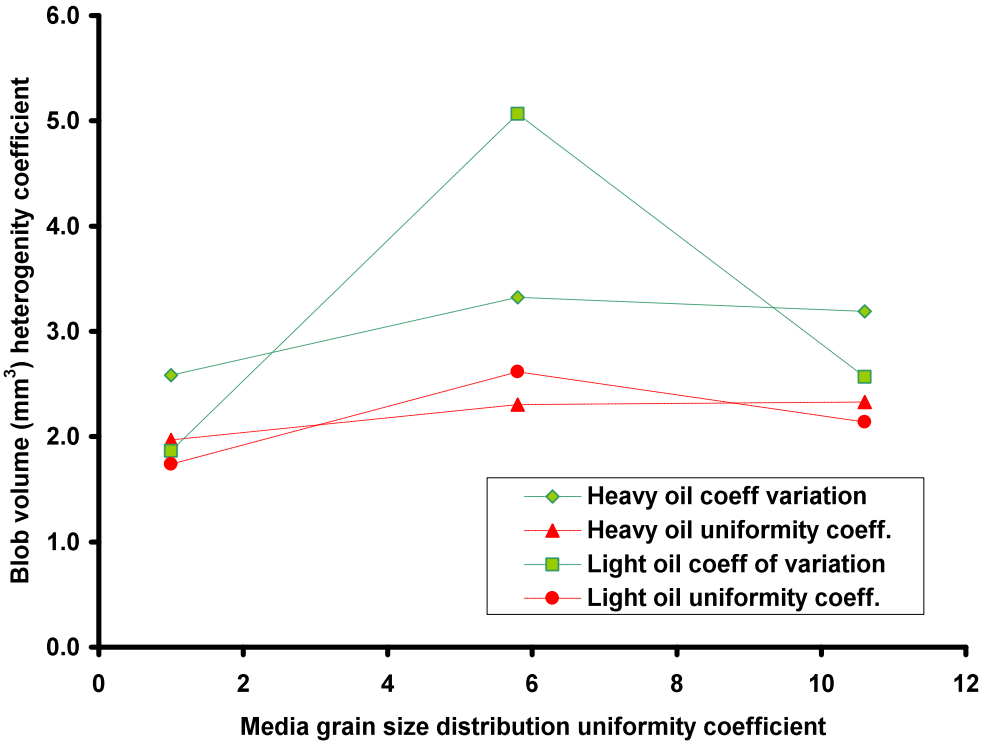

Figure 2.29. Plot showing correlation between grain-size distribution and oil-blob volume distribution. The coefficient-of-variation and the uniformity-coefficient represent the degree of heterogeneity in blob volume distribution, where the value of 1 represents a homogeneous distribution. Both light and heavy crude oil blobs show highly heterogeneous distribution in the mildly heterogeneous porous medium. The distributions are relatively more homogeneous (extreme left) in the homogeneous 40/50 Accusand. Note: the homogeneous sand has the highest permeability and the mildly-heterogeneous sand has the lowest permeability (absolute).

EXTRA-HEAVY CRUDE OIL DISTRIBUTION IN POROUS MEDIA AND RECOVERY POTENTIAL: AN APPLICATION OF SYNCHROTRON X-RAY MICROTOMOGRAPHY

ABSTRACT

Extra-heavy-crude oil and Bitumen commonly trapped within unconsolidated high porosity and high permeability sand are usually of fluvial or deltaic origin. Surfactant induced cold recovery techniques are feasible upon conventional thermal recovery, for the heavy oil deposits in shallow (< 200ft), thin pay-zones in California, eastern Missouri and Kansas. This method relies on spontaneous emulsification due to interfacial-tension-reduction, and wettability-alteration yielding greater recovery. In this research an innovative, non destructive high resolution (9-10μm) imaging technique, synchrotron X-ray microtomography (SXM) was used to study the trapping mechanisms and in-situ emulsification processes in terms of extra-heavy-oil-blob distribution in unconsolidated sands of varying micro-scale heterogeneity (sorting). Additional studies have been carried out to understand the interfacial processes at the pore-scale in response to an anionic surfactant application. Detailed analyses were conducted to quantify the changes in individual blob morphology before and after surfactant flooding events to identify correlation with recovery process. Three columns, packed with three types of water-saturated sands, were injected with extra-heavy-crude oil, and then flooded with anionic surfactant in several episodes. Multiple SXM images were taken at various episodes. Results show relatively low (6%) net recovery from the homogeneous sand after 5 pore volumes (PVs) or surfactant flooding, due to the formation of continuous-oil-phase attributed to oil wet media. Limited contact of heavy-oil with surfactant-solution resulted in less interfacial activity. Negligible net

oil recovery was achieved from the mildly-heterogeneous-sand mainly due to low associated permeability. Although a spontaneous in-situ-stable-emulsion was formed, minimal net oil recovery resulted due to the "jamin" effect producing local oil saturation after 2 PVs surfactant flooding and 6% recovery after 5 PVs of flooding (with respect to the saturation after the 2-PV flood). The highly heterogeneous sand yielded an average of 20% recovery after each surfactant flooding attributed to water wet media. Under these conditions, a stable-spontaneous-emulsion yielded greater displacement efficiency. These results demonstrate the versatility and invaluable application of SXM imaging techniques for evaluating critical pore scale processes which control oil displacement efficiency which can be extremely beneficial for evaluating systems conducive for enhanced heavy oil recovery for particular porous media systems.

3.1 INTRODUCTION

Recent studies predict a near-future worldwide energy crisis as a result of declining production of crude oil. It has been estimated that the maximum world oil production has already been reached, or will be achieved by 2023, under the current 2% growth rate for average world production (Carlson 2011, Guseo et al. 2007). Studies also show that with the estimated crude oil reserve of the U.S., production has already reached the peak, and has been declining since 1990 (Figure 1, appendix). Consequently, there is a growing interest to explore and extract the enormous resources from unconventional oil sources such as Canadian "oil sand" and "shale oil" (Green et al. 2006). Oil sand or tar sand is a source of shallow subsurface extra-heavy-crude oil and Bitumen having ºAPI gravity less than 10º and viscosity of more than 10 Pa·s (or 10,000 cP), trapped in unconsolidated high porosity and high permeability sand of fluvial or deltaic origin (Schramm 2000). Oil sand deposits are found worldwide mainly along the foreland basins of North and South Americas bordering the major conventional reservoirs (Head et al. 2003). 91% of the total world deposit of heavy oil is found in Venezuela (Orinoco, 1200BBO) and in Canada (Athabasca, 900BBO) which is 5 times greater in size than the largest conventional deposit in Saudi Arabia (Head et al. 2003, Schramm 2000). USGS fact sheet (Schenk et al. 2006) shows an estimate of 54095 million barrels (MMBO) of available extra-heavy-oil/bitumen in place in the U.S., including 6360 MMBO in Alabama (includes the measured in place resource and the speculative resources). API gravity for this heavy oil/bitumen varies from -0.5 to 10 ºAPI at reservoir temperature ranging from 12 to 38ºC. Viscosity of heavy oil ranges from 12 to 2×10^4 Pa·s. Meyer et al. (2007) defines any crude oil having API gravity ranging from 10º - 20º, and viscosity greater than 10^{-1} Pa·s as heavy oil, whereas Bitumen can be defined as the hydrocarbon having API gravity less than 10º API and a viscosity greater than 10 Pa·s. It should be noted that

viscosity varies with temperature, and Bitumen of the above specific gravity range but having lower viscosities can also be found in nature. Therefore, viscosity is primarily defined on the basis of API gravity (Meyer et al. 2007).

Thermal recovery techniques such as Cyclic Steam Stimulation, In Situ Combustion, Steam-Assisted Gravity Drainage (SAGD) and the Vapor Extraction (VAPEX), which are alternative modified versions of SAGD have been used to reduce viscosity, and therefore enhance the recovery ratio for heavy oil (Das and Butler 1997, Albahlani and Babadagli 2008). SAGD is the most popular method, which has been successfully used for extracting economic quantities of heavy oil from oil-sand with some limitations in energy efficiency, and pay zone thickness (>20 m.). This process is used for subsurface reservoirs composed of high porosity sand/sandstone at a depth ranging from 1500-4500 ft. Vertical permeability required for this process is 200-2540 mD (Taber et al. 1997). Recovery factors of heavy crude oil from oil-sand vary from 10-15% in the various parts of the world with a maximum of up to 19% in North America and recovery factors of Bitumen vary from 9-16% in the various parts of the world with a maximum of 32% in North America (Meyer and Attanasi, 2003). Limitations of thermal recovery have been reported for shallow reservoirs (< 500ft.) due to low formation fracture pressure attributed to low depth. Hunky et al. (2010) reported that the high viscosity of heavy oil, low reservoir depth (< 200 ft) and underlying water contact creates a challenging environment for using conventional thermal recovery methods in the heavy oil fields of shallow Pennsylvanian sands in Southwestern Missouri and Southeastern Kansas. Moreover, expensive thermal recovery methods are also not economically feasible for thin pay zones (Bryan and Kantzas 2009). Inexpensive cold enhanced recovery techniques, which apply surfactant solutions

to reduce interfacial tension, have proved to be useful for these ultra-shallow heavy oil reservoirs.

3.1.1 Porous Media Heterogeneity, Interfacial Tension, Emulsion Formation

Trapping mechanisms of crude oil blobs are controlled by capillary action as function of porous media heterogeneity, viscosity of crude oil, and wettability of a reservoir medium for a particular oil-brine system. Detailed discussion on trapping mechanisms in terms of capillary pressure and pore size heterogeneity has been provided in Chapters 1 and 2. The magnitude of capillary pressure in a small pore of a heterogeneous porous medium is directly proportional to the product of interfacial tension between the oil-brine phases and the cosine of the contact angle, and is inversely proportional to the radius of the oil-water interface (Hirasaki 2004, Mercer and Cohen 1990, Levorsen 2001, Hubbert 1953). When an oil blob reaches a water-wet pore constriction, the oil-water interfacial radius is equal to the pore radius, and from the above relationship it can be concluded that smaller the pore throat size greater is the capillary pressure, limiting blob mobility. Chapter 1 provides a detailed discussion on the interaction of viscosity driven inertial force and the capillary force on recovery efficiency. A dimensionless number called the capillary number (N_C) estimates the ratio of these counteracting forces (Morrow and Chatzis, 1982): $N_C = \frac{\eta v}{\gamma \phi}$

Where, η = viscosity of the flooding fluid (water),
v = velocity of the flooding fluid (water),
γ = interfacial tension between oil and water,
ϕ = media porosity,

By convention, systems with higher capillary numbers yield greater oil recovery. One way to increase this capillary pressure is reducing interfacial tension between the oil-water

interfaces through the application of surfactant solution. Surfactant induced enhanced recovery is a common practice in various parts of the world for both conventional and unconventional oil resources. Several pore-scale mechanical processes have been described in previous literature and are attributed to the high recovery of heavy-oil related to surfactant induced reduced interfacial phenomena. These processes include emulsification of oil phase, followed by either entrainment or re-entrapment of the oil blobs, and change in wettability of solid media-grain-surface (Johnson 1976). As the interfacial tension between the oil-water is reduced, the two immiscible phases try to behave as one phase, attributed to formation of greater interfacial area. New interfacial area can be formed in two ways, either by changing the blob morphology or by breaking down of larger blobs into smaller blobs. For a very low interfacial tension, discontinuous phase (e.g. oil) yields smaller droplets and disperses into the continuous phase (water) producing an oil-water emulsion. These fine blobs then flow (or can be entrained) with the continuous phase. Re-entrapment of oil blobs within smaller pore diameters (in a heterogeneous, relatively less permeable medium) can thereby increase the sweep efficiency of the surfactant flood by allowing the brine to invade the other low permeability regions of the medium.

Boom (2008) and Walstra (1993) discussed in detail the rheology of heavy oil blobs during emulsion formation. The change in individual blob-morphology and the critical conditions for breaking down a particular blob are due to interactions between the external stress and the internal-cohesive-force acting on the blob. When a high viscosity heavy-oil-blob flows as a suspended droplet in water, the external stress applied is a coupled action of the local velocity field and the viscosity ratio of the two immiscible phases, offset by the interfacial tension. The

ratio of these interacting forces can be expressed by the dimensionless expression called the Weber number,

$$N_W = \frac{G\mu_W r}{\gamma_{O/W}}$$

Where, G = magnitude of the velocity gradient tensor

μ_W = viscosity of the continuous fluid (water or surfactant solution)

r = radius of the individual oil blob

$\gamma_{O/W}$ = interfacial tension between oil-water.

When a heavy oil blob is squeezed through a small pore diameter, an extensional flow field is applied into it. As a result, it changes shape to an ellipsoid and breaks down into smaller blobs when a critical Weber number is reached. Weber number of blob disintegration for an individual pore model is equivalent to the capillary number (N_C), a macroscopic property that determines the recovery efficiency of a porous medium at the field scale. Therefore knowing the blob size distribution can help predict the capillary number for a particular field (or reservoir system) and establish a correlation between the lab scale and field scale parameters.

In macro-scale many methods have been proposed by several researchers. McAuliffe (1973) discussed the fundamental concepts of oil-water emulsion blob trapping and mobilization processes. During hydrodynamic displacement of oil blobs, “fingering” process can be observed in heterogeneous porous media. In this case, an oil-water emulsion will initially flow primarily through preferential flow paths or along the high permeability zones, resulting in the temporary restriction in mobility. Then, more water can flow through the unswept zones resulting greater sweep efficiency. The other important mechanism proposed was due to what is termed the “Jamin effect”. As oil blobs in an emulsion mobilize, they tend to be captured in relatively

smaller pore throats. Consequently water starts flowing to the less permeable zones, producing greater sweep efficiency. Thomas and Ali (1989) showed that light gravity oil blob distribution which forms an oil-water emulsion, within a porous medium of a given pore size distribution, strongly affects the recovery potential. Many other laboratory scale studies have been carried out to understand the importance of emulsion formation for heavy oil recovery, stability of emulsion formation, and transport phenomena of oil blobs in response to the application of various types of alkali-surfactant for cold recovery techniques (Hunky et al. 2010, Romero 2009, Bryan 2007, Liu et al. 2006). The processes described above from all of these studies were based on microscopic images of emulsified blobs that were prepared externally and injected into the porous media. The blob distribution properties were characterized using microscopic images of the emulsion outside the system. The unique and innovative research as part of this dissertation was the first detailed study to conduct an in-situ, three dimensional (3-D) pore scale investigation of heavy oil recovery and blob distribution under spontaneous emulsion formation within a typical reservoir porous medium type in order to understand the interfacial processes due to surfactant application for enhanced (heavy) oil recovery (EOR).

3.1.2 Wettability Changes and Mobility

Wettability is an important factor controlling recovery potential of heavy oil from unconsolidated sand. At the molecular level, wettability of a medium is an interaction between the molecular attraction by the van der Waals force, and repulsion by the electrostatic force. A third force, the hydration force, can be hydrophilic or hydrophobic depending upon the nature of the solid media. If the van der Waals attraction between the water-molecules and the solid-media is greater than that of the repulsive force, the porous media turns into water wet (Hirasaki 1991,

Liu et al. 2007). In a previously water wet porous medium the thin water film is bound between the solid-water and oil-water interfaces. The electrostatic force existing along these two interfaces also determines the wettability of the medium. If they are of same charge, they repel each other and the water film will be thickened. If the charge is opposite on the two interfaces, they will squeeze the water film, resulting in an oil-wet medium as the oil comes in contact with the solid surface (Dubey and Doe 1993). Wetting-behavior changes with composition of oil fraction and pH of the system (Morrow 1990). High asphaltene (large heterocyclic aromatic compounds) content in heavy crude oil (e.g., California crude) shows greater adsorption on glass and synthetic silica core at low pH (≤4), whereas sand grains show greater water-wet behavior at high pH (≥8) condition in the presence of NaCl brine and heavy oil (Buckley 1996, Kaminsky and Radke 1997). Dubey and Doe (1993) discussed this wetting behavior of California crude (heavy) using the concept of zeta potential (determines the electrostatic charge) of the crude oil and silica surfaces in response to changing pH condition. The surface of silica sand always has a negative electrostatic charge above pH of 2, whereas at high pH (up to pH 7) California crude surface is strongly positively charged. pH 7 is the isoelectric point for this particular crude oil when there is no charge. Above this pH the wettability changes as the two surfaces posses the same electrostatic charge (negative), and repel each other. Morrow (1990) discusses stability behavior due to the wettability of a medium with time, which is an important factor controlling heavy oil recovery. Carbonate cement and clay particles, although present in small fractions in heterogeneous porous media, have significant control on pH buffer and, consequently, controls the wettability behavior due to their occurrence on top of the pore wall surface. Wettability behavior is measured by the oil-water contact angle measurement on a solid medium, where complete water wet means a contact angle of 0°, and complete oil wet means an angle of 180°.

For water wet heavy-oil-sand (e.g., most of the Athabasca oil sand) connate water exists as thin coating of 10 nm thickness on top of the medium grain boundary (Schramm 2000, Blunt 1999). The non-wetting phase (oil) can exist as continuous or discontinuous chain in multiple pores through the pendular ring of wetting phase, which is directly in contact with the media grains.

Wettability of heterogeneous sand depends on the sorting of the grains in a porous medium. The interaction of the capillary pressure, the interfacial tension, and pore diameter has control on the wettability of a porous medium (discussed in Chapter 1). When a heterogeneous medium contains larger pores surrounded by smaller pores it can be shown empirically (using Young-Laplace equation) that pores with smaller diameter are occupied by water, whereas oil-blobs (i.e. non-wetting phase) are preferentially trapped into the larger pores. For example, Carrigy (1962) showed that the wettability variation is a function of the clay content of Athabasca oil sand, and correlated heavy oil saturation as function of grain size heterogeneity. This study showed that a decreasing amount of oil saturation with increasing clay content resulted in a continuous wetting phase within the reservoir. Greater heavy oil saturation can be found in larger grained sediment deposited which likely originated under relatively higher energy conditions. Relatively greater saturation of heavy oil into this sediment can be attributed to the existence of continuous oil phase trapped into the homogeneous larger sand grains and little clay materials (< 2μm). The majority of the Athabasca oil sand is water wet and the trapped oil-phase is not in direct contact of the sand grain surface. However, this behavior is unlikely in the other heavy oil reservoirs found in California, New Mexico, and Utah, where the reservoir materials are oil wet. Commercial hot water floatation of these oil wet reservoirs is not advantageous under these conditions due to difficulty associated with mobilizing the adsorbed oil phase from the porous media grain (Schramm 2000).

In macroscopic scale, Johnson (1976) discussed the pros and cons associated with wettability reversal processes. An originally oil-wet medium can be changed to preferentially water wet by changing the pH or salinity by chemical flooding yielding higher recovery. However, this method can also change the oil-permeability of the system reducing the mobility and the recovery process. Conversely, the other mechanism of changing a water-wet medium to oil-wet can also occur and the trapped disconnected oil phase can be changed to a continuous phase. Adding surfactant solution into the system may create a low interfacial tension environment resulting in the formation of water-in-oil emulsion. This emulsion reduces the permeability elsewhere, imposing a high-pressure gradient on the continuous oil-phase. Therefore, enhanced recovery of oil can be attained if the continuous-oil-phase overcomes the capillary force that has been reduced by lowering the interfacial tension.

3.1.3 X-ray Imaging in Flow Behavior

Emulsification of viscous fluids, using micro-engineered capillaries, is an emerging field where the blob shape and the blob size distribution can be controlled by varying the pore size distribution of the capillary tubes and the nature of surfactant (Boom 2008). With this idea it can be concluded that heterogeneity of the reservoir, and therefore the pore size distribution, has greater control on heavy oil blob size distribution. Characterization of the oil blob size distribution is critical in understanding trapping mechanisms and mobilization processes by means of emulsion formation and entrainment. Additionally, changes in blob morphology in response to an applied flow field and change in surface area due to the application of surfactant (induced lower interfacial tension) may have significant control on the heavy oil recovery process. Much research has been carried out to understand flow behavior of various immiscible

liquids including crude oil fractions, in 2-dimensional and 3-dimensional glass micromodels (Wardlaw and Yu 1988, Chatzis and Dullien 1983, Chatzis et. al. 1983, Wardlaw 1982) using glass beads (Wardlaw and McKellar 1985, Morrow and Chatzis 1982, Morrow et al. 1988), unconsolidated sand (Craze 1950, Powers et al. 1992), and homogeneous Berea sandstone (Chatzis et. al. 1983) as the model porous medium. Many of these techniques used in the early 1950s to 1980s were destructive, whereby the quantitative calculations associated with the oil phase or the non-aqueous-phase have been carried out by separating phases out from the system (i.e. ex-situ). Additionally, flow behavior studies were based on the final result of the multiphase flow rather than evaluating changes in flow or distribution temporally.

Advancements in computer tomography (CT) techniques have facilitated processes in which imaging of multiphase flow and quantitative calculation of various phases is possible in high resolution (less than 10μm). Because of its non-destructive behavior, CT scanning techniques have been used extensively in the petroleum industry in the two main areas such as core description and multiphase flow behavior of oil-water-air phases in fractured and porous media. Studies have been conducted to investigate in-situ heavy oil dispersion and flow behavior in terms of spontaneous emulsion formation and mobilization from unconsolidated sand. Following are some studies particularly relevant for this research. Kantsaz et al. (1994) studied the porous media (unconsolidated) heterogeneity on heavy-oil-sand. Salma and Kantsaz (2005), and Luo and Kantsaz (2008) studied an enhanced oil recovery (EOR) technique and mass transfer profile of solvent through heavy oil trapped in unconsolidated oil-sand by means of density and concentration data using X-ray CT. Tremblay and Sedgwick (1995) studied cold enhanced recovery process of heavy oil from sand using X-ray CT technology. Peters and

Hardham (1990) used X-ray CT to study various enhanced recovery techniques, and successfully estimated quantitative data to use in numerical modeling.

Synchrotron X-ray microtomography (SXM) is an emerging technology, which has only been used for very few multi-phase fluid flow studies to date. Coles (1998) tried to apply this method to obtain core properties and 3-D fluid distribution and successfully correlated these image resolved data with computational results. Al Roush and Wilson (2004) provide a detailed description on the recent use of SXM to determine porous media properties and discussed the application of this novel technique in characterizing pore network, connectivity, porosity, and specific surface area. Schnaar and Brusseau (2006a, 2006b) successfully applied SXM imaging to study immiscible phase residual saturation and dissolution within various unconsolidated porous media. As part of the dissertation research herein SXM imaging was applied to conduct an in-depth analysis of the pore scale distribution and recovery processes of San Joaquin Valley heavy crude oil within unconsolidated sand. The purpose of this research is to understand the trapping mechanisms and oil blob emulsification processes in terms of distribution pattern as function of porous medium heterogeneity. The heterogeneity in the porous media is mainly characterized by porosity, permeability, and the sorting of unconsolidated sand. Three types of sands (one homogeneous and two other heterogeneous types) were saturated with heavy oil and flooded with brine to establish residual saturation, and then followed by a series of anionic surfactant floods (multiple episodes). This SXM imaging technology gives the capability to quantify the volume and the surface area of individual blobs in an emulsion within the porous medium. It can be hypothesized that individual blob volume morphology has, in part, control on the recovery volume. Blob distribution pattern and the change in oil blob morphology were characterized and compared, in both residual saturation and after each surfactant flooding

episode. These results will help reinforce the preexisting conceptual model, as well as aid in predicting the total recovery of residual oil due to surfactant flooding through pore scale relationships and quantification. Additionally, this research will substantiate the application of synchrotron X-ray microtomography (SXM) as an important tool to understand the spontaneous emulsion process in terms of 3-D distribution of heavy oil blobs and other interfacial pore scale phenomena due to reduced interfacial tension by the application of an anionic surfactant. These results can be interpolated or extrapolated to predict oil reserves and potential recovery from reservoirs having heavy oil, and therefore predict a reservoir system most amenable for maximum recovery.

3.2 MATERIALS AND METHODS

Three columns were packed with three types of sands and saturated with double deionized water. All of the columns were then injected with heavy crude oil. The columns were flushed with an anionic surfactant in several episodes. Multiple SXM images were taken, including one initial and two to four others after each subsequent surfactant-flooding event.

3.2.1Materials

The model oil phase chosen was San Joaquin Valley crude (Chevron) having API gravity 14º. The oil sample was doped with iodobenzene (10-12% by volume) to improve the image contrast for a particular iodine critical X-ray absorption energy using synchrotron X-ray microtomography (SXM). The aqueous phase (double-deionized water) was doped with 60 g/L ACS grade cesium chloride (CsCl) (Sigma-Aldrich Co.) for the same purpose, so that the aqueous phase can be captured by the cesium critical absorption energy interval for appropriate image contrast using SXM. Previous research (Schnaar and Brusseau 2006b) showed no or insignificant change in interfacial tension, due to the addition of CsCl dopant, in the aqueous phase. These dopants showed the least partitioning to the non-target fluids (Schnaar and Brusseau 2006b). However, oil phase doping with iodobenzene (IB) showed changes in interfacial tension. Also, the doping with IB (density 1.82 g/cm^3) increased the specific gravity of the heavy crude oil, and the API gravity was changed from 14º to 4.2ºAPI. According to USGS standards, in the absence of viscosity data any crude oil sample having API gravity less than 10º is considered as extra-heavy-oil. Henceforth, the oil sample will be termed a extra-heavy-oil in this paper. A 0.1% (by volume) solution of an anionic surfactant branched alcohol propoxy sulfate (Stepan Chemical Company; Houston, TX) was used for the surfactant flooding

experiments. This surfactant was chosen for its ability to reduce interfacial tension at very low concentration (0.1%). Moreover, this surfactant was formulated specifically for EOR applications and also has been effectively used in remediation applications to mobilize crude oil from shallow aquifers. It also showed high salinity tolerance and is therefore assumed to be applicable for reservoirs with high salinity (Wu et al. 2005). Goddard et al. 2004 found that this surfactant showed minimal adsorption to the solid phase. It is to be noted that initially all of the porous media used in these experiments were water wet. The time interval between surfactant flooding and image capturing was less than 24 hours, limiting any possibility of surfactant adsorption on solid grains.

Three types of unconsolidated sands, with increasing heterogeneity, have been used as representative reservoir media. The heterogeneity of the medium can be expressed in terms of uniformity coefficient ($U_c = d_{60}/d_{10}$), estimated by the ratio of the 60th percentile to the 10th percentile grain-size diameters in a grain-size distribution curve. The sediments are commercially available, homogeneous 40/50 Accusand ($U_c = 1$), mildly heterogeneous Accusand ($U_c = 5.8$), and highly heterogeneous Accusand (Unimin Corporation, Le Sueur, MN). He latter two heterogeneous porous media types were prepared in the laboratory, and added with fractions of fine-grained carbonate clay ($U_c = 10.6$) to achieve particular uniformity coefficients of interest. Parameters for three types of sand are presented in table 3.1. Porosity values for the homogeneous, the mildly heterogeneous, and the highly heterogeneous sands are 0.33, 0.27 and 0.25 respectively, and the absolute permeability values for the three are 9E-11 m^2, 3.6E-11 m^2 and 5.4 E-11 m^2, respectively. It is important to emphasize that the mildly heterogeneous sand has the minimum permeability amongst all three of the porous media.

3.2.2 Residual Saturation and Surfactant Flooding

Thin-walled aluminum columns were dry-packed with three types of porous media. The columns were approximately 4.4 cm long, with Swagelok end-fittings on the top and the bottom. The inner diameter of the columns was approximately 0.5 cm. However, the available imaging length varied from approximately 1.0-1.7 cm because the top and the bottom of the columns were fitted with Swagelok end-fittings, which inhibited the penetration of the X-ray beam through these portions. Therefore, two aluminum caps were used at the column top and bottom, to occupy these obscured shaded regions. Polypropylene frits were used between the sand and the aluminum caps to hold the loose particles intact along the column boundaries, and to avoid any preferential flow of the fluids through the porous medium.

The sand pack columns were purged with carbon-dioxide to displace all air bubbles captured along the pore spaces. The columns were then saturated with de-aired double-deionized water for several pore volumes (PV) vertically upward, using a single piston, HPLC pump (Acuflow series II). The saturation process continued for 48 hours with a linear velocity ranging from 10-20 cm/hour. After the initial saturation was completed, columns were injected with 4 PVs of crude oil, vertically downward, at a linear velocity of 4 cm/hour with a syringe pump (Model: 780100, KD Scientific, Holliston, MA). The columns were then flushed with the cesium chloride solution to attain residual saturation, by displacing the oil blobs, in a discontinuous distribution. The residual saturation process was carried out in two steps: 2 PV with a flushing rate of 6-10 cm/hour (linear velocity) and 10 PV with a flushing rate of 20 cm/hour. Capillary numbers (Table 3.2) calculated for this displacement process (considering 20 cm/hr) were 4.5×10^{-4}, 5.5×10^{-4} and 5.91×10^{-4} for the homogeneous, the mildly heterogeneous, and the highly heterogeneous sand, respectively. Previous research related to trapping and mobilizing oil

phase in the unconsolidated bead packs of high porosity and permeability (Wardlaw and Mckellar 1985, Morrow et al. 1988) showed that residual saturations in the range of 50% to more than 75% can be attained with capillary numbers of this range. This additional entrapment force can be attributed to the high aspect ratio due to relatively greater radius of the bead pack pores and can be compared with the capillary number estimated in this research. However, these capillary numbers are comparatively higher than that expected in consolidated sandstone. After residual saturation was completed, the columns were sealed and imaged by SXM.

The columns were flooded with 0.1% anionic surfactant solutions doped with cesium chloride. Prior experiments were carried out to ensure that the concentration of the surfactant solution was below the critical micelle concentration (CMC) level so that mobilization would be the dominant mechanism of oil removal. It was assumed that no or insignificant dissolution of crude oil would have taken place below CMC level and during the time-scale of the experiments. Therefore, as mentioned previously, it is expected that the oil blobs would be mobilized and extracted from the system only due to reduced interfacial tension. Interfacial tension measurements were carried out using a Du Noüy ring tensiometer. A detailed discussion of the method and estimation of CMCs for the crude oil and surfactant solution is given in Chapter 4. Subsequent to the establishment of residual oil saturation and initial SXM scan, surfactant flooding was implemented in two to four steps (episodes). Surfactant flooding was done in a series of two to four episodes. First, 2-PVs of surfactant solution were pumped through initial oil saturated column at a linear pore velocity of 20 cm/hr, and then scanned using SXM to resolve the oil distribution. The column was then pumped with 3-PVs (5-PVs total) of surfactant solution at the same velocity (20 cm/hr) and then scanned using SXM to resolve the resulting oil distribution within the column. An extended period of flooding continued for extra-heavy-oil

trapped within the highly heterogeneous medium for 2 additional episodes consisting of 4PVs of flushing (20 cm/hour) each time (i.e. total of 9 and 13 PVs, respectively). A total of up to five SXM scans were made for each column, including one initial scan and four scans after each surfactant flooding event (i.e. total 2, 5, 9, 13 PVs, respectively).

3.2.3 Synchrotron X-Ray Microtomography

All images were taken at the GeoSoilEnviroCARS (GSECARS) BM-13D, at the Advanced Photon Source (APS) Argonne National Laboratory, Illinois. Synchrotron X-ray Microtomography has many advantages such as the high intensity (high photon flux density), highly collimated and monochromatic or single energy rays, which are uniform across the entire beam, resulting in exceptionally high-resolution imaging capabilities (Wildenschild 2002, Flannery et al. 1987). Images of different phases (oil and water) can be taken simultaneously by changing the X-ray incident energies using a monochromator. When the X-ray beam passes through a particular object, it is absorbed and attenuated at particular threshold energy, called the critical absorption energy. After passing through the object the X-rays pass through a synthetic scintillator to be converted into the visible light. These visible rays are then reflected at an angle of 45˚ and magnified, before being captured by CCD camera (Al-Raoush and Willson 2005). A series of images can be captured from multiple directions by rotating the object at particular angular interval. The final image shows a linear depth-integrated grayscale image, where the darker gray indicates greater absorption. This gray scale level is a function of the atomic number and the X-ray energy, and can closely be correlated with the density of the imaged object (Ketcham 2001, Wildenschild 2002). Approximately 1400 to 1600 two-dimensional slices were produced for the 1.0-1.5 cm imaging length of one column. The images were preprocessed

(correction for dark current and white field) and reconstructed using software called Tomo_Display (written by Dr. Mark Rivers, ANL) at the APS. The reconstruction process was performed in multiple steps associated with the building of sinograms in terms of logarithmization, and correction of rotation axis with respect to the center of the image. The reconstruction process also involves removing any artifacts and it applies a reconstruction algorithm to estimate the spatial variation of the attenuated values in inverse method, producing 2-D reconstructed slices. After the reconstruction process is completed, the fluid phases with high absorption appear brighter.

The images of the three phases have been captured at three incident energy levels with a spatial resolution ranging from 9.9-10.3 μm. The images scanned at energies above (36.085 KeV) and below (33.269 KeV) the cesium critical absorption edge and were subtracted to resolve the aqueous phase doped with cesium chloride. The images scanned at energies below the cesium edge (or above the iodine edge, 33.269 KeV), and below the iodine edge (33.0169) have been subtracted to resolve the oil phase (i.e. nonaqueous fluid). Additional post-processing was carried out to stack all two-dimensional images of a single column, to generate a three-dimensional image for the entire column and portions along the column boundary were "cropped" to avoid unwanted artifacts due to wall effects such as preferential flow or unrealistic pools. Ketcham (2005) describes all these post processing methodologies, in detail, carried out by software called Blob3D. Several tools available in Blob3D have been used to improve image quality prior to stacking. Median smoothing (grayscale-to-grayscale algorithm) was used to reduce inherent noise in order to enhance the edge of the oil blobs from the surrounding non-target phases. This process involves the application of a particular grayscale value, which is the median value of all other gray-scale values for a chosen radius. A determined gray-scale value

was assigned as the threshold value for each oil fraction to convert the images from gray-scale to binary (two-component). In general, a gray-scale value intermediate to the target phase and non-target phase is considered as the threshold value (ASTM 1992). Binary images separate the target fluid as white (gray-scale value 255) from any other phases as black. Finally the images were cropped along X and Y directions (approximately 4mm×4mm) to ignore any saturation attributed to the preferential flow along the column wall. Quantitative data such as volume and surface area for each individual blob have been extracted after binary image separation.

3.3 RESULTS AND DISCUSSION

3.3.1 Interfacial Tension and Capillary Number

Table 3.2 lists the changes in the interfacial tension due to surfactant flooding, and the capillary numbers before and after the flooding events. Compared to the extra-heavy-oil/water system, the effect of the surfactant resulted in a 41% reduction of interfacial tension (between extra-heavy-oil and 0.1% surfactant-solution) from 42.25 mN/m to 24.65mN/m. A corresponding increase in capillary number (N_c) resulted (approximately 71%) for all three porous media. Although increased, the capillary numbers are still on the order of 10^{-3} to 10^{-4}, which is within an expected range for systems near the well bore flooding with alkaline surfactant for the Athabasca oil sand (Cuthiell et al. 1995). It should be emphasized that in this experiment the capillary number was increased only as a result of decreased interfacial tension. Therefore, this observed increase remained constant for all of the three porous media systems. The bond number, which gives an estimate of gravitational or buoyancy forces involved in trapping are on the order of 10^{-13} to 10^{-14}. Since the buoyancy (gravitational) component is negligible compared to capillary forces, any possibility of oil blob trapping due to gravity can be ignored.

3.3.2 Distribution of Extra-Heavy-Oil Blobs in 2-D and 3-D Sections

Figures 3.1, 3.2 and 3.3 show the distribution of the extra-heavy crude oil in the homogeneous, the mildly heterogeneous, and the highly heterogeneous sands respectively. All of these figures show the initial residual saturation conditions and the respective time series of the surfactant flooding events, in a particular 2-D section along the X-Z (vertical section) direction of the columns. The oil phase is shown in bright white color in binary subtracted images. Visual observation shows that a relatively high volume of extra-heavy-oil present as a continuous phase

within the homogeneous porous medium (Figure 3.1). Although no major changes occur in oil phase distribution, some mobilization process can be observed after the 5-PV surfactant flood. Extra-heavy oil recovery primarily occurred through preferential flow paths along high permeability zones within the homogeneous medium. The other two heterogeneous porous media (Figures 3.2 and 3.3) showed a discontinuous oil-phase present under the initial residual saturation conditions. The extra-heavy oil in the mildly heterogeneous medium experiment exhibited a relatively heterogeneous blob distribution with some larger blobs existing at the top and the bottom part of the column. Oil recovery processes affected the larger distribution of oil blobs initially as time-series images revealed the preferential disappearance of the larger blobs from the system. Residual saturation within the highly heterogeneous porous medium is also characterized by a heterogeneous distribution of large and small oil blobs in 2-D image section. Changes can clearly be seen after subsequent flooding events. Larger blobs disappear and the pores are gradually dominated by smaller blobs after each flooding episode, resulting in minimum oil saturation after 13 PVs of surfactant flooding. One notable phenomena observed in this system was the appearance of preferential oil mobilization along the column boundaries (Figures 3.1 and 3.2), which is known as the "wall effect". In order to minimize this boundary effect, images were later cropped, and the quantitative data have been calculated only from the central portion of the columns to estimate the recovery potential from each of the medium.

Figures 3.4, 3.5 and 3.6 show the time series of three dimensional distribution of the oil blobs in a part of the cropped section (approximately $1.5 \times 1.5 \times 4$ mm^3) for each column, for the initial residual saturation condition and the subsequent surfactant flooding episodes. Observed three dimensional distributions of the oil blobs, in all three porous media, are in good agreement with those that were observed in the two dimensional vertical sections. A relatively high initial

residual saturation of heavy oil in the homogeneous medium is characterized by a continuous interconnected oil phase distributed through multiple pores. In terms of mobilization, no major changes occurred after each surfactant flooding event for this particular 3-D image section. However, discontinuous oil blobs were present as a homogeneous distribution within the other two heterogeneous media (i.e. mildly heterogeneous and highly heterogeneous) (Figures 3.5 and 3.6). For both of these heterogeneous porous media experiments, the formation of spontaneous oil-blob emulsion can be clearly observed within the initial residual saturation conditions. The mildly heterogeneous medium was dominated with a fine distribution of oil blobs after all three surfactant flooding episodes. The influence of the porous media characteristics (i.e. pore size distribution and heterogeneity) on oil distribution was clearly observed by the distribution of small oil blobs as initial residual saturation. It can be concluded, that initially, the emulsion was formed during the establishment of the residual saturation as a function of pore distribution heterogeneity. After the surfactant flooding was conducted, the original blobs were broken down into even smaller blobs (red square in Figure 3.5) and eventually disappeared as they were mobilized from the system. This small imaged section also showed simultaneous saturation and desaturation of the blobs at specific grain boundary places, likely due to the "jamin" effect described in the introduction section. This effect is a common phenomenon found in a heterogeneous porous medium with low permeability conditions. A comparison of oil distribution after all three surfactant flooding episodes reveals an overall increase in the oil-blob-saturation from initial residual conditions to after 5 PVs of flooding (Figure 3.5). It should be noted that this process of increasing local saturation was likely due to the trapping of oil blobs by smaller pore diameters with the porous medium. This ultimately leads to an increase in the sweep efficiency attributed to preferentially water saturation (invasion) in the relatively impermeable

zones. Although advantageous, this process can delay the recovery process, and greater recovery can only result after flooding with many pore volumes of solution.

The oil blob distribution within the highly heterogeneous porous medium also clearly depicts spontaneous emulsification during the formation of the initial residual saturation condition (Figure 3.6a). A heterogeneous oil distribution containing both the large and smaller blobs can be seen with the latter being dominant in number. The emulsion present under the initial residual saturation condition was stable after subsequent surfactant flooding events, attributed to the formation of the finer blobs due to reduced interfacial tension (red box region in Figures 3.6c and 3.6d). However, this system also showed the presence of some larger blobs after the 5-PV and 9-PV flood (Figures 3.6c and 3.6d) and this may be in part due to the coalescence of some smaller blobs. Significant oil recovery was observed after 13-PV of surfactant flooding (Figure 3.6e). The blob distribution was completely dominated by the smaller blobs after the total 13-PV flood. This local distribution imaged in 3-D was also consistent to that observed in the 2-D vertical image sections (Figure 3.3) and was considered to be representative for the entire system.

Previous discussion noted that the spontaneous emulsion process is a consequence of the interaction of reduced interfacial tension and the hydrodynamic shear force applied on the heavy oil blobs, in conjunction with the capillary action as function of permeability of the porous medium. The above observations reveal that the heterogeneity of the medium is primarily responsible for spontaneous emulsion formation, which became stable over the course of subsequent flooding episodes by the formation of smaller blobs due specifically to interactions of the surfactant itself. Chapter 1 and 2 showed that significant change in blob morphology of light and heavy gravity crude oil resulted due to the surfactant application process. However, the

extra-heavy-oil emulsion trapped in the two heterogeneous media shows no significant change in oil blob morphology or shape over flooding episodes. The larger blobs distributed within both the heterogeneous media exhibited elongated and tabular surface area which were easily differentiated from the blob morphology of light and medium gravity oil blobs described in Chapter 2 whereby most of the larger blobs were rounded and ellipsoid in shape. It can be assumed that larger oil surface areas would result in greater surfactant solution contact (i.e. with the oil phase) resulting in greater mobilization and faster recovery. With this assumption, a quantitative approach was conducted in the following sections to characterize the oil blob morphology distribution pattern and determine if it has any correlation with the recovery potential.

3.3.3 Quantitative Results

Quantitative results for recovery from the three porous media based on 3-D image data have been reported in the tables 3.2, 3.3, and 3.4, respectively. Recovery results are in good agreement with the observed results from the representative 2-D and 3-D image sections as mentioned in the previous sections. The homogeneous porous medium yielded a negative recovery or gain of 4.5% extra-heavy-oil after the first 2-PV surfactant flood, and approximately 6% net recovery (with respect to initial residual saturation) after the 5-PV flood. Moreover, the total surface area of the entire-phase distribution increased by 7% after the 2-PV flood, and decreased by 1.4% after the 5-PV flood. Clearly the surfactant application was not able to reduce the interfacial tension of the oil or initiate significant recovery. In this case, the high permeability of the medium resulted in the formation of a continuous oil-phase of heavy oil through the pendular ring of initially water-wet pores. Since the hydrodynamic gradient is imposed over the entire length of the continuous oil distribution, greater capillary number (critical capillary

number) may have been required for mobilization of the continuous phase of larger ganglia. Wardlaw and Mckellar (2005) proposed that a critical capillary number has to be achieved for mobilization of the blobs, and that any capillary number less than the critical number results in blob separation and redistribution within the pore spaces. Additionally, wettability is another factor which enhances the trapping mechanism in this particular example. The 2-D vertical imaged section of extra-heavy-oil showing oil-brine distribution, under the initial residual saturation condition, showed (Figure 1.1 in Article 1) a discontinuous aqueous phase. Initially the homogeneous medium was water wet. During crude oil injection into the system the oil phase displaced the water phase, and at places ruptured the thin film of water changing it to oil wet conditions. It is important to note that the San Joaquin Valley (California) extra-heavy-oil shows wetting behavior to silica sand (Schramm 2000) at a pH of 7 (Dubey and Doe 1993). Establishing residual saturation of extra-heavy-oil with CsCl flushing proved to be challenging and unsuccessful due to the strongly oil wet system. Moreover, the surfactant application into the system helped maintain the oil-wet conditions. The pH measurement for the anionic surfactant in contact with 40/50 silica sand was approximately 3.6, which created oil-wetting conditions (Buckley 1996) on the silica sand, resulting in immobilization of the oil phase. All SXM images were taken within 24 hours of surfactant application, and the system pH stabilized at 3.94 after 24 hours. Since there was no measurable oil recovery after 2 PVs of surfactant flooding and approximately only 10% recovery after 5 PVs of flooding, it can be concluded that the critical capillary number may have been achieved at some point during the 5-PV flood, thereby producing some recovery. The whole process clearly demonstrates the utility of pore scale 3-D imaging for understanding the trapping mechanisms in this particular case.

The quantitative data demonstrated a negative recovery or addition of extra-heavy-oil (-9%

recovery) in the mildly heterogeneous sand after the 2-PV surfactant flood, and approximately 6.6% recovery after the 5-PV surfactant flood (with respect to the gain in saturation after the 2-PV flood). The previous discussion on 3-D distribution (Figure 3.5) of oil blobs clearly showed spontaneous emulsification processes attributed to the formation of new smaller blobs after sequential surfactant flooding events. Consequently, the total blob surface area increased by 11.3% after the 2-PV flood and 15.2% after the 5-PV flood (3.5% increase with respect to that after the 2-PV flood). Since the water phase was the continuous phase in this case, the surfactant should maximize contact with the trapped oil phase therby aiding in the mobilization of the oil blobs. However, the data reveal that no significant net recovery was achieved even after the 5-PV flood. However, there was approximately a 6.6% oil recovery by volume with respect to the saturation resulting (including additional 9% by volume) after the 2-PV flood. This additional oil saturation may have been incorporated into this small scale system during the surfactant flooding process from oil potentially trapped in the Swagelok end-fitting on top of the column. The pH for this system measured 8.25 during the surfactant flood and stabilized at 8.13 after 24 hours. This high pH can be attributed to the pH buffer due to the carbonate fine fraction of the porous medium. The relatively high pH condition was likely to keep the system water wet, leading to greater recovery. Therefore, in this case, the "jamin effect" may be responsible for the initial negative recovery (net oil gain). It is to be noted that the permeability of the mildly heterogeneous medium is 3.6 E-11m^2, which was the minimum amongst all three media. Although the reduced interfacial tension enhances breaking the oil blobs into smaller fragments, some of the blobs were large enough to be trapped within the smaller pore diameters. However, with subsequent flooding (i.e. 5-PV) the sweep efficiency may have been increased as the aqueous phase preferentially invaded the reduced-permeability regions within the system over

time, yielding more efficient oil recovery with each subsequent surfactant flood. Additional surfactant flooding experiment in this system may have provided further insight in the understanding of mobilization and recovery processes.

The highly heterogeneous system shows continuous recovery after each surfactant flooding episode. On average, 20% oil recovery was achieved after each flood and a maximum of 81% recovery was achieved at the end of 13 PVs of flooding. Previous discussion based on the 3-D distribution of oil blobs, showed that spontaneous emulsification resulted by dispersion of the oil blobs into a continuous phase of water. This result clearly shows how surfactant flooding events may act in reducing interfacial tension of extra-heavy oil thereby yielding spontaneous emulsion and higher recovery. However, it should be noted that the total initial trapped oil volume in this system was relatively lower (1.94 mm^3) compared to that within the homogeneous sand (34 mm^3) and the mildly-heterogeneous (3.8 mm^3) sand. Although new smaller blobs were formed continuously, generating new surface areas in response to reduced interfacial tension, total surface area decreased continuously after each flooding episode. This phenomenon was a result of the continuous recovery behavior due to the removal of a greater number of blobs from the system. Additionally, the formation of larger blobs by coalescence processes (reducing surface area) may also have had some effect on surface area reduction. The pH measured for this system was stable at 8.31 even after 24 hours. This measurement ensured the stability of water wet conditions for this system and was likely responsible for yielding greater recovery with time. Again, the carbonate fine fraction of the porous medium was attributed to this pH buffering process for this system.

3.3.4 Statistical Analysis of Blob Distribution

Knowledge of the oil blob distribution and the blob volume morphology in an emulsion formation are important for understanding the recovery process for a particular porous medium. The synchrotron-based imaging techniques make it possible to estimate the blob volume and the surface area for each individual blob when a spontaneous emulsion is formed in-situ. Characterization of the blob-distribution pattern provides important information about the stability of the emulsion and mobilization processes within a porous medium with known porosity and permeability. Since the pore size distributions of the three media are different, the resulting blob volume distributions are also different. The distribution pattern for emulsion formation is usually characterized by a large number of fine blobs and few larger blobs. Although few in number the larger blobs include the major fraction of the oil by volume. Conventionally this type of distribution is characterized and compared by log-normal cumulative distribution plots. Figure 3.7 shows the distribution pattern of extra-heavy-oil blobs trapped within the homogeneous porous medium. However, this type of plot is more useful for characterizing disconnected emulsified blobs. Since, the larger fraction of the oil phase in the homogeneous medium is present as interconnected ganglia, it was only possible to plot it as a single multi-pore large blob. Therefore this plot provides limited information about the distribution pattern for this particular system. However the distribution patterns of the other two heterogeneous media were well characterized and compared using the log-normal cumulative distribution analysis process. Figure 3.8 shows the distribution of the surface area of the blobs within the homogeneous medium, where the dark bold line represents the model curve representing the blob distribution as perfect spheres (minimum surface area condition) for all respective equivalent blob volumes. In other words, for a particular volume any deviation (along

a vertical line) from that model curve represents larger surface area, or a complex-nonspherical morphology. However, this plot also has limitations describing ganglia type distributions. Therefore the discussion for these plots is limited to the disconnected blobs trapped and mobilized within the two more heterogeneous media (i.e. mildly heterogeneous and highly heterogeneous).

The cumulative distribution of the blobs in the mildly-heterogeneous porous medium was characterized by a relatively heterogeneous distribution under the initial residual saturation condition, and the trend remained approximately the same after surfactant flooding episodes. The blob volumes ranged from 10^{-5} mm^3 to 10^{-1} mm^3, for all three series of surfactant flooding episodes. For all flooding episodes the mean and median blob sizes vary on the order of 10^{-4} mm^3 and 10^{-5} mm^3, respectively. Detailed observation of the distribution pattern reveals small change in blob size after 2 PVs of flooding. For example, the larger blobs increased slightly by volume, most likely by coalescence or redistribution processes. Over the duration of 5 PVs of flooding the oil blobs became smaller which is consistent with the previous observation (Figure 3.5). Two parameters can be used to compare the heterogeneity of the blob size distribution pattern, such as uniformity coefficient (C_U) and coefficient of variation (C_V). The coefficient of variation is the ratio of the standard deviation with the mean volume in a blob distribution. C_V varies from 6 (relatively homogeneous) as initial residual saturation condition to approximately 6.4 (relatively heterogeneous) after the total 5-PV surfactant flood. C_U ranged from 3.5 to 3.9 and is consistent with the previous result in terms of representing a relatively homogeneous blob distribution. No major change was observed in the blob morphology under initial residual saturation conditions and after each subsequent surfactant flooding event. As expected, the larger the blobs exhibited maximum deviation from a spherical shape. All blob volumes greater than

10^{-4} mm^3 (mean volume), under initial residual saturation conditions and after surfactant flooding, deviated markedly from a spherical shape. Quantitative data also demonstrated no significant change in the total blob surface area, as initial residual saturation and after sequential surfactant flooding. These overall results suggest that although interfacial activities in terms of the spontaneous emulsification processes can be clearly observed at the pore scale, cold recovery processes, in this case, was controlled by the permeability of the porous medium. Similar recovery behavior and blob surface area change was observed for the light and heavy oil in this same porous medium (mildly heterogeneous) (Chapter 2). For these specific studies, only the light oil showed obvious changes in blob morphology and consistent increase in surface area to more non-spherical shape in response to surfactant flooding. However, the heavy gravity oil showed an increase in total surface area primarily by the formation of new smaller blobs in response to reduced interfacial tension (i.e. due to surfactant). Similar to the extra-heavy oil recovery behavior, relatively low oil recoveries (~10%) were observed for both the light and heavy oil in this mildly heterogeneous medium after the 2-PV flood but significantly greater recovery after 5 PVs of flooding due to the "jamin effect".

The blob distribution pattern in the highly heterogeneous medium can be characterized by two phenomena: 1) an overall gradual decrease in blob volume from the initial residual saturation condition to the other episodes of surfactant flooding. This result is consistent with that observed within the representative 3-D SXM imaged sections; 2) the blobs exhibit a trend from relatively heterogeneous distribution to more homogeneous distribution after each sequential surfactant flooding event. Blob sizes ranged from 10^{-5} mm^3 to 10^{-2} mm^3 under initial residual saturation condition. The maximum blob volume in this medium (highly heterogeneous) was one order of magnitude less than the blobs present within the mildly-heterogeneous medium

(initial residual saturation condition). Both mean and median blob volumes were approximately 1×10^{-5} mm^3. The mean blob volume was 9.2×10^{-5} mm^3 as initial residual saturation and decreased to 4×10^{-5} mm^3 after 13 PVs of surfactant flooding. However, median blob volume changed from 2.9×10^{-5} mm^3 to 2×10^{-5} mm^3. The change in distribution pattern from the heterogeneous to the relatively more homogeneous was evaluated by C_U and C_V. C_U changed from 2.7 (initial residual saturation condition) to 1.8 after the 13-PV flood, and C_V changed from 12.6 to 2.9, respectively. As mentioned previously, lower C_U and C_V represent more homogeneous blob distribution conditions. Changes in the blob morphology pattern also exhibited a generally consistent and continuous trend from more non-spherical in shape (initial residual saturation condition) to more spherical in shape after each respective surfactant flooding event as the blob volume reduced with time (over the series of flushing). This observation differs from that observed for the light and heavy oil recovery discussed in Chapter 2. Under qualitative assessment, a correlation was determined between the total blob surface area and oil recovery after surfactant flooding events. In this particular system, it was shown in the 3-D SXM-imaged small section, that new blobs were formed due to surfactant-reduced interfacial tension leading to an increase in the total blob surface area. However, this increase was less than the total surface area of the blobs removed from the system by recovery process, resulting in a total decrease in surface area from the system. The overall results of this study demonstrate the promising and effective utility of synchrotron X-ray microtomography imaging for understanding heavy oil distribution under spontaneous emulsion conditions and resulting mobilization and flow behavior as related to oil recovery. Therefore, studies such as this will provide critical information for assessing the feasibility of larger systems most amenable to enhanced cold recovery techniques.

3.4 SUMMARY AND CONCLUSIONS

Synchrotron X-ray microtomography (SXM) has been used to conduct a comprhensive high resolution pore scale study of extra-heavy-oil distribution trapping in various unconsolidated sands of increasing heterogeneity. Experiments and observations were also carried out to study the interfacial processes in response to surfactant application for enhanced extra-heavy-oil recovery. This technique reduces oil-brine interfacial tension, resulting in oil blob distributions through spontaneous emulsion and enhanced mobilization through pore spaces. As part of this study, a series of experiments were conducted to understand temporal changes of oil distribution patterns and oil blob morphology on recovery behavior in response to multiple episodes of anionic surfactant flooding events. A time series assessment of blob mobilization and transport and associated recovery was studied under initial residual saturation conditions and after respective sequential surfactant flooding episodes. The following conclusions can be made from the results obtained from this research:

1. In homogeneous sand systems (due to high permeability, and pH conditions) trapping of the continuous oil phase (ganglia type distribution) displaced initially water-wet pore spaces to become oil wet. Wettability of the homogeneous sand was changed from water-wet to oil-wet, imposing greater challenges for the surfactant induced recovery process. Additional challenges were caused by the discontinuous water phase, which limited the surfactant solution contact with the oil phase resulting in less interfacial activity, and consequently, less recovery from this particular system.

2. Porous media sorting and permeability are primary factors controlling discontinuous oil blob trapping and distribution. Spontaneous in-situ emulsion of oil-in-water was produced under initial residual saturation conditions within both the heterogeneous porous media. Blob

distribution in the oil-water emulsion in the mildly-heterogeneous-medium was stable after surfactant flooding events, attributed to the formation of smaller blobs due to reduced oil-water interfacial tension. No major changes in the oil-blob morphology have been observed in this medium. Delayed recovery after the 5-PV flood may be the result of the "jamin effect", characterized by local saturation of oil blobs which are restricted by smaller pore diameters (absolute permeability 3.6 E-11m^2). Greater recovery was obtained at the later stages of surfactant flushing due to the formation of smaller blobs, and increased saturation of oil-water emulsion in relatively impermeable zones giving rise to larger and better sweep efficacy.

3. Steady recovery was achieved from the highly heterogeneous medium which was attributed to the emulsion formation under the initial residual saturation condition and which became stable after subsequent surfactant floods. A more homogeneous blob distribution resulted after each flooding episode and a greater number of smaller blobs were formed due to reduced interfacial tension effects related to sequential surfactant application. Blob morphology changed from non-spherical, as initial residual saturation condition, to more spherical as the flooding continued and progressed. A steady oil recovery rate of (~ 20%) was achieved after each respective surfactant flooding event. Higher pH aided in maintaining water-wet condition yielding a higher recovery through time.

The overall results of this study demonstrate that synchrotron X-ray microtomography can be a very useful tool for characterizing and enhancing the current understanding of pore-scale multiphase mobilization and transport for the application of oil recovery techniques. Results obtained from this research showed an unprecedented level of oil distribution characterization to better understand the influence of pore scale processes on oil recovery during EOR in which a surfactant solution was used. In addition, this research

provided an enhanced understanding of spontaneous emulsion formation processes on extra-heavy oil recovery when implementing cold recovery techniques. These factors are critical when evaluating the conditions, such as oil blob size distribution and particular blob morphologies, most favorable for enhanced recovery from a particular oil-porous medium system.

REFERENCES

Albahlani, A.M., and Babadagli, T. (2008). A critical review of the status of SAGD: Where are we and what is next? *Society of Petroleum Engineers, SPE Western Regional and Pacific Section AAPG Joint Meeting, 29 March-2 April 2008, Bakersfield, California, USA Paper Number 113283-MS. d*oi: 10.2118/113283-MS

Al-Raoush, R. I.and Willson, C. S. (2005). Extraction of physically realistic pore network properties from three-dimensional synchrotron X-ray microtomography images of unconsolidated porous media systems, *Journal of Hydrology 300 (1-4)*, 44-64. doi: 10.1016/j.jhydrol.2004.05.005.

Boom R. M. (2008). Emulsion-Based Products, Types of Emulsions and Their Uses, In Aguilera, J. M. and Lillford, P. J. (Ed), *Food Materials Science*, Springer, New York pp.305-339, doi: 10.1007/978-0-387-71947-4_15

Bryan, J., and Kantzas, A. (2009). Potential for Alkali-Surfactant Flooding in Heavy Oil Reservoirs Through Oil-in-Water Emulsification, *Journal of Canadian Petroleum Technology, 48(2)*, 37-46, doi: 10.2118/09-02-37

Buckley, J.S., Bousseau, C., and Liu, Y. (1996). Wetting alteration by brine and crude oil: from contact angles to cores, *Soc. Pet. Eng*., 1, 341-350, doi: 10.2118/30765-PA

Carlson, W. B. (2011). The Modeling of World Oil Production Using Sigmoidal Functions-Update 2010, *Energy Sources Part B: Economics, Planning and Policy, Vol. 6(2),* 178-186, doi: 10.1080/15567249.2010.516310

Carrigy, M. A. (1962). Effect of texture on the distribution of oil in the Athabasca oil sands, Alberta, Canada, *Journal of Sedimentary Petrology, vol. 32(2)*, 312-325

Chatzis, I. and. Dullien, A. L. (1983). Dynamic Immiscible Displacement Mechanisms in Pore Doublets: Theory versus Experiment, *Journal of Colloid and Interface Science,* 91(1), 199-222, doi: 10.1016/0021-9797(83)90326-0.

Chatzis I., Morrow N.R., and Lim H.T. (1983). Magnitude and detailed structure of residual oil saturation. *Soc. Pet. Eng*., 23, 311-326.

Coles, M.E., Hazlett, R.D., Spanne, P., Soll, W.E., Muegge, E.L., and Jones, K.W. (1998). Pore level imaging of fluid transport using synchrotron x-ray microtomography. *Journal of Petroleum Science and Engineering, 19 (1-2)*, 55–63

Craze, R.C. (1950). Performance of limestone reservoirs. *Trans. Amer. Inst. Min. Eng., 189*, 287-294.

Das, S. K., and Butler, R. M. (1998). Mechanism of the vapor extraction process for heavy oil and bitumen, *Journal of Petroleum Science and Engineering, 21(1-2)*, 43-59, doi: 10.1016/S0920-4105(98)00002-3

Dubey, S.T., and Doe, P.H. (1993). Base Number and Wetting Properties of Crude Oils, *SPE Reservoir Engineering, 8 (3)*, 195-200, doi: 10.2118/22598-PA

Flannery, B.P., Deckman, H.D., Roberge, W.G. and D'Amico, K.L. (1987). Three-dimensional x-ray microtomography, *Science, New Series*, *237* (4821), 1439-1444

Goddard, W.A., Tang, Y., Shuler, P., Blanco, M., Jang, S.S., Lin, S.T., Maiti, P., Wu, Y., Iglauer, S., and Zhang, X. (2004). Lower cost methods for improved oil recovery via surfactant flooding: final report. Department of Energy DE-FC26-01BC15362

Greene, D. L., Hopson, J. L., and Li, J. (2006). Have we run out of oil yet? Oil peaking analysis from an optimist's perspective, *Energy Policy 34*, 515–531, doi:10.1016/j.enpol.2005.11.025

Guseo, R., Dalla Valle, A., and Guidolin, M. (2007). World Oil Depletion Models: Price effects compared with strategic or technological interventions, *Technological Forecasting and Social Change, 74, (4),* 452-469

Head, I. M., Jones, D. M., and Larter, S. R. (2003). Biological activity in the deep subsurface and the origin of heavy oil, *Nature 426, 344-352,* doi:10.1038/nature02134

Hirasaki, G., and Zhang, D. L. (2004). Surface Chemistry of Oil Recovery From Fractured, Oil-Wet, Carbonate Formations, *SPE Journal, 9(2)*, 151-162, doi: 10.2118/88365-PA

Hirasaki, G.J., (1991). Wettability: Fundamentals and Surface Forces, *SPE Formation Evaluation, 6, (2),* 217-226, doi: 10.2118/17367-PA

Hubbert, M. K. (1953). Entrapment of petroleum under hydrodynamic conditions *American Association of Petroleum Geologist Bulletin, 37,* 1954-2026 doi: 10.1306/5CEADD61-16BB-11D7-8645000102C1865D

Hunky, R. M.,Wu, Y., Bai, B., and Dunn-Norman, S.(2010). An Experimental Study of Alkaline Surfactant Flooding for Ultra Shallow Heavy Oil Reservoirs, *Society of Petroleum Engineers, Western Regional Meeting,* 27-29 May 2010, Anaheim, California, doi:10.2118/132537-MS

Johnson Jr., C.E., (1976). Status of Caustic and Emulsion Methods, *Journal of Petroleum Technology, 28, (1)*, 85-92

Kaminsky, R., and Radke, C. J. (1997). Asphaltenes, water films, and wettability Reversal. *SPE Journal*, *2(4),* 485–493. doi: 10.2118/39087-PA

Kantzas, A., Marentette, D. F., Erno, B., and Harding, S. (1994). Characterization of a Heavy Oil Reservoir Using Computer Assisted Tomography of Core Material, *Journal of Canadian Petroleum Technology, 33 (6),* doi: 10.2118/94-06-03

Ketcham, R.A. (2005). Computational methods for quantitative analysis of three-dimensional features in geological specimens. *Geosphere, 1*, 32-41.

Ketcham, R.A., and Carlson, W.D. (2001). Acquisition, optimization and interpretation of x-ray computed tomographic imagery: application to the geosciences. *Comput. Geosci*., *27*, 381-400.

Levorsen, A. I. (2001). *Geology of petroleum (2nd Ed.).* The AAPG Foundation. Tulsa, Oklahoma.

Liu, Q., Dong, M., and Ma, S. (2006). Alkaline/Surfactant Flood Potential in Western Canadian Heavy Oil Reservoirs. *SPE/DOE Symposium on Improved Oil Recovery, 22-26 April 2006*, Tulsa, Oklahoma USA, doi: 10.2118/99791-MS

Luo, H., and Kantzas, A. (2011). Study of Diffusivity of Hydrocarbon Solvent in Heavy-Oil Saturated Sands Using X-Ray Computer Assisted Tomography. *Journal of Canadian Petroleum Technology*, *50(2),* 24-34. doi: 10.2118/145309-PA.

McAuliffe, C. D., (1973). Oil-In-Water Emulsions And Their Flow Properties In Porous Media, *Journal of Petroleum Technology, 25, (6),* 727-733, doi: 10.2118/4369-PA

Mercer, J.W., and Cohen, R.M. (1990). A review of immiscible fluids in the subsurface: properties, models, characterization and remediation, *journal of Contaminant Hydrology, 6 (2)*,107-163. doi:10.1016/0169-7722(90)90043-G

Meyer, R.F., Attanasi, E.D., and Freeman, P.A. (2007). Heavy oil and natural bitumen resources in geological basins of the world: *U.S. Geological Survey Open-File Report*, 2007-1084. Retrieved on 7/12/11 from http://pubs.usgs.gov/of/2007/1084/.

Meyer R.F., and Attanasi, E.D. (2003). *Heavy Oil and Natural Bitumen- Strategic Petroleum Resources*, USGS Fact Sheet. Retrieved on 7/12/11 from http://walrus.wr.usgs.gov/infobank/programs/html/factsheets/pdfs/2003_0070_FS.pdf

Morrow, N. R. (1990). Wettability and its effect on oil recovery. *Journal of Petroleum Technology*, *42(12),* 1476–1484. Doi: 10.2118/21621-PA

Morrow, N.R., Chatzis, I., and Taber, J.J. (1988). Entrapment and mobilization of residual oil in bead packs, *SPE Reservoir Engineering, 3 (3)*, 927-934, doi: 10.2118/14423-PA

Morrow, N.R., and Chatzis, I. (1982). Measurement and correlation of conditions for entrapment and mobilization of residual oil. *Dept. Energy Report, 10310* (20), 59.

Peters, E. J., and Hardham, W. D. (1990). Visualization of fluid displacements in porous media using computed tomography imaging *Journal of Petroleum Science and Engineering*, *4(2),* 155-168

Powers S.E., Abriola L.M., and Weber W.J. (1992). An experimental investigation of nonaqueous phase liquid dissolution in saturated subsurface systems: steady state mass transfer rates. *Water Resour. Res., 28*, 2691-2705.

Romero, M. I. (2009). Flow of Emulsions in Porous Media. *SPE Annual Technical Conference and Exhibition, 4–7 October 2009,* New Orleans, Louisiana, paper SPE 129519-STU.

Salama, D. and Kantzas, A. (2005). Monitoring of Diffusion of Heavy Oil with Hydrocarbon Solvents in the Presence of Sand. *Proceedings: SPE/PS-CIM/CHOA International Thermal Operations and Heavy Oil Symposium*, *1-3 November 2005, Calgary, Alberta, Canada*, doi: 10.2118/97855-MS

Schenk, C. J., Pollastro, R. M., and Hill, R. J. (2006). Natural Bitumen Resources of the United States, *USGS Fact Sheet.* Retrieved on 7/12/11 from http://pubs.usgs.gov/fs/2006/3133/pdf/FS2006-3133_508.pdf

Schnaar, G., and Brusseau, M.L. (2006a). Characterizing pore scale configuration of organic liquid in multiphase systems with synchrotron X-ray microtomography. *Vadose Zone Journal*, *5*, 641-648.

Schnaar, G., and Brusseau, M.L. (2006b). Characterizing pore-scale dissolution of organic immiscible liquid in natural porous media using synchrotron X-ray Microtomography. *Environ. Sci. Technol*., *40*, 6622-6629.

Schramm, L.L. (2000). *Surfactants: fundamentals and applications in the petroleum industry.* Cambridge, N.Y., Madrid. Cambridge University Press.

Taber, J.J., Martin, F.D. and Seright, R.S. (1997). EOR Screening Criteria Revisited- Part 1: Introduction to Screening Criteria and Enhanced Recovery Field Projects. *SPE Reservoir Engineering*, *12(3),* 189-198, doi: 10.2118/35385-PA.

Thomas, S., and Ali, S. M. F. (1989). Flow of Emulsions in Porous Media, and Potential for Enhanced oil recovery. *Journal of Petroleum Science and Engineering*, *3(1-2),* 121-136, doi: 10.1016/0920-4105(89)90038-7.

Tremblay, B., Sedgwick, G., and Forshner, K., (1996). Imaging of Sand Production in a Horizontal Sand Pack by X-Ray Computed Tomography. *SPE Formation Evaluation*, *11(2),* 94-98, doi: 10.2118/30248-PA.

Walstra, P. (1993). Principles of Emulsion Formation. *Chemical Engineering Science*, *48(2),* 333-349, doi: 10.1016/0009-2509(93)80021-H.

Wardlaw, N. C., and Yu, L. (1988). Fluid topology, pore size and aspect ratio during imbibition. *Transport in Porous Media, 3(1),* 17– 34, doi: 10.1007/BF00222684

Wardlaw, N. C., and McKellar, M. (1985). Oil blob populations and mobilization of trapped oil in unconsolidated packs. *Canadian Journal of Chemical Engineering*, *63*, 525-531, doi: 10.1002/cjce.5450630401

Wardlaw, N. C. (1982). The effects of geometry, wettability, viscosity and interfacial tension on trapping in single pore-throat pairs, *Journal of Canadian Petroleum Technology, 21(3)*, 21-27, doi:10.2118/82-03-01

Wildenschild, D., Hopmans, J.W., Vaz, C.M.P., Rivers, M.L., Rikard, D., and Christensen, B.S.B. (2002). Using X-ray computed tomography in hydrology: systems, resolutions and limitations. *Journal of Hydrology, 267*, 285-297.

Wu, Y., Shuler, P., Blanco, M., Tang, Y., and Goddard, W. A. (2005). A Study of Branched Alcohol Propoxylate Sulfate Surfactants for Improved Oil Recovery. *SPE Annual Technical Conference and Exhibition, 9-12 October 2005,* Dallas, Texas, SPE Doi: 10.2118/95404-MS

Table 3.1 Properties of three types of porous media.

Properties	Accusand 40/50: Homogeneous medium	Mildly Heterogeneous medium	Mixed accusand carbonate: Highly Heterogeneous Medium
Median Grain Diameter, d_{50} (mm)	0.35	0.27	0.37
Uniformity Coefficient, Cu	1.00	5.8	10.6
Bulk Density (disturbed) [g/cm^3]	1.75	1.97	1.95
Wet Porosity	0.33	0.27	0.25
Permeability (m^2)	9E-11	3.6E-11	5.4E-11

Table 3.2 Physical parameters controlling the mobilization process in three types of porous media.

	Homogeneous	Mildly heterogeneous	Highly heterogeneous
Residual Saturation			
True IT (γ) dyne/cm	42.25	42.25	42.25
Capillary number	4.48E-04	5.48E-04	5.92E-04
Bond Number	1.24E-13	4.13E-14	6.88E-14
After flooding with 0.1% Surfactant			
True IT (γ) dyne/cm	24.68	24.68	24.68
Capillary number	7.68E-04	9.39E-04	1.01E-03
Bond Number	2.12E-13	7.07E-14	1.18E-13

Table 3.3 Quantitative data for extra-heavy oil (4.2˚ API) in the homogeneous (C_U = 1) porous medium.

Parameters	Residual	After 2PV flood	After 5 PV flood
No. of blobs	ganglia	ganglia	ganglia
Mean Volume (cu mm)	N/A	N/A	N/A
Coefficient of variation (C_v)	N/A	N/A	N/A
Total Surface Area (mm^2)	1034.456	1108.619 (change 7%)	1092.859 (Change -1.4 %)
Total volume (mm^3)	34.036	35.553(Recovery -4.5%)	32.045(Recovery 9.9%)
Net recovery (w.r.t. residual)		-4.5%	5.8%

Table 3.4 Quantitative data for extra-heavy oil (4.2˚ API) in the mildly-heterogeneous sand (C_U = 5.8).

Parameters	Residual	After 2PV flood	After 5 PV flood
No. of blobs	25810	28518	32831
Mean Volume (cu mm)	1.48E-4	1.46E-4	1.19E-4
Median Volume (cu mm)	2.94E-5	2.86E-5	2.61E-5
Standard Deviation (cu mm)	0.00089	0.00093	0.00076
Coefficient of variation (C_V)	6.003	6.365	6.380
Uniformity coefficient (C_U)	3.543	3.935	3.556
Total Surface Area (mm^2)	402.414[*]	448.029[#] (+ 11.3%)	463.639 (+3.5%)[#], (+15.2%)[*]
Total volume (mm^3)	3.820	4.165(-9%)	3.892 (6.6%)
Net recovery (w.r.t. residual)		-9%	-1.9%

Table 3.5 Extra-heavy oil (4.2˚ API) distribution and recovery data from the highly heterogeneous sand (C_U =10.6).

Parameters	Residual Saturation	After 2PV Surfactant flood	After 5 PV Surfactant flood	After 9 PV Surfactant flood	After 13 PV Surfactant flood
No. of blobs (single particles)	21038	20142	17567	14818	8813
Mean Volume (cu mm)	9.2E-5	8.0E-5	6.6E-5	5.0E-5	4.0E-5
Median Volume (cu mm)	2.9E-5	2.6E-5	2.5E-5	2.2E-5	2.0E-5
Standard Deviation (cu mm)	0.000365	0.000359	0.000246	0.000144	0.000116
Coefficient of variation(C_V)	12.616940	4.455173	3.702358	2.857173	2.901247
Uniformity coefficient (C_U)	2.671352	2.557239	2.369084	2.754082	1.849530
Surface area (mm^2)	226.453	203.726 (-10%)	161.497 (-20.7%)	113.701 (-29.6%)	57.018 (-49.9%)
Total volume (mm^3)	1.941002	1.620766 (-16.2%)	1.165686 (-28.1%)	0.745225 (-36.1%)	0.353684 (-52.5%)
Net increased surface		-16.2%	-28.7%	-49.8%	-74.8%
Net recovery (w.r.t. residual)		16.2%	39.9%	61.6%	81.8%

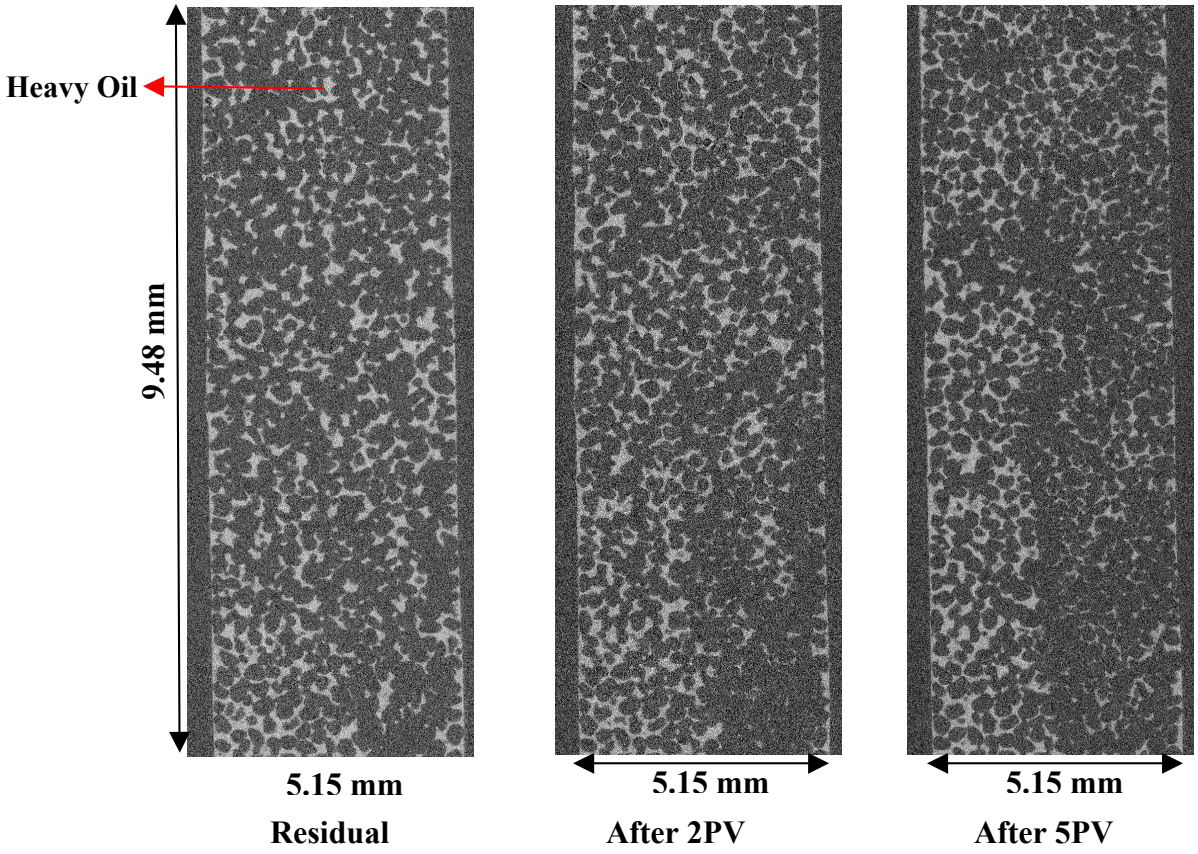

Figure 3.1. Vertical 2-D sections (binary image) of one column along the X-Z plane showing the distribution of extra-heavy-crude oil (San Joaquin Valley Crude) within the homogeneous-porous-medium (40/50 accusand, $C_U = 1$). Figure showing the trapping of the continuous oil phase due to oil-wet state attributed to the low pH condition for the initial residual saturation (pH = 5.6) system and after the 2-PV and 5-PV surfactant (0.1% v/v, pH = 3.6) flooding events. Limited oil recovery or oil mobilization occurs along the preferential flow paths.

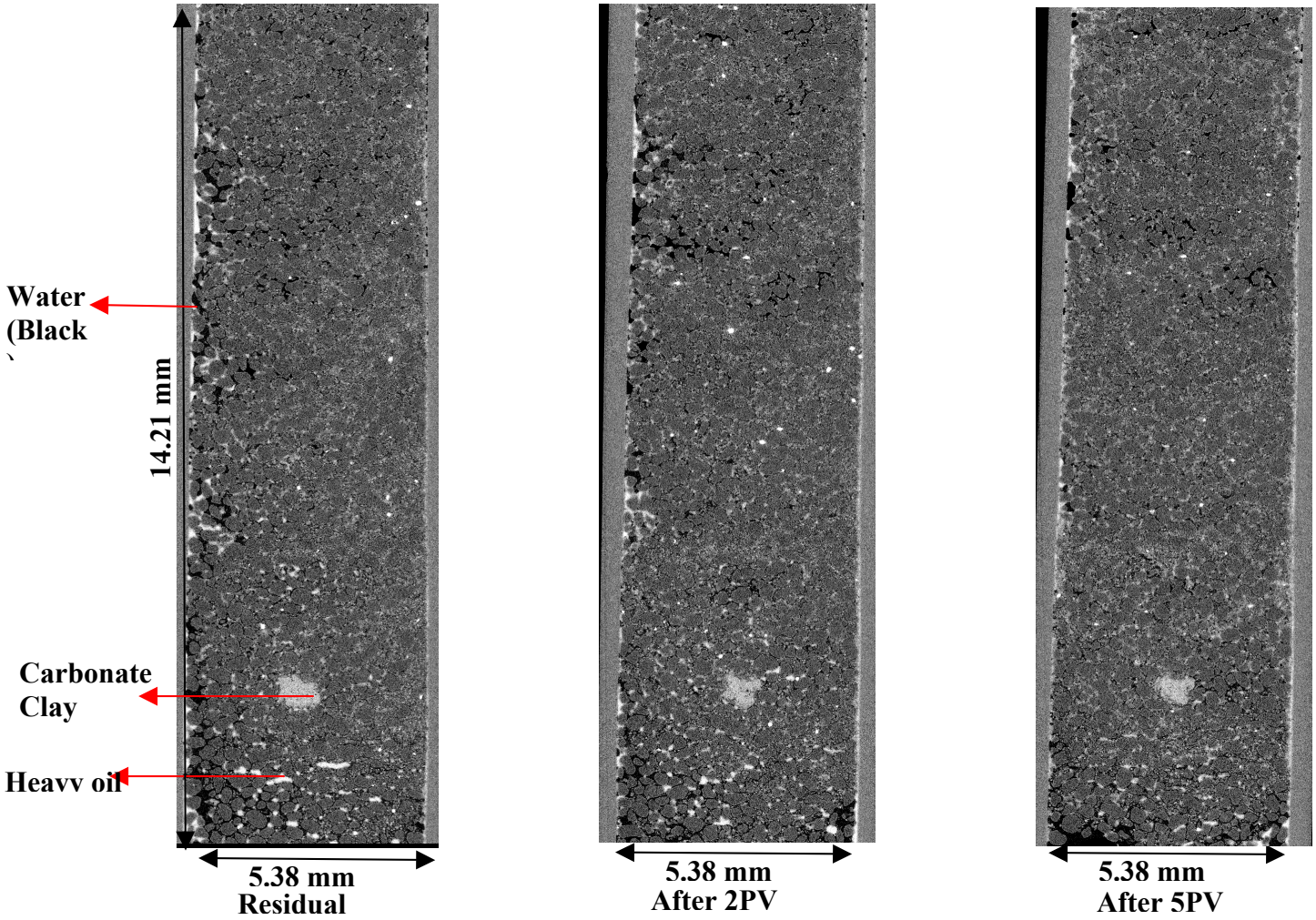

Figure 3.2. Vertical 2-D sections of the column along the X-Z plane showing extra-heavy-oil (San Joaquin Valley Crude) and aqueous phase distributions over various surfactant flushing episodes, within the mildly heterogeneous sand ($C_U = 5.8$). From left to right: initial oil residual saturation, saturation after the 2-PV surfactant flood, and saturation after the 5-PV surfactant flood. Any effects or quantification errors due to potential preferential mobilization of oil phase along the column boundaries was mitigated by cropping these boundaries out of the images (for all columns) before the estimation of quantitative recovery data (e.g. see Figure 3.3).

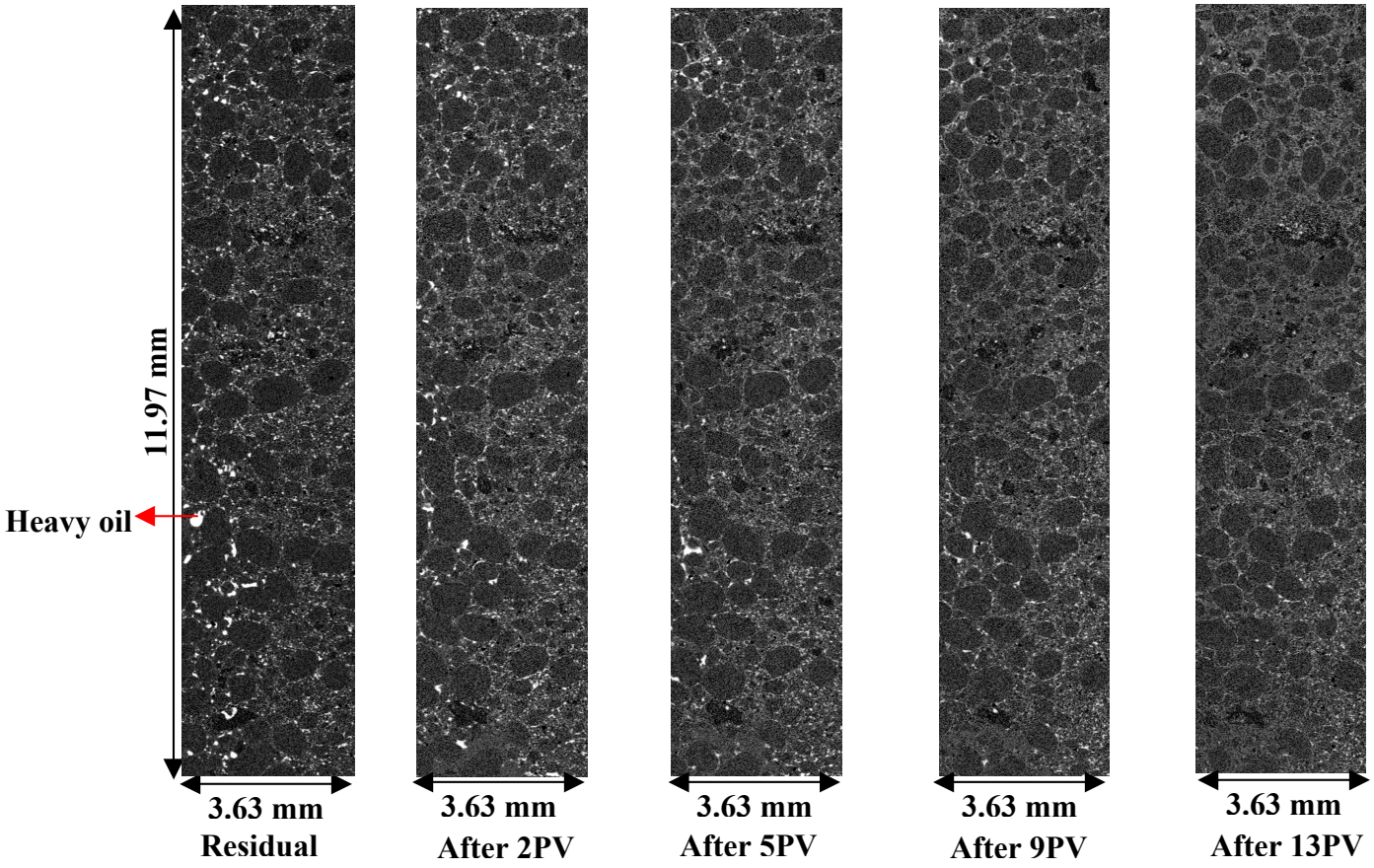

Figure 3.3. Vertical 2-D sections of a column (cropped along the boundaries) showing extra-heavy-oil (San Joaquin Valley Crude) distribution in the highly heterogeneous sand (C_U = 10.6). From left to right: initial residual saturation, after 2-PV, 5-PV, 9-PV, and 13-PV flooding events with anionic surfactant. Distributions are characterized by disconnected oil blobs in each system. Consistent recovery resulted after each surfactant flood (16%, 39%, 61% and 81% respectively) due to water-wet conditions attributed to pH >8.

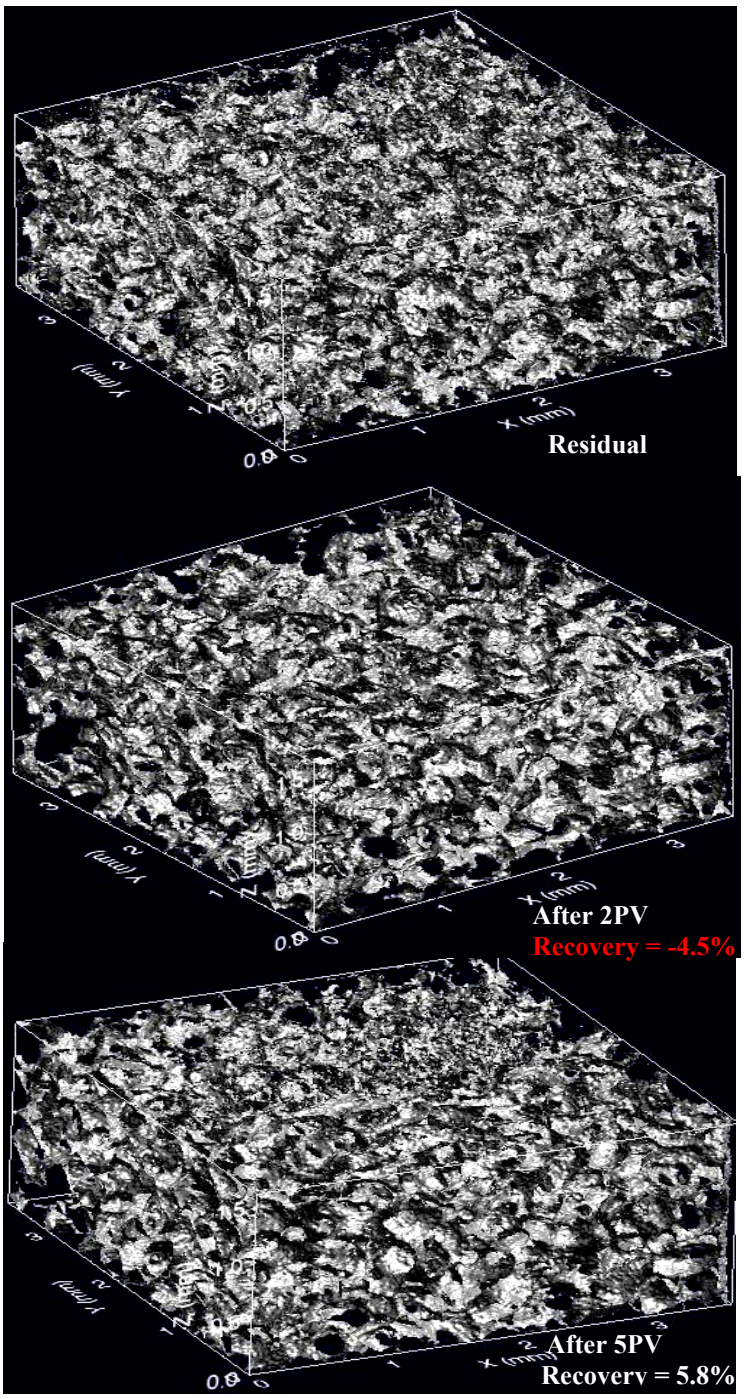

Figure 3.4. 3-D images showing cropped sections (3.83×3.83×1.5 mm^3) of the column (see Figure 3.1) containing extra-heavy-crude oil within the homogeneous porous medium (40/50 Accusand). Distributions are characterized by continuous interconnected ganglia attributed to oil-wet conditions at pH less than 7. Negative recovery resulted after the 2-PV flooding event and 6% net recovery was achieved after 5 PVs of surfactant flooding.

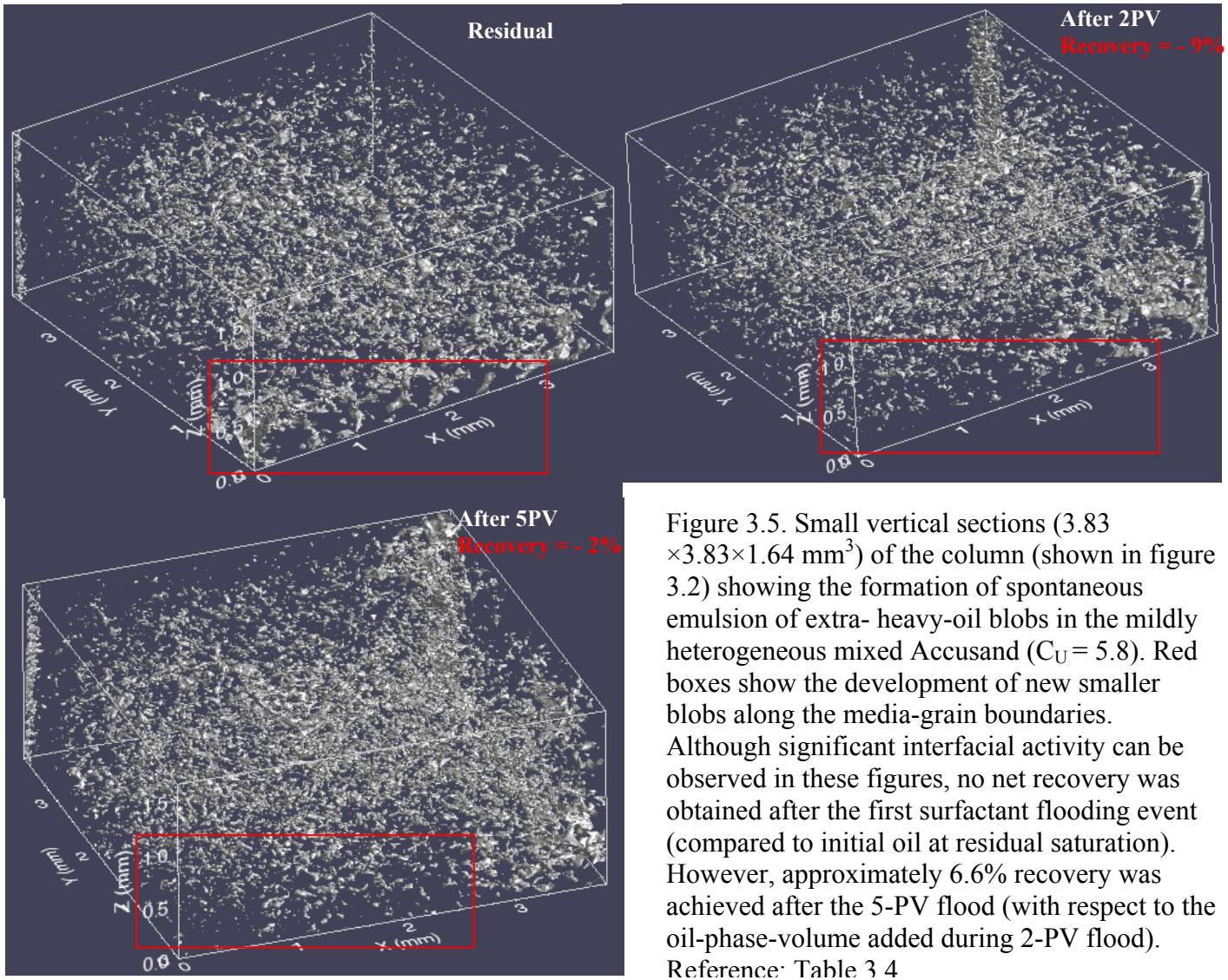

Figure 3.5. Small vertical sections (3.83 ×3.83×1.64 mm^3) of the column (shown in figure 3.2) showing the formation of spontaneous emulsion of extra- heavy-oil blobs in the mildly heterogeneous mixed Accusand (C_U = 5.8). Red boxes show the development of new smaller blobs along the media-grain boundaries. Although significant interfacial activity can be observed in these figures, no net recovery was obtained after the first surfactant flooding event (compared to initial oil at residual saturation). However, approximately 6.6% recovery was achieved after the 5-PV flood (with respect to the oil-phase-volume added during 2-PV flood). Reference: Table 3.4

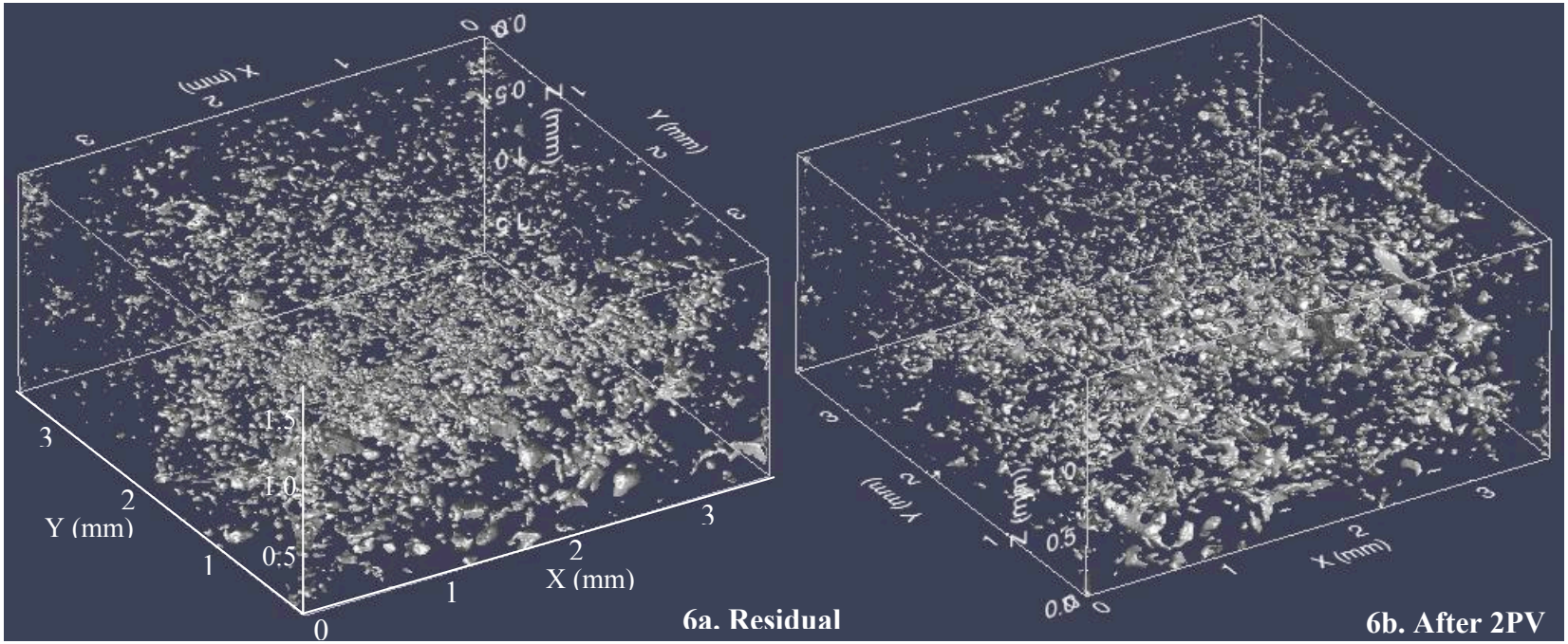
Y (mm)
X (mm)
Z (mm)
0.5
1.0
1.5
0
1
2
3
6a. Residual
6b. After 2PV

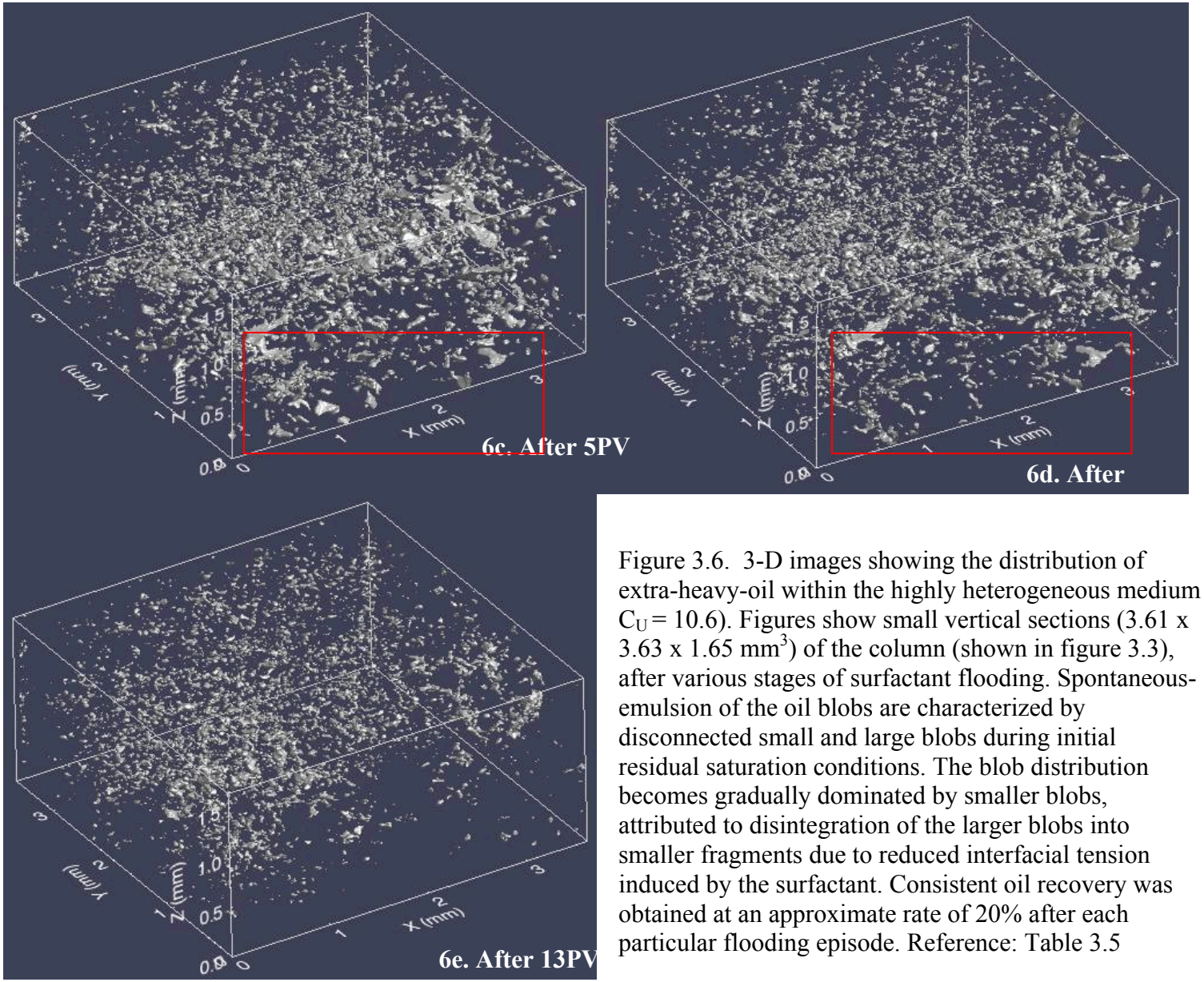

Figure 3.6. 3-D images showing the distribution of extra-heavy-oil within the highly heterogeneous medium (C_U = 10.6). Figures show small vertical sections (3.61 x 3.63 x 1.65 mm^3) of the column (shown in figure 3.3), after various stages of surfactant flooding. Spontaneous-emulsion of the oil blobs are characterized by disconnected small and large blobs during initial residual saturation conditions. The blob distribution becomes gradually dominated by smaller blobs, attributed to disintegration of the larger blobs into smaller fragments due to reduced interfacial tension induced by the surfactant. Consistent oil recovery was obtained at an approximate rate of 20% after each particular flooding episode. Reference: Table 3.5

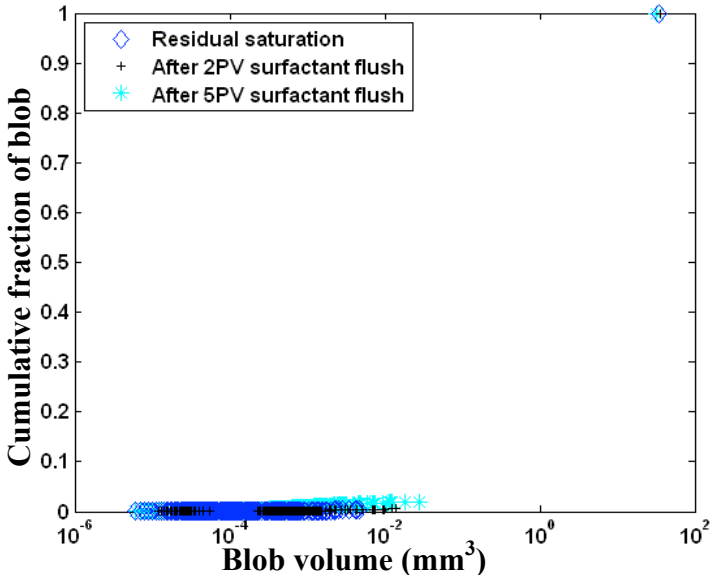

Figure 3.7. Figure showing cumulative distribution of extra-heavy oil-blob/ganglia in the homogeneous sand (40/50 Accusand). The distribution of the initial oil residual saturation, and distributions after the 2-PV and 5-PV surfactant flooding events do not show significant change in the distribution pattern. The single large blob (top right) represents large continuous oil-ganglia that includes most of the oil-phase volume present within the system. All other smaller blob fragments, which may also include the part of the thin layer adsorbed on to the grain boundaries, represent insignificant fraction of the total oil saturation (see Figures 3.1 and 3.4).

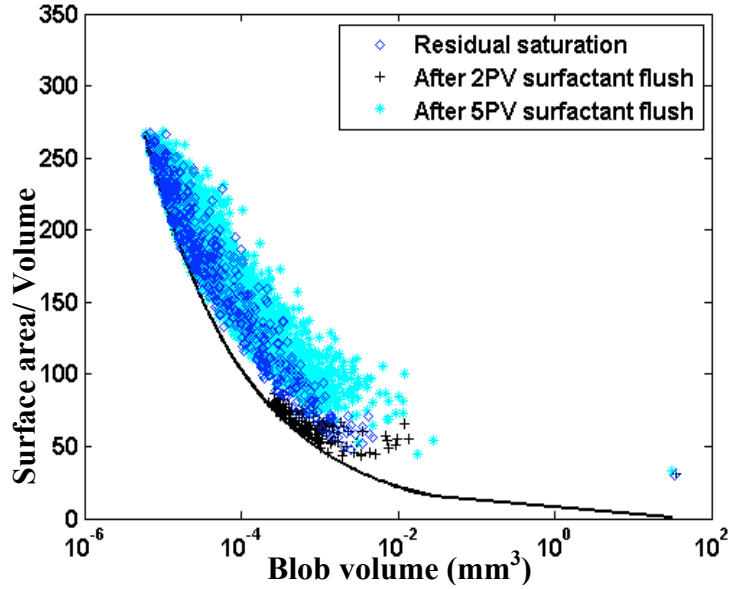

Figure 3.8. Plot showing the deviation of extra-heavy oil blobs from spherical shape for the system shown in Figure 3.7. The smaller blobs, representing only a very small fraction of the total oil saturation, show progressively greater deviation from a spherical shape (represented by black curve) as a function of flooding duration (i.e. greater deviation after the 2-PV and 5-PV surfactant flooding events). The large ganglia (extreme right) includes the majority of the trapped oil volume after all three flooding episodes and is primarily attributed to the wettability change due to low pH conditions (< 7) of the system (see figures 3.1 and 3.4).

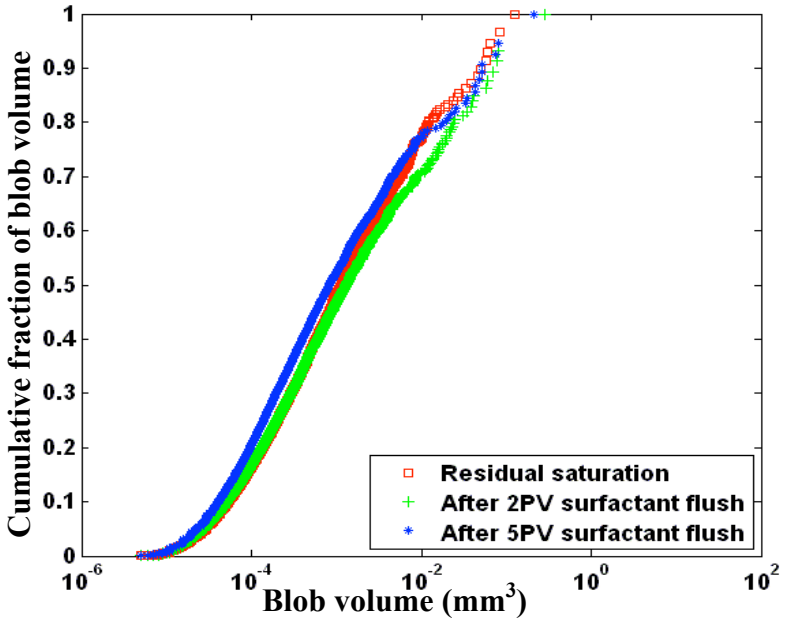

Figure 3.9. Figure showing the cumulative distributions of the extra-heavy blobs in spontaneous emulsion, within the mildly heterogeneous sand (C_U = 5.8) (see figures 3.2 and 3.5). A relatively heterogeneous oil distribution pattern was observed under initial residual saturation conditions. No major change occurred in the distribution pattern after subsequent flooding events.

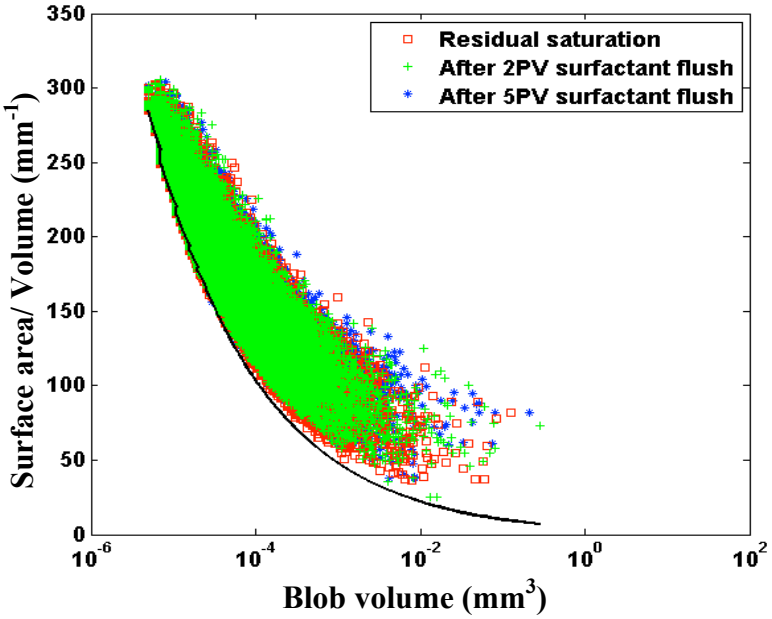

Figure 3.10. Plot showing distribution of extra-heavy oil blob surface area and deviation from spherical shape for the system shown in Figure 3.9 (also see figures 3.2 and 3.5). The bold black line represents a model curve for spherical shape for a particular volume. Deviation from spherical shape represents greater surface area. Extra-heavy oil blobs show maximum deviation from spherical shape after all three flooding episodes. The majority of the oil blobs having volumes greater than 10^{-4} mm^3 show significant deviation from spherical shape after all flooding episodes.

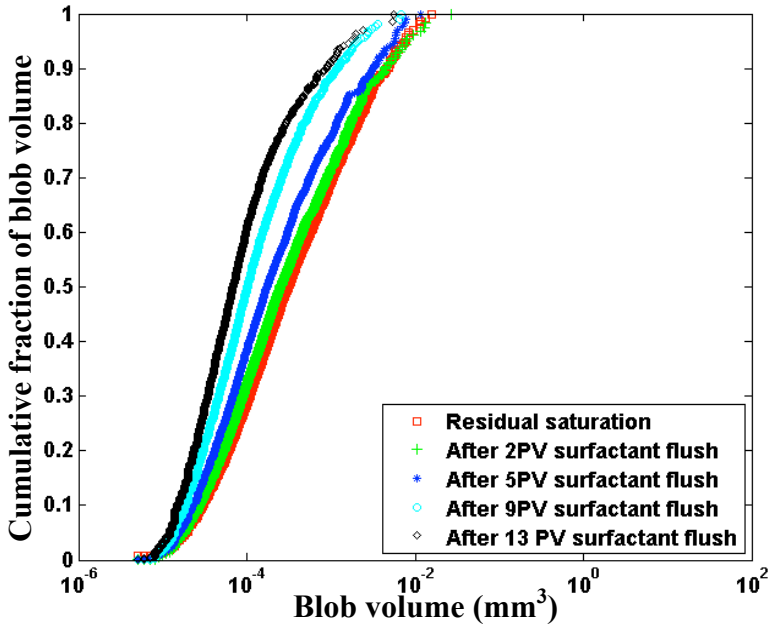

Figure 3.11. Cumulative distributions of extra-heavy oil blob volume in the highly heterogeneous sand (C_U = 10.6) (see figures 3.3 and 3.6). A relatively heterogeneous oil distribution pattern was observed under initial residual saturation conditions and progressively changed to a more homogeneous distribution after subsequent flooding events. Resulting oil blob volumes, for the overall distribution became progressively smaller in size after each surfactant flooding event.

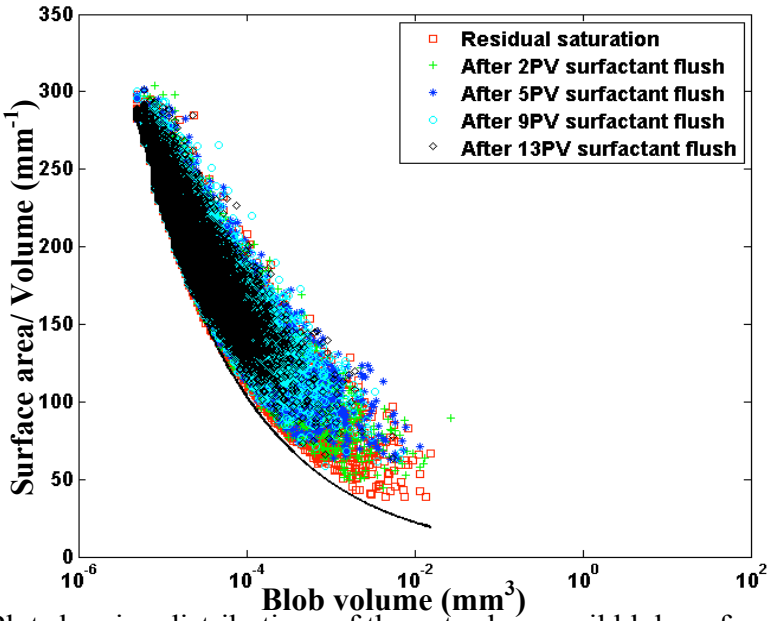

Figure 3.12. Plot showing distributions of the extra-heavy oil blob surface area and deviation from spherical shape for the system shown in Figure 3.11 (also see figures 3.3 and 3.6). The bold black line represents a model curve for spherical shape for any particular volume. Deviation from spherical shape represents greater surface area. The extra-heavy oil blobs showed maximum deviation from spherical shape after all three flooding episodes. Resulting oil blob volumes became gradually smaller in size and closer to spherical shape after each subsequent surfactant flooding event.

ESTIMATION OF CRITICAL MICELLE CONCENTRATION FOR VARIOUS CRUDE OIL-ANIONIC-SURFACTANT SYSTEMS BASED ON INTERFACIAL TENSION MEASUREMENT

ABSTRACT

Experiments were carried out to estimate critical-micelle-concentration (CMC) for three fractions of crude oils (e.g., light, heavy, and extra-heavy) in the presence of an anionic surfactant-brine solution. The branched alcohol propoxylate sulfate surfactant was used for its ability to reducing interfacial tension (IFT) at very low concentration, and its high temperature and pH tolerance for field scale applications of enhanced oil recovery (EOR) or remediation. A Du Noüy ring tensiometer was used to take multiple measurements of static IFT values for each particular oil and surfactant-concentration system. An abrupt change in the IFT values indicated the threshold of micelle formation and the corresponding surfactant concentration was considered as the CMC for a particular oil-surfactant solution system. Results showed that for the light and heavy oil fractions, the CMC could be achieved for concentration ranges between 0.5% and 1%. A relatively gradual decrease in IFT values was observed for the extra-heavy oil system and the CMC was estimated at a surfactant concentration of less than 1%. Based on this collective set of results, a low surfactant concentration of 0.1% was considered to be an overall optimal concentration for enhanced recovery at least for the oil-surfactant systems investigated as part of this study.

4.1 INTRODUCTION

The use of surface-active agents (surfactants) for enhanced oil recovery (EOR) is an existing technology for extraction of conventional and unconventional oil resources. The presence of surfactant acts to reduce the oil-water-grain interfacial tension thereby enhancing the mobilization of oil otherwise trapped as residual saturation within the pore spaces of a reservoir after primary and secondary recovery processes. Schramm and Marangoni (2000) and Kaniky et al. (2001) provide more thorough descriptions of surfactant based chemistry and effects on removal of multi-phase water-oil systems. Surfactants are chemical compounds which possess amphiphilic or amphipathic behavior. For example, a surfactant molecule consists of two moieties: a hydrophilic head, which has an attraction for polar media such as water, and a lypophilic tail, which has the attraction for non-polar media such as oil. The lypophilic group is generally a long chain (branched or non-branched) of carbon atoms (C_8- C_{18}). The hydrophilic group is the ionic or functional group, which determines the category of the surfactant as anionic, cationic, nonionic, and/or zwitterionic. The anionic variety dissociates in water producing an anion with the negative charge on the head group. This is the most widely produced and utilized surfactant (found as soap, emulsifier, foaming and wetting agent) for various purposes. The cationic variety dissociates in water as a cation with a positive charge on the head group. This type is least used due to its high manufacturing cost. The nonionic variety does not produce a cation or an anion in water, and the zwitterionic variety ionizes both anions and cations (Green and Willhite 1998).

Njus (2000) described the interfacial phenomenon of surfactant mechanisms in terms of thermodynamics. Under this description, two consecutive water molecules are held by a hydrogen bond, defined by the electrostatic bond existing between an oxygen atom of one water

molecule to a hydrogen atom of another molecule. The water molecules, which are not at the surface, are surrounded by many other molecules from all possible directions. These molecules are able to achieve high entropy. However, the molecules along the air-water or oil-water interface have fewer number of other molecules linked through hydrogen bonding, which creates lower entropy. In order to increase the entropy, the surface area must be reduced, which also minimizes the free surface energy. In an oil-water immiscible system, the existence of oil molecules (i.e. non-polar) disrupts the hydrogen bonding. Thus, the presence of the multi-phase system acts to decrease the entropy of the system and therefore phase separation (hydrophobic and hydrophilic) will occur to achieve thermodynamic stability. In other words, the non-polar hydrophobic nature of the oil phase separates out from the polar phase in an attempt to increase entropy (or minimize the free energy) of the system. When surfactant is added in low concentration in an oil-water (or brine) immiscible system, the individual molecules, called monomers, assemble at the oil-water interface in order to achieve a thermodynamically stable condition. In this case the polar end (hydrophilic) of the monomers can attach to the water molecules. The non-polar (lypophilic) tails preferentially attach to the oil phase. This amphiphilic behavior helps reduce the interfacial tension between the two immiscible phases, behaving more like one single phase and resulting in the extension of the interfacial area. Consequently, the oil phase breaks down into smaller droplets and disperses within the continuous water phase.

When the surfactant reaches a particular threshold concentration, known as the critical-micelle-concentration (CMC), the monomers form aggregates surrounding the oil-blobs usually in the form of a sphere or as other complex morphologies. These aggregates of the monomers surrounding the oil blobs are called micelles. Schramm (2000) discusses the fundamental

principle of CMC formation and estimation procedures. Within one micelle aggregate the hydrophilic heads project towards the continuous aqueous phase, whereas the hydrophobic tails are attached to the oil blobs. It has been reported that the physico-chemical properties of a surfactant changes abruptly at the CMC (Schramm 2000, Mulligan et al. 2000, Green and Willhite 1998). In recent years, with the advancement of petroleum production technology, it is important that the injected surfactant solution has higher concentration than the CMC value in order to achieve the interfacial tension (IFT) value as low as 10^{-3} mN/m (Wu et al. 2005). An ultralow IFT value ensures the formation of a stable spontaneous-emulsion of oil blobs within the reservoir, restricting coalescence phenomena. Another important factor includes the fact that the CMC indicates the saturation limit of a particular surfactant up to which it can be adsorbed onto the porous-media-surface. Additionally, the CMC for a particular system also indicates the rapid increase in solubility of the oil phase. In general the CMC value is measured by using a particular physico-chemical property (such as conductivity, density changes, foaming, osmotic pressure, IFT, etc.) of the system as function of the surfactant-concentration.

Previous research shows that the dynamic behavior of IFT is a function of several parameters such as temperature, salinity (Wu et al. 2005), pH (Buckley and Fan 2007), composition of the crude oil and surfactant (Wu et al. 2005, Green and Willhite 1998, Mercer and Cohen 1990), and aging of the interface (Liu et al. 2006, Taylor and Schramm 1990, Buckley and Fan 2007). Liu et al. (2006) showed that IFT measurements, under equilibrium conditions, (using alkali/anionic surfactants), were one order of magnitude higher than dynamic IFT measurements. Based upon experiments on 250 various fractions of crude oil samples, Buckley and Fan (2007) concluded that the dynamic change in IFT values follow an exponential relationship and reach equilibrium after a particular time period. The experiments were

conducted for 2000 seconds (33 minutes) and an average IFT value reduction of 23% from the initial value was obtained (4.7 ± 2.9 mN/m), and the maximum change was observed for higher pH values up to a maximum reduction of 15.6mN/m at a pH of 9 for a light crude oil (48˚API, viscosity 1.2cP at 20˚C, acid number 0.08). Based on the experiments carried out on 25 crude oil samples (which include light, medium and heavy oils) with 0.1M NaCl, this research also concluded that IFT values increased with increasing acidity and decreased with increasing viscosity. However, all fractions showed stable IFT values within the range of pH 3-6 and reduced values at higher pH of approximately 6 or greater.

As part of this study, IFT experiments were carried out to estimate the CMC for the three fractions of crude oil (e.g., light, heavy and extra heavy) in the presence of surfactant solutions with various concentrations within a bulk 60g/L CsCl brine solution. The CMC of a particular system indicates rapid increase in solubility of the oil phase. The purpose of this research was to characterize the impact of a specific surfactant, with varying concentrations, on the interfacial behavior with various fractions of crude oil (e.g., light, heavy and extra heavy). More specifically, the objectives included quantifying the critical micelle concentration for these oil/surfactant-brine systems to evaluate optimal interfacial tension reductions most amenable to oil recovery for each particular system.

4.2 MATERIALS AND METHODS

Three fractions of crude oil were used as the representative oil phase including West Texas Intermediate crude (BP) of light (41.4°) API gravity, Poseidon crude (BP) of medium (29.6°) API gravity, and San Joaquin Valley crude (Chevron) of heavy (14˚) API gravity. The oil samples were doped with iodobenzene (10% by volume) for synchrotron X-ray microtomography imaging purposes required as part of this research project. The doping process with iodobenzene (density 1.82 g/cm^3) slightly changed the API gravity of the crude oil fractions. After density measurements were recalculated, the crude oil samples were characterized as light (23.4˚API), heavy (14.8˚API), and extra heavy (4.2˚API), respectively (USGS standard). The aqueous phase consisted of a 60 g/L CsCl (99.9% ACS grade, Sigma Aldrich Co.) solution to provide appropriate image contrast for synchrotron microtomography imaging purposes and to simulate a representative brine solution. These dopants showed the least partitioning to the non-target fluids (Schnaar and Brusseau 2006). The pH measured for the CsCl solution was 5.6 under environmental laboratory temperatures (i.e. 20°C), which is equivalent to the pH of a brine solution within reservoir conditions (Sverjensky 1984). The CMC was estimated based on the reduction of IFT values (Green and Willhite 1998) as a function of various concentrations of the anionic surfactant. The research was conducted under controlled laboratory temperature and pH conditions. The anionic surfactant used in this research was a branched alcohol propoxylate sulfate (Stepan Chemical Company, Northfield, IL). The pH measured for the 0.1% surfactant solution (60 g/L CsCl) was 3.6 under the controlled laboratory conditions. IFT measurements were carried out for the following concentrations of the surfactant in 60 g/L CsCl solution: 0.01%, 0.025%, 0.05%, 0.1%, 0.25%, 0.5%, 1%, and 5%. Previous research shows that the branched alkyl surfactant has the greater ability to reduce interfacial

tension in comparison to straight chain alkyl group at very low concentrations (Rosen et al. 2005). Moreover, this surfactant was specifically formulated for oil extraction purposes (EOR) and for oil remediation and it has been effectively used to mobilize crude oil remediation from shallow aquifers (Jayanti et al. 2002). It also showed high salinity tolerance and is therefore assumed to be applicable for reservoirs with high salinity. In addition, this surfactant showed minimal adsorption to the solid phase (Goddard et al. 2004).

Static IFT values were measured using a manual du Noüy ring tensiometer (Fisher Scientific Tensiometer, Model 20). Although the currently available dynamic methods provide (drop volume and drop shape techniques) relatively more accurate time series of the IFT values, the conventional static method using du Noüy ring tensiometer is commonly used in many laboratories and advantageous for its cost effectiveness (Weiss 2003). Moreover, the primary purpose of CMC measurement can be achieved using the static method with small variations and robust reproducibility attributed to the measuring technique (Schramm 2000). Multiple IFT measurements were carried out for each oil-surfactant solution system. Oil and surfactant samples were placed in a glass container of more than 45mm diameter in order to limit any surface tension activity interference by the container-wall. ASTM method D-971 was followed for glassware cleaning regarding the IFT measurement of crude oil samples. The platinum-iridium ring was cleaned using benzene, acetone, and Bunsen burner flame before each measurement. A period of 15 minutes was allowed for the interface to achieve an equilibrium condition before each measurement. True IFT values for each system was calculated using a correction factor based on the ratio of radius of the platinum ring and the radius of the platinum wire, and the difference in densities of the two liquids present in a particular crude oil-surfactant solution system.

4.3 RESULTS AND DISCUSSION

IFT values were plotted for each specific oil-fraction/surfactant as a function of surfactant concentration. Figure 4.1 shows the measured static IFT values for the light oil (doped with iodobenzene or IB) and the anionic-surfactant-solution interface, plotted as function of various concentrations of the surfactant solution (in 60g/L CsCl solution). The average IFT value showed a reduction from 15.4 mN/m, for oil-water interface (no surfactant added), to a minimum of less than 1mN/m for the surfactant concentration of 2.5%. There was an observed rapid decrease of the IFT values at a concentration of 0.5% but became approximately constant at 1mN/m for the higher surfactant concentrations. Under these conditions, the critical micelle concentration (CMC) was estimated to occur at a surfactant concentration of approximately 0.6%. Figure 1 also shows the range of IFT data (plotted as red dots) measured for a particular concentration. It can be observed that equilibrium of the static IFT values was achieved and confirmed by no major change in the range of values for a particular concentration. Figure 4.2 shows the IFT values for heavy oil (doped with IB) as function of surfactant concentration. A rapid decrease in IFT can be observed from a maximum value of 15.1 mN/m for no surfactant (or only with DI water), to a minimum of 3.8 mN/m at a surfactant concentration of 5%. The maximum IFT reduction occurred at a surfactant concentration between 0.75% and 1% and reached a constant equilibrium IFT value of approximately 4 mN/m. Under these conditions, the CMC was estimated to occur at a surfactant concentration of 1%. Figure 4.2 shows a maximum change in the range (green dots) of measured data for low concentrations of surfactant solution in comparison to IFT data measured for the high concentration systems whereby multiple measurements showed constant equilibrium values (behavior). IFT values for the extra-heavy oil (doped with iodobenzene) plotted as a function of surfactant concentration showed relatively less overall reduction in IFT

compared to the other lighter oil fractions (Figure 4.3). The average IFT value was reduced from a maximum of 42.3 mN/m for oil-deionized water system (no surfactant added) to a minimum of 21.2 mN/m for a surfactant concentration of 5%. Although the estimation of the CMC value was challenging for this system, the best interpretation of the constant equilibrium IFT value occurred at a surfactant concentration of approximately 0.1%. The maximum IFT rate of change was estimated at 0.025% based on a change of IFT values from 38.2 mN/m to 34.4 mN/m and from 32mN/m at 1% to 21mN/m at 5% surfactant concentration, respectively. For the other two lighter fractions, the rate of IFT change became constant for high concentration of surfactant solutions. Whereas, there was a gradual rate of change of IFT values in case of extra heavy crude oil with higher concentration surfactant solutions. With these observations, it can be assumed that the CMC value was achieved at a concentration of less than 1% when compared with the trends showed by the two other lighter fractions. Under the conditions of these experiments, a 0.1% surfactant solution was determined to be the overall optimal concentration to test the effects crude oil mobilization for pore-scale studies of surfactant-enhanced oil recovery (EOR) for these three oil/surfactant systems. These results support the fact that the dominant mechanism of oil recovery will occur by mobilization of the oil phase, as intended, when flooding with this particular surfactant concentration rather than through significant dissolution processes.

4.4 SUMMARY AND CONCLUSIONS

Careful examination and characterization of enhanced oil recovery (EOR) reagents, such as surfactants, must be conducted before applying in the field or even at smaller experimental scales. Part of this characterization requires determining optimal surfactant concentrations for the removal of oil through mobilization processes while minimizing surfactant concentration and lower associated costs. The purpose of these experiment included providing estimates of critical-micelle-concentration (CMC) for three selected fractions of crude oils (e.g., light, medium, and heavy) in the presence of an anionic surfactant-brine solution. The branched alcohol propoxylate sulfate surfactant was chosen for its effectiveness at reducing interfacial tension (IFT) at very low concentration and its high temperature and pH tolerance for field scale applications of EOR or remediation. A series of experiments were carried out to measure the IFT values for each crude oil fraction as function of aqueous surfactant concentration. A conventional Du Noüy ring tensiometer was used to take multiple measurements of static IFT values for each particular oil and surfactant-concentration system. An abrupt change in the IFT values indicated the threshold of micelle formation and the corresponding surfactant concentration considered as the CMC for a particular oil-surfactant solution system. Results showed that for the light and heavy oil fractions, the CMC could be achieved for concentration ranges between 0.5% and 1%. For extra-heavy oil system there was a relatively gradual change in IFT values and the CMC was estimated to occur at a surfactant concentration less than 1%. Additional experiments with advanced IFT measurement techniques could provide increased accuracy and precision for the determination of CMC for the extra-heavy oil-surfactant system. Based on these collective set of experiments, a low surfactant concentration of 0.1% was determined to be an overall optimal concentration for enhanced oil recovery at least for the oil-surfactant systems investigated as part of this study.

REFERENCES

Buckley, J. S. & Fan, T., (2007), Crude oil/brine interfacial tensions, Petrophysics, 48 (3), 175–185

Kaniky, J. R., Carlos, J. Pandey, S. & Shah, D. (2001), Surface chemistry in petroleum industry, In Holmberg, K. (Ed.), Handbook of applied surface and colloid chemistry, ISBN 0471 490830 2001 John Wiley & Sons, Ltd.

Green, D. W. & Willhite, G. P. (1998), *Enhanced oil recovery*, SPE Textbook Series, Volume 6

Mercer, J.W., & Cohen, R.M. (1990), A review of immiscible fluids in the subsurface: properties, models, characterization and remediation, *journal of Contaminant Hydrology, 6 (2)*,107-163. doi:10.1016/0169-7722(90)90043-G

Mulligan, C.N, Yong, R.N, & Gibbs, B.F (2001), Surfactant-enhanced remediation of contaminated soil: a review, *Engineering Geology, Volume 60 (1-4)*, 371-380 doi:10.1016/S0013-7952(00)00117-4

Njus, D. (2000), *Fundamental principles of membrane biophysics, Chapter 2: Thermodynamics of Micelle Formation*, retrieved on July 20, 2011, retrieved from http://sun.science.wayne.edu/~bio669/index716.html#MainPage

Goddard, W.A., Tang, Y., Shuler, P., Blanco, M., Jang, S.S., Lin, S.T., Maiti, P., Wu, Y., Iglauer, S., & Zhang, X. (2004), Lower cost methods for improved oil recovery via surfactant flooding: final report. Department of Energy DE-FC26-01BC15362

Jayanti, S., Britton, L. N., Dwarakanath,V. & Pope, G. A., (2002), Laboratory evaluation of custom-designed surfactants to remediate NAPL source zones, *Environmental Science & Technology, 36 (24)*, 5491–5497, DOI: 10.1021/es020566i

Liu, Q., Donga,M, Yue, X., Houb, J. (2006), Synergy of alkali and surfactant in emulsification of heavy oil in brine, *Colloids and Surfaces A: Physicochem. Eng. Aspects 273*, 219–228

Rosen, M. J., Wang, H. Shen, P.& Zhu, Y., (2005), Ultralow interfacial tension for enhanced oil recovery at very low surfactant concentrations, *Langmuir, 21*, 3749-3756

Schnaar, G., & Brusseau, M.L. (2006b), Characterizing pore-scale dissolution of organic immiscible liquid in natural porous media using synchrotron X-ray Microtomography. *Environ. Sci. Technol*., *40*, 6622-6629.

Schramm, L.L. (2000), *Surfactants: fundamentals and applications in the petroleum industry.* Cambridge, N.Y., Madrid. Cambridge University Press.

Schramm, L.L. &Marangoni, D. G. (2000), Surfactants and their solutions: basic principles, In Schramm, L.L. (Ed.). *Surfactants: fundamentals and applications in the petroleum industry.* Cambridge, N.Y., Madrid. Cambridge University Press.

Sverjensky, D. A. (1984), Oil Field Brines as Ore-Forming Solutions, *Economic Geology Vol. 79*, 213-137

Taylor, K. C., & Schramm, L. L. (1990), Measurement of short-term low dynamic interfacial tensions: application to surfactant enhanced alkaline flooding in enhanced oil recovery, *Colloids and Surfaces, 47*, 245-253

Weiss, J. (2003), Static and dynamic interfacial tension analysis, In *Current Protocols in Food Analytical Chemistry*, Published Online: 1 MAY 2003. John Wiley and Sons, Inc. doi: 10.1002/0471142913.fad0306s07. Retrieved on July 20, 2011.

Wu, Y., Shuler, P., Blanco, M., Tang, Y., & Goddard, W. A. (2005), A Study of Branched Alcohol Propoxylate Sulfate Surfactants for Improved Oil Recovery. *SPE Annual Technical Conference and Exhibition, 9-12 October 2005,* Dallas, Texas, SPE Doi: 10.2118/95404-MS

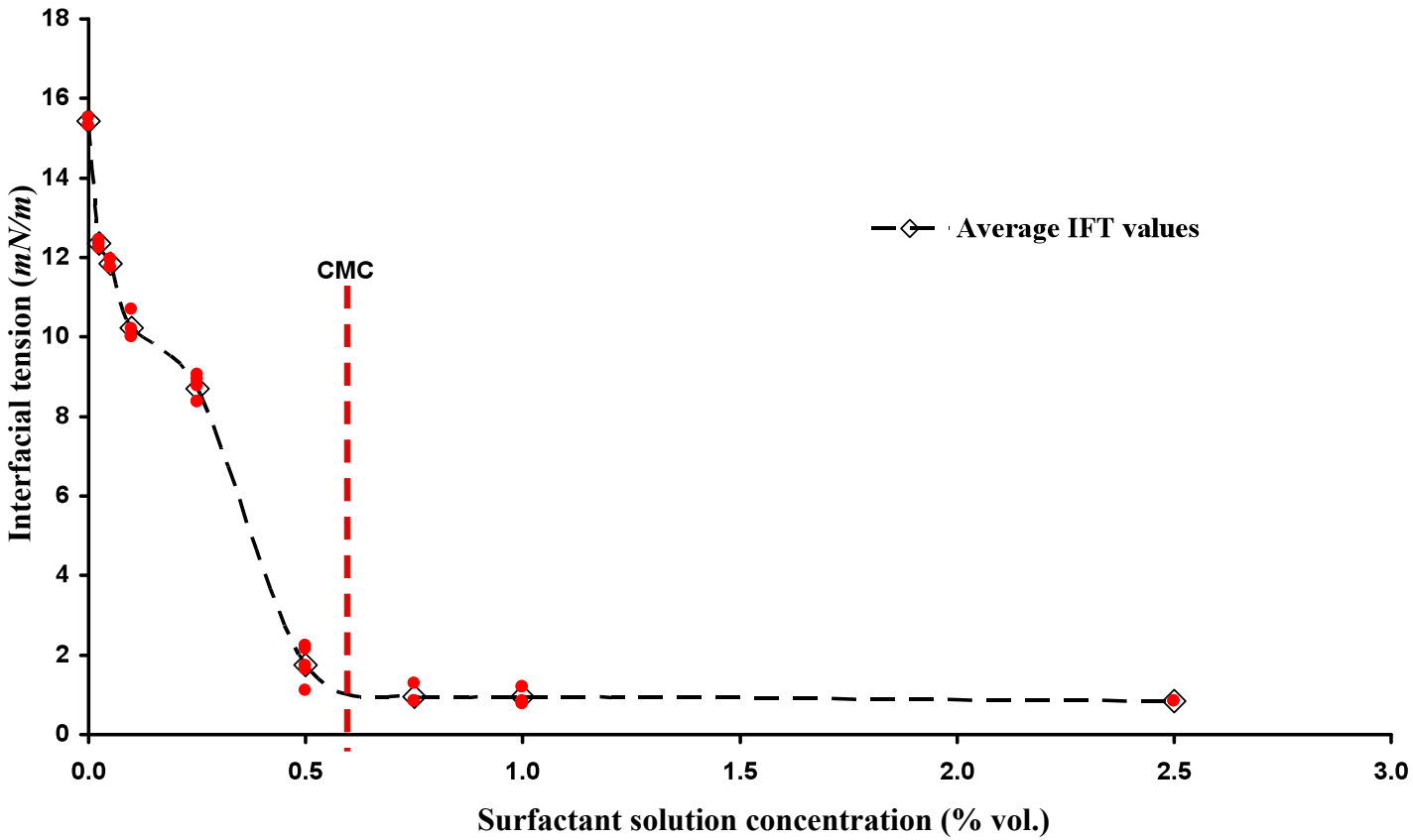

Figure 4.1. Interfacial tension measurements for light oil (after doping with iodobenzene) are plotted against various concentrations of anionic surfactant solution (in 60g/L CsCl solution). The dashed line connects the average IFT values for each corresponding surfactant concentration. Critical micelle concentration (CMC) can be estimated at 0.6% surfactant solution.

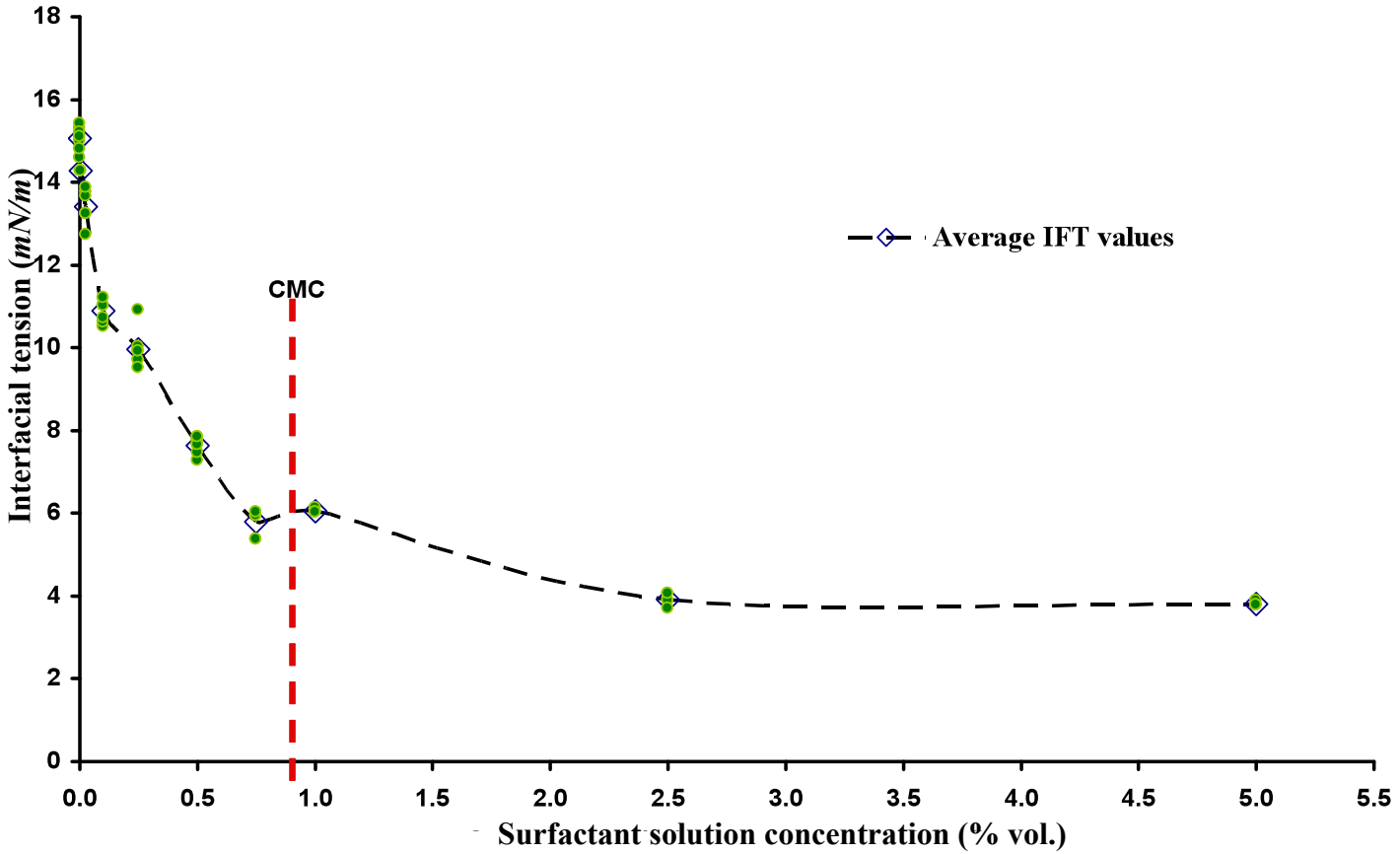

Figure 4.2. Interfacial tension measurements for heavy oil (after doping with iodobenzene) are plotted against various concentrations of anionic surfactant solution (in 60g/L CsCl solution). The dashed line connects the average IFT values for each corresponding surfactant concentration. Critical micelle concentration (CMC) can be estimated at 0.9%.

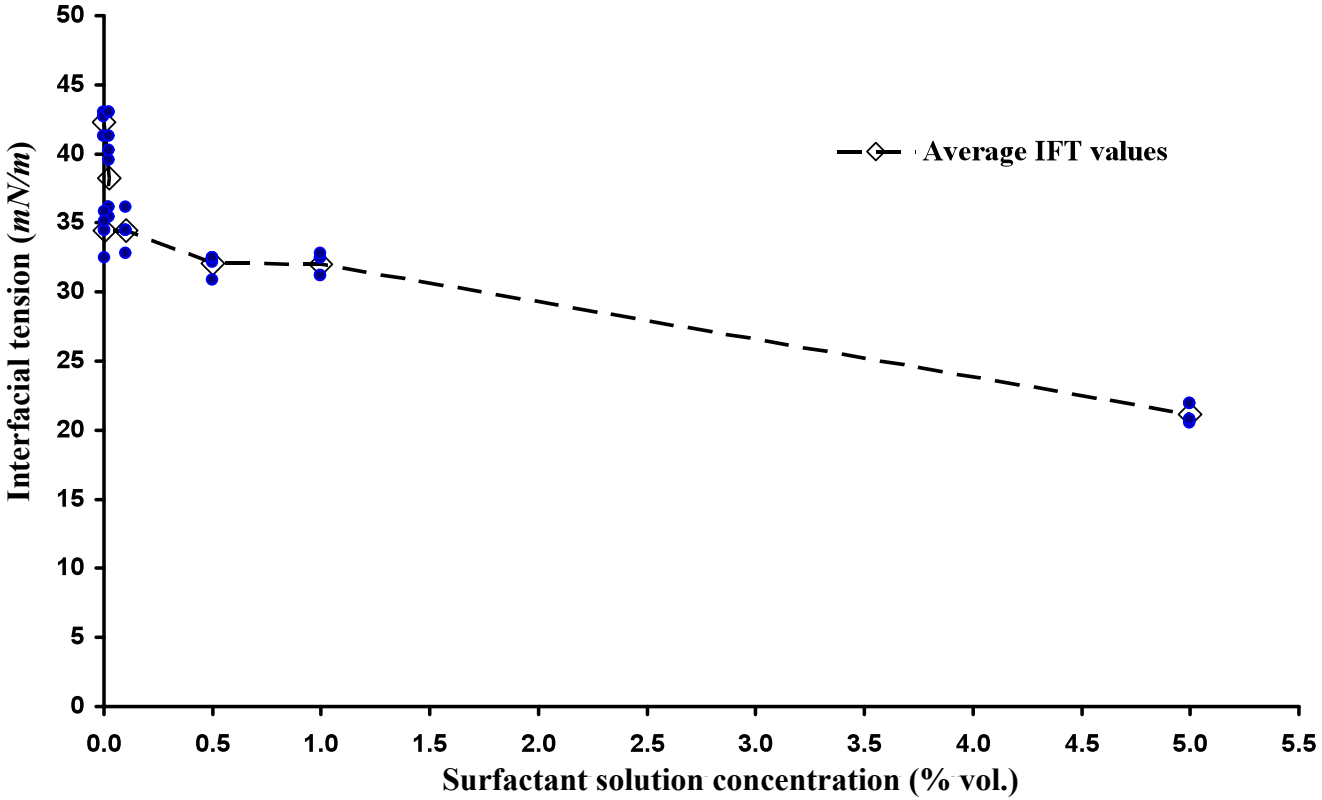

Figure 4.3. Interfacial tension measurements for extra heavy oil (after doping with iodobenzene) are plotted against various concentrations of anionic surfactant solution (in 60g/L CsCl solution). The dashed line connects the average IFT values for each corresponding surfactant concentration. Although an appropriate CMC value estimation is difficult to isolate on this plot, an approximate CMC threshold appears to exist at concentrations between 0.2 and 1.0 % and are therefore the surfactant solution used in the column flooding experiments are assumed to be appropriate.

DISCUSSION AND CONCLUSIONS

A comprehensive set of studies was conducted to determine and understand the primary pore-scale processes controlling crude oil distribution, mobilization, and recovery (displacement efficiency) from various porous media ('model reservoir') systems. A series of column experiments implementing three different fractions of crude oil (light, heavy, and extra-heavy API° gravity) were distributed in three different types of porous media with varying grain size heterogeneity (i.e. homogeneous, mildly heterogeneous, and highly heterogeneous in terms of grain size distribution). A newly developed surfactant, branched alcohol propoxy sulfate (Stepan Chemical Company, Northfield, IL), was used to induce flooding through the column systems to evaluate resulting effects on oil distribution, morphology, and recovery during enhanced mobilization processes. An innovative non-destructive imaging technique, synchrotron X-ray microtomography, was used successfully to produce time series of three-dimensional (3-D) in-situ distribution of oil phases at the pore scale to elucidate crude-oil transport and interfacial processes acting in the various systems. This is the first known research of this kind to evaluate 3-D pore-scale displacement efficiency of crude oil during surfactant induced tertiary recovery. All three phases within the each experimental column system including the oil, aqueous-brine and solid media phases were resolved in high-resolution (<10 μm) images for precise quantification and characterization. The oil phase was successfully separated to provide the ability to quantify oil-blob-volume distribution and morphological changes due to lowering interfacial tension during surfactant flooding. Changing oil-phase morphology is a measure of

available contact surface with the surfactant solution, which is an important parameter controlling micro-scale sweep (displacement) efficiency.

Results obtained for three fractions of oil distributions in the homogeneous porous medium are provided in detail within article 1 and are summarized as follows. Results showed that a relatively homogeneous initial distribution of disconnected blobs of light and heavy gravity crude oil exist as residual saturation prior to surfactant flooding, whereas, extra-heavy oil existed as a continuous interconnected ganglia type distribution. Both the light and heavy oil fractions showed an increase in number of blobs and total blob surface area, and a reduction in the total blob-volume after 2 pore volumes (PV) of surfactant flooding. The light and the heavy oil blobs showed significant change in morphology after the 2-PV surfactant flooding event, and became more laminar and flattened, coating the media grain boundaries to a greater extent. The extra-heavy oil exhibited an interconnected distribution of blobs, primarily as a large ganglia mass after all three stages of flushing (i.e. residual establishing aqueous flush, and the two successive surfactant floods) with negligible visual or quantifiable change in distribution pattern. The light-oil distribution showed a 200% increase in total surface area after the 2-PV surfactant flooding event. The heavy-oil distribution showed 87% increase in total surface area after 2 PVs of surfactant flooding. This increase in surface area is attributed to the change in blob morphology from spherical to more complex non-spherical lenticular with laminar ganglia shape characteristics. Moreover, the observed increase in the number of oil blobs from larger to smaller particles after the 2-PV surfactant flood contributed to the greater cumulative oil surface area. However, the extra-heavy-oil distribution showed only a 7% increase in surface area after 2 PVs of surfactant flooding and a 1.4% decrease in surface area after the 5-PV flood. Disintegration or ‘breaking up’ of larger blobs into smaller fragments in response to reduced interfacial tension

was the primary factor responsible for increasing total surface area for this system. Both the light and heavy oil experiments showed complete recovery after 5 PVs of surfactant flooding, whereas the extra-heavy oil experiment showed minimal recovery after the 5-PV surfactant flood. The results of these experiments demonstrate the high extraction potential of light and heavy oil fractions from the homogeneous medium during tertiary surfactant induced recovery process. However, the results of the experiments reveal that the extraction potential of extra-heavy oil fraction distributions within these types of reservoirs are expected to be severely limited even under significant surfactant flooding under these conditions.

Article 2 provided a comprehensive set of results for both the light and the heavy oil fractions distributed within the three types of porous media (i.e. homogeneous, mildly heterogeneous, and highly heterogeneous). Both the light and the heavy oil fractions showed relatively more heterogeneous distributions within the two higher heterogeneous porous media types. The heterogeneity of the porous media (i.e. grain-size distribution) and permeability were the dominant factors controlling the oil-blob-size-distribution and mean blob volume present as residual saturation (initial distribution condition). Both light and heavy oil blobs showed similar trends or characteristics in that they existed primarily as heterogeneous oil-blob distributions within the homogeneous and the highly heterogeneous media. However, the mean-blob-volumes present in the highly heterogeneous medium were one to two orders of magnitude smaller in all the episodes (i.e. initial residual saturation and all subsequent surfactant flooding events) compared to that in the homogeneous medium. The initial residual saturation distribution, in the mildly heterogeneous porous medium, showed highest heterogeneity (i.e. non-uniform distribution) for both the light and the heavy oil fractions. It is important to note that the distribution in this medium contains the smallest mean blob volume, for both oil fractions (light

and heavy) compared to the other systems tested as part of these studies. Additionally, it should be noted that although 'mildly heterogeneous' in grain size distribution, this sand mixture had the least permeability among all three types (e.g., 9.0E-11 m^2, 3.60E-11 m^2 and 5.40E-11 m^2 for the homogeneous, mildly heterogeneous, and highly heterogeneous sand, respectively). Both the light and the heavy oil blob distributions became relatively more heterogeneous after each subsequent surfactant flooding episode for all porous-media systems. The mildly heterogeneous porous medium produced a limited recovery after the 2-PV flood (i.e. 1.3% and 10% for the light and heavy, respectively), and greater recovery after the 5-PV flood (i.e. 23% and 41% recovery for the light and heavy fractions, respectively). The highly heterogeneous porous medium showed no recovery after the 2-PV surfactant flood; however, significant recovery resulted after the 5-PV flood (i.e. 44% for light oil and 34% gross recovery for heavy oil).

Both light and heavy oil blobs increased in surface area within the homogeneous medium. In contrast, total surface area for both fractions either slightly increased or continuously decreased in the mildly heterogeneous medium after surfactant flooding. However, both fractions showed an increase in total surface area within the highly heterogeneous medium after the 2-PV surfactant flood and a slight decrease after the 5-PV flood, mainly due to high recovery process during this later flooding episode. With these observations, and the fact that permeability of the mildly heterogeneous medium is the lowest, it can be concluded that for higher permeability media (i.e. the homogeneous and the highly heterogeneous media) more surfactant solution comes into contact with the oil phases yielding increased surface area through increased re-distribution and increased recovery (displacement).

Results obtained for the extra-heavy oil distributed in all three types of media were compared and are provided in article 3 as follows. Relatively low (6%) net recovery was

achieved for extra-heavy oil from the homogeneous sand after the 5-PV surfactant flood, due to the formation of a continuous-oil-phase attributed to a change to an oil wet media system. Limited contact of extra-heavy oil with surfactant-solution resulted in less interfacial activity. Negligible net (extra-heavy oil) recovery was achieved from the mildly-heterogeneous-sand mainly due to low associated permeability. Although, a spontaneous in-situ-stable-emulsion was formed during this experiment (i.e. mildly heterogeneous medium), minimal net oil recovery resulted due to the "jamin" effect producing a local oil saturation after 2 PVs of surfactant flooding and 6% gross recovery after 5 PVs of flooding (with respect to the saturation after the 2-PV flood). The extra-heavy oil within the highly heterogeneous sand experiment yielded an average of 20% recovery after each surfactant flooding event and the initially heterogeneous blob distribution changed significantly to a more homogeneous distribution as flooding progressed. Under these conditions, a stable-spontaneous-emulsion yielded consistent and notable oil recovery. The oil phase (extra-heavy) within the homogeneous and mildly-heterogeneous porous media showed a small increase (7% and 11% respectively) in total surface area over the duration of flooding. However, the oil (extra-heavy) within the highly heterogeneous porous medium showed a gradual reduction in the total surface area after each successive surfactant flood.

The integration of the results from the comprehensive series of studies, conducted as part of this dissertation research, has led to several important and notable overall conclusions that can be applied to understanding and predicting oil recovery for many different oil-reservoir systems. An overall linear trend in oil recovery pattern was observed as function of pore-volumes flushed for light and heavy crude oil distributed within homogeneous sand. Better sweep efficiency due to greater contact surface with the displacing fluid is responsible for higher recovery from this

medium. The displacement efficiency is controlled by the chemical properties of all phases (i.e. oil, aqueous-brine, gas, and solid matrix phases), and the geology of the porous media. With proper rescaling of injection rate, and pore volume imbibed into a well-sorted homogeneous reservoir, a liner trend in recovery pattern can be expected at greater scale. Although direct extrapolation of percent oil recovery is difficult if not impossible to determine from pore-scale experiments, the general recovery trends are expected. Crude oils ranging from light to heavy in API° gravity, distributed within homogeneous well-sorted porous reservoirs, are expected to produce relatively high recoveries in the presence of uniform surfactant applications.

Results obtained from poorly sorted porous-media systems (C_u between 5.8 - 10.5) (i.e. mildly heterogeneous and highly heterogeneous), with overall lower permeability, showed limited recovery (light and heavy gravity oil) during initial stages of surfactant flooding (0 - 2 PVs), and greater recovery for later stages of flooding (≥ 5 PVs). This suggests that higher oil recoveries can be expected in poorly sorted ("heterogeneous") reservoirs, however, only after extended flooding duration (pore volumes).

Green and Willhite (1998) describe scale issues and methods for correlating laboratory-scale results with reservoir-scale parameters. Since the complexity of heterogeneity increases at the reservoir scale, other factors such as areal and vertical displacement efficiency, effect of gravity (density differences between the oil and flushing solution), well patterns, and the rate of injection must be adjusted for greater sweep efficiency. The concept of heterogeneity for describing a reservoir medium is scale dependent. Generally, the degree of heterogeneity increase with scale of the system. Significant challenges exist when trying to correlate the recovery efficiency obtained in laboratory scale with that in field scale. Under laboratory scale conditions, the displacement efficiency is primarily controlled by the interaction between viscous

and interfacial forces, which is represented by capillary number. However, under field scale conditions, gravity or in other words the buoyancy forces (attributed to density difference between crude oil and displacing aqueous solution) has additional control (Moreno et al. 2011) into the system, which is estimated by bond number. Results obtained from this research shows bond number is insignificant (on the order of 10^{-11} to 10^{-14}) compared to capillary number (on the order of 10^{-3} to 10^{-4}) for all the crude oil-media systems investigated in this dissertation research. Capillary number is a dimensionless coefficient, which has been shown to be consistent between laboratory scale and field scale when modeling or characterizing the mobility potential of oil residual saturations (Green and Willhite 1998). In this research the micro-scale displacement efficiency has been measured in terms of recovery potential (% of original oil in place) for various crude-oil porous-media systems. Higher displacement efficiency (function of residual saturation) can be achieved in laboratory scale experiments since the surfactant injection surface area is much larger compared to that in the field situation. As a result, maximum number of pore spaces can be flooded with surfactant solution in laboratory condition, which is unlikely in the field situation, attributed to the complexity in heterogeneity at the macro-scale (Moreno et al. 2011). For example, results from this research, show that the micro-scale-displacement-efficiency (E_D) for light and heavy oil recovery from homogeneous sand, reaches 1 (100% recovery). However, for field scale applications, a realistic approach should consider overall displacement efficiency, which is the product of both microscopic and macroscopic displacement efficiency. Input parameters (such as capillary number, pore volume, etc.) estimated from this laboratory scale research can be used to conduct numerical modeling analyses for field-scale (macro-scale) situations. Data obtained from this laboratory scale research not only can be up-

scaled for field scale modeling, but can also be effectively used to calibrate and validate the results obtained for micro-scale modeling for various conditions (Moreno et al. 2011).

Pore scale trapping mechanisms of the extra-heavy oil in porous media were controlled by changing wettability conditions and were clearly observed and quantified from the 3-D distribution images over the duration of surfactant flooding. Wettability is a function of the pH conditions of the reservoir (i.e. surfactant solution, salinity, carbonate cement, pore-fluid chemistry, etc.). Alkaline conditions favor a water-wet reservoir/porous medium situation, producing greater sweep efficiency for the oil-phase. Higher recoveries of extra-heavy oil can be achieved from any type of reservoir media by maintaining alkaline conditions. Surfactant induced enhanced oil recovery (EOR) techniques can be optimally applied for relatively shallow subsurface conditions with thin pay zones containing extra-heavy crude oil, whereby conventional thermal recovery techniques are not economically feasible.

The results and conclusions of these sets of studies demonstrate the versatility and invaluable application of SXM imaging techniques for evaluating critical pore scale processes, which control displacement efficiency. The enhanced understanding of the pore scale factors controlling crude oil recovery processes was extremely beneficial for evaluating particular systems most conducive and amenable for enhanced oil recovery. The ability to quantify in-situ blob distribution patterns resulted in a comprehensive understanding of the pore-scale processes affecting oil recovery and will help researchers, chemical engineers, and other practitioners alike develop more effective measures in production technology in terms of surfactant chemistry and characterization of emulsion formation for enhanced recovery from particular oil-porous-media systems.

REFERENCES

Al-Raoush, R.I., Abu-Salem Z., and Willson, C.S. (2003). Characterization of non-wetting phase fluids in porous media systems using high-resolution, three-dimensional, synchrotron x-ray microtomography. *American Chemical Society Conference Proceeding, Division of Environmental Chemistry, 43*, 1031-1035.

Bryan, J., and Kantzas, A. (2009). Potential for Alkali-Surfactant Flooding in Heavy Oil Reservoirs Through Oil-in-Water Emulsification, *Journal of Canadian Petroleum Technology, 48(2)*, 37-46, doi: 10.2118/09-02-37

Chatzis I., Morrow N.R., and Lim H.T. (1983). Mmagnitude and detailed structure of residual oil saturation. *Soc. Pet. Eng*., 23, 311-326.

Craze, R.C. (1950). Performance of limestone reservoirs. *Trans. Amer. Inst. Min. Eng., 189*, 287-294.

Culligan K.A., Wildenschild D., Christensen B.S.B., Gray W.G., and Rivers M.L. (2004). Pore-scale characteristics of multiphase flow in porous media: a comparison of air-water and oil water experiments. *Advances in Water Resources., 29*, 227-238.

Dullien, F.A.L. (1979). *Porous Media: Fluid Transport and Pore Structure.* Academic Press, New York

Dullien, F.A.L., and Dhawan, G.K. (1974). Characterization of pore structure by a combination of quantitative photomicrography and mercury porosimetry. *Colloid Interface Science*, *47*, 337-349

Green, D. W. and Willhite, G. P. (1998). *Enhanced Oil Recovery.* SPE Text Book Series. Vol 6. Richardson, Texas

Hirasaki, G., and Zhang, D. L. (2004). Surface Chemistry of Oil Recovery From Fractured, Oil-Wet, Carbonate Formations, *SPE Journal, 9(2)*, 151-162, doi: 10.2118/88365-PA

Hunky, R. M.,Wu, Y., Bai, B., and Dunn-Norman, S.(2010). An Experimental Study of Alkaline Surfactant Flooding for Ultra Shallow Heavy Oil Reservoirs, *Society of Petroleum Engineers, Western Regional Meeting,* 27-29 May 2010, Anaheim, California, doi:10.2118/132537-MS

Kerr, R. A. (2005). Bumpy road ahead for world's oil, *Science, 310 (5751)*, 1106-1108

Mayer A.S., and Miller C.T. (1992). The influence of porous medium characteristics and measurement scale on pore-scale distributions of residual nonaqueous-phase liquids. *J. Contam. Hydrol*., *11*, 189-213.

Moreno, J., Flew, S., and Gurpinar, O., (2011). Challenges of Translating Fine Scale Displacement into Full Field Models, *Society of Petroleum Engineers,* SPE Enhanced Oil Recovery Conference, 19-21 July 2011, Kuala Lumpur, Malaysia. DOI: 10.2118/143568-MS

Morrow, N.R., and Heller, J.P. (1985). Fundamentals of Enhanced Recovery. In Donaldson, E.C.; Chillingarian, G.V.; and Yen, T.F. (1985). *Enhanced Oil Recovery, I: Fundamentals and Analysis.* Elsevier, New York

Morrow, N.R., and Chatzis, I. (1982). Measurement and correlation of conditions for entrapment and mobilization of residual oil. *Dept. Energy Report, 10310* (20), 59.

Powers S.E., Abriola L.M., and Weber W.J. (1992). An experimental investigation of nonaqueous phase liquid dissolution in saturated subsurface systems: steady state mass transfer rates. *Water Resour. Res., 28*, 2691-2705.

Schnaar, G. (2006). Pore-scale characterization of organic immiscible liquid in natural porous media using synchrotron X-ray microtomography. Dissertation, University of Arizona.

Schnaar, G., and Brusseau, M.L. (2006a). Characterizing pore scale configuration of organic liquid in multiphase systems with synchrotron X-ray microtomography. *Vadose Zone Journal*, *5*, 641-648.

Stegemeier, G.L. (1976). Mechanism of entrapment and mobilization of oil in porous media. In Shah, D. O., Schechter, R. S. (Eds.), *Improved Oil Recovery by Surfactant Flushing and Polymer Flooding*. Academic Press, New York.

Wildenschild, D., Hopmans, J.W., Vaz, C.M.P., Rivers, M.L., Rikard, D., and Christensen, B.S.B. (2002). Using X-ray computed tomography in hydrology: systems, resolutions and limitations. *Journal of Hydrology, 267*, 285-297.

Zhang, C.Y., Werth, C.J., and Webb, A.G. (2002). A magnetic resonance imaging study of dense nonaqueous phase liquid dissolution from angular porous media. *Environmental Science and Technology, 36*, 3310-3317.

APPENDIX

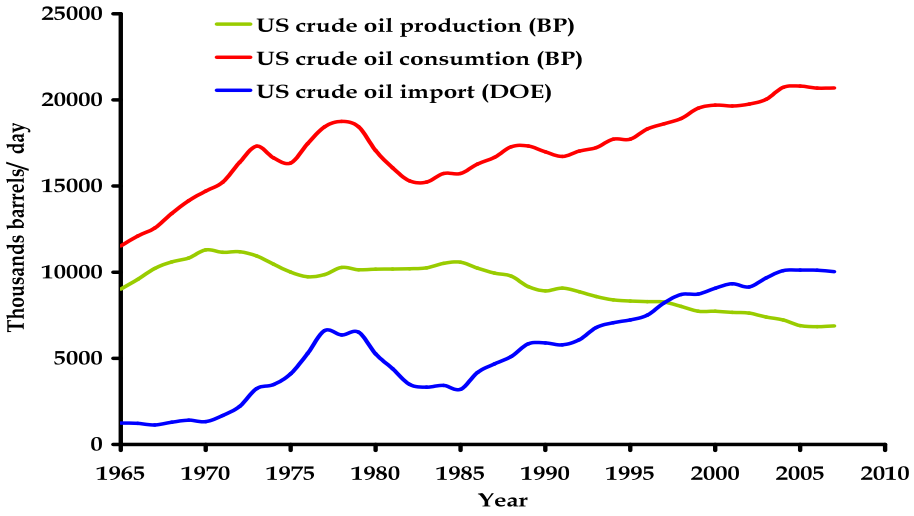

Figure A1. Crude oil production, importation and consumption in the United States since 1965.

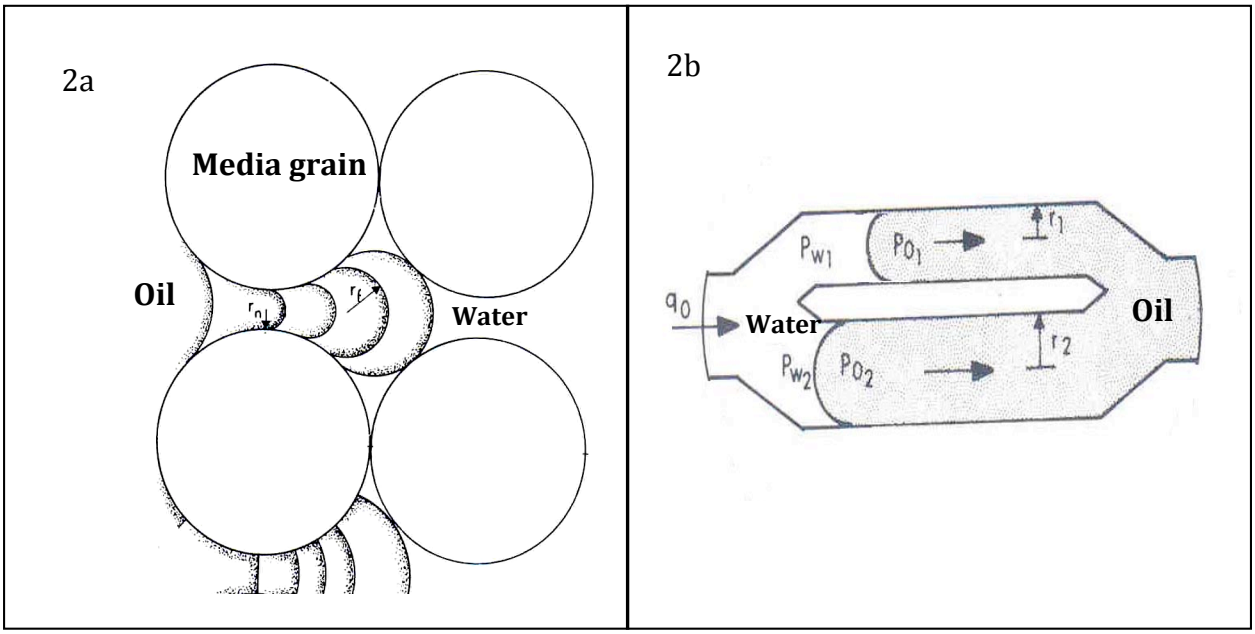

Figure A2. Oil trapping mechanisms: (a) The snap off mechanism is more common in pore spaces having a greater aspect ratio (the ratio of pore body to the pore neck radius, r_f/r_n, where $r_f > r_n$); (b) A simulation of the bypassing mechanism. Capillaries of two different radii ($r_2 > r_1$), connected at both inlet and outlet. During residual saturation the aqueous phase will preferentially penetrate the smaller radius channel, due to greater capillary pressure ($P_{W1} > P_{O1}$). Gradually, the smaller diameter channel will be filled completely with water, simultaneously squeezing the oil phase into the larger diameter pore channel. Eventually, the aqueous phase bypasses the oil phase and flows through the pore-doublet outlet, completely trapping the oil phase in the larger pore. (*Schematic diagrams modified from Stegemeier 1976*)

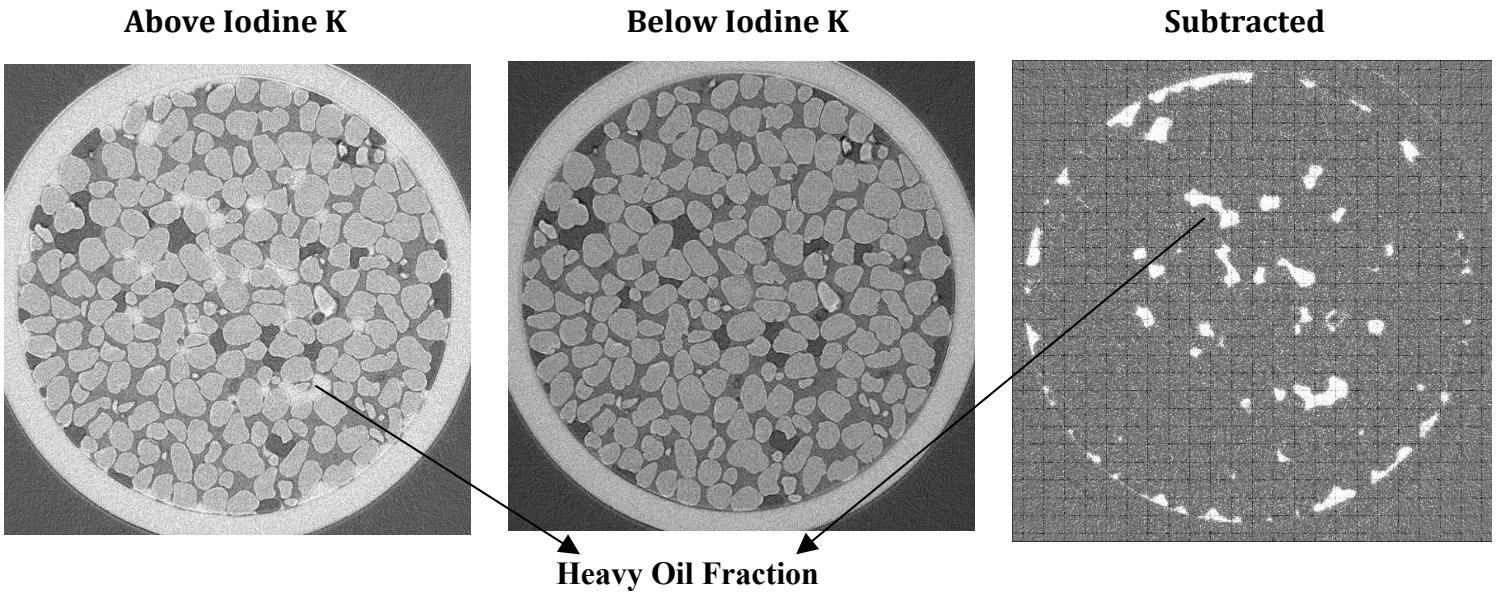

Figure A3. Subtraction of images taken above and below the iodine critical absorption energy to resolve the oil fraction (medium oil in this picture) doped with iodobenzene.

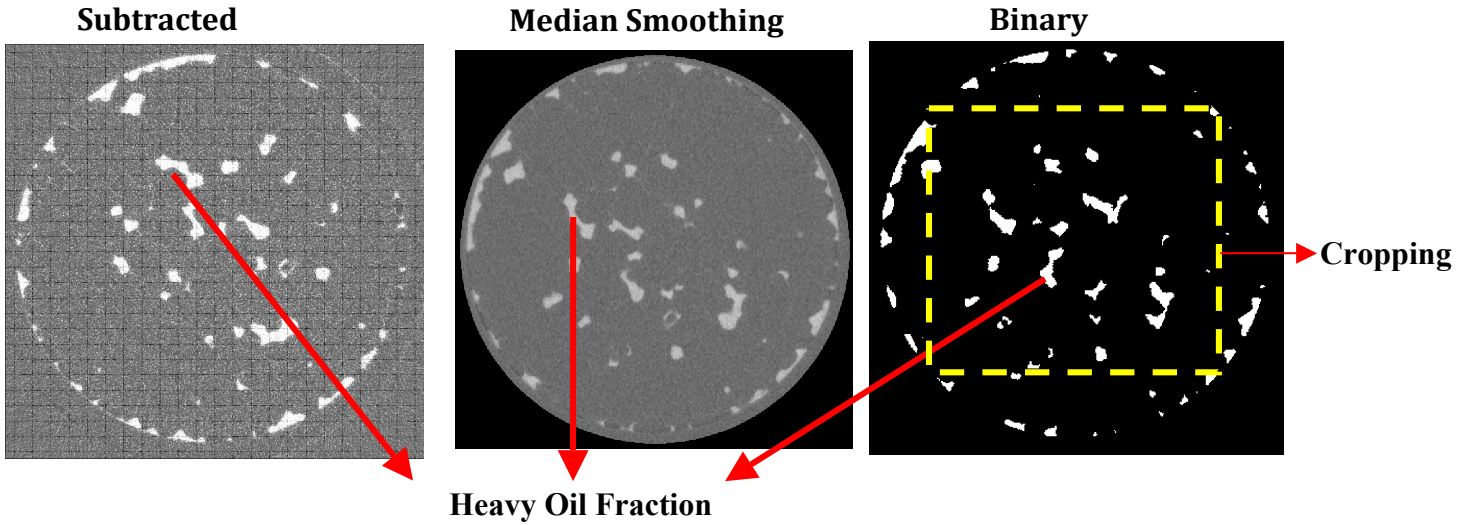

Figure A4. Noise reduction and transformation of SXM images into binary format, assigning the highest grey-scale value (255) to the target fluid (oil) and anything else as black (0 grey-scale value). The yellow dashed line shows the zone of cropping (3.97×3.97 mm^2) applied in order to avoid any interfacial control associated with the crude oil flow through preferential flow path along the boundary.